MEDDELELSER OM GRØNLAND

The Hans Tausen Ice Cap

Glaciology and Glacial Geology

Edited by C. U. Hammer

GEOSCIENCE • 39 • 2001

The Hans Tausen Ice Cap

Glaciology and Glacial Geology

Edited by
Claus Uffe Hammer

MEDDELELSER OM GRØNLAND • GEOSCIENCE 39 • 2001

The Hans Tausen Ice Cap. Glaciology and Glacial Geology. Edited by Claus Uffe Hammer. Meddelelser om Grønland, Geoscience 39. Copenhagen, the Danish Polar Center, 2001.

Editor in publication: Kirsten Caning
Layout by Special-Trykkeriet Viborg as
Printed by Special-Trykkeriet Viborg as

Cover: Researchers Camp on top of Hans Tausen Ice Cap.
Photo Department of Geophysics, University of Copenhagen.

Scientific Editor:
Dr. Svend Funder, University of Copenhagen, Geological Museum,
Øster Voldgade 5-7, DK 1350 Copenhagen K.
Phone+ 45 3532 2345, fax + 45 3332 2325, svf@savik.geomus.ku.dk

About the monographic series *Meddelelser om Grønland*
Meddelelser om Grønland, which is Danish for *Monographs on Greenland*, has published scientific results from all fields of research in Greenland since 1879. *Meddelelser om Grønland* is published by the Commission for Scientific Research in Greenland, Denmark.
Since 1979 each publication is assigned to one of the three subseries:
- *Man & Society*
- *Geoscience*
- *Bioscience*

*Geoscienc*e invites papers that contribute significantly to studies in Greenland within any of the fields of geoscience (physical geography, oceanography, glaciology, general geology, sedimentology, mineralogy, petrology, palaeontology, stratigraphy, tectonics, geophysics, geochemistry).

For more information and a list publications, please visit the web site of the Danish Polar Center *http://www.dpc.dk*

All correspondence concerning this book or the series *Meddelelser om Grønland* (including orders) should be sent to:

Danish Polar Center
Strandgade 100 H
DK-1401 Copenhagen
Denmark
tel +45 3288 0100
fax +45 3288 0101
email dpc@dpc.dk

Accepted October 2000
ISSN 106-1046
ISBN 87-90369-45-9

Contents

Foreword

The Hans Tausen Project was originally anticipated as two separate but closely linked projects within the Nordic Environmental Research Programme 1993-1997. The letters of intent were centered on two main issues:

1) Drilling of an ice core through the Hans Tausen Iskappe (ice cap) at a suitable place on this fairly large high Arctic ice cap;
2) To investigate the dynamic aspects of the ice cap and the surrounding area in both a glaciological and a geological sense.

Shortly after the field season in 1995 the participants decided to publish several papers on the project in one volume. Not only would it be easy for the reader to find the relevant papers in the same publication, but it would also demonstrate the importance of relating the various informations obtained by the project. Alas, this kind of publication is often time-consuming as authors, referees, and editors do not always follow the time schedule. In any case, we finally succeeded in collecting a fairly comprehensive set of papers.

Mixing more recent data of the Hans Tausen Iskappe with investigations of the post-glacial dynamics in the area is of special interest, as Peary Land is believed to be especially sensitive to global change. Amelioration of the Arctic climate conditions could have drastic effects on the local glaciers.

Our findings from the Hans Tausen Iskappe do tell a story of an ice cap which melted away during the Climatic Optimum and later started to rebuild; it has still not reached a dynamic equilibrium. In this perspective it is worth comparing our findings with those of the Northeast Canada.

The Hans Tausen Iskappe Project and the post glacial geo-glaciological history of the area is of significant interest due to the concern about global change as the data demonstrates that the area is sensitive to climate change.

Even though the project was focused on Global Change it also offered information of a more regional character, which adds to our understanding of geo-glaciological relations and to our understanding of the chemistry of the low troposphere in remote areas.

Copenhagen, 2000
Claus Hammer

Neoglacial Glaciations around Hans Tausen Iskappe, Peary Land, North Greenland

By Anker Weidick

Abstract

Weidick, A. 2001. Neoglacial glaciations around Hans Tausen Iskappe, Peary Land, North Greenland. Copenhagen, Danish Polar Center. Meddelelser om Grønland Geoscience 39, pp. 5-26.

All present glacier units in central Peary Land, North Greenland, have been systematically indexed in order to register existing documentation on glacier changes. The basis for this inventory work is the series of wide angle vertical aerial photographs flown in 1978 for Kort- og Matrikelstyrelsen. Determination of the glaciation limit on this base indicates a rise from 200 m a.s.l. at the outer coast of the Arctic Ocean to between 900 and >1000 m a.s.l. in the central areas of Peary Land. This trend is related to relatively higher precipitation and lower summer temperature at the outer coast compared to further inland.

The present glacier activity of individual glacier units has been investigated by study of all available aerial photographs from the years of 1950, 1960-63 and 1978. Locally photographic documentation can be extended back to 1938. In general, the glacier changes in this century have been very small, and significant changes are restricted to outlets of the Inland Ice, and to a minor degree outlets of local glaciers with mainly western and northern aspect.

Semi-permanent ice cover in the fjords leads to formation and retention of extensive floating lobes of glacier fronts. The climate of the 20th century appears to have been characterised by borderline conditions between periods of ice-free fjords and those of semi-permanent ice cover.

Neoglacial maximum is generally referred to A.D. 1900, with major thinning (downwasting) and recession in the first half of the 20th century, followed by slower recession, stand-still or even readvances during the last half of the century.

Keywords: Calf ice production, Glacier inventory, Glaciation limit, Neoglacial glaciations.

Anker Weidick, The Geological Survey of Denmark and Greenland, Thoravej 8, DK-2400, Copenhagen NV, Denmark.

Introduction

This paper describes recent glaciological developments around Hans Tausen Iskappe, central North Greenland (Fig. 1), i.e. the development of the glacier cover since the Holocene climatic optimum (the Neoglacial, e.g. Kelly 1980), but with special emphasis on the events of the 20th century.

Due to the scattered information available and lack of place names for most glaciers, the first step was to estab-

lish a reference base for all glaciers in the region. This was undertaken following the recommendations of Müller *et al.* (1977), in the same way as that established for West Greenland by Weidick *et al.* (1992). This new reference system for eastern and central North Greenland has been used for recording glaciological and glacial geological information, and is employed in the text and illustrations of this paper. Supplementary inventory data, such as the areal extent of each glacier unit, is not given here.

Description of the high arctic glaciers of the region includes their response characteristics, and their relationship to older Holocene glacial events.

Geological setting

Geology and geomorphology

Topographically and geologically, eastern and central North Greenland can be divided into broad E-W trending zones (e.g. Bengaard & Henriksen 1984). From north to south these are:

1. An alpine and fjord-dissected zone of folded Cambrian formations in Johannes V. Jensen Land (Fig. 1) and islands to the west, i.e. north of Frederick E. Hyde Fjord and the outer parts of J.P. Koch Fjord. Isolated peaks reach to c. 2000 m and the area is characterised by the widespread occurence of valley glaciers.
2. A broad zone of high plateaus dominated by Silurian formations, bounded to the north by Frederick E. Hyde Fjord, and to the south by Independence Fjord and Wandel Dal. The highest peak reaches 1850 m, but the extensive plateau surfaces are at around 1000 m a.s.l. with ice caps and ice fields of different sizes; Hans Tausen Iskappe is the largest (Fig. 1). A correct delineation of Hans Tausen Iskappe is complicated by the fact that its two northern branches (Fig. 2) coalesce with local valley glaciers.
3. A southern zone made up of flat-lying Proterozoic formations extending southwards from the heads of Victoria Fjord and J.P. Koch Fjord in the west to south of Wandel Dal and Independence Fjord in the east (Fig. 1). The Inland Ice in the west part of the zone slopes down at a low angle to the ice-free land areas, which generally reach altitudes of 800-900 m a.s.l.

West of Hans Tausen Iskappe, between the heads of Victoria Fjord and J.P. Koch Fjord the northern local ice caps over Freuchen Land almost merge with the Inland Ice proper. This may provide an illustration of the early phases of the Holocene disintegration of the ice cover over the present coast land, leading to successive isolation of local ice caps from the ice sheet margins.

Climate

Climate records for the continental area of North Greenland are limited to Brønlundhus in Jørgen Brønlund Fjord, c. 100 km east of Hans Tausen Iskappe and cover the period 1948-50 (Fristrup 1961). January temperatures average –31°C, July +6°C and the annual mean temperature is –15°C. Precipitation is low at about 100 mm/year.

For Hans Tausen Iskappe the present precipitation (accumulation) at the southern dome is about 10 cm water equivalent/year whereas the northern domes receive slightly higher accumulation (Reeh 1995).

Measurements of accumulation on Chr. Erichsen Iskappe and on Heinrich Wild Iskappe (Fig. 3) c. 100 km northeast of Hans Tausen Iskappe in the period 1948-1950 (Høy 1970) are of the same extreme low order. Descriptions of all three ice caps witness to a rapid formation of superimposed ice in the firn. The temperature in 10 m depth on Chr.

Fig. 1. Locality map for Peary Land and surroundings. On the map sheet water sheds dividing the area into the hydrological districts 2H to 2M are shown.

Erichsen Iskappe at 1000 m a.s.l. is given as –18°C, compatible with the figure of –20° to –17°C on Hans Tausen Iskappe at 1200 m a.s.l. (Reeh 1995).

Davies (1972) divided northern Greenland into two distinct climatic zones: a subhumid zone along the coastal fringe, including the lower parts of Danmark Fjord and Independence Fjord, and an arid inland zone. Temperature conditions in both zones are nearly the same, but annual precipitation in the subhumid zone is up to 40 cm annually compared to only 10 cm/year for the inland arid zone.

Present Glaciation, Fjords and Glacier Margins

Glaciation limit

In connection with the systematic registration of the glaciers of the area, an updating of the glaciation limit was made on the basis of the 1:100 000 orthophoto maps of Kort- og Matrikelstyrelsen (KMS, National Survey and Cadastre, Copenhagen). These maps were prepared using the series of vertical aerial photographs at 1:150 000 taken in 1978, and new fixed points surveyed throughout North Greenland. The

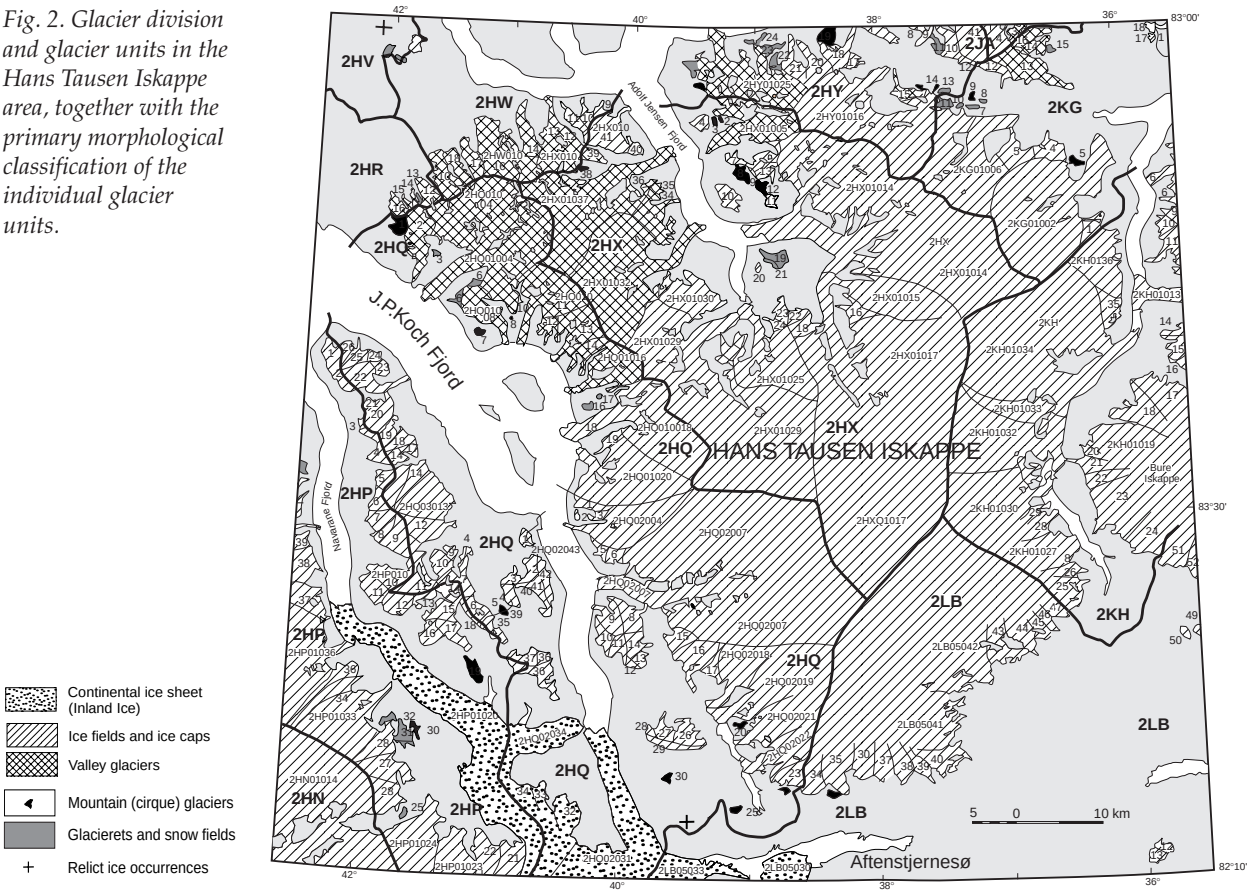

Fig. 2. Glacier division and glacier units in the Hans Tausen Iskappe area, together with the primary morphological classification of the individual glacier units.

map of glaciation limits is given in Fig. 4, and indicates generally the same trend of low coastal glaciation limit increasing inland towards the Inland Ice, as that published more than 70 years ago by Koch (1928). The new map gives maximum elevations (over 1000 m a.s.l.) around the mountains of Nordkronen west of Hans Tausen Iskappe, the area of greatest aridity.

The map also reflects that major sources of moisture must be from the open water areas among the pack ice and leads along coastal regions (Langway 1961, p. 1028), together with vapour transported by summer winds (Ohmura & Reeh 1991). The embayment of relatively low glaciation limit on the western flanks of Hans Tausen Iskappe seems to be influenced by the network of deeply incised fjords connecting the area with the Arctic Ocean.

The low level of the glaciation limit and widespread occurrence of valley glaciers in the coastal areas of eastern North Greenland imply a faster response of the glaciers to climate change than that of the large glaciers (ice caps) of central Peary Land around Hans Tausen Iskappe.

Fjords and calving outlets

The specific high arctic conditions of the glaciers of North Greenland, especially those draining from the Inland Ice to the heads of the fjords, are illustrated by strongly lobate or saw-tooth forms of the calving fronts floating in the fjords. Koch (1928) had attributed their preservation to the low surface slope (only minor crevasse development at the grounding line) and the constraining effect of the semi-permanent ice cover of the fjords in

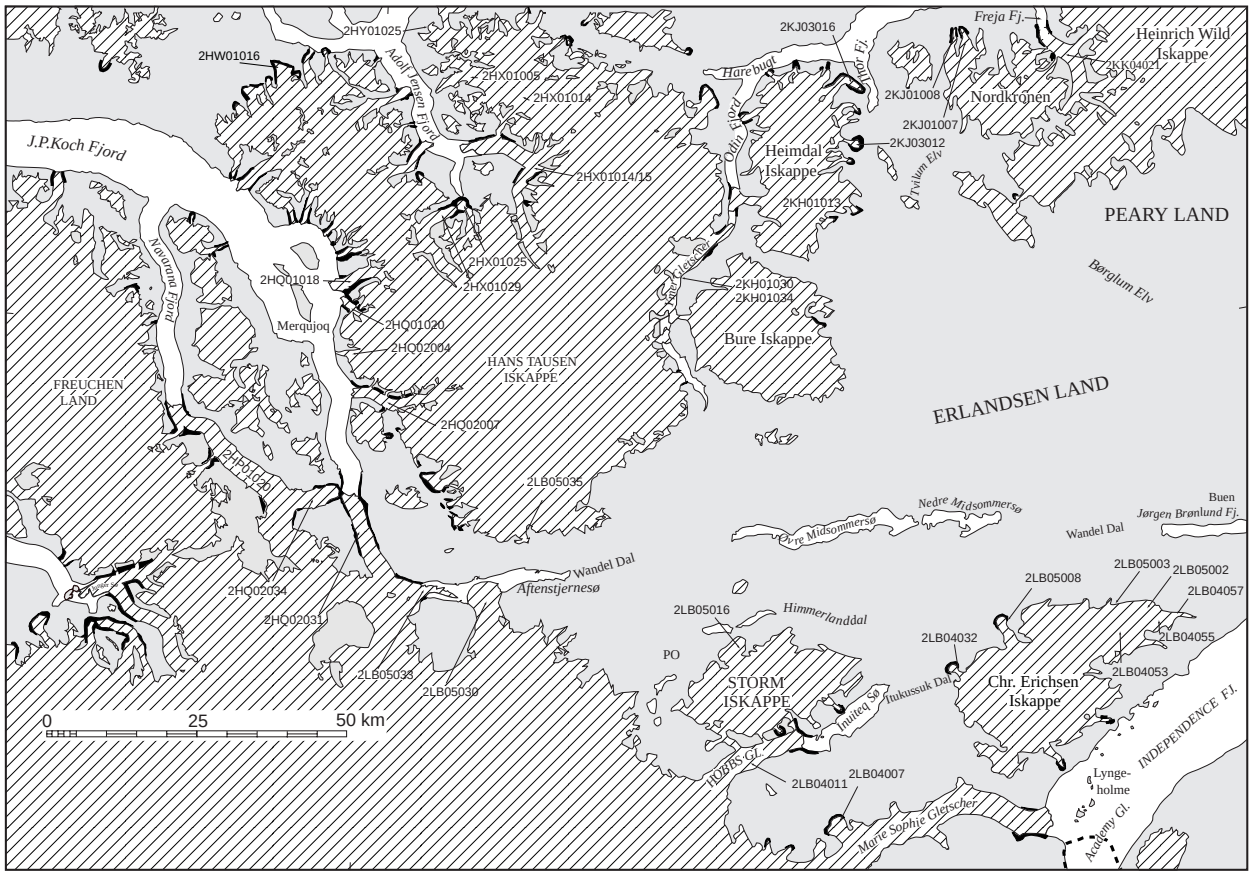

Fig. 3. Extension of neoglacial terrain around glaciers and ice caps in central Peary Land, shown with black colour. Glacier units described in the text are indicated by their location numbers.

front of the glaciers. Their changes and movement rate have been described by Higgins (1989, 1991), who also related the origin of Greenland ice islands to the infrequent break-up of large floating glaciers of this type. Several excellent examples of this type occur today north of 77°N on the east coast of Greenland (Reeh *et al.* 1999), of which the most intensively studied is the floating glacier filling Nioghalvfjerdsfjorden; this type of floating glacier is thus characterised as NFG-mode after the type locality of Nioghalvfjerdsfjorden glacier at 79°N. Essential characteristics of these NFG-mode outlets are:

1. They often have extending floating sections that partly or entirely fill the fjord.
2. Calving and dispersal of icebergs takes place on the rare occasions when the connected fjords are icefree; average calf ice production is low, compared to those of the more southerly outlets in East and West Greenland (see below).
3. Essential ice loss from the floating glacier outlets is not by calf ice production, but by bottom melting (Reeh *et al.* 1999), a consequence of thermohaline and tidal circulation under the floating ice.

By contrast, most calving glaciers south of 77°N are characterised by nearly rectilinear or concave frontal forms, and the front is usually located at or near the grounding line with often a nearly constant and high calf ice production. The calving glaciers of this type are referred to as the DJG-mode, after Daugaard-Jensen Gletscher at 72°N, East Greenland (Reeh & Olesen 1986; Reeh *et al.* 1999).

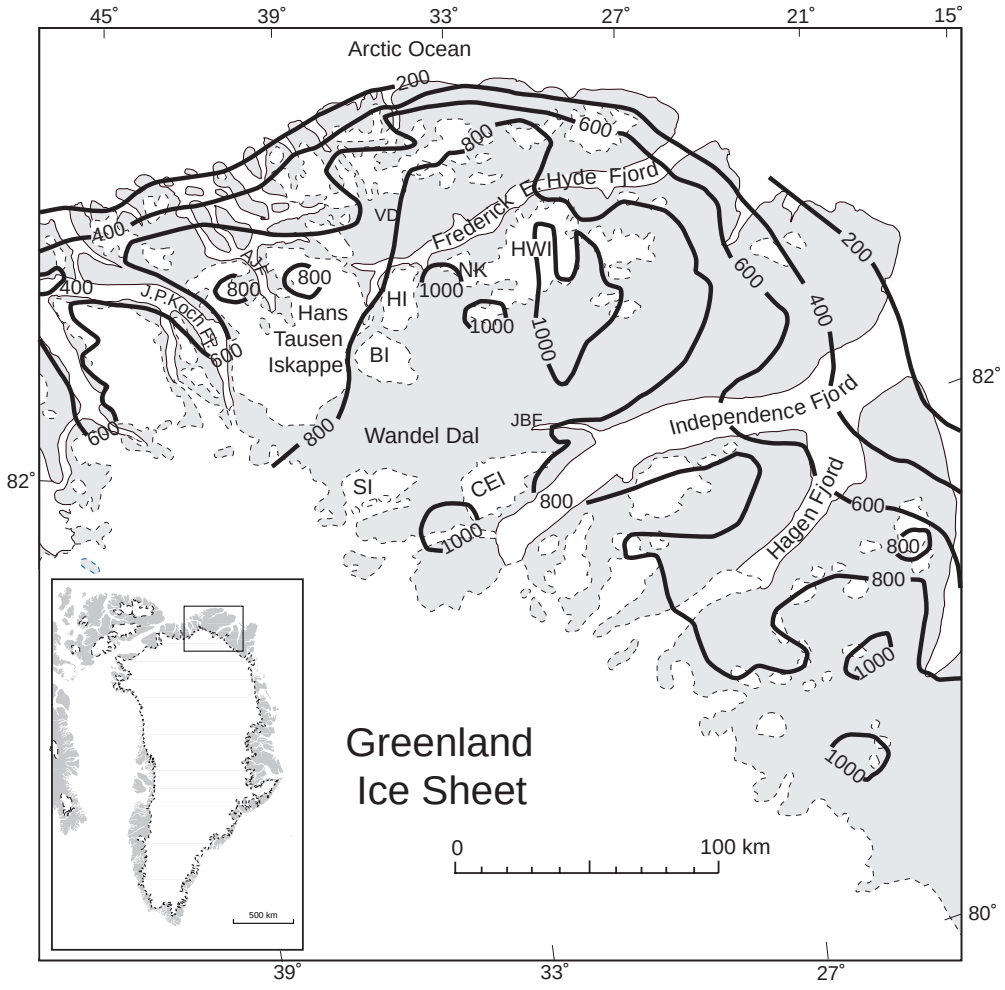

Fig. 4. Peary Land and surroundings. Altitude of glaciation limit in meter a.s.l. Abbreviations: AJF: Adolf Jensen Fjord, VD: Vølvedal, BI: Bure Iskappe, HI: Heimdal Iskappe, NK: Nordkronen, HWI: Heinrich Wild Iskappe, SI: Storm Iskappe and CEI: Chr. Erichsen Iskappe.

In Reeh *et al.* (1999) it is concluded that a slight temperature rise would be sufficient to cause a reduction of the present semi-permanent fjord ice in North Greenland, and induce a rapid disintegration of the floating glacier sections of North Greenland from the Inland Ice. However, the bathymetric and shifting hydrographic conditions of the different fjords and adjoining parts of the Arctic Ocean must also influence the changes of glacier fronts and ice coverage of the fjords.

^{14}C dates from the heads of North Greenland fjords (Bennike 1987; Kelly & Bennike 1992, Weidick *in* Landvik *et al.* 2001) show that during the early Holocene retreat, glaciers attained their present position as early as 8-9 cal. ka B.P. in wider fjord systems such as in Independence Fjord, whereas the outlets in narrow fjords such as in J.P. Koch Fjord first reached their present position at 6-7 cal. ka B.P. This reflects the importance of changes of hydrographic conditions and a relatively rapid glacier change in the larger fjord systems during the first phase of the Holocene deglaciation. Deglaciation of narrow fjords, valleys and especially the coastal uplands must then be regarded as later phases in the deglaciation.

The occurrence of both NFG-mode for most North Greenland glaciers and DJG-mode at the glaciers at the head of Independence Fjord, eastern North Greenland in this century may imply that present climatic conditions are intermediate between the two modes in the area. Possibilities for observing the change be-

tween the two modes therefore should be present. Unfortunately, aerial photograph coverage for the region is very limited, and searches of other historical material (old diaries, photographs) would be extremely time consuming. However, a single example of recent change between the two frontal modes is found at the head of J.P. Koch Fjord at Adams Gletscher (2HQ02031, Fig. 5).

The calving outlets from local glaciers into the ice covered fjords in the western and central parts of the Hans Tausen Iskappe area also generally show an

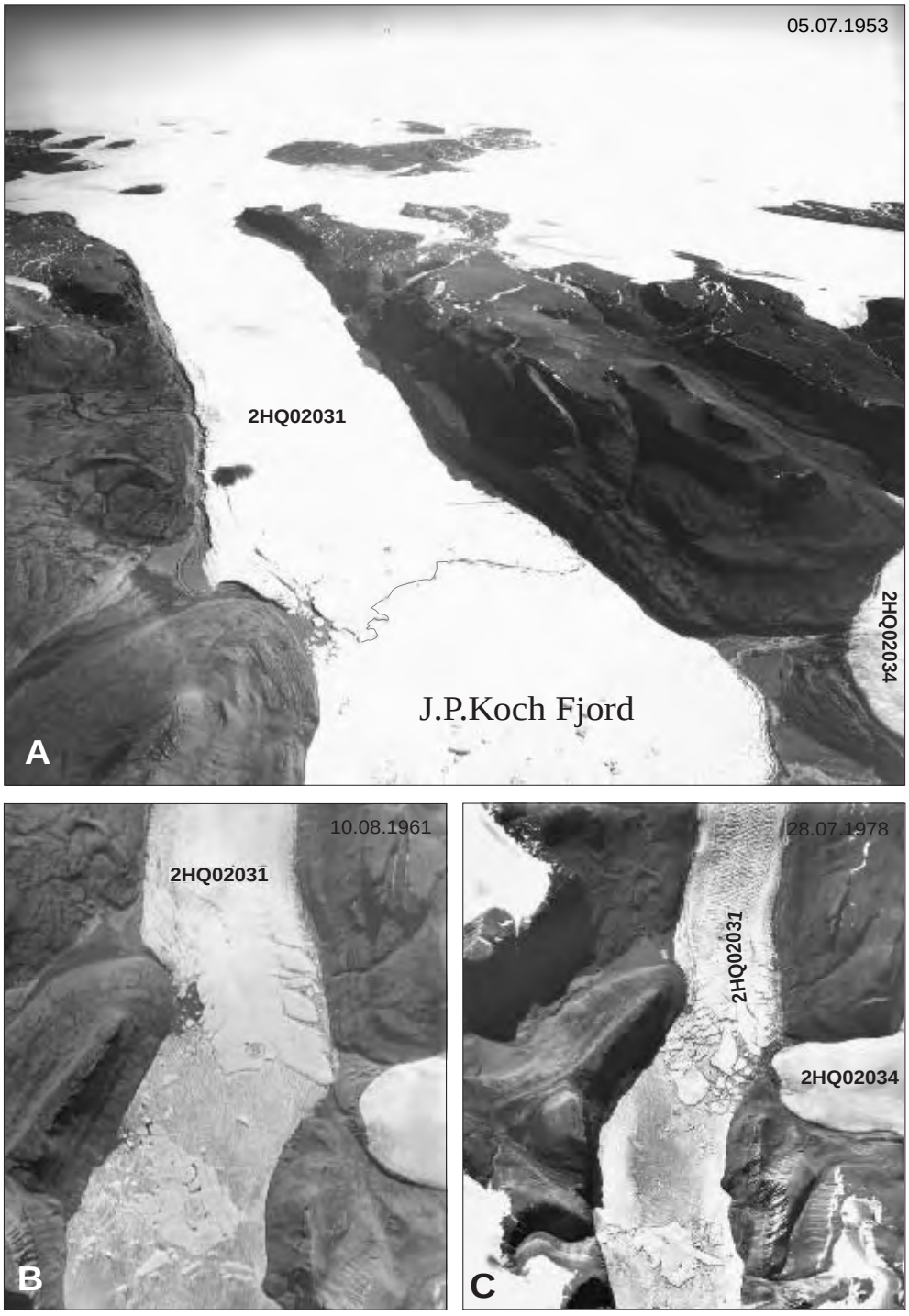

Fig. 5. Documentation of the changes of Adams Gletscher (2HQ02031), and Henson Gletscher (2HQ02034).

A: Photograph of July 5th, 1953, KMS route D-SØ, no. 1165.

B: Photograph of August 10th, 1961, KMS route 256H, no. 754

C: Photograph of July 28th 1978, KMS route 874F, no.2200

Copyright Kort- og Matrikelstyrelsen. A indicates the front of 2HQ02031 in DJG mode with a nearly rectilinear or concave glacier front, whereas B and C show the same front in NFG mode with strongly lobate front extending out into the fjord.

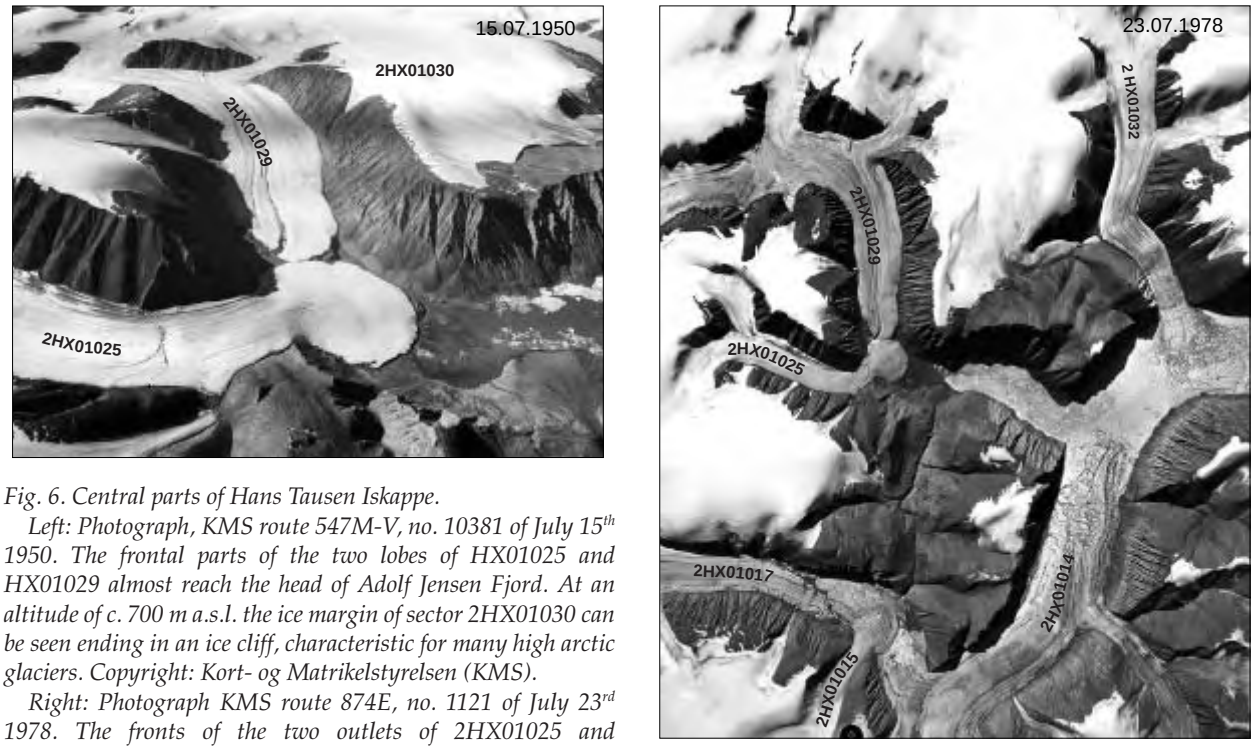

Fig. 6. Central parts of Hans Tausen Iskappe.

Left: Photograph, KMS route 547M-V, no. 10381 of July 15th 1950. The frontal parts of the two lobes of HX01025 and HX01029 almost reach the head of Adolf Jensen Fjord. At an altitude of c. 700 m a.s.l. the ice margin of sector 2HX01030 can be seen ending in an ice cliff, characteristic for many high arctic glaciers. Copyright: Kort- og Matrikelstyrelsen (KMS).

Right: Photograph KMS route 874E, no. 1121 of July 23rd 1978. The fronts of the two outlets of 2HX01025 and 2HX01029 are in almost the same position as in 1950 (a slight expansion has possibly occurred). The typical high arctic calving fronts of 2HX01014 and 2HX01032 are seen surrounded by semi-permanent fjord-ice. At the border between 2HX01014 and 2HX01015, strongly folded moraines are seen. Copyright: Kort- og Matrikelstyrelsen.

NFG-mode (see examples in Fig. 6, glaciers 2HX01014 and 2HX01032) whereas this is not the case in the eastern parts of the area around Frederick E. Hyde Fjord.

Land-based ice margins and glacier fronts

Land-based ice margins and glacier fronts also show characteristic high arctic features such as marginal superimposed ice or fringing glaciers, ice cliffs and steep ramps (Nobles 1961). At higher altitudes, ice cliffs (Goldthwait 1971) are usually well developed. An example from the central part of Hans Tausen Iskappe (glacier 2HX01030) is shown in Fig. 6 and here, as well as at lower altitudes, shear moraines in the fronts may indicate formation of superimposed ice. Another example from the area is glacier 2HW01016 at the northwestern section of Hans Tausen Iskappe, the location of which is shown in Fig. 3. However, the connection between the marginal forms and advancing or retreating ice in the high Arctic is still uncertain (e.g. see discussion on ice cliffs in Goldthwait 1961, p. 114 and Hooke 1970, p. 322) so they cannot be used as indicators of advance or retreat of ice margins.

Another specific form frequently seen is the piedmont glacier or expanded foot glacier. A characteristic and well developed form from Nares Land west of the entrance to J.P.Koch Fjord is shown in Weidick (1995, Fig. 36). Other examples from the study area are the glaciers 2HX01015 and 2HX01025 (Fig. 6). In places frontal reduction of such

glaciers has taken place, e.g. glacier 2KJ03012 from Heimdal Iskappe, the position of which is shown in Fig. 3. The glacier outlet 2LB04032 (Elefantfoden) from the north-western part of Chr. Erichsen Iskappe (Fig. 3) was stable between 1950 and 1978 (1950: 548G-V no. 10220; 1978: 874J no. 2966 and 874K no. 921) and showed very slight recession since the neoglacial maximum, whereas the outlet of glacier 2HX01025 in central parts of Hans Tausen Iskappe at the head of Adolf Jensen Fjord (Figs 2, 3, 6) appears to have had a slight expansion between 1950 and 1978 by provisional estimate.

Location and Definition of the Present Ice Cover

The systematic registration of the glaciers on the map of Fig. 2 was carried out on the basis of studies of the 1978 vertical aerial photographs with respect to location, type and frontal conditions. For comparison, these observations were supplemented by scattered investigations of glaciers between Hans Tausen Iskappe and Hans Egede Land (Fig. 1), i.e. the area covered by Fig. 3.

The distribution of glacier types around Hans Tausen Iskappe is shown in Fig. 2. Of the 303 glacier units distinguished, 61 constitute Hans Tausen Iskappe proper and another 50 units make up two northern extensions of this ice cap, with a gradual change from ice cap sectors through ice fields to valley glaciers; the entire Hans Tausen Iskappe complex thus comprises 111 units.

Comments on the individual types of glaciers are given below.

The continental ice sheet margin (Inland Ice)

The part of the Inland Ice represented in Fig. 2 is divided into 9 units; the western parts form glacier sector 2HP01020 (Navaraneq Gletscher), and the eastern parts 2LB05030 (Astrup Bræ), which debouches into Aftenstjernesø (lake, surface 300 m a.s.l.).

The upland gradation from ice margin over snow patches to bare rock is only seen above 700 m a.s.l. Land-based outlets below this altitude usually have ice cliffs or ice ramps (Nobles 1961), with lacking or very narrow trim lines or Neoglacial moraine terrain such as at 2HQ02034 (Henson Gletscher).

Two floating glacier outlets of very different form occur in Aftenstjernesø. Glacier 2LB05033 is a perfect example of a saw-tooth glacier, typical of high arctic floating glaciers, whereas the eastern outlet of 2LB05030 (Astrup Bræ), exhibits a typical piedmont lobe (Fig. 7, 10). Bathymetric conditions in Aftenstjernesø are unknown; presumably the lake is deepest at its west end (towards the drainage outlet to J.P. Koch Fjord) so that only the damming lobes of 2LB05033 are floating whereas 2LB05030 is grounded. The extent of these lobes and the location of detached icebergs in aerial photographs from 1961 and 1978 suggests little ice movement.

For the major outlet which reaches the sea, 2HQ02031 (Adams Gletscher), the movement has been estimated at 170 m/year (Higgins 1991). This outlet is surrounded by neoglacial moraines and trim line zones that extend c. 3 km north of the 1978 frontal plain.

Ice fields

Ice fields are defined by Müller *et al.* (1977) as masses of sheet or blanket types of ice, whose thicknesses are not sufficient to obscure the subsurface topography. They are here viewed as transitional between ice caps and valley glaciers; their frontal characteristics correspond to those of ice caps (see below) and they are grouped with ice caps on Fig. 2. The units corresponding to this type are found in the northern parts of the Hans Tausen Iskappe complex.

Fig. 7. South-east corner of Hans Tausen Iskappe showing the lake of Aftenstjernesø with the fronts of glaciers 2LB05033 and 2LB05030 (Astrup Bræ). Parts of J.P.Koch Fjord show the floating Inland Ice outlet of Adams Gletscher (2HQ02031). The front of Adams Gletscher is surrounded by neoglacial moraines extending c. 4 km beyond the glacier front on this 1978 aerial photograph.

The cirque glaciers of 2HQ02025, 2HQ02030 and the frontal cirque tributary to outlet 2LB05035 illustrate different degrees of down wasting.

Locations of radiocarbon dated organic material (Ua-4586, Ua-4587, GSC-2279 and I-9130) indicate a retraced position of glacier lobe 2HQ02031 from c. 6000 years ago and up to the Little Ice Age (cf. Landvik et al. 2001). KMS route 874G, no. 2230 of July 28th 1978. Copyright, Kort- og Matrikelstyrelsen.

Ice caps

Ice caps are the dominant ice type of the area. The largest is Hans Tausen Iskappe and Table 1 shows the size of Hans Tausen Iskappe compared to other local ice caps of the region.

Land-based glacier outlets are often surrounded by narrow trim line zones or by neoglacial moraines, in particular around small outlets which descend steeply from ice caps, and around some of the floating outlets in the northern and western parts of the Hans Tausen Iskappe complex (Fig. 3). The most important floating outlets are here typically characterised by protruding fronts of calf ice assemblages but these are also bordered by trim lines or fresh moraines indicating a net thinning in most recent time.

For the largest outlets of Hans Tausen Iskappe complex, Higgins (1991) measured rates of movement varying from 175 m (2HQ02007) to 30 m (2HQ01016) annually for the west and north sides of the ice cap complex. However, while Higgins (1991) stated that the large eastern outlet from Hans Tausen Iskappe: 2KH01034 (Ymer Gletscher) had insignificant movement, stake movements in connection with mass balance measurements in 1994/95 in the nor-

Table 1. Estimated areas and volumes of ice caps in Peary Land.

Ice cap	Area	Thickness	Volume (ice)
Hans Tausen	4208 sq.km (a)	175 m	736 cubic km (b)
Heinrich Wild	1042 sq.km (a)	100 m	104 cubic km (b)
Chr. Erichsen	529 sq.km (a)	80 m	42 cubic km (b)
Bure	397 sq.km (a)	80 m	32 cubic km (b)
Heimdal	368 sq.km (a)	80 m	29 cubic km (b)
Storm	300 sq.km (a)	80 m	24 cubic km (b)

(a) Area according to W. Starzer (personal communication).

(b) According to Cailleux et Lagarec (1977) as related mean glacier thickness to glacier size. Measured volume of Hans Tausen iskappe complex with the area figure of 4208 sq.km is calculated to relate a volume of 761 cubic km on the basis of radar measurements by Gundestrup et al. (W. Starzer, pers. Communication).

thern part of the ice cap (2KG01002, Fig. 2) showed the maximum rate of movement at the equilibrium line is about 50 m/year, declining to 5 m/year at the land-based glacier terminus (Reeh 1995).

Valley glaciers

Valley glaciers are mainly found in the north-western part of the area (Fig. 2). In their lower parts they are often surrounded by well developed trim line zones and moraines, indicative of net recession.

Cirque glaciers

The group was originally termed mountain glaciers (Müller *et al*. 1977), i.e. small glaciers of any shape, sometimes similar to a valley glacier, but much smaller; frequently located in cirque or niche. Most of those in the study area here could be described as cirque glaciers. The cirque glaciers occur scattered throughout the upland areas of otherwise ice-free terrain. The few (cf. Fig. 2) registered cirque (mountain) glaciers have little frontal development of neoglacial moraines, such as are known from other parts of the world. In place of recessive features they show a state of general waning or downwasting, with dust covered surfaces such as 2HQ02025 and 2HQ02030 on Fig. 2 and 7. Examples of "fossil" glaciers of this type have been observed on aerial photographs, where the glaciers can scarcely be distinguished from the surrounding land (depicted in Fig. 2 as "relict ice occurrences").

Glacierets and ice fields

Glacierets and ice fields are defined by Müller *et al*. (1977) as a small ice mass of indefinite form in hollows, river beds and protected slopes. They occur frequently throughout the area. Their mergence with other glacier forms, especially at the eastern and southern margins of Hans Tausen Iskappe and at the Inland Ice margin, makes delineation and differentiation of these ice cover types difficult.

General trends of the ice cover of the area

The general trends of the ice cover are summarised in the map of Fig 3, which shows the extent to which the glaciers were surrounded by fresh Neoglacial moraines or trim line zones in 1978, indicative of recent net recession.

The recession is in general related to larger outlets from ice caps and valley glaciers, and in particular to western and northern facing examples. Usually

the net recession is modest, of the order of tens to hundreds of metres since the neoglacial maximum. One extreme exception on the map of Fig. 3 is the outlet of 2HQ02031 (Adams Gletscher) from the Inland Ice, which shows a net retreat of *c*. 3 km.

The permanence of the upland cirque glaciers may indicate positive mass balance for most recent decades, but this is contradicted by the occurrences of relict ice. In this context it is possible that downwasting rather than recession is characteristic for the upper reaches of the region. This process has been described for the western parts of North Greenland by Davies & Krinsley (1962; Brother John Gletscher, p. 124). In respect of the Holocene recession of the ice cover over North Greenland the same process is described by Kelly & Bennike (1992, p. 19). Low slope of the subsurface, relatively small thickness of the ice cover, confinement of the glaciers to narrow valleys and the low temperatures in the glacier body with extensive freezing of the glacier to the subsurface, may favour conditions for downwasting and relict ice formation.

Historically Documented Glacier Activity in Peary Land

The presentation of Neoglacial terrain around the glaciers in Peary Land (Fig. 3) can only give an impression of recent net recession of the glacier cover over specific areas, a recession which may be compensated by advances or readvances of other areas.

Earlier glaciological investigations of the area

Recent glacier changes in North Greenland were investigated by Davies & Krinsley (1962) and on the basis of conditions in the period 1956-1960 they concluded for Peary Land that "of the 309 glacier fronts in the area, 208 are apparently stable, 99 show definite indications of recent retreat and 2 show evidence of recent advance. Of 11 small isolated ice caps, 9 are apparently stable and 2 show sign of recent retreat" (Davies & Krinsley 1962, p. 127). Their investigations covered the entire area of Peary Land north of Independence Fjord and east of J.P. Koch Fjord, but the location of the observed glaciers is not given in most cases and it is therefore not possible to update the observations given.

Early glaciological work on the ice caps of the region is reported by Høy (1970). Mass balance measurements on Chr. Erichsen Iskappe were initiated by B. Fristrup and Th. Høy in 1948-49, continued in 1951 and 1952, and terminated with a re-survey in 1963. Høy (1970) records an accumulation figure of 10-12 cm water equivalent per year, and a marginal net recession of the north-eastern ice margin, around the sectors 2LB05002 and 2LB05003 in Fig. 3, of 80-150 m in the period 1950-1963, i.e. 6-12 m/year at an altitude of c. 870 m a.s.l. Investigations on the south-eastern ice cap margin around sector 2LB04055 (Fig. 3), at near the same height showed no signs of change during this period. As a follow-up of this observation a comparison of the conditions at this margin on aerial photographs of July 7th 1960 (route 256M no. 754) with aerial photographs for July 21st 1978 (route 874K no. 915) revealed little change of the ice margin position.

Present evaluation of glacier changes

The maximum age of the Neoglacial trim line zone mapped in Fig. 3 can only be documented for those glaciers in North and North-East Greenland where observations extend back to the beginning of the 20th century, i.e. Petermann Gletscher, Ryder Gletscher, Academy Gletscher and Hagen Bræ; fluctuations of these glaciers have been summarised by Davies & Krinsley (1962), Higgins

(1991) and Weidick (1995). On this evidence the oldest neoglacial moraines are considered to be *c.* 100 years old.

The documentation for subsequent glacier fluctuations during this century is very sparse. For the area of study regular observations began with the oblique photographs of 1938 (Koch 1940) and the oblique photographic routes of the Geodetic Institute, dating from the early 1950s, but without uniform coverage of the area. Full coverage by vertical aerial photography was first achieved in the early 1960s, and repeated by the high altitude wide-angle photography of 1978. Evaluation of the often small glacier changes is hindered even here by shadow positions of the glacier fronts and, for floating glacier tongues, the common gradation between glacier and floating calf ice of the glacier fronts.

Examples of fluctuations given below illustrate some trends in the behaviour of glaciers in the area.

Fluctuations of the Inland Ice margin

The largest extension of the Neoglacial trim line zone can be observed around the outlet of Adams Gletscher (2HQ02031), which debouches into the head of J.P. Koch Fjord and has a 2-3 km wide calving front. Since the neoglacial maximum extent (about 1900?) the glacier front has retreated by over 4 km and was observed in this retracted position in 1950; subsequently it gradually advanced by 1-2 km to its 1978 position. In Fig. 8 these changes are given as loss or gain in the glacier area, and the changes are here compared with those of other calving outlets of the Inland Ice in eastern North Greenland (Academy Gletscher and Hagen Bræ). With reservations for the scatter and scarcity of observations there seems to be the same general trend in the glacier behaviour. A major recession of the outlet glaciers in the first half of the 20th century is followed by minor readvances in the second half. Ryder Gletscher and Steensby Gletscher elsewhere in North Greenland seem to show similar trends (Higgins 1991) which can be linked to a period of break-up of the semi-permanent fjord ice corresponding with maximum temperatures for this century as revealed in the Hans Tausen Iskappe ice record (Hammer & Thomsen 1998).

The changes of the frontal positions of Adams Gletscher (Fig. 5) also appear to reflect a transformation of the glacier front from a DJG-mode in 1953 to an NFG-mode in 1963 and 1978.

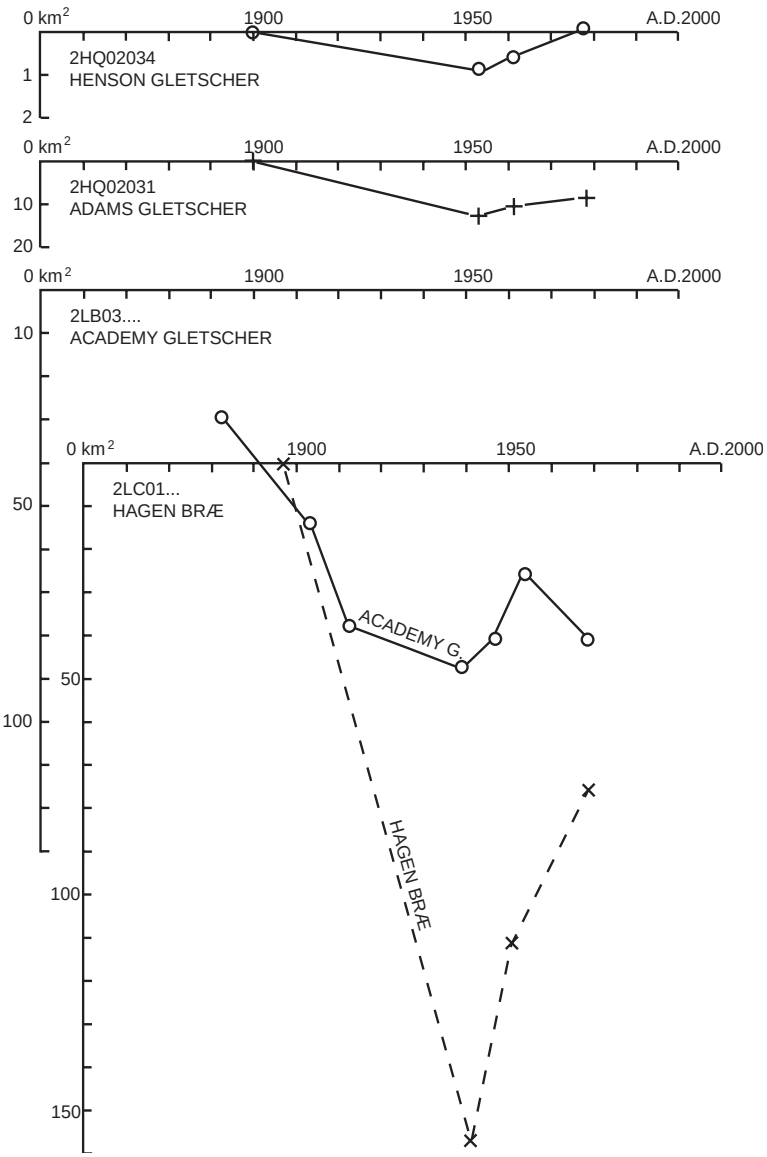

Fig. 8. Estimated changes of area of some Inland Ice outlets in eastern and central North Greenland. NB: The vertical scale for the land-based outlet Henson Gletscher (2HQ02034) differs from the scales of the floating outlets of Adams Gletscher, Academy Gletscher and Hagen Bræ.

The neighbouring land-based glacier 2HQ02034 (Henson Gletscher, cf . Figs 5, 8) also shows the same trend of recession prior to 1950 and the subsequent readvance, whereas other higher altitude outlets draining into the lake Aftenstjernesø (2LB05033; no name, and 2LB05030; Astrup Bræ, Fig. 7) show no change throughout the period 1950-1978.

Glacier changes 1938-1978 at outlets from ice fields, ice caps and valley glaciers

For most glacier outlets, the zones of trim line or Neoglacial moraines apparent on the 1950 series of aerial photographs show little subsequent change in their extension in the fjords, or their extension on land. Their main recession must therefore have been achieved prior to 1950. For example, the protruding glacier fronts on the west side of Hans Tausen Iskappe (Higgins 1991) show essentially the same configuration on the aerial photographs of the early 1950s and those of 1978.

The earliest photographs of some of the glacier lobes from April 15th 1938 are published in Koch (1940) and give only local and restricted information of the status of the glacier at that time. However, the age of the observations justify comments on the updating of glacier changes at these localities, as given below. The positions of these glaciers are shown in Fig. 3.

2KK04021 (Balder Gletscher)
This glacier is situated at the head of Freja Fjord, a southern minor tributary to Frederick E. Hyde Fjord. The glacier is the largest drainage outlet of Heinrich Wild Iskappe and terminated with a 1.5 km wide, "normal" calving front (DJG-mode) in 1978. Photographs of the glacier in 1938 and 1978 are shown in Fig. 9.

The glacier had presumably receded from its Neoglacial maximum *c*. 1.8 km north of its 1978 position before 1938 (cf. Fig. 9). The subsequent recession between 1938 and 1978 (route 874F, no. 281) is between 200 and 500 m.

2KJ01007 and 2KJ01008 (no names)
These outlets are lobes from the ice fields covering the mountain Wistar Bjerg (1850 m high). They descend down to altitudes of respectively 300 and 200 m. Their flanks are characterised by ice cliffs, and a trim line zone is apparently lacking or very narrow at the 1938 position. Only the front of 2KJ01007 can be observed on the 1938 photograph. Both glaciers were close to their Neoglacial maximum in 1938 and only a slight thinning of both glaciers took place in the period up to 1978 (route 874E no. 1105).

2KJ03016 (no name)
This glacier is an outlet from Heimdal Iskappe draining down to Thor Fjord, a southern tributary to Frederick E. Hyde Fjord. The lobe descends rather steeply in a narrow gorge down to the shore of Thor Fjord, where the front in 1938 (Koch 1940, fig. 49) formed a small piedmont. Subsequent thinning and disappearance of the front from the coastal plain occurred in the period up to 1978.

2KH01013 (no name)
This is a *c*. 1.5 km wide glacier outlet descending from Heimdal Iskappe (Fig. 3). Its front expands to a piedmont lobe which blocks Odin Fjord for more than 4 km. With some reservation it can be concluded that the front in 1938 may have had a position a little more retracted than that of 1978 (route 874F, no. 2188). In Koch (1940, fig. 50) the glacier illustrated is described as Ymer Gletscher, but Ymer Gletscher is in fact located farther to the south and cannot be seen on the 1938 photograph.

2HQ01018 and 2HQ01020 (no names)
Both glaciers are outlets from Hans

Fig. 9.
Top: Freja Fjord with Balder Gletscher (2KK04021) photographed May 15th 1938 (Koch 1940).
Bottom: Section of KMS 1:100 000 orthophoto map 82 Ø3, based on aerial photographs of 1978 (route 874E, no. 1105, July 23rd 1978). Copyright: Kort- og Matrikelstyrelsen.

Tausen Iskappe draining to J.P.Koch Fjord (Fig. 3). They descend at a moderate gradient to the fjord where their fronts appear as an assemblage of packed calf ice concentrations (Higgins 1991, Fig. 12) protruding *c.* 2 km out into the fjord. The frontal widths of the two outlets are 2.2 km (2HQ01018) and 1 km (2HQ01020) and their rates of movement are given by Higgins (1991) as 60 m/year and 70 m/year respectively.

On the 1938 photographs reproduced in Koch (1940, Figs 51-52) calf ice concentrations can also be seen reaching out into J.P.Koch Fjord from the neighbouring outlet 2HQ02004 (Fig. 3). All the

concentrations of packed calf ice from the outlets into J.P.Koch Fjord have the same general extent on the photographs from 1938 and those of 1978 (route 874E, no. 1125). The well developed trim line zone on the 1978 photograph seems not so widely developed in 1938 where the features are veiled by a thin snow cover, and a thinning of the glaciers 2HQ01018 and 2HQ01020 in the period 1938-1978 must therefore be concluded.

2LB05016 (no name)

This is a 5 km wide piedmont glacier outlet on the northern side of Storm Iskappe, which descends from the firn area at *c*. 1000 m altitude down to the front at 500 m altitude. Precise determination of the frontal position in 1938 cannot be made due to the distant view of the glacier, but apparently little or no change had taken place up to 1978 (route 874J, no. 2971).

Glacier changes 1960-1978 at outlets from ice fields, ice caps and valley glaciers

Only the glaciers described above are covered by photographs back to 1938; many other glaciers are covered by information back to the oblique photographs of *c*. 1950, but the first regional coverage is by the vertical aerial photographs of 1960-63. A total of 33 glaciers can be evaluated in terms of their activity between 1960 and 1978.

The 33 glacier units are listed in Table 2 by their location number, name if any, geographical coordinates, lowest and highest parts of the glacier (highest part omitted for Inland Ice sectors or outlets), morphological code and main exposure directions.

The morphological code is described in the matrix form given in Table 3 (originally proposed by Müller *et al.* 1977), modified for Greenland by Weidick *et al.* (1992). Of the 33 glaciers listed in Table 2, 23 are related to ice fields, ice caps and valley glaciers (first digits 2, 3 and 5 in the morphological code Table 2), seven units are related to the Inland Ice (first digit 1) and three are cirque glaciers (first digit 6). For the 23 glaciers related to the ice fields, ice caps or valley glaciers, 16 are stationary or show slight retreat, and only one has slightly advanced in the decades since 1950. The reported cases of possible surges are very uncertain; they are based on the appearance of pitted glacier surfaces and/or strongly foliated moraines. In all cases there has been no change in the glaciers between 1950 and 1978, so surges have not been demonstrated. The glacier changes are in all cases small, which is the reason that the three remaining glacier units of ice fields, ice caps and valley glaciers are labelled "uncertain".

Specifically high arctic features such as ice cliffs generally occur in the higher reaches of the ice margin, but can also occur in lower frontal regions. Thus at glacier 2HWJ01016, located in Fig. 3, the recession given is a recession of superimposed ice deposited in front of the real glacier lobe.

Cirque glaciers

The few cirque glaciers (cf. the plots on the map Fig. 2) show generally little area change in the period 1950-1978. Isolation and slight thinning of a cirque glacier from the outlet of 2LB05035 on the south side of Hans Tausen Iskappe is shown here in Fig. 10. It will be noted that the reduction of the area of the cirque glacier between 1950 and 1978 is small.

Summary of the historical changes of glaciers in central Peary Land

Recent recessional features (neoglacial moraines, trim line zones) are plotted in a very generalised way in Fig. 3. For the land-based outlets, net recession for this century is usually confined to the fjord systems north and west of Hans Tausen

Location number and name	Coordinates		Elevation		Morphol.	Exposition	Reference to
	N	W	Low	Heigh	Code		figure in text
2HP01020 Navaranaq Gletscher	82°40'	48°25'	0	–	164112	NW	2, 3
2HQ01020 n.n.	82°32'	39°52'	0	1200	364312	NW	2, 3
2HQ02004 n.n.	82°29'	40°05'	0	1200	364210	W	2, 3
2HQ02007 n.n.	82°27'	39°00'	0	1250	364112	W	2, 3
2HQ02025 n.n.	82°12'	39°07'	550	750	633112	E	2, 7
2HQ02030 n.n.	82°14'	39°38'	650	750	633112	SW	2, 7
2HQ02031 Adams Gletscher	82°10'	39°49'	0	–	164114	N	2, 3, 5, 7, 8
2HQ02034 Henson Gletscher	82°16'	40°51'	20	–	163114	E	2, 3, 5, 8
2HW01016 n.n.	82°52'	41°11'	250	1350	523112	N	2, 3
2HX0l00S n.n.	82°54'	39°04'	50	1150	533114	W	2, 3
2HX01014Tjalfe Gl.	82°46'	38°19'	0	1350	324116	W	2, 3, 6
2HX01015 n.n.	82°44'	37°53'	100	1350	362216	NW	2, 3, 6
2HX01025 n.n.	82°39'	38°48'	10	1150	301213	N	2, 3, 6
2HX01029 Lurgletscher	82°39'	39°43'	50?	1200	323213	NE	2, 3, 6
2HY01025 n.n.	82°58'	39°00'	0	900	524110	N	2, 3
2KG01002 Hare Gl.	82°50'	36°27'	110	1250	323113	NE	2
2KH01013 n.n.	82°43'	35°32'	0	1250	362213	W	2, 3
2KH01030 n.n.	82°31'	36°53'	10?	1300	366116	NE	2, 3
2KH01034 Ymer Gl.	82°39'	36°54'	0?	1300	366110	NE	2, 3
2KJ01007 n.n.	82°55'	33°00'	300	1800	233112	N	3
2KJ01008 n.n.	82°54'	33°12'	200	1800	233112	N	3
2KJ03012 n.n.	82°48'	34°37'	100	1400	362212	E	3
2KJ03016 n.n.	82°51'	34°45'	200	1500	363212	E	3
2KK04021 Balder Gl	82°54'	31°45'	0	1500	364112	N	3, 9
2LB04011 Hobbs Gl.	81°49'	36°30'	150?	–	166113	NE	3
2LB04007 Marie Sophie Gletscher	81°40'	35°00'	0	–	164113	E	3
2LB04032 Elefantfoden	82°00'	33°30'	200	1200	361313	NW	3
2LB05008 Skjoldet	82°02'	33°00'	180	1200	361313	NW	3
2LB05016 n.n.	82°02'	35°58'	490	1051	362113	N	3
2LB05030Astrup Bræ	82°04'	38°34'	300	–	166113	N	2, 3, 7, 10
2LB05033 n.n.	82°07'	39°36'	300	–	166113	E	2, 3, 7
2LB05035a n.n.	82°14'	38°22'	480	1200	363112	SE	2, 3, 7, 10
2LB05035b n.n.	82°13'	38°21'	550	740	630112	E	2, 7, 10

2LB05035a: Main glacier

2LB05035b: Cirque glacier, now isolated from main glacier.

Table 2. Glacier activity – Central Peary Land.

Iskappe, and further south to the regions around inner Independence Fjord.

The map of Fig. 3 only reflects the distribution of a "neoglacial" formation, representing the maximum extension of the "Steensby stade" of Kelly & Bennike (1992), i.e. the culmination of the readvances of the local glaciers after the Holocene climatic optimum. This culmination is, by analogy with neighbouring areas, believed to have taken place at the end of the Little Ice Age, i.e. around A.D. 1900.

The borders of ice showing no recession in Fig. 3 mark a nearly stationary ice margin. The stability is in places documented by aerial photographs from 1938 to 1978, which show that the pre-

	Digit 1 Primary classification	Digit 2 Form	Digit 3 Frontal characteristics	Digit 4 Longitudinal profile	Digit 5 Major source of nourishment	Digit 6 Activity of tongue
0	uncertain or miscellaneous	uncertain or miscellaneous	uncertain or miscellaneous	uncertain	normal or miscellaneous	uncertain or miscellaneous
1	continental ice sheet	compound basin	piedmont	even, regular	snow and/or drift snow	marked retreat
2	ice field	compound basin	expanded foot	hanging	avalanche ice and/ or snow	slight retreat
3	ice cap	simple basin	lobed	cascading	superimposed ice	stationary
4		cirque	calving in sea	ice-fall		slight advance
5	valley glacier	niche	calving in sea grounded	interrupted		marked advance
6	mountain glacier	outlet	calving in lake			possible surge
7	glacieret and snow field	ice apron	confluent			known surge
8	ice-shelf	group				
9	rock glacier	remnant				

Table 3. Explanation of the morphology code of the glaciers.

sent ice margin here is stable and not a product of a 20th century maximum re-advance.

In the areas of recent glacier recession, minor variations occur. For the Inland Ice margin outlets reaching to near sea level, e.g. 2HQ02031 and 2HQ02034, Figs 3 and 8, a clear recession seems mainly to have occurred in the first half of the 20th century, followed by a minor readvance in the second half of the century. This development is known from other outlets of the Inland Ice in North and North-East Greenland (cf. Fig. 8). The recessional period may be related to warm spells with break-up of the fjord ice (e.g. Higgins 1989), and a correlation between glacial retreat and decrease in precipitation between 1920 and the 1950s (Diamond 1956) is suggested by Davies & Krinsley (1962). A decrease in precipitation during the past century is also suggested by the Hans Tausen ice corings (Reeh 1995).

The outlets of local glaciers , mainly from ice caps and ice fields, show for some lower and near-fjord lobes a minor recession during this century, whereas the inland areas situated close to the glaciation limit are dominated by stationary outlets (cf. Fig. 3). The thinning was locally initiated before 1938, to be followed by a slow-down (2KK04021), stationary (2LB04032) or readvancing (2HX01005) periods.

A downwasting of minor glaciers such as cirque glaciers, and presumably also some larger features such as ice caps, must be considered to have occurred throughout the 20th century. However, the net retreat and possibly also the thinning of the glaciers, is by the smallest amount so far encountered in Greenland.

Concluding Remarks

The assessment of Davies & Krinsley (1962) that most glacier margins in central Peary Land are extremely stable, also holds true for the situation in 1978. The apparant stability of glaciers approaches the conditions of Antarctic glaciers in the "Dry valleys" of Victoria Land (Chinn 1988), where it is precipitation changes rather than temperature

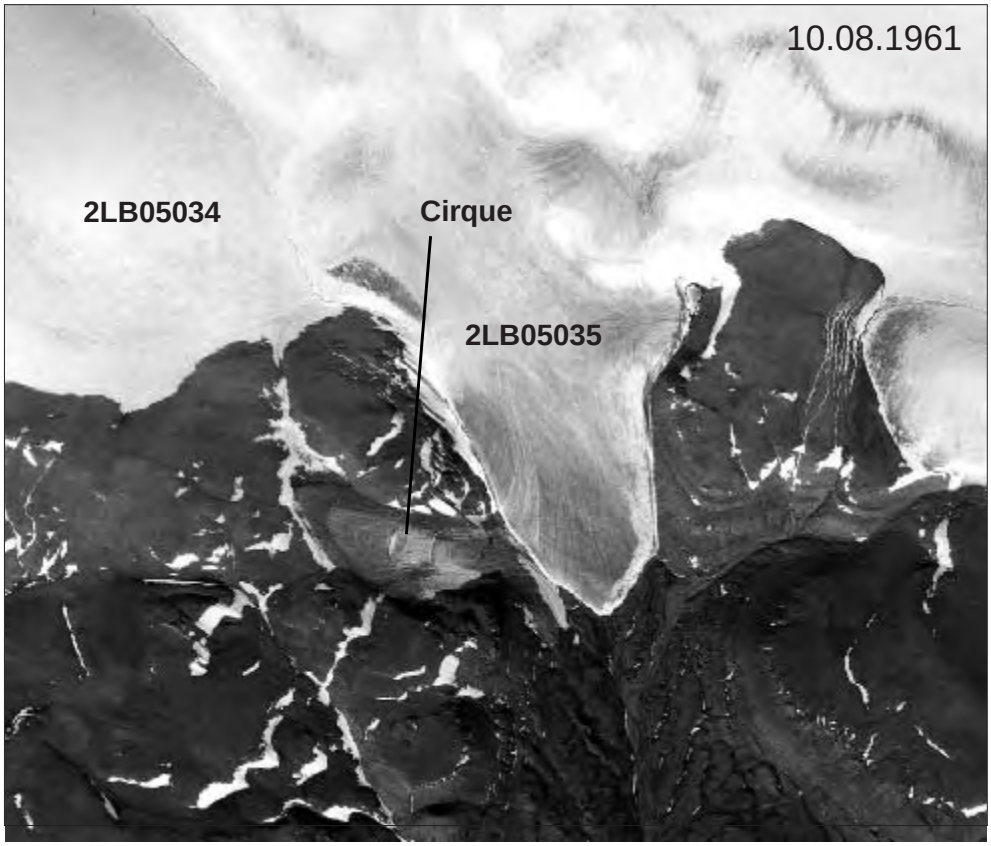

Fig. 10.
Top: South side of Hans Tausen Iskappe with the outlet of 2LB05035 and the adjoining cirque. On the far side of the lake Aftenstjernesø, the floating outlet of 2LB05030 (Astrup Bræ) can be seen. Photograph, KMS route 547M-V, no. 10403 of July 15th 1950.
Bottom: Outlet 2LB05035 and the adjoining cirque on August 10th 1961. Photograph, KMS route 256K no. 827. Both photographs copyright: Kort- og Matrikelstyrelsen.

changes that control the glacier changes; mean annual temperatures here are under –20°C.

The apparent stability of many central Peary Land glaciers may therefore be related to the thermal englacial and subglacial conditions such as freezing to the subsurface, low movement, i.e. low turn-over rate of the glacier mass. A partial control of glacier fluctuations by precipitation should also be considered, which again leads back to the question of the relationship of precipitation to fjord conditions, periodically ice-free and penodically semi-permanently ice covered during the arctic summer. The question is as to whether the ice-free fjords imply increased precipitation and accumulation on glaciers which might rule out the impact of higher temperature and ablation.

The record of net thinning of present ice caps and cirques points to a marginal, vertical downwasting rather than a horizontal recession (e.g. Reeh *et al.* 2001). Downwasting was also an important process during the Holocene deglaciation of North Greenland, as witnessed by extensive occurrences of dead ice terrain according to the descriptions of Kelly & Bennike (1992).

The largest fluctuations in Peary Land, as elsewhere in Greenland, are exhibited by the large calving outlets from the Inland Ice to the heads of the fjords (cf. Figs 5, 8). The high arctic NFG-mode (saw-tooth formed protruding fronts) is today a pronounced feature for most North Greenland Inland Ice outlets, and must be taken as a criterion for a semi-permanent ice cover of the interior fjord systems during most of the 20th century. Exceptions to this are the "normal" calving fronts (DJG-mode) from the large ice cap outlets into Frederick E. Hyde Fjord and the Inland Ice outlets (Academy Gletscher and Marie Sophie Gletscher) at the head of Independence Fjord. Since the NFG-mode again appears further south in East Greenland (in Hagen Fjord and Niog-halvfjerdsfjorden), these exceptions may be connected to oceanic circulation in these fjords related to the polynya off Northeast Greenland (e.g. Hjort 1997).

That oceanic circulation also played an important role for the onset and spread of the Holocene deglaciation in North and North-East Greenland can also be seen from the rate of recession of the Inland Ice outlets through the fjords. Attainment to the present positions was reached as early as 8-9 cal. ka B.P. in the larger fjords (local example: Independence Fjord, e.g. Bennike 1987) whereas it was reached later in narrow fjords as in the case of J.P. Koch Fjord near Hans Tausen Iskappe, where it was reached at about 6 cal. ka B.P.; this is also approximately the time of the isolation of this ice cap from the Inland Ice proper by the deglaciation of the valley Wandel Dal and the lake Aftenstjernesø (Fig. 10). The recession of Adams Gletscher in J.P. Koch Fjord continued beyond the present extent, and this retracted situation may have continued until the Little Ice Age (cf. Landvik *et al*. 2001), after which the glacier readvanced to its maximum at about A.D. 1900. Fluctuations in the 20th century are given in Fig 8.

The climatic deterioration occurred in a step-like fashion (Funder & Abrahamsen 1988; Bay & Fredskild 1997; Hjort 1997) and the occurrence of driftwood from 6.6 to 2.6 cal. ka B.P. (Landvik *et al*. 2001) indicates that the climate was periodically warmer than now more than 2600 years ago. The question as to whether ice-free fjords could contribute to increased snow accumulation in the surrounding highlands is still open.

The fluctuations of the local glaciers and of the Inland Ice can only in a very generalised way reflect the climatic development. The major recession from a neoglacial maximum in the first part of the 20th century and the quasi-stability or minor fluctuations in the last half of the century reflect the major tempera-

ture developments in the region, as also preserved in the Hans Tausen ice core record. A closer evaluation of this temperature record may contribute to an evaluation of periods of ice-free fjords as given by Reeh *et al.* (1999).

Acknowledgements

This paper is essentially based on archive studies of published and unpublished material relating to the Holocene and Neoglacial of Peary Land. In this context the present Hans Tausen Iskappe Project initiated this work and supported publication of the results. The help of the Nordic Environmental Research Programme 1993-1997 is greatly appreciated.

The work has benefited from discussions with colleagues at the Survey (O. Bennike, C.E. Bøggild, O.B. Olesen, H.H. Thomsen, W. Starzer), the Danish Technical University (N. Reeh) and the University Courses on Svalbard (J. Landvik) and also by the comments of two unknown referees to the manuscript. Last but not least, thanks are due to A.K. Higgins for help in editing the final manuscript and suggesting improvements to the English of the text.

References

Bay, C. and B. Fredskild 1997. Present and past vegetation in the high arctic, easternmost North Greenland and the relation to the Northeast Water Polynya. *Journal of Marine Systems* 10: 35-39.

Bengaard, H. J. and N. Henriksen 1984. *Geological map of Greenland 1:500 000, sheet 8, Peary Land*. Copenhagen: Geological Survey of Greenland.

Bennike, O. 1987: *Quaternary geology and biology of the Jørgen Brønlund Fjord area, North Greenland*. Meddelelser om Grønland, Geoscience 18, 23 pp.

Cailleux, A. and D. Lagarec 1977. Nombre, Surface et Volume des Glaciers du Globe. *Studia Geologica Polonica* 52: 83-96.

Chinn, T. J. 1988: The "Dry Valleys" of Victoria Land. In: Williams, R.S. and J. G. Ferrigno (editors). *Satellite Image Atlas of Glaciers of the World. Antarctica.* United States Geological Survey, Professional Paper 1386-B: 39-41.

Davies, W. E. 1972. *Landscape of Northern Greenland.* Cold Regions Research and Engineering Laboratory, Special Report 164, 67 pp.

Davies, W. E. and D. B. Krinsley 1962. *The recent Regimen of the Ice Cap margin in North Greenland*. U.G.G.I. International Association of Scientific Hydrology, Publication 58: 119-130.

Diamond, N. 1956. *Precipitation trends during the past 30 years.* Snow, Ice and Permafrost Research Establishment, U.S.Army. Research Report. 22, 4 pp.

Fristrup, B. 1961: Climatological Studies of Some High Arctic Stations in North Greenland. *Folia Geographica Danica* 9: 67-78.

Funder, S. and N. Abrahamsen 1988. Palynology in a polar desert, eastern North Greenland. *Boreas* 17: 195-207.

Goldthwait, R.P. 1961. Regimen of an Ice Cliff on Land in Northwest Greenland. *Folia Geographica Danica* 9. 107-115.

Goldthwait, R.P. 1971. *Restudy of Red Rock ice cliff, Nunatarssuaq, Greenland.* Cold Regions Research and Engineering Laboratory. Technical Report 224, 27 pp.

Hammer, C. U. and H. H. Thomsen 1998. Fælles nordisk indsats – tæt på verdens top. Geologi – *Nyt fra GEUS* 2: 2-14.

Higgins, A. K. 1989. North Greenland ice islands. *Polar Record* 25: 207-212.

Higgins, A. K. 1991. North Greenland glacier velocities and calf ice production. *Polarforschung* 60(1): 1-23, 1990 (issued 1991).

Hjort, C. 1997. Glaciation, climate history, changing marine levels and the evolution of the Northeast Water Polynya. *Journal of Marine Systems* 10: 25-33.

Hooke, R. le B. 1970. Morphology of the ice-sheet margin near Thule, Greenland. *Journal of Glaciology* 9 (57): 303-324.

Høy, Th. 1970. *Surveying and mapping in southern Peary Land, North Greenland.* Meddelelser om Grønland 182(3), 50 pp.

Kelly, N. 1980. *The status on the Neoglacial in Western Greenland. Rapport* Grønlands Geologiske Undersøgelse 96: 24 pp.

Kelly, N. and O. Bennike 1992. *Quaternary geology of western and central North Green-*

land. Rapport, Grønlands Geologiske Undersøgelse 153: 34 pp.

Koch, L. 1928. Contributions to the Glaciology of North Greenland. Meddelelser om Grønland 65(2), pp. 161-464.

Koch, L. 1940. *Survey of North Greenland*. Meddelelser om Grønland 130(1), 364 pp.

Landvik, J., Weidick, A. and A. Hansen 2001. The last glaciation of Peary Land, North Greenland, as seen from the glacial history of the Hans Tausen Ice Cap. Meddelelser om Grønland Geoscience, this volume, pp. 27-44.

Langway, C.C. 1961. Accumulation and temperature on the inland ice of North Greenland, 1959. *Journal of Glaciology* 3 (30): 1017-1044.

Müller, F., T. Caflisch and G. Müller 1977. *Instructions for Compilation and Assemblage of Data for a World Glacier Inventory.* International Commission for Snow and Ice, Department of Geography, Eidgenössische Technische Hochschule, Zürich: 28 pp. + appendix.

Nobles, L. H. 1961. Structure of the Ice Cap Margin, Northwestern Greenland. *Folia Geographica Danica* 9: 188-204.

Ohmura, A. and N. Reeh 1991. New precipitation and accumulation maps for Greenland. *Journal of Glaciology* 37 (125): 140-148.

Reeh, N. 1995 (co-ordinator). *Report on activities and results 1993-1995 for Hans Tausen Ice Cap Project – Glacier and Climate Change Research.* Report to the Nordic Minister Council. 52 pp.

Reeh, N. and O. B. Olesen 1986. Velocity measurements on Daugaard-Jensen Gletscher, Scoresby Sund, East Greenland. *Annals of Glaciology* 8: 146-150.

Reeh, N., C. Mayer, H. Miller, H. H. Thomsen and A. Weidick 1999. Present and past climate control on fjord glaciations in Greenland: Implications for IRD-deposition in the sea. *Geophysical Research Letters* 26(8): 1039-1042.

Reeh, N., O. B. Olesen, H. H. Thomsen, W. Starzer and C. E. Bøggild 2001. Mass Balance parameterization for Hans Tausen Iskappe, Peary Land, eastern North Greenland. Meddelelser om Grønland Geoscience, this volume, pp. 57-69.

Weidick, A. 1995. Greenland. In: Williams, R.S. & Ferrigno, J.G. (editors). *Satellite Image Atlas of Glaciers of the World, Greenland*. United States Geological Survey, Professional Paper 1386-C: 141 pp.

Weidick, A., C. B. Bøggild and N. T. Knudsen 1992. *Glacier inventory and atlas of West Greenland*. Rapport, Grønlands geologiske Undersøgelse 158: 194 pp.

The glacial history of the Hans Tausen Iskappe and the last glaciation of Peary Land, North Greenland

By Jon Y. Landvik, Anker Weidick and Anette Hansen

Abstract

Jon Y. Landvik, Anker Weidick and Anette Hansen 2001. The glacial history of the Hans Tausen Iskappe and the last glaciation of Peary Land, North Greenland. Meddelelser om Grønland, Geoscience 39, Copenhagen, pp. 27-44.

Studies of glacial geology near the Hans Tausen Iskappe, 82°N, suggest that the Greenland Ice Sheet covered Peary Land during the Late Weichselian. The ice sheet experienced successive marginal retreat due to calving along the major fjords, and an extensive thinning in response to the climatic amelioration during the early Holocene. Local ice caps had melted by ca. 8100 cal years ago, a result which is compatible with the studies of an ice core record from the Hans Tausen Iskappe. The present ice caps are thus not relicts from the Weichselian, but have formed during the Holocene. Findings of 5000-6000 year-old driftwood along fjords that connect to the Arctic Ocean indicate that the perennial sea-ice cover was gone during the mid-Holocene.

Keywords: Greenland; glacial history; ice caps; Weichselian; Holocene; climate.

Jon Y. Landvik, The University Courses on Svalbard (UNIS), P.O. Box 156, N-9171 Longyearbyen, Norway (Present address: Agricultural University of Norway, Department of Soil and Water Sciences, P.O. Box 5028, N-1432 Ås, Norway.

Anker Weidick, Geological Survey of Denmark and Greenland (GEUS), Thoravej 8, DK-2000 Copenhagen NV, Denmark.

Anette Hansen, COWI, Thulebakken 34, DK-9000 Aalborg, Denmark.

Introduction

During recent decades, investigations of the Quaternary history of the land areas surrounding the North Atlantic have demonstrated a close coupling between the oceanic conditions and terrestrial climate. The Greenland ice core studies as well as stratigraphic studies (Johnsen *et al.* 1992, Dansgaard *et al.* 1993) in the ice-free areas of Greenland and Svalbard (Funder *et al.* 1998, Mangerud *et al.* 1998) have shown a correlation with the paleoceanographic records of the North Atlantic (Bond *et al.* 1993). Even though our present understanding of the climatic interaction between the North Atlantic and the adjacent land areas has increased, more needs to be learned about the parts of the Arctic that are closer to sources of moisture such as the Arctic Ocean.

This study is a part of the Hans Tausen Iskappe project which was designed to investigate the present and

Fig. 1. Location map.

past climate and glacier dynamics of North Greenland by means of ice-core records (Hammer *et al.* 2001), mass balance studies and the local glacial history on a geologic time scale (this paper).

The research strategy for the geological investigations has been to search for stratigraphic and geomorphologic evidence for fluctuations in volume and extent of the Hans Tausen Iskappe. The northern and northwestern margins of the ice cap were considered as most suitable for new field investigations. In this area, the outlet glacier and associated deposits can be found below the Holocene marine limits. Due to this interaction with Late Quaternary fjord environments, marine fossils enable radiocarbon age control on glacial fluctuations. The paper will also review and discuss previous investigations and unpublished observations from the southern margin of the ice cap and the major fjords systems such as Independence Fjord and J. P. Koch Fjord (Fig. 1).

Methods

The new field studies were based on air photo interpretations succeeded by field investigations in three selected areas, supported by helicopter reconnaissance during camp moves.

The geographic sample positions were determined by use of a GPS receiver, using the WGS-84 datum. Altimetry was

Sample	Lab ref.	Location	Co-ordinates	Elevation	Material	^{14}C Reservoir corrected	Conventional ^{14}C age	Calibrated age	Remarks
Northern margin:									
GGU 417602	T-11769	Nordpasset E	82°53.7'N 36°09.2'W	32	Mt	7260±55	7810±55	8120	In growth position above till.
GGU 417611	T-11773	Nordpasset E	82°54.9'N 36°23.4'W	37	Mt	7245±95	7795±95	8100	Growth position in marine sed.
GGU 417601	T-11768	Nordpasset E	82°53.8'N 36°08.6'W	49	Ha, Mt	7085±95	7635±95	7930	On delta surface
GGU 417609	T-11772	Nordpasset E	82°54.7'N 36°10.5'W	43	Ha, Mt	6910±140	7460±140	7750	Raised shoreline
GGU 417606	T-11771	Nordpasset E	82°54.0'N 36°11.1'W	18	Ha	6450±120	7000±120	7370	Frozen up on delta front
GGU 417605	T-11770	Nordpasset E	82°53.7'N 36°09.1'W	24	*Picea* sp.	–	5855±50	6710 or 6670	
GGU 417620	T-11776	Nordpasset W	82°58.0'N 37°41.3'W	28	Shell frag.	6945±140	7495±140	7790	In redeposited silt.
GGU 417621	TUa-1079	Nordpasset W	82°58.2'N 37°43.9'W	29	Ha	6680±70	7230±70	7560	AMS-date of single valve
GGU 417612	T-11774	Kap Bopa	82°59.4'N 39°40.1'W	33	Ha, Mt	7140±85	7690±85	7970	
GGU 417614	T-11775	Kap Bopa	82°59.4'N 36°40.6'W	13	*Larix?*	-	5470±100	6280	
GGU 417613	TUa-1078	Kap Bopa	82°59.3'N 39°40.2'W	46	Shell frag.	36,870± 605	36,980±605		
Southwestern margin:									
GGU 226451	I-9664	E. of J.P. Koch Fj.	82°24'N 40°30'W	30-35	Shells	5550±110	5700±105	6350	Weidick (1977)
GGU 226450	Ua-4586	E. of J.P. Koch Fj.	82°17'N 39°55'W	Ca 25	Ha	5085±60	5635±60	5880	
GGU 226451	Ua-4587	E of J.P. Koch Fj.	82°16'20''N 39°59'W	30-36	Ha	5480±80	6030±80	6280	
GGU 215308	GSC-2279	Adams Gletcher	82°21.2'N 40°51'W	2-3	Shells	4040±150	4590±140	4590	Weidick (1977)
GGU 215308	I-9130	Adams Gletcher	82°21.2'N 40°51'W		Twigs	-	220		Weidick (1977)

Table 1. Radiocarbon dates from the Hans Tausen Iskappe area. The conventional radiocarbon age has been normalised to $\delta^{13}C = -25$ ‰. The dates from Weidick (1977) have been normalised by the authors. All dates on marine material have been corrected for a reservoir age effect of –550 yrs (Funder 1982). A recent survey suggests that the reservoir age could be up to 760 yrs. in North Greenland (Rasmussen & Rahbek). Prefixes TUa- and Ua- are AMS-dates. Calibration to calendar years is obtained using the CALIB programme (Stuiver & Reimer 1993). Ha = Hiatella arctica, Mt = Mya truncata.

carried out through parallel use of two electronic altimeters, and readings were corrected for air pressure changes during the day. The elevations refer to the high tide mark. The tidal range in the area appeared to be small, and in Jørgen Brønlund Fjord (Fig. 1) it is reported to be only 20-30 cm (Høy 1970).

For comparison with the ice core record, all radiocarbon ages (Table 1) have been converted to calendar years according the calibration data-sets by

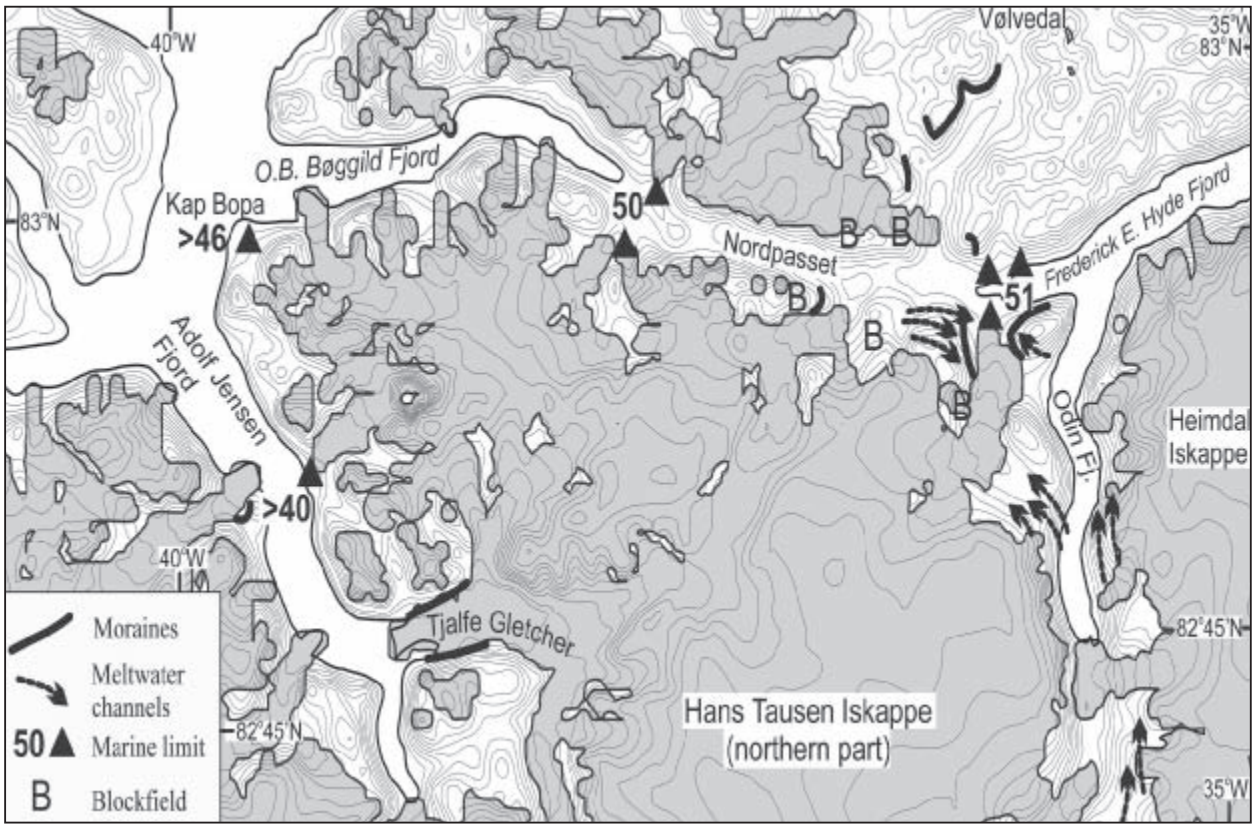

Fig. 2. The glacial geology along the northern margins of Hans Tausen Iskappe and Nordpasset. Moraines and meltwater channels have been mapped in the field. Black triangles: deltas; numerals: elevation of marine limit in metres. The map is extracted from a digital terrain model constructed by Wolfgang Starzer, GEUS.

Stuiver *et al*. (1998a) and Stuiver *et al*. (1998b) using the CALIB 4.1 calibration programme (Stuiver & Reimer 1993).

Physiography

Hans Tausen Iskappe is the second largest ice cap in North Greenland, covering an area of 4208 km^2. It is not only one of the northernmost ice caps in the world, but also one of the few that is located close to the Arctic Ocean. Most of the present day ice cap has an elevation exceeding 1000 m a.s.l. Its southern parts rest on a 800-900 m high plateau, whereas the northern part of the ice cap sits on more rugged bedrock (Reeh 1995, Reeh *et al*. 2001). To the south, the Wandel Dal valley, connecting J. P. Koch Fjord to the west with Independence Fjord to the east, separates the ice cap from the Greenland Ice Sheet. The southern margin of the ice cap (Fig. 1) terminates on dry land at ca. 500 m a.s.l. To the north, however, outlet glaciers reach elevations of ca 100 m a.s.l. in Nordpasset and terminate as tidewater glaciers at the head of Adolf Jensen Fjord to the north-west (Fig. 2).

Nordpasset is a 2-3 km-wide and 25 km long u-shaped, probably glacially eroded valley that connects Frederick E. Hyde Fjord to O.B. Bøggild Fjord. The central part of the pass is 150-200 m a.s.l. and mountains to the north and south reach elevations up to 800 m a.s.l. (Fig. 2). Rock glaciers are developed along the mountain slopes in the central part of the valley, and the valley floor is characterised by vigorous periglacial activity and cryoturbation of the Quaternary deposits. Outlet glaciers from the Hans Tausen Iskappe reach Nordpasset in its eastern parts.

The bedrock of North Greenland is dominated by Late Precambrian to Palaeozoic sedimentary rocks that become successively younger towards

the north. They are generally found in east-west trending zones related to the formation of the North Greenland fold belt in the Devonian/Early Carboniferous (Henriksen 1992). The Greenland Ice Sheet probably covers the crystalline basement. The finding of erratics of high-grade metamorphic and plutonic origin along the north coast of Peary Land points to sources under the present ice sheet (Dawes 1986).

The present glaciation limit rises from ca. 200 m along the coast to ca. 800 m a.s.l. in the Hans Tausen Iskappe area (Weidick 2001).

The North Side of Hans Tausen Iskappe

The studies along the northern margin of the Hans Tausen Iskappe were based on air photo interpretation and helicopter reconnaissance, supported by field work in both ends of Nordpasset, and at Kap Bopa where O.B. Bøggild Fjord and Adolf Jensen Fjord meet (Fig. 2). The observations will be discussed from east to west.

Odin Fjord

Odin Fjord cuts the eastern part of the Hans Tausen plateau (Fig. 2). Its southern part is filled by two outlets from the surrounding ice caps: a northern outlet from the Heimdal Iskappe east of Odin Fjord (2KH01013 in Weidick 2001), and a southern outlet called Ymer Gletcher from the Hans Tausen Iskappe west of the fjord (2KH01034 in Weidick 2001). The rims of the plateau on both sides of Odin Fjord and Ymer Gletcher are ca. 600 m a.s.l. These plateaus, particularly east of the fjord, are all characterised by glacial and glaciofluvial sediments and a series of well-developed lateral meltwater channels that were formed by water draining towards the north. The vertical distribution of these channels suggests erosion along the margin of a successively lower fjord glacier in Odin Fjord. A suite of channels drain an over 500 m-high pass towards the northwest, which are today cross-cut by the north-eastward outlet of the Hans Tausen Iskappe (Fig. 2). This relationship shows that the ice cap was less extensive at the time when the meltwater channels were formed.

Eastern Nordpasset

The eastern part of Nordpasset is a key area for the reconstruction of the glacial history of the Hans Tausen Iskappe. The lower parts of the mountain slopes are generally covered by a diamicton of glacial origin. However, they have been subject to extensive downslope movement by solifluction and only a few distinct moraine ridges are found above the marine limit (Fig. 2). Large glaciofluvial deltas, partly covered with beach sediments, are found in front of major meltwater pathways, whereas cryoturbated pebbly silt deposits, interpreted to be of glaciomarine and littoral origin, cover the valley floor below the marine limit.

As for the Odin Fjord area, the eastern part of Nordpasset shows evidence of downwasting of a former glacier. Three sets of geomorphological features are important for the interpretation of the glacial history: a) glacial meltwater channels; b) moraine ridges; c) glaciofluvial deltas.

Meltwater channels

Two transects of the southern slope of Nordpasset were studied in detail. The area between ca. 900 and 600 m a.s.l. is dominated by blocks and a silty matrix derived from weathering of the underlying siltstone. Patches of sub-rounded gravel are found locally in the blockfield. In a horizontal zone at 600 m a.s.l., no blocks are found and only *in situ* weathered bedrock is exposed, probably due to removal of the blocks by glacial

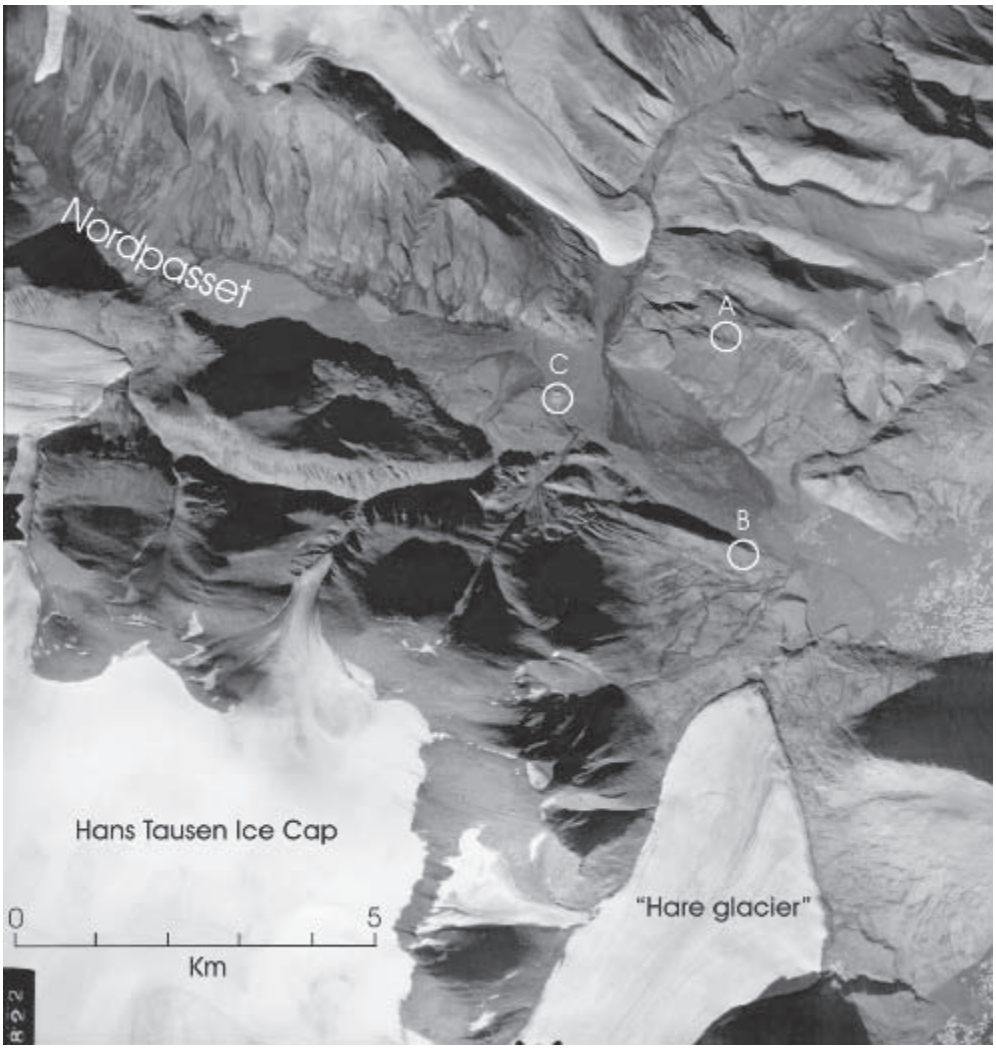

Fig. 3. Vertical air photo of the eastern part of Nordpasset. Localities discussed in the text are marked A to C. Aerial photograph 255K 822, July 1960. Copyright: Kort- og Matrikelstyrelsen, Copenhagen.

meltwater. Below this level, there is a series of distinct ice marginal features, predominately meltwater channels cut into bedrock at successively lower altitudes (Figs. 2 and 3). Several of the channels are 20-30 m deep, dip towards the east, and begin and end in open air (Fig. 4). Their formation requires that meltwater from a valley glacier in Nordpasset turned into ice marginal drainage before it re-entered the glacier either supra- or subglacially.

Moraines

Evidence that a thick glacier filled Nordpasset is also found on the steep northern side of the valley. On a ledge 405 m a.s.l. (Fig. 3, A), there is a ca. 50 m-long moraine ridge comprised of a diamicton with subrounded to rounded boulders in a silty sandy matrix. The ridge has a sharp crest and a fresh-looking appearance (Fig. 5). The lobate shape indicates deposition from a glacier flowing eastwards through Nordpasset, compatible with the dip of the meltwater channels on the south side.

A set of more continuous moraine ridges formed during a later stage of the Nordpasset glacier can be found below ca. 300 m a.s.l. At the eastern end of Nordpasset, a 14 km-long valley connects to the wide east-west running Vølvedal valley to the north. On the western slope of the connecting valley, a

Fig. 4. One of the meltwater channels in the southern slope of Nordpasset.

moraine ridge with declining elevation to the north can be mapped over a distance of 6 to 8 km (Fig. 2). The elevation of the moraine is >600 m a.s.l. in the southern part of the valley, and the northward dip of the moraine shows that it was deposited from a glacier that once filled Nordpasset. The slopes and valley floor below the moraines are characterised by glacial and glaciofluvial deposits.

Another set of moraine ridges is found south of Harebugt at the head of Frederick E. Hyde Fjord. A moraine lobe deposited from the 200 m-high pass between Odin Fjord and Nordpasset crosscuts the lowermost meltwater channels discussed above (Fig. 2). As we infer that no ice existed on the Hans Tausen plateau at his time, it shows that an outlet glacier from Odin Fjord entered the eastern part of Nordpasset during a late stage of the last deglaciation.

Glacial erratics (Fig. 6) are found at

Fig. 5. Moraine ridge on a ledge 450 m a.s.l. on northern side of Nordpasset.

Fig. 6. Erratic boulders 470 m a.s.l. on the mountains south of Nordpasset.

several elevations on the mountains surrounding Nordpasset. The lithologies have not been traced to their area of origin, but the erratics demonstrate the overriding by a glacier prior to the formation of the meltwater channels.

Raised deltas and the marine limit

The marine limit in the area was formed during the last deglaciation. In eastern Nordpasset it can be determined by the elevation of three glaciofluvial deltas (Figs. 2 and 3). The largest one is located 1 km north of the present snout of the outlet from Hans Tausen Iskappe (informally named Hare Glacier by Reeh *et al.* 2001, 2KG01002 by Weidick 2001). The delta surface is ca. 1000 m wide, has its apex close to the present meltwater river from the glacier, and slopes gently with a distinct break towards the delta front. The raised delta is cut by the present river that forms a large modern delta at sea level (Figs. 2 and 3). The distal break of the delta plain is 49 m a.s.l. which is assumed to have formed a few metres below sea level during deposition. Shell fragments of *Hiatella arctica* and *Mya truncata* that were brought to the surface by cryoturbation at the outer part of the delta plain were radiocarbon dated to 7085±95 BP (7930 cal. yrs. BP, T-11768). In a 5 m-high section in the delta front, glaciomarine silty sand is observed above a diamicton interpreted as till. Shells of *Mya truncata* in living position 1.75 m above the diamicton were dated to 7260±55 BP (8120 cal. yrs. BP, T-11769).

A series of raised shorelines where the uppermost beach deposit was hand-leveled to 51 m a.s.l. is found ca 1000 m north-west of the delta (Fig. 3, B). The beach sediments are overrun in places by solifluction deposits suggesting that they represent a minimum estimate for the elevation of the marine limit. When compared to the elevation of the delta plain, however, 51 m seems to be a fair determination of the marine limit in the area. The uppermost occurrence of shell fragments in the beach sediments at 43 m a.s.l is dated to 6910±140 BP (7750 cal. yrs. BP, T-11772).

On the north side of the valley are two smaller raised deltas (Fig. 2). The western one has a steeper fan-delta like surface with a front break at 41 m a.s.l., whereas the eastern one is built up to 50 m a.s.l. Shells brought to the surface by

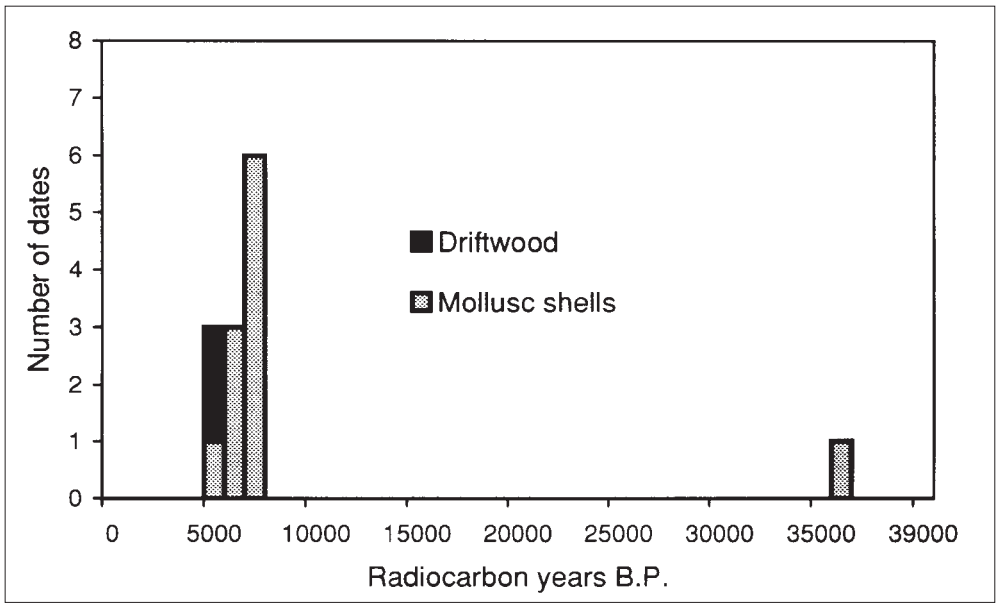

Fig. 7. Distribution of new radiocarbon dates from the Hans Tausen Iskappe area.

cryoturbation in the latter delta front were dated to 6450±120 BP (7370 cal. yrs. BP, T-11771).

Below the marine limit, the valley slopes and floor are covered predominately by solifluction deposits, which comprise a mixture of marine fine-grained sediments, beach gravel and diamicton. In the centre of the valley (Fig. 3, C) there is a mound of marine silt. Redeposited sediments mantle most of the deposit, and the 20 cm-thick active layer only melts the outer part of this mantle. However, the appearance of larger clasts in the lower part of the slopes suggests that the silt deposit is stratigraphically underlain by a diamicton. At the surface, ca. 3 m above the top of the diamicton, numerous valves of *Mya truncata* were found in living position and dated to 7245±95 BP (8100 cal. yrs. BP, T-11773).

Inner Frederick E. Hyde Fjord

As discussed above, the marine limit in western and eastern Nordpasset is 50 and 51 m a.s.l., formed at ca 6900 and 7200 BP (7800 and 8100 cal. yrs. BP), respectively (Fig. 7).

A glaciofluvial delta at the mouth of Vølvedal (83°00′N 34°10′W) is related to the deglaciation of both Vølvedal and Frederick E. Hyde Fjord, and was deposited during a sea level of 53 m a.s.l. However, the exact age of this deposit is not known. A similar height of 55 m a.s.l. was reported by Bennike (1983) from a kame delta at the entrance to the Vølvedal valley. Along the northwestern margin of the Hans Tausen Iskappe, mapping of the marine limit along the eastern coast of Adolf Jensen Fjord gave estimates of >46 m a.s.l.

The drop in the marine limit from 53 m a.s.l. in Frederick E. Hyde Fjord to 51 m in eastern Nordpasset may indicate a slightly earlier deglaciation of the fjord basin, probably due to calving of the glacier. This is also supported by the dip of the moraines from Nordpasset into Vølvedal (see below), which also suggests a deglaciation of the Vølvedal/Fredrick E. Hyde Fjord valley prior to the final deglaciation of Nordpasset.

Western Nordpasset

Areas below the marine limit are also found in the westernmost 5 km or so of Nordpasset, at the head of O.B. Bøggild Fjord (Fig. 2). The morphology of the

glacial deposits is not as well expressed as in the eastern part of the valley, partly due to disturbance by cryogenic processes.

A large raised delta is found at the mouth of a tributary valley entering Nordpasset from the north. The delta is ca. 1 km wide, and reaches halfway into Nordpasset. To the west, it is dissected by river erosion, and terraces are formed at different levels. All terrace surfaces are dissected by up to 1 m-deep ice-wedge polygons. The frontal part of the uppermost terrace surface is slightly offset by a series of front-parallel faults, and the elevation on the ice-proximal side of the innermost fault is 50 m a.s.l. Paired *Hiatella arctica* and *Mya truncata* were found in sediments on the delta front, and a single valve of *Hiatella* was radiocarbon dated to 6680±70 BP (7560 cal. yrs. BP, TUa-1079).

A slightly higher minimum age for the deglaciation is recorded from the southern side of the valley, where shell fragments in a silt subjected to solifluction were dated to 6945±140 BP (7790 cal. yrs. BP, T-11776).

Three km from the coast, a fan delta deposited from Nordpasset sits in the middle of the valley. The lowermost mapable river channels on the fan surface were found at 55 m, an elevation which is compatible with a marine limit of 50 m a.s.l., as discussed above.

Valleys north of Nordpasset

An air photo study and helicopter reconnaissance of the Vølvedal and Nornegæst Dal valleys were carried out in order to track the northward distribution of the glacial deposits mapped in Nordpasset. The moraines and associated glacial sediments that were mapped in the valley connecting Nordpasset and Vølvedal (see above) continue over the 400 m-high pass into Vølvedal. The valley floor of the inner part of Vølvedal is 200-300 m a.s.l. and characterised by thick glacial and glaciofluvial deposits dissected by meltwater channels. Several large meltwater channels are also cut into bedrock, and there has been a stage of meltwater overflow from Nordpasset into Vølvedal over a pass ca. 600 m a.s.l.

Also in Nornegæst Dal north of Vølvedal, a similar distribution of sediments is found. Here, the glacial and glaciofluvial sediments cover the valley floor and continue up along the slopes. However, the upper limits of glacial sediments or any marginal moraines could not be determined during our reconnaissance. Outlet glaciers from Roosevelt Fjelde apparently overrun the glacial deposits along the northern side of the valley. Several large meltwater channels and kame terraces, especially along the southern side of Nornegæst Dal and Frigg Fjord, show that considerable meltwater drainage entered Frederick E. Hyde Fjord through the Frigg Fjord tributary during the last deglaciation.

The South Side of Hans Tausen Iskappe

The present information on the Holocene deglaciation of the region from J.P. Koch Fjord to Independence Fjord is illustrated in the map of Fig. 8. The simplified trend lines are based on detailed mapping of recessional ice marginal features such as moraines, meltwater channels, etc., by W. Davies (in GEUS files, unpublished). A more comprehensive account of these maps is given by Weidick & Dawes (1999). The trend lines indicate a deglaciation pattern in which rapid deglaciation along Independence Fjord and the lowland along Jørgen Brønlund Fjord and Wandel Dal resulted in ice remains over the land areas presently covered by Hans Tausen Iskappe and Heinrich Wild Iskappe.

The chronology of this recessional pattern is fragmentary. In the J. P. Koch Fjord basin, the recession of the Green-

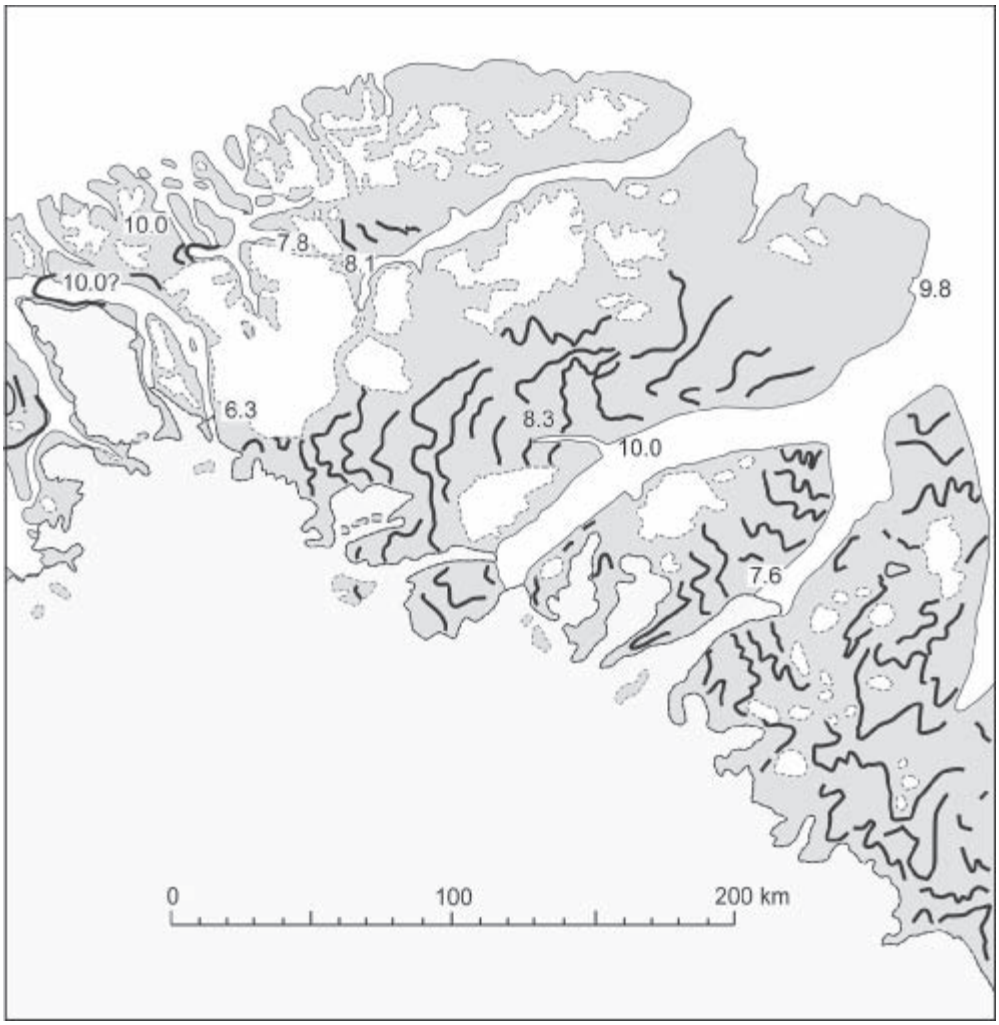

Fig. 8. Trend lines of early and mid-Holocene deglaciation simplified from morphological maps of North Greenland made by W. Davies, U.S. Geological Survey (Weidick & Dawes 1999). The maps are not published, but can be found in the files of GEUS. The age of deglaciation expressed in cal. yrs. BP.

land Ice Sheet margin is not well dated. The Warming Land stade, represented by moraines in the central part of J. P. Koch Fjord (Fig. 8), were assumed by Kelly & Bennike (1992) to date from 9500-8000 BP (ca 11,200-8900 cal. yrs BP). West of this fjord, in Wulff Land, Warming Land and Nyeboe Land, this recession was related to extensive downwasting of the ice, resulting in the formation of dead ice terrain at these localities (Kelly & Bennike 1992). We also know that the ice retreat in Independence Fjord had reached the mouth of the tributary Jørgen Brønlund Fjord by 8000 BP (ca. 8900 cal. yrs. BP)(Bennike 1987).

Inner J.P. Koch Fjord

Extensive deposits of Holocene age are located around the head of J. P. Koch Fjord and in the east-west trending valley between the fjord head (terminus of Adam Gletcher, an outlet of the Greenland Ice Sheet) and the outlets of the Hans Tausen Iskappe. Marine terraces are found up to the marine limit, estimated to be ca. 42 m a.s.l.

During fieldwork in 1976, shells were collected from silt in a terrace 30-36 m a.s.l. The silt is overlain by gravel that can be mapped up to the marine limit of ca. 42 m a.s.l. The shells yielded ages of 5550±105 BP (6350 cal. yrs. BP, I-9664) and 5480±80 (6280 cal. yrs. BP, Ua- 4587)

(Table 1). Shells embedded in fine-grained sand and laminated silt in a slightly lower terrace, 1.5 km downstream, were dated to 5085±60 BP (5880cal. yrs. BP, Ua-4586) (Table 1), whereas shells and twigs from the outermost silty neoglacial moraines of Adams Gletcher were dated to 4040±150 BP (4590 cal. yrs. BP, GSC-2279) and 220 BP (I-9130).

These dates from the southwestern margin of the Hans Tausen Iskappe suggest that the ice cover was close to or less than present prior to 5500 BP (6300 cal. yrs. BP), and that the Adams Gletcher had a readvance to its present position some time during the last 300 years, i.e. at the end of the Little Ice Age.

Independence Fjord

A reconstruction of the marine limit distribution in Northern Greenland has emerged from the increasing number of field observations in recent decades (Funder & Hjort 1980, Bennike 1987, Kelly & Bennike 1992, see also compilation by Funder & Hansen 1996). Relative sea-level curves (Fig. 9) for the inner part of Independence Fjord have been supplied from Jørgen Brønlund Fjord and from the mouth of the fjord at Kap København and Prinsesse Ingeborg Halvø, respectively (Funder & Abrahamsen 1988).

For the outer part of Independence Fjord, a marine limit of 65-100 m a.s.l. was determined by Funder & Hjort (1980). Based on the shoreline diagram (Fig. 10), the initial deglaciation of the area probably took place at about 9000 BP (10,200 cal. yrs. BP), which complies with earlier age estimates of an ice margin in the area at 9000-10,000 yrs. BP (10,200-11,500 cal. yrs. BP).

Based on the relative sea level curve (Fig. 9) and a marine limit of 80 m a.s.l. (Bennike 1987), we assume that the deglaciation of Independence Fjord reached Jørgen Brønlund Fjord by 8000 BP (8900 cal. yrs. BP), and about 7500 BP (8350 cal. yrs. BP) at the head of Jørgen Brønlund Fjord. This is somewhat younger than the age of 9500 ± 500 cal. yrs. BP as suggested by Bennike (1987).

The emergence curve for the inner part of the Independence Fjord shows that the relative sea level reached present level around 1000 years ago. The information is based on a Thule eskimo

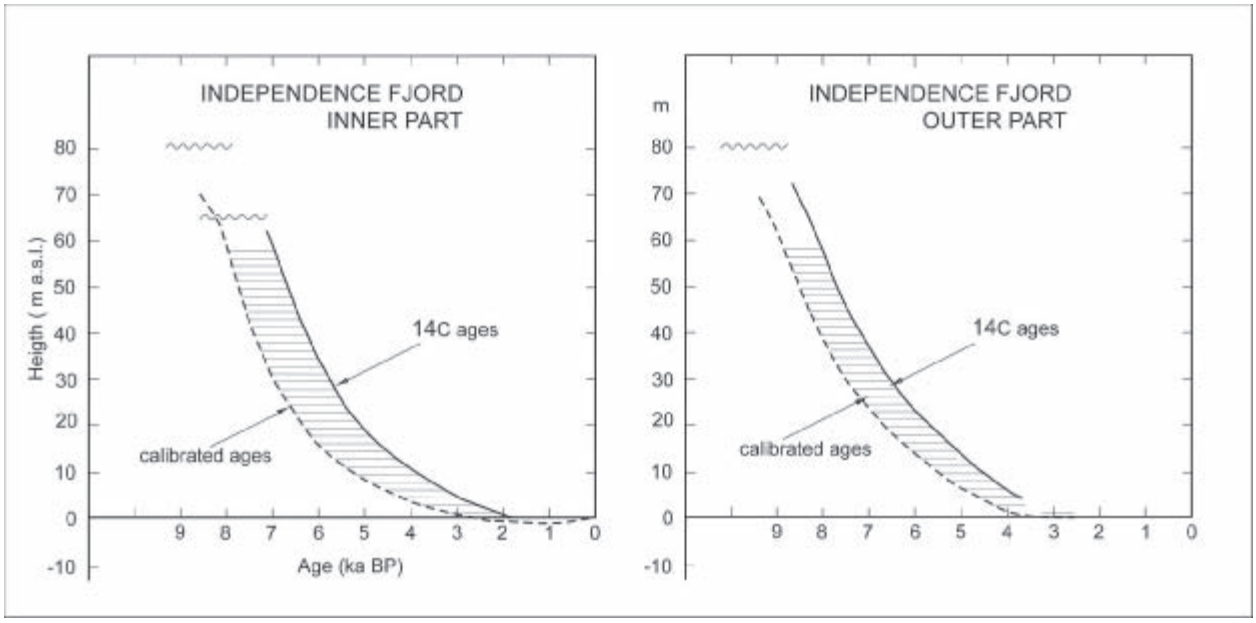

Fig. 9. Emergence curves of inner and outer part of Independence Fjord. Inner part covers the region around Jørgen Brønlund Fjord, the outer part the region around the mouth of Independence Fjord between Kap København and Prinsesse Ingeborg Halvø (see Fig. 10). Curves drawn by full lines are based on compilation of ^{14}C-datings, for the interior region by Bennike (1987) and for the outer region by Funder & Abrahamsen (1988). The broken lines are emergence curves based on calendar years.

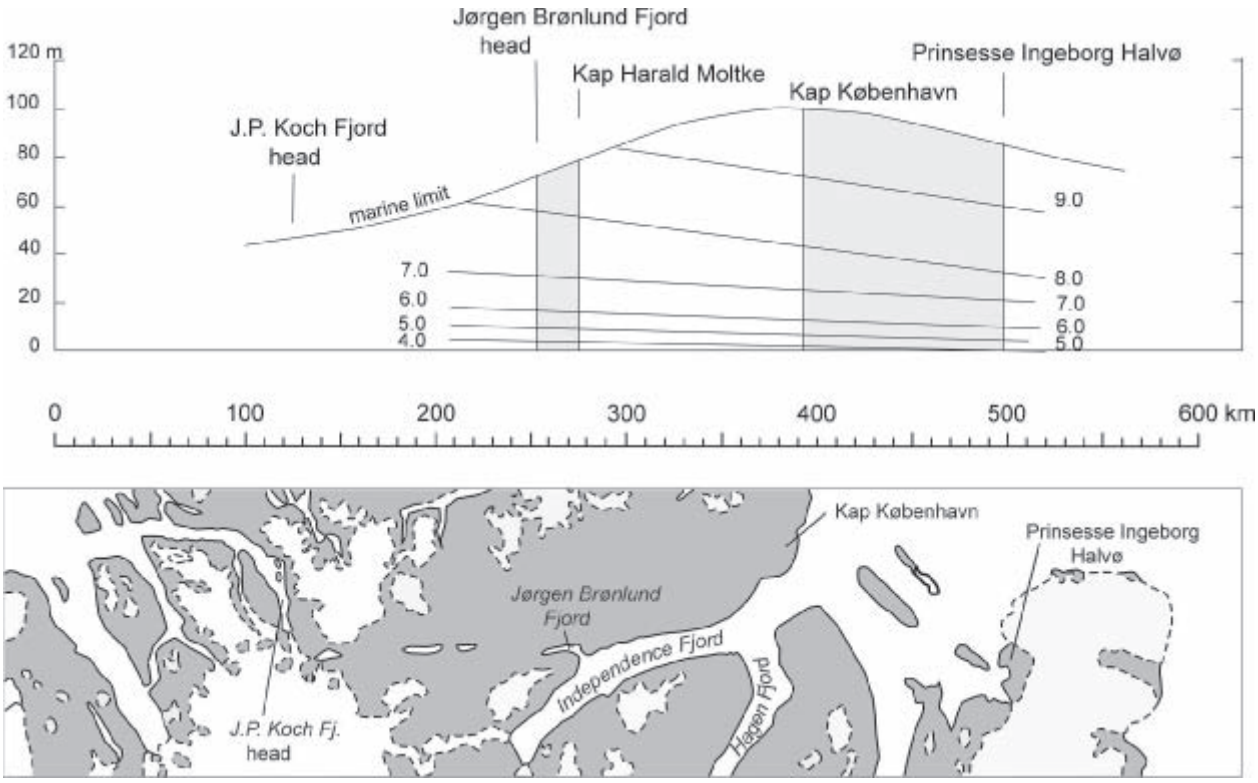

Fig. 10. Simplified outline of the marine limit and the conceptual trends of strandlines in a profile from the head of J.P. Koch Fjord in the west to the mouth of Independence Fjord in the east. Large figures: Estimated time for deglaciation expressed in calibrated ka BP. Hatched areas of the curves: areas covered by the two emergence curves of Fig. 9.

ruin on the south coast of Jørgen Brønlund Fjord which is transgressed by the sea (Bennike 1987). The emergence curves of the outer Independence Fjord do not extend to this period. However, drowned Thule culture ruins from this region (Kronprins Christian Land) were also reported by Hjort (1997). In both cases the sea level related to the Thule culture is only slightly (1 m or so) under the present one.

The calendar ages of the emergence curves of Fig. 9 are applied in the construction of the conceptual equidistant shoreline diagram along Independence Fjord (Fig. 10). A shoreline dip towards the outer coast can be seen, even if the gradient of the highest shorelines (8000 to 9000 cal. yrs BP) is only ca 10 cm/km. This is significantly lower than the 50 cm/km of a 9400 cal. yrs BP shoreline at Germania Land 600 km further to the south (Landvik 1994, Weidick *et al.* 1996). However, this could be an artifact due to limited control of the exact direction of the isobases in the area. The relatively low marine limits close to the Hans Tausen Iskappe indicate a late local deglaciation compared to the middle and outer parts of Independence Fjord.

Glacial History of the Hans Tausen Iskappe – Discussion

The extent of the last ice sheet

Our studies in Nordpasset show that an ice sheet that also filled adjacent fjords and valleys during the last glaciation inundated the 900-1000 m high bedrock plateau, which is covered by the northern dome of the Hans Tausen Iskappe. There is also strong evidence for a confluence between this ice sheet and the Greenland Ice Sheet to the south. Evidence for such a continuous ice cover during the Late Weichselian has also been found in the Jørgen Brønlund Fjord area, at the eastern end of the

Wandel Dal ice-free corridor, by Bennike (1987). He showed that outlets from both the Greenland Ice Sheet and a "Peary Land ice cap" reached Independence Fjord through the Wandel Dal, and that there was a halt in ice recession at the mouth of Jørgen Brønlund Fjord ca. 9000 to 7600 BP. Such an easterly ice flow in Jørgen Brønlund Fjord is not possible without a full confluence between the Late Weichselian Greenland Ice Sheet and the ice over the Hans Tausen plateau.

The extensive glaciofluvial deposits in the large valleys north of Nordpasset suggest further confluence with ice over the mountains of northern Peary Land (namely, Johannes V. Jensen Land). Weidick (1976) pointed out that only a slight depression of the present glaciation limit would lead to the formation of an ice cap over Peary Land. As reviewed by Funder & Hansen (1996), there are still large uncertainties whether large ice shelves existed along the coast of Peary Land (Funder & Larsen 1982, Dawes 1986), or only restricted piedmont glaciers reached the western parts of the coastline.

The last deglaciation

Northern margin of Hans Tausen Iskappe

The successive lowering of the glacier surface in Nordpasset shows that the whole ice mass must have experienced large surface melting during the deglaciation. Even the highest areas were brought under the equilibrium line due to the climatic amelioration. Such a style of deglaciation over the area implies that the whole Hans Tausen plateau must have been ice-free before the formation of the ice marginal features we have reported from Odin Fjord and Nordpasset. The higher ground, including the Hans Tausen plateau, must have been deglaciated prior to ca. 7200 BP (8100 cal. yrs. BP), as indicated by the deglaciation dates in eastern Nordpasset.

The consequence of this deglaciation model is that the present-day Hans Tausen Iskappe formed after 8100 cal. yrs. BP as a result of an equilibrium line lowering during the Middle or Late Holocene. This conclusion is supported by the results of the ice core from the ice cap. The age estimates of the 345 m-long core suggests that the entire ice cap formed after 3500-4000 years BP (Hammer *et al*. 2001).

The margins of several outlet glaciers along the northern margins of the Hans Tausen Iskappe were studied in order to reconstruct any Late Holocene glacier fluctuations. There are fresh-looking moraine ridges in close contact with the glacier snout. In front of most of the outlet glaciers there is a clear morphological contrast between these ridges and the old landscape which lacks pronounced moraine ridges. This maximum position in the area was generally reached ca AD1900, with a subsequent recession or still-stand (Weidick 2001). The morphological contrast and lack of older moraine ridges suggest that the present glacier margins were at their outermost position during the whole Holocene. The terminal moraines of two outlet glaciers from the northern dome, the one in eastern Nordpasset and in Tjalfe Gletcher at the head of Adolf Jensen Fjord, were visited in 1994. Despite a thorough search for radiocarbon-datable material, neither of the advances to the present day position could be dated.

The southern margin and the Independence Fjord basin

The onset of the Holocene ice retreat in the area between the Hans Tausen Iskappe and the Greenland Ice Sheet cannot be settled exactly. With allowance for the preceding readvances of

the Warming Land stade (Kelly & Bennike 1992) in North Greenland (around J. P. Koch Fjord) and the dated events of Independence Fjord, the retreat might be ascribed to around 9000 BP (10,200 cal. yrs. BP)(Bennike 1987). The ice margin retreat must have occurred as a fast break-up due to calving in the fjords. This is supported by the annual recession rate of 100 m/year or more that we have calculated in Independence Fjord, which contrasts with only 50 m/year in the narrower Jørgen Brønlund Fjord. Here, as elsewhere, topographic conditions (sills, narrowings of the fjords) might have caused halts of the recession through the fjords (cf. Mercer 1961). However, with exception of the 85 m-deep Jørgen Brønlund Fjord (Høy 1970), the bathymetry of the North Greenland fjords is unknown.

The approximate rate of ice recession over the land area can be calculated from the deglaciation of Jørgen Brønlund Fjord, i.e. 50 m/year. This is similar to a recession rate of 47 m/year over Germania Land further south (Weidick *et al.* 1996). The recession to the present extent of most larger ice caps in the area north of Independence Fjord then would have taken 1-2 ka.

The fast recession of the outlet glaciers occurred at the same time as the first openings in the permanent fjord ice cover (see below) which is probably related to the early Holocene temperature increase of the surface waters in the Greenland Sea (Koç *et al.* 1993, Koç & Jansen 1994). During this change, the glaciers presumably shifted their frontal characteristics to a "temperate mode". The recession rates were dependent on fjord width and calving rate. We conclude that the ice in the larger fjords (e.g., Independence Fjord) attained its present position at about 8000-9000 cal. yrs. BP, whereas this was reached at about 6300 cal. yrs. BP in the narrower fjord systems such as J. P. Koch Fjord.

Here, the ice recession to a position behind the present margin occurred shortly before 5600 BP (6350 cal. yrs. BP). This development is comparable to other dated sites in North Greenland. Reworked shells in the present moraines are dated to 5000 BP (5700 cal. yrs. BP) at C.H. Ostenfeldt Gletscher, ca. 100 km WSW of Adams Gletscher, and to 4700 BP (5400 cal. yrs. BP) at Steensby Gletscher, nearly 250 km WSW of Adams Gletscher at 12 km behind its front (Kelly & Bennike 1992). Similar evidence is obtained from the Inland Ice outlet Nioghalvfjerdsfjorden Gletscher at 79(N in Northeast Greenland. The fjord was deglaciated to 80 km behind its present front shortly after 8000 cal. yrs. BP and became glacier-filled to its present extent after ca 4500 cal. yrs. BP (Bennike & Weidick 1999).

As shown by our studies from Hans Tausen Iskappe, the glacier recession in the fjords occurred at the same time as surface ablation and thinning of the ice cap. It must be presumed that the apparently thin ice caps such as Storm Iskappe and Chr. Erichsen Iskappe, as well as those to the south of Independence Fjord, disappeared. The trend lines of the deglaciation around these ice caps are cross-cut by the present ice cap margins (Fig. 8), which indicates a substantial regrowth of the ice caps after the initial deglaciation of the region. Some of the largest ice caps (e.g., Hans Tausen, Nordkronen, Heinrich Wild) conceal a subglacial alpine topography, covered by several hundred metres of glacier ice, as shown for the Hans Tausen Iskappe.

Post-Glacial Climate

The fjords in this part of north Greenland today experience a semi-permanent sea-ice cover where the fjord ice melts only at rare intervals (>30 years)(Higgins 1990). The finding of driftwood both at the eastern end of Nordpasset and Kap Bopa (Table 1) shows that the fjords were seasonally ice-free 5850-5500

BP (6700-6300 cal. yrs. BP). The two driftwood samples have been identified as either *Picea* sp. or *Larix* sp., but could not be identified to species level due to poor preservation (L.M. Paulssen, written comm. 1995). Thus, their geographical growth area could not be determined.

There are several reports of driftwood from North Greenland. From the Jørgen Brønlund Fjord area, Bennike (1987) compiled radiocarbon dates from different sources, including 17 samples of wood, both driftwood and charcoal. These dates cover a time-span from 5900 to 2500 BP (6600-2550 cal. yrs. BP), which is in agreement with our dates showing that the fjords were seasonally free from fjord ice shortly after 6000 BP. Several pieces of driftwood below the 2500 BP date at 6 m a.s.l. (Bennike 1987) suggest that predominantly seasonally open conditions prevailed until at least 1000-1500 BP, when sea-level dropped below present (Fig. 9). However, there seems to be a contrast in sea-ice survival between the fjords facing the Arctic Ocean, as discussed by Higgins (1990), and the fjords facing the northern Fram Strait, such as Independence Fjord and the tributary Jørgen Brønlund Fjord.

Hjort (1997) suggested ice-free fjords during the early and mid-Holocene warming in Northeast Greenland, followed by intermittent periods of ice-covered and ice-free fjords during the subsequent neoglacial climate decline after ca. 5700 cal. yrs. BP. It is unknown to what degree such periods of ice-free fjords increased the regional precipitation, especially in summer months, but its importance for the acceleration of calving from outlet glaciers is substantiated by the descriptions by Higgins (1989, 1990).

The vegetation records give some other constraints on the Holocene climatic optimum in North Greenland. In a study of the vegetation history from Klaresø on the south coast of Jørgen Brønlund Fjord, Fredskild (1969, 1973) showed that the period from 5000 to 3300 BP (5700 to 3500 cal. yrs. BP) was characterised by richer vegetation than today, probably caused by enhanced precipitation due to locally open fjords. Distinct drops in the local sedimentation rate and pollen influx occurred at 3300 BP (3500 cal. yrs. BP) and 2100 BP (2100 cal. yrs. BP). A slightly earlier transition to colder summers at 3900 BP (4400 cal. yrs. BP) was concluded for lake Sommersø close to Station Nord (Funder & Abrahamsen 1988). The fact that this lake has a more oceanic setting than the lake in the Jørgen Brønlund Fjord area suggests that a cooling of regional significance occurred, as is also suggested by Funder & Abrahamsen (1988).

These intervals also coincide with the interpretation of the ice core records from the Hans Tausen Iskappe, which suggests that the build-up of the ice cap started after ca. 3500-4000 cal. yrs. BP, probably as a response to increased precipitation during summer (Hammer *et al.* 2001).

The period of ice-free conditions in the fjords also encompasses the date range of the paleo-eskimo cultures in Peary Land. They have been dated to 4400-4000 BP (4900-4500 cal. yrs. BP) (Independence I) and 2800-2400 BP (2900-2400 cal. yrs BP) (Independence II) (Knuth 1984, Andreasen 1996). The end of Independence II occurs at the same time as the driftwood stranding ceased in the fjord region.

Conclusions

The plateau covered by the Hans Tausen Iskappe, and adjacent areas, were fully glaciated during the last glaciation (Late Weichselian).

The ice cap was probably confluent with the Greenland Ice Sheet to the south, and with ice caps over northern Peary Land to the north.

The last deglaciation occurred as a

downwasting of the ice sheet and ice caps, combined with a rapid recession by calving along the large fjords, leaving the Hans Tausen plateau ice-free by 7200 BP (8100 calendar years BP).

There was a rapid ice recession along the large Independence Fjord, which was essentially completed by 9000 cal. yrs. BP.

Dates of driftwood show that the presently sea-ice covered fjords were seasonally ice-free during the Mid-Holocene (6800-2500 cal. yrs. BP). This correlates with the presence of the paleo-eskimo cultures in North Greenland.

Acknowledgements

The investigations were funded by *The Nordic Environmental Research Programme 1993-1997* of the *Nordic Council of Ministers*. Fieldwork in 1994 was supported by the North Greenland expedition of the Geological Survey of Greenland. Platinova A/S and BGR, Hannover, also kindly provided additional helicopter transport in the field. The manuscript has benefited from critical reviews by Ole Bennike and Arthur S. Dyke.

References

Andreasen C. 1996. A survey of paleo-eskimo sites in northern Eastgreenland. In: B. Grønnow (ed). *The paleo-eskimo cultures of Greenland. New perspectives in Greenlandic archaeology.* Copenhagen, Danish Polar Center, pp. 177-189.

Bennike, O. 1983. Paleoecological investigations of a Holocene peat deposit from Vølvedal, Peary Land, North Greenland. *Grønlands Geologiske Undersøgelse Rapport* 115: 15-20.

Bennike, O. 1987. *Quaternary geology and biology of the Jørgen Brønlund Fjord area, North Greenland*. Meddelelser om Grønland, Geoscience 18, 23 pp.

Bennike, O. and A. Weidick 1999. Observations on the Quaternary geology around Nioghalvfjerdsfjorden, eastern North Greenland. *Geology of Greenland Survey Bulletin* 183: 57-60.

Bond, G., W. S. Broecker, S. Johnsen, J. Mcmanus, L. Labeyrie, J. Jouzel and G. Bonani 1993. Correlations Between Climate Records from North Atlantic Sediments and Greenland Ice. *Nature* 365: 143-147.

Dansgaard, W., S. J. Johnsen, H. B. Clausen, D. Dahl Jensen, N. S. Gundestrup, C. U. Hammer, C. S. Hvidberg, J. P. Steffensen, A. E. Sveinbjørnsdóttir, J. Jouzel and G. Bond 1993. Evidence for General Instability of Past Climate from a 250- kyr Ice-Core Record. *Nature* 364: 218-220.

Dawes, P. R. 1986. Glacial erratics on the Arctic Ocean margin of North Greenland: implications for an extensive ice-shelf. *Geological Society of Denmark Bulletin* 35: 59-69.

Fredskild, B. 1969. A postglacial standard pollen diagram from Peary Land, North Greenland. *Pollen et Spores* 11: 573-583.

Fredskild, B. 1973. *Studies in the vegetational history of Greenland. Palaeobotanical investigations of some Holocene lake and bog deposits.* Meddelelser om Grønland 198: 1-245.

Funder, S. 1982. ^{14}C-dating of samples collected during the 1979 expedition to North Greenland. *Grønlands Geologiske Undersøgelse Rapport* 110: 9-14.

Funder, S. and N. Abrahamsen 1988. Palynology in a polar desert, eastern North Greenland. *Boreas* 17: 195-207.

Funder, S. and L. Hansen 1996. The Greenland ice sheet – a model for its culmination and decay during and after the last glacial maximum. *Geological Society of Denmark Bulletin* 42: 137-152.

Funder, S. and C. Hjort 1980. A reconnaissance of the Quaternary geology of eastern north Greenland. *Grønlands Geologiske Undersøgelse Rapport* 99: 99-105.

Funder, S., C. Hjort, J. Y. Landvik, S. I. Nam, N. Reeh and R. Stein 1998. History of a stable ice margin – Greenland during the Middle and Upper Pleistocene. *Quaternary Science Reviews* 17: 77-123.

Funder, S. and O. Larsen 1982. Implications of volcanic erratics in Quaternary deposits of North Greenland. *Geological Society of Denmark Bulletin* 31: 57-61.

Hammer, C. U. , S. J. Johnsen, H. B. Clausen, D. Dahl-Jensen, N. Gundestrup and J. P. Steffensen 2001. The paleoclimatic record

from a 345 m long ice core from the Hans Tausen Ice Cap. *Meddelelser om Grønland, Geoscience* 39: 87-95.

Henriksen N. 1992. *Geological map of Greenland 1:500,000. Nyeboe Land sheet 7 and Peary Land sheet 8. Descriptive text.* Grønlands Geologiske Undersøgelse, Copenhagen: 40 pp.

Higgins, A. K. 1989. North Greenland ice islands. *Polar Record* 25: 207-212.

Higgins, A. K. 1990. North Greenland glacier velocities and calf ice production. *Polarforschung* 60: 1-23.

Hjort, C. 1997. Glaciation, climate history, changing marine levels and the evolution of the Northeast Water Polynya. *Journal of Marine Systems* 10: 23-33.

Høy, T. 1970. *Surveying and mapping in southern Peary Land, North Greenland.* Meddelelser om Grønland 182: 1-50.

Johnsen, S. J., H. B. Clausen, W. Dansgaard, K. Fuhrer, N. Gundestrup, C. U. Hammer, P. Iversen, J. Jouzel, B. Stauffer and J. P. Steffensen 1992. Irregular glacial interstadials recorded in a new Greenland ice core. *Nature* 359: 311-313.

Kelly, M. and O. Bennike 1992. Quaternary geology of western and central North Greenland. *Grønlands Geologiske Undersøgelse Rapport* 153: 1-34.

Knuth E. 1984. *Reports from the Musk-ox Way. A compilation of previously published articles with the insertion of some new illustrations and with a slightly altered radiocarbon dating list.* Copenhagen.

Koç, N. and E. Jansen 1994. Response of the high-latitude northern hemisphere to orbital climate forcing – evidence from the Nordic Seas. *Geology* 22: 523-526.

Koç, N., Jansen, E. and H. Haflidason 1993. Paleoceanographic Reconstructions of Surface Ocean Conditions in the Greenland, Iceland and Norwegian Seas Through the Last 14-KA Based on Diatoms. *Quaternary Science Reviews* 12: 115-140.

Landvik, J. Y. 1994. The last glaciation of Germania Land and adjacent areas, northeast Greenland. *Journal of Quaternary Science* 9: 81-92.

Mangerud, J., T. M. Dokken, D. Hebbeln, B. Heggen, Ó. Ingólfsson, J. Y. Landvik, V. Mejdahl, J. I. Svendsen and T. O. Vorren 1998. Fluctuations of the Svalbard-Barents Sea Ice Sheet the last 150,000 years. *Quaternary Science Reviews* 17: 11-42.

Mercer, J. 1961. The estimation of the regimen and former firn limit of a glacier. *Journal of Glaciology* 3: 1053-1062.

Rasmussen K. L. and U. Rahbek 1996. The ^{14}C reservoir effect in Greenland. In: B. Grønnow (ed). *The paleo-eskimo cultures of Greenland. New perspectives in Greenlandic archaeology.* 237-242. Danish Polar Center, Copenhagen.

Reeh N. 1995. *Hans Tavsen Ice Cap Project – Glacier and Climate Change Research, North Greenland.* Report. Geological Survey of Denmark and Greenland, Copenhagen. 1-52.

Reeh, N., O. Olesen, H. H. Thomsen, W. Starzer and C. E. Bøggild 2001. Mass balance paramerization for Hans Tausen Iskappe, Peary Land, eastern North Greenland. *Meddelelser om Grønland, Geoscience* 39: 57-69.

Stuiver, M. & Reimer, P. 1993. Extended ^{14}C data base and revised Calib 3.0 ^{14}C age calibration program. *Radiocarbon* 35: 215-230.

Stuiver, M., P. J. Reimer, E. Bard, J. W. Beck, G. S. Burr, K. A. Hughen, B. Kromer, G. McCormac, J. van der Plicht and M. Spurk 1998a. INTCAL98 radiocarbon age calibration, 24,000-0 cal BP. *Radiocarbon* 40: 1041-1083.

Stuiver, M., P. J. Reimer and T. F. Braziunas 1998b. High-precision radiocarbon age calibration for terrestrial and marine samples. *Radiocarbon* 40: 1127-1151.

Weidick, A. 1976. Glaciations of Northern Greenland – New evidence. *Polarforschung* 46: 26-33.

Weidick, A. 1977. C14 dating of Survey material carried out in 1976. *Grønlands Geologiske Undersøgelse Rapport* 127-129.

Weidick, A. . Neoglacial glaciations around Hans Tausen Iskappe, Peary Land, North Greenland. *Meddelelser om Grønland, Geoscience* 39: 5-26.

Weidick, A. *et al*. 1996. Neoglacial glacier changes around Storstrømmen, North-East Greenland. *Polarforschung* 64: 95-108.

Weidick, A. and P. R. Dawes 1999. W.E. Davies, hans arbejde i Nordgrønland og hans systematiske kortlægning af de istidsgeologiske aflejringer. *Tidsskriftet Grønland* 7-8 1999: 270-282.

Digital elevation models of the Hans Tausen ice cap

By Wolfgang Starzer and Niels Reeh

Abstract

Starzer, W. and N. Reeh 2001. Digital elevation models of the Hans Tausen ice cap. Copenhagen, Danish Polar Center. Meddelelser om Grønland Geoscience 39, pp. 45-56.

In the field seasons from 1993 to 1995 several data set describing glacier surface and thickness have been collected at the Hans Tausen Ice Cap in Peary Land, North Greenland. This is the description of how this geophysical data have been used in order to produce digital elevation models for both the surface and the bedrock topography of the area. The two models are consequently used to construct a digital ice thickness model of the Hans Tausen Ice Cap. Based on this model, calculated estimates for both the surface area and the total glacier volume are computed.

Keywords: Digital elevation model; bedrock topography; ice thickness; ice-dynamic modelling and interpolation.

Wolfgang Starzer, Geological Survey of Denmark and Greenland, Thoravej 8, DK-2400 Copenhagen NV, Denmark.

Niels Reeh, Danish Centre for Remote Sensing, Dept. of Electromagnetic Systems B. 348, Technical University of Denmark, DK-2800 Lyngby, Denmark.

Introduction

This paper describes the construction of digital elevation models, DEMs, of the Hans Tausen ice cap and surrounding areas. Three DEMs are built for (1) surface elevation, (2) subglacial/bedrock topography and (3) ice thickness. These DEMs will be used as input for ice-dynamic modelling. In the following sections the different data sources used for the compilation of the DEMs are described, geographical and technical decisions are explained and the compilation of each of the three maps is discussed in detail (the words DEM, map and grid refer to the same concept).

Data sources

The different data sources used in the compilation of the maps of surface and subglacial topography include:

1. Surface topography data from photogrammetric mapping based on aerial photographs from 1978. These data are produced at the photogrammetric laboratory of the Geological Survey of Denmark and Greenland, and represent the largest and most important single data source (Fig. 1).
2. Surface elevation and ice-thickness data obtained by airborne radar survey in 1993 over the central higher part of the ice cap (Hammer, 1995).

3. Surface elevation and ice-thickness data obtained by two ground radar surveys, one on the central dome around the drill site (Jonsson, 1994) and one covering a glacier basin in the north-eastern part of the ice cap (Jonsson, 1995).
4. Finally, where no other information was available, surface elevation data from a digital elevation model covering entire Greenland were used. This elevation model was produced by the National Survey and Cadastre of Denmark (Ekholm, 1996).

Method

The DEM for the ice thickness is constructed by subtracting the grid for the subglacial topography from the grid for surface elevation. The DEMs for subglacial topography and surface elevation were constructed from the four original data sets above by using a gridding method. Gridding is the process of using original data points/observations in an XYZ data file to generate interpolated data points on a regularly spaced grid. If extra observation points exist, then their number is reduced to create a firm input file for the interpolation. This file has an even distribution of data points over the total area, and an observation density that is roughly similar to the point density of the resulting grid. The resulting grid was used to generate a contour map.

Different interpolation routines have been tested and Kriging has proven to be the most useful geostatical gridding method for the construction of the DEMs. Kriging produces visually appealing contour and surface plots from irregularly spaced data. The method is developed to express trends that are suggested in the source data. For example, high points might be connected along a ridge, rather than in isolated bulls-eye type contours. Nevertheless, in locations where the interpolation result were not satisfactory, the data source had to be improved by additional data points. It is explained later how these extra points, for both the surface and the subglacial maps, are found.

The three maps of the Hans Tausen ice cap are based on a grid of UTM coordinates. The area is located in UTM zone 23 and stretches from the coordinates 535000 to 640000 from west to east and the coordinates 9120000 to 9230000 from south to north. Thus, the total size of the grid is 105 by 110 kilometres. An optimal grid resolution of 500*500 metres was found, taking into account the distribution of the original data and the characteristics of the interpolation method. Accordingly, the DEMs are defined by a grid of 46,631 data points, laid out by 211 columns by 221 rows.

Surface elevation map

The main data source for the compilation of the surface elevation map is data from photogrammetric mapping. These data are divided into five groups: two specify elevation contours in 100 meter steps on glacier and land, and three specify glacier, river and coastline delineations. Within the frame of the DEM, the photogrammetric data set contains 191,524 points, that are laid out tightly along lines. To break up this line structure and to achieve a more equal data distribution over the total area, the point data, that are used from each of the five groups, was reduced. A most effective factor for this reduction was determined by experimental testing. This testing shows that a useful intersection of elevation points for the interpolation can be constructed by reducing river and coastline data by the factor 1 to 30, contour lines on land by 1 to 24, contour lines on ice by 1 to 6 and the delineation by 1 to 5. Thus the total data set was reduced to 22,389 data points. These selected data points, together with the original photogrammetric delineation lines, are shown in Fig. 1.

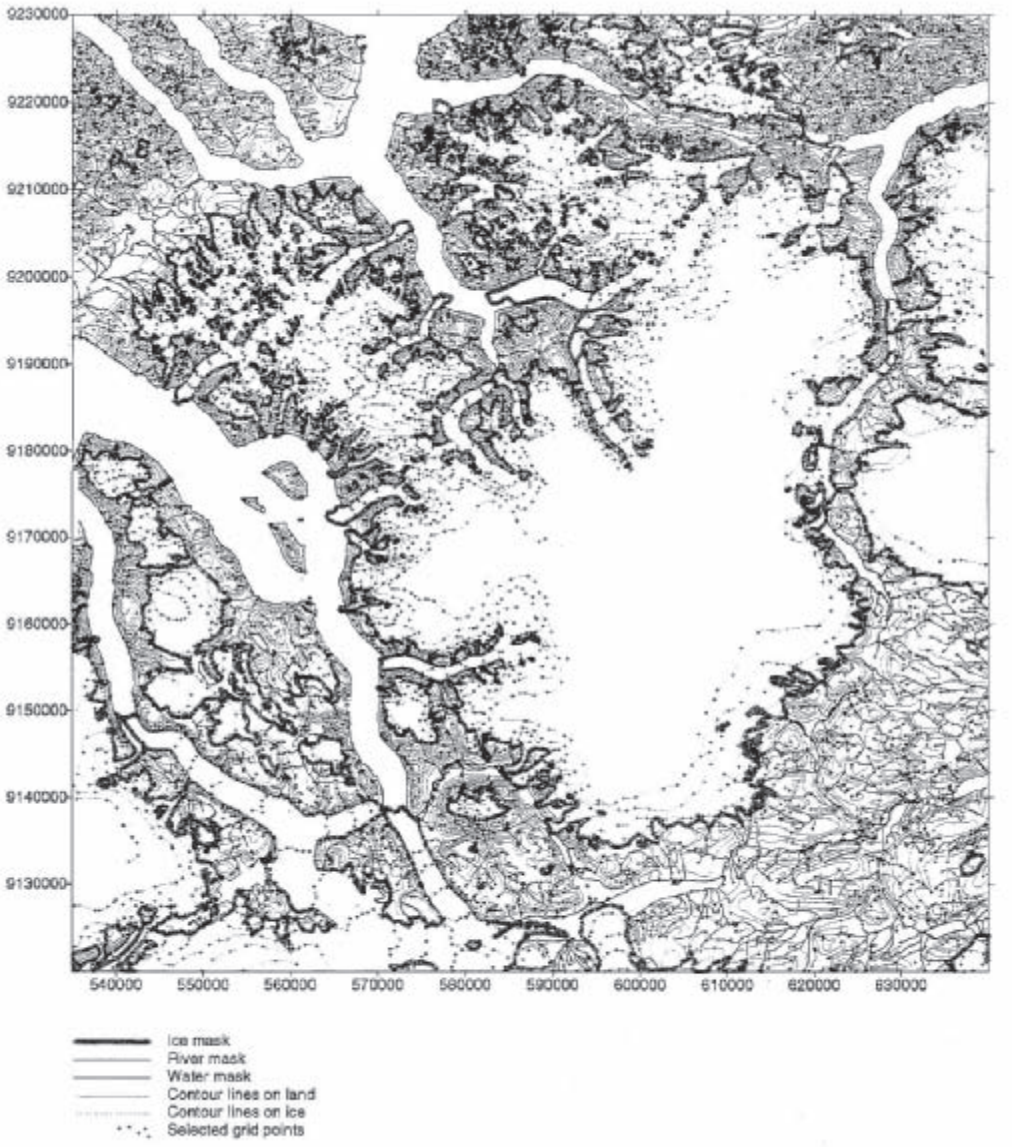

Fig. 1. Topographic data from photogrammetric mapping.

Surface data for the central higher part of the ice cap were measured by airborne radar-echo sounding in 1993. This data set contains a total of 5631 measurements along two separate flying routes, of which every one in five has been selected as input for the interpolation. The chosen set of points is called s2 and is shown in Fig. 2.

Around the central dome ground data describing surface and bedrock elevation were collected in 1994, using a geographical positioning system (GPS) and radar surveys. These data have a better accuracy and a higher density than the flight measurement data from the previous year. Therefore, 538 surface elevation points (1 out of 15) from this data set have been selected as input for the interpolation. Fig. 2 displays the points by the name s3. Simultaneously, 42 data points of the airborne radar measurements of the previous year in the same area have been removed. Thus, a total of 1622 surface points defining the central higher part of the ice sheet were selected as input for the DEM.

The north-eastern part of the Hans Tausen ice sheet was explored by field work in 1994. GPS and radar-echo

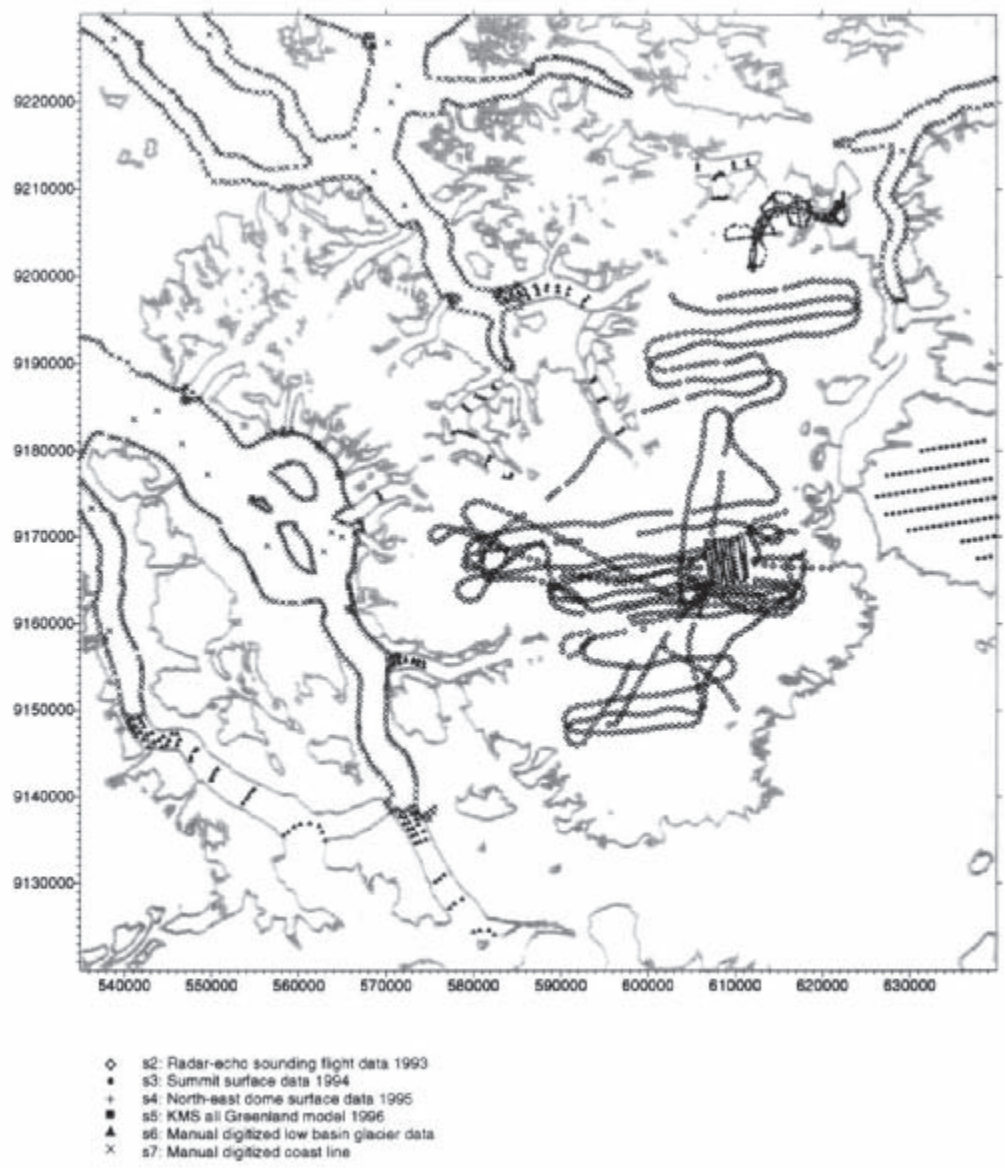

Fig. 2. All data sets used for the compilation of the surface map except photogrammetric data.

sounding measurements were performed in an outlet glacier basin stretching from a local dome at 1300 meter elevation to the glacier terminus near Harebugt at about 300 meter elevation. Along 4 snowscooter trolls a total of 11310 data points were measured with kinematic GPS and every tenth of these was selected as input for the model. The points are called data set s4 and are shown in Fig. 2.

The above data sets define most locations on the surface map, except for the fjords and the Bure ice cap to the east of the Hans Tausen glacier. Surface data for the Bure ice cap were extracted from the topographic Greenland model developed at the Danish National Survey and Cadastre (Ekholm, 1996). This model contains elevation estimations for entire Greenland, in a grid of geographical coordinates with a spacing of 0.02 degree latitude and 0.05 degree longitude. In the Hans Tausen region this results in a grid of about 0.6 by 2 km, and 89 of these points were assigned for input to the DEM. These topographic data are shown in Fig. 2 as dataset s5.

Fjord data defining the water depth have not been measured yet and the first interpolation of the intersection of all selected points so far shows very poor results for the bottom topography of the fjords. For several locations in the fjords the interpolated elevations were hundred m a.s.l. and more. To improve this result, a coastline at elevation zero along selected river and water delineation lines was constructed manually from the photogrammetric data set. Existing photogrammetric coastline data could not be used directly, due to the errors and inconsistency of labelling and the extensive coverage of rivers and lakes, features that are not relate to the coastline. For the coastline, one point in every 200 metre was digitised. This sums up to a total of more than 2000 data points. These points were added to the above intersection of selected source data. The high density of these points assures that any data point situated on land only indirectly influences the interpolation of a grid point in the fjord, as the intersection with the coastline points with value zero m a.s.l. directly corrects the fjord elevation values to below zero m a.s.l..

Interpolating this extended intersection of data now largely improves the surface grid and the values for the depth of the fjords become more realistic. Only in a few locations, namely in areas between flat or smoothly rolling coastal landscapes, the values for the fjord bottom topography are still calculated as above sea level. To improve these interpolation results, additional negative elevation points with an estimated value of minus 50 m b.s.l. are assigned to certain locations in the fjords. Fig. 2 shows these negative elevation points together with the manually digitised coastline as data set s7.

The last problem that had to be solved for the interpolation of the surface DEM is the grid points on narrow glacier tongues. Grid points located on relatively narrow glacier tongues, confined by steep valley walls, acquire negative or otherwise subtracted elevation values due to lack of elevation information on their surface. This problem is solved by locally drawing estimated 10 metre contour lines for every interval, particularly on low lying and/or floating glacier tongues. This manually digitised data set describing additional ice elevation contours was added to the data source as well (Fig. 2).

Now all the source data for the interpolation of the surface grid are defined. The input dataset contains 27,520 data points and the resulting grid exists of 46,631 points. The data are distributed evenly except for the lesser density of elevation data on the top of some glaciers and the missing data for fjord depth. A graphical representation of the result of this interpolation is shown in Fig. 3.

Subglacial Map

The subglacial topography is constructed in a similar way as the surface elevation topography and more than fifty percent of the points were reused. New input data were only needed for ice covered areas and along the boundary line between floating glacier tongues and coastal waters. However, both river, water and glacier delineation lines, and contour lines on land contribute to the main set of data point use for the interpolation and each group was reduced by the same factor as before.

The manually digitised fjord coastline was used once more for the interpolation of grid points in the fjords. The data points at the boundary line between calving glacier tongues and coastal waters, the zero m.a.s.l contour, were removed from the input data as well as photogrammetric glacier front data of floating glaciers. This guarantees the unrestrained interpolation of the subglacial grid, also underneath floating glacier tongues. Removing the described

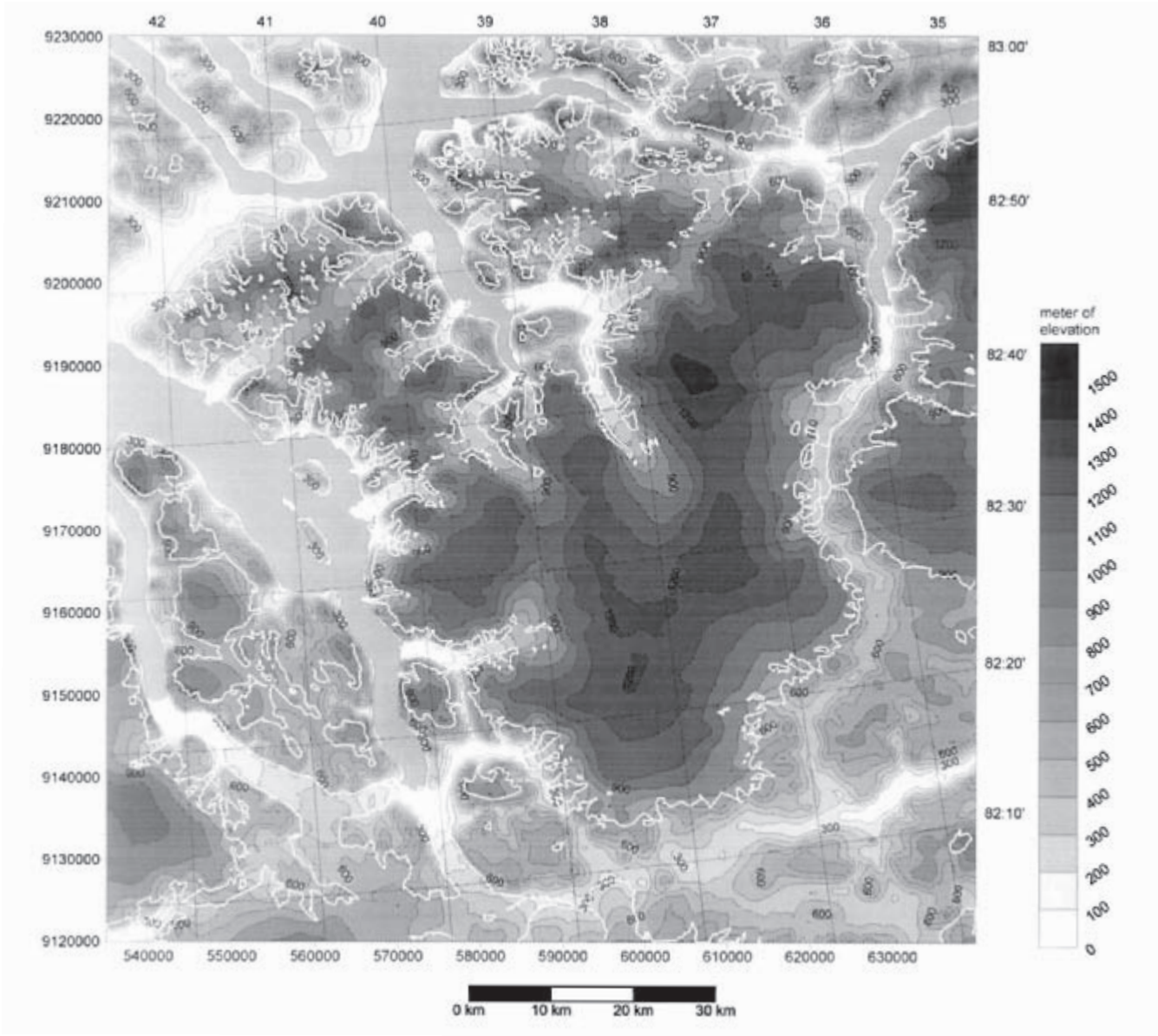

Fig. 3. Contour map of surface elevation.

information from the two data sets leaves respectively 15,354 and 1,920 data points as source for the interpolation of the subglacial DEM. In Fig. 4 both the selected photogrammetric datapoints and the reduced digitised coastline, are shown respectively as data set b1 and b5.

Three data sets containing ground and airborne radar-echo sounding data describe the ice thickness. Each point in this data set was assigned two elevation values: one for surface elevation and one for the underlying bedrock elevation. Since the selected surface points already were used for the construction of the surface map, the same points were used again for the construction of the subglacial DEM. Thus, the points in the data sets b2 (airborne radar echo sounding), b3 (summit data) and b4 (north-east dome data) refer to the same points on the glacier as the points in the sets s2, s3 and s4 as described earlier. The data sets b2, b3 and b4 are shown in Fig. 4.

The five data sets above do only include bedrock information for glaciers that are part of the main Hans Tausen ice

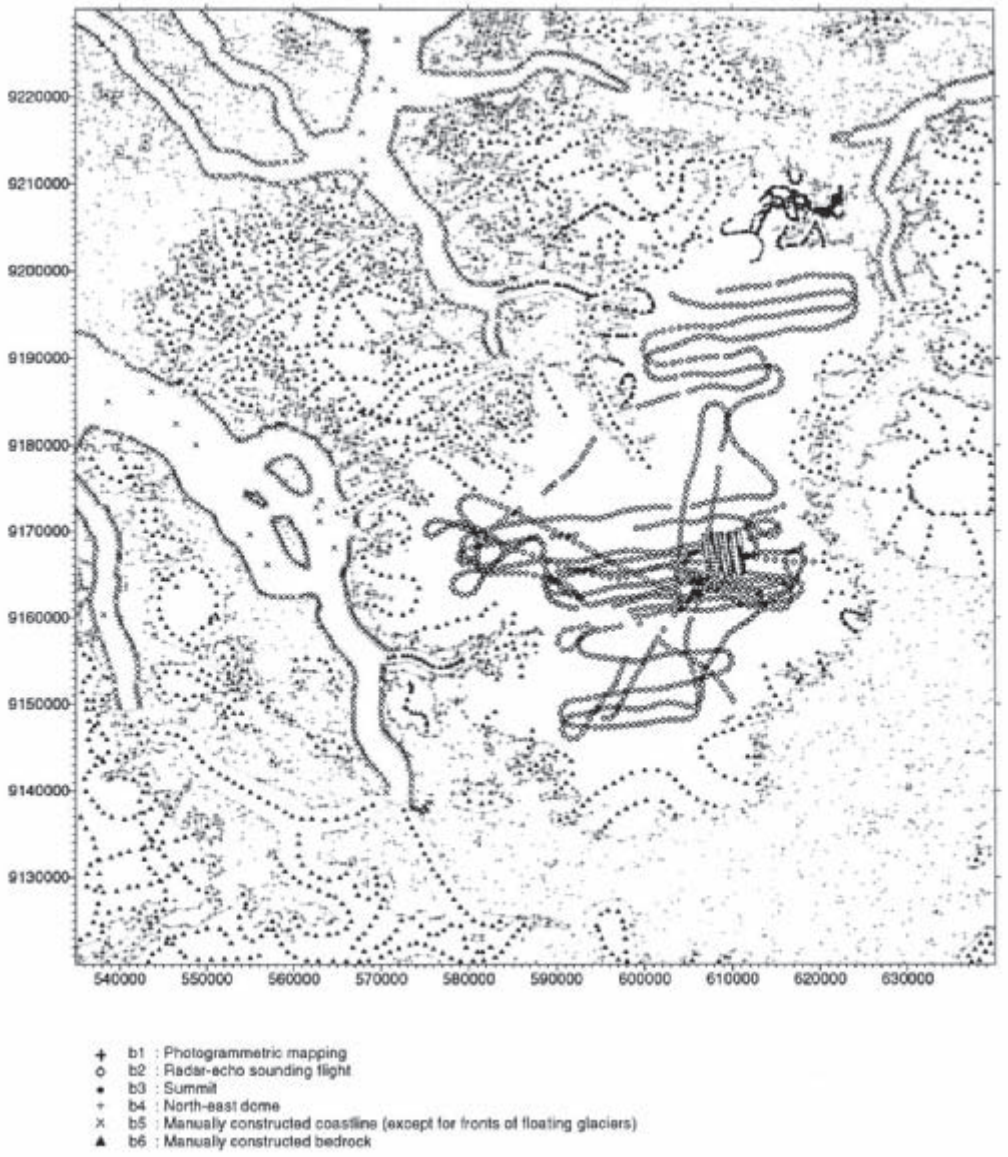

Fig. 4. Data sets used for the compilation of the DEM for bedrock/subglacial topography.

sheet. More than 200 local valley or mountain glaciers, minor ice caps and ice fields in the area need to be specified as well. There is no measured data available for these glaciers and therefore a simple model was constructed to describe the ice thickness. This model is based on the assumption that a relation between ice thickness and surface elevation can be deduced from the radar-echo sounding data of the glacier basin in the north-east, assuming that this glacier basin is typical for all glaciers in the area. In other words: the north-east glacier basin was used to identify the general mid glacier profile for all local glaciers. Accordingly, the quality of this model depended on two data sets: (1) a profile of the 1995 ice thickness data from the outlet glacier basin in the northeast, and (2) photogrammetric data, describing the surface elevation of local glaciers.

The geographical location of this profile and its characteristics are shown in Fig. 5 and Fig. 6. The ice thickness decreases from 300 m a.s.l. at the top to about 150 m a.s.l. at the glacier snout.

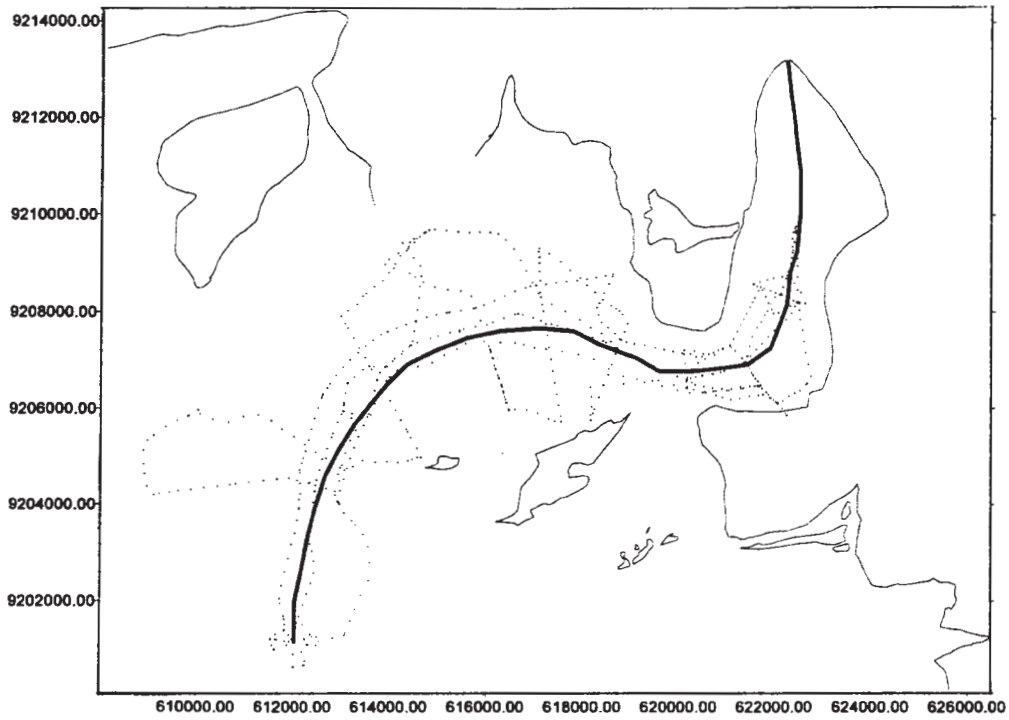

Fig. 5. Central flow-line from the local dome to the glacier terminus of the outlet glacier basin in the north-eastern corner of the Hans Tausen ice cap. The dots represent the measurement points that are used to define surface and subglacial profiles along the flow-line.

The relation between ice thickness and surface elevation can be generalised as:

$$I = 3/20 * E + 105 \qquad (1)$$

where I stands for ice thickness and E for surface elevation in metres. This equation defines the midprofile elevation of an outlet glacier down to about two kilometres upglacier from terminus. It will be used to identify the subglacial topography along flowing lines of similar valley and mountain glaciers in the area and as an estimate for the ice thickness of neighbouring ice fields and local ice caps.

Having specified the relation between ice thickness and surface elevation, the next step was to find the mid glacier

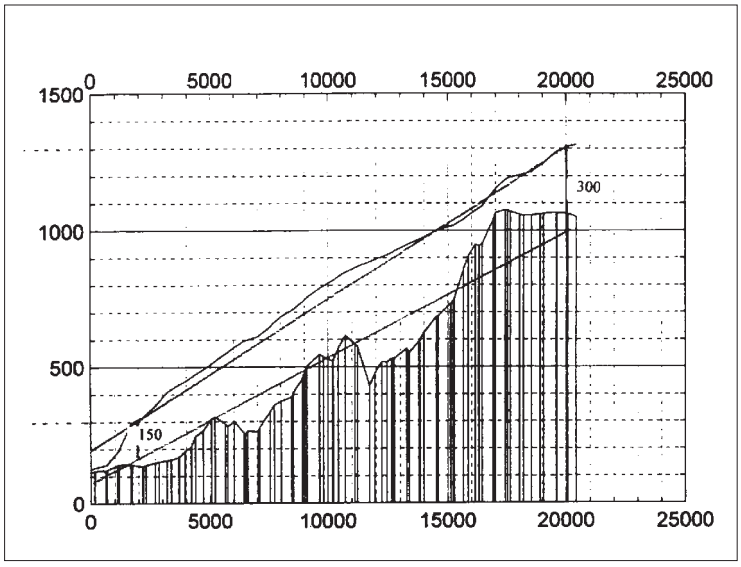

Fig.6. Surface and bottom elevation profiles along the central flow-line from the local dome to the glacier terminus. The two straight lines illustrate an approximate relation between bottom topography and surface elevation. This approximate will be used in the model to determine the ice thickness of neighboring glaciers.

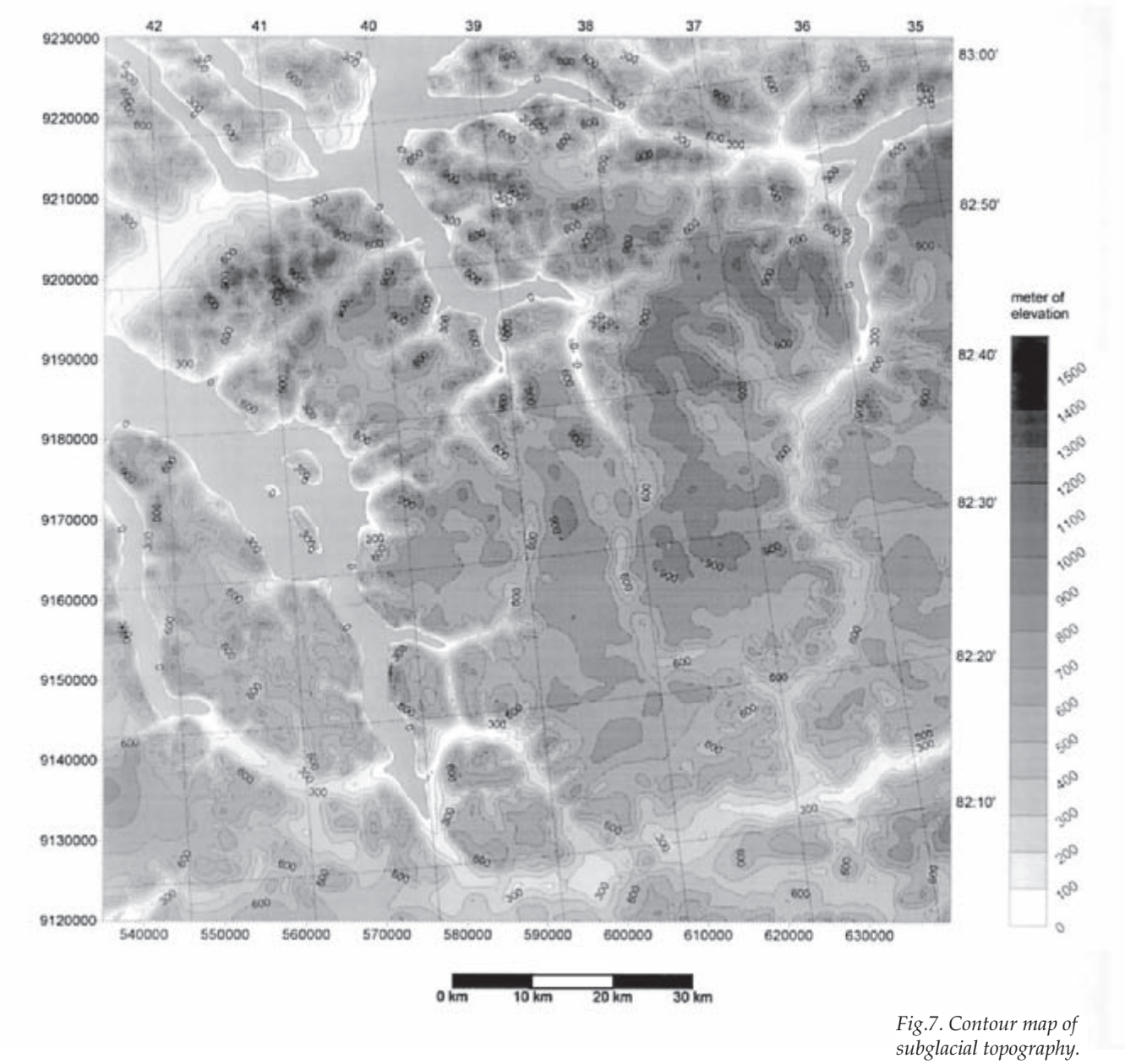

Fig.7. Contour map of subglacial topography.

surface elevation along the flow-line or similar terrain characteristics of neighbouring glaciers. For this purpose, numerous points along 143 profile lines were digitised manually. Then the surface elevations was calculated along these profile lines for every 300 to 500 meter. This was done by cutting slices into the previously constructed DEM for surface elevation and interpolating for each point the elevation values for the selected points. Finally, the subglacial elevation was found applying equation (1) to calculate the ice thickness and then subtracting the ice thickness from the elevation. The result is a data file containing 3,646 bedrock points along 143 profile lines. These points make the data source b6 and are shown in Fig. 4.

By merging of the 6 data sets, the subglacial topography map can be inferred. The intersection of source data for the interpolation now contains 23,723 points. The resulting grid is of the same size as before and exists of 46,631 points. The result of this interpolation is represented as a contour map in Fig. 7.

Glacier Model

The last step in the compilation was the construction of a DEM for ice thickness. This was done by subtracting the subglacial elevation data from the surface elevation data for every grid point in the DEMs. For areas representing floating glaciers is assumed that the whole section between surface and bedrock is glacier ice. This is obviously a generalisation. However, as these areas are relative insignificant in size around the Hans Tausen ice cap, the effects on the model are insignificant. In the resulting grid for ice thickness, all grid values greater than or equal to five metres were accepted for the DEM. Values less that five metres were not used because they are beyond the accuracy of the interpolation routine, and also because these small ice thicknesses are not significant for glaciological modelling. In the grid of the glacier DEM all points with values of less than five metres were assigned a dummy value for ice thickness of -1.

The result of the subtraction procedure showed a final problem, once more con-

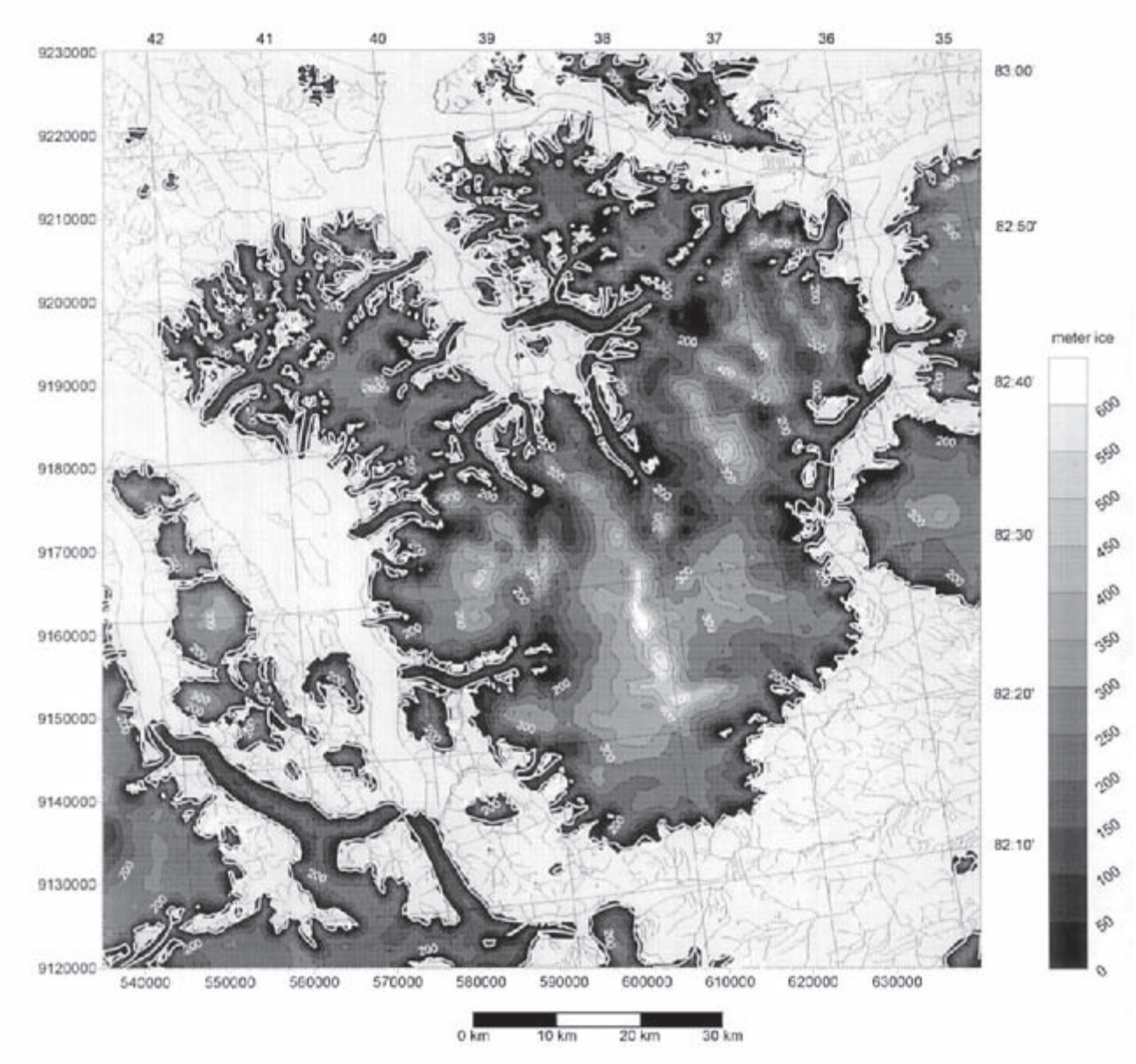

Fig. 8. Ice thickness map.

cerning the calving fronts of floating glaciers. Subtracting the two interpolated maps resulted in an unrealistic situation, because of the elevation step between the surface of the glacier fronts, at zero m a.s.l., and the fjord depth, at up to a hundred m b.s.l.. This elevation step misplaced the calving front of many of these glaciers by several kilometres out into the fjords. The problem was solved by comparing the two DEMs for glacier thickness and surface elevation and removing any glacier ice from open fjords. Technically, every ice thickness grid point that had corresponding surface points at elevations below zero, was set zero.

Finally the grid was edited and checked for its accuracy. The gridding boundaries were compared to the ice delineation lines from the photogrammetric mapping and irregularities along the calving fronts were corrected manually. Fig. 8 shows the result of the construction of the DEM for ice thickness as a contour map.

Volume calculation

The DEM of ice thickness of the HT ice cap can be used to compute the total volume of the ice cap. The volume of ice is calculated using three different methods. The difference in the results of the three methods gives a qualitative measure of the accuracy of the volume calculations and thus an indication of the quality of the selected grid size. The methods used are the Trapezoidal Rule, Simpson's Rule and Simpson's 3/8 Rule. The results of applying the three rules to the ice thickness DEM yields total volume estimates for the HT ice cap of 763.699, 763.358 and 763.465 cubic kilometres respectively. The relative error of the results can be expressed as a percentage of the average volume and can be computed as:

$$RE = 100 * (LR - SR) / AVER \quad (2)$$

where RE is the relative error, LR is the largest result from the three methods, SR is the smallest result and AVER is the average of the three methods. Applying this formula the relative error is computed to be 0.045 percent. This rather small number shows that the selected grid size of 500 by 500 meters, related to the topographical changes, was reasonable and emphasises the reliability of the volume calculations. Thus, the average volume of the Hans Tausen ice cap is estimated to be 763,507 km3. Given a planar area of the ice cap of 3975 km2, the average ice thickness of the glacier is estimated to be 192 metres.

Conclusion

A DEM of ice thickness of the HT ice cap was constructed by subtracting the bedrock elevation from the ice surface elevation grid. This model was used to compute the total volume of the ice cap. In the future the model can be used as source for all types of glacier modeling in the area.

Acknowledgements

This project was supported by *The Nordic Environmental Research Programme 1993-1997* of the *Nordic Council of Ministers*. Since January 1997 this project was coordinated by Henrik Højmark Thomsen, Geological Survey of Denmark and Greenland. We would like to thank Peter Jonsson for his great effort in preparing the ground radar-echo sounding data from the 1994 and 1995 field seasons. Niels Gundestrup is thanked for sharing his unique logistical material of the area and for providing the airborne radar-echo sounding data. Christian Keller is thanked for the technical support in preparing GPS data. Finally our special thanks go to the employees of the photogrammetric laboratory under the leadership of Hans Jepsen. Their data and collaboration have been of invaluable importance for this project.

References

Ekholm, S. 1996. A full coverage, high-resolution, topographic model of Greenland computed from a variety of digital elevation data. *Journal of Geophysical Research* vol 10 1, no. B 10, 21,961-21,972.

Hammer, C. U. 1995. Ice core drilling. In: Reeh, N. (ed). *Report on activities and results 1993-1995 for Hans Tausen Ice Cap Project – Glacier and Climate Change Research, North Greenland*. Nordisk Minister Råd, Miljøforskningsprogram – klimaforskning, 16-28.

Jonsson, P. 1994. *Mission report on an impulse radar experiment at NE Greenland*. Lund University. Department of Engineering Geology, Report no ISRN: LUTVDG/TVTG-3046-SE, 7 pp.

Jonsson, P. 1995. *Mission report on an impulse radar experiment at NE Greenland*. Lund University, Department of Engineering Geology, Report no ISRN: LUTVDG/TVTG-3047-SE, 8 pp.

Mass balance parameterisation for Hans Tausen Iskappe, Peary Land, North Greenland

By Niels Reeh, Ole B. Olesen, Henrik Højmark Thomsen, Wolfgang Starzer, and Carl Egede Bøggild

Abstract

Reeh, N., O. B. Olesen, H. H. Thomsen, W. Starzer, and C. E. Bøggild 2001. Mass balance parameterisation for Hans Tausen Iskappe, Peary Land, North Greenland. Copenhagen, Danish Polar Center. Meddelelser om Grønland Geoscience 39, pp. 57-69.

A mass balance model based on a positive degree-day approach is used to model the mass balance-elevation relationship for Hans Tausen Iskappe (82.5°N, 37.5°W). Model parameters are estimated by means of field data from a glacier basin in the north-east corner of the ice cap. The mass balance model is run for the total Hans Tausen Iskappe by using additional information on the snow fall distribution based on accumulation data from three local ice cores. The model indicates that, in the period 1975-1995, the total balance of Hans Tausen Iskappe was negative (–0.14 m/y of ice equivalent averaged over the ice cap, corresponding to –104% of the annual average accumulation in the period). During the same period, the central part of the ice cap was very likely thickening. The sensitivity of the total mass balance to changing summer temperature is –0.17 m ice/y/K. With a 5% increase of snow fall per degree increase of summer temperature, the sensitivity is changed to –0.14 m ice/y/K. Model studies with larger deviations of the summer temperature from the present value indicate that a 5 K warmer temperature would result in ablation over the entire ice cap, which would then melt away completely in a few hundred years. Even a three-fold, simultaneous increase of the accumulation rate would not in general restore the mass balance, but might secure survival of small isolated ice caps in the northern mountainous landscape. The firn warming (the increase of the temperature at 10 m depth above the mean annual air temperature) of the central area of the ice cap is also studied. Extreme changes of climate conditions as those mentioned above, are needed in order to change the thermal regime of the central region of Hans Tausen Iskappe from cold to temperate. This indicates that Hans Tausen Iskappe was a cold glacier during most of its existence.

Keywords: Glacier mass balance; firn warming; North Greenland

Niels Reeh, Department of Electromagnetic Studies, Technical University of Denmark, Building 348, Ørsteds plads, DK-2800 Lyngby, Denmark.

Ole B. Olesen, Henrik Højmark Thomsen, Wolfgang Starzer, Carl Egede Bøggild, The Geological Survey of Denmark and Greenland, Thoravej 8, DK-2400 Copenhagen NV, Denmark

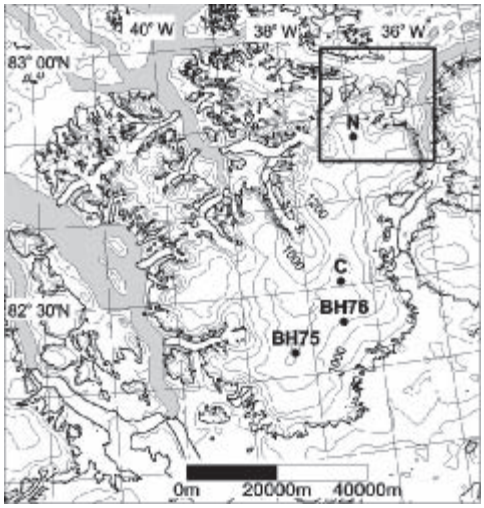

Fig. 1. Map of Hans Tausen Iskappe. North Dome (N), Central Dome (C), and drill locations BH75 and BH 76 are indicated. The square delimited by a thick line in the north-east corner of the map shows the area covered by the map in Fig. 2.

Introduction

The main purpose of this paper is to set up a model for estimating the present mass balance of Hans Tausen Iskappe and its sensitivity to climate change. Hans Tausen Iskappe is a local ice cap, about 75 km from north to south and 50 km from east to west, located in western Peary Land (Fig. 1). Covering an area of 3975 km^2 (Starzer and Reeh 2001), it rests on one of the widespread c. 1000 metre high plateau of Silurian rocks, dominating the landscape of Peary Land. The ice cap has several domes (outflow centres) which reach elevations of 1200 to 1300 m above sea level (a.s.l.). Several outflow glaciers drain the ice cap to the west, north and east, often terminating at elevations of a few hundred metres or reaching sea level with a calving front. The southern margin of the ice cap can be characterised as a "quiet" sector, covered by snow drifts that often survive the summer melt period. Here, the subice landscape is relatively smooth. The maximum ice thickness is around 300 metre, except in a marked, deep valley trending north-south, where the thickness locally reaches a value of 600 metre. In contrast, the northern part of the ice cap rests on a mountainous terrain with ice-thickness variations typically between 100 and 450 metre (Starzer & Reeh 2001).

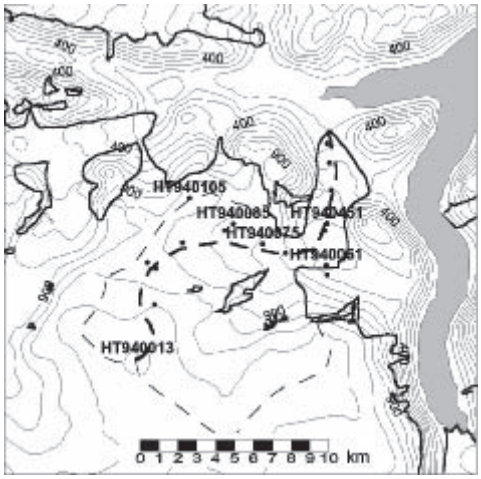

Fig. 2. Map of Hare glacier basin. Basin limit is shown by a thin dashed line. The central flow line is shown by a thick dashed line. Stake and pit locations for mass balance measurements are shown as dots.

Mass Balance Observations

In the summers of 1994 and 1995, field work was carried out on the tongue and in the drainage basin of an outlet glacier located in the north-east corner of the ice cap, in the following referred to as Hare glacier (Fig. 2). An important part of the field work was mass balance studies and related measurements of glacier climate and englacial temperatures. The mass balance measurements were performed as snow-pit/firn-core studies and stake readings along the centre line of the drainage basin. They show that considerable summer melting takes place even on the higher parts of the ice cap. In peak summer, several decimetres thick slush develops over extended areas of the glacier basin. A significant part of the melt water penetrates into the snow/firn pack where it re-freezes and creates high-density layers or ice layers in the snow pack. This process releases energy (latent heat) causing local warming of the surface-near layers of the glacier, as confirmed by repeated measurements of ice temperatures down to 10 m depth at several locations on the glacier. From the local dome at 1320 m a.s.l. to the glacier terminus at c. 100 m

a.s.l, the following zones are represented (in descending order): A snow zone (percolation zone, wet and soaked snow), a superimposed ice zone (covered by slush in peak summer), a second snow zone, a second superimposed ice zone, and an ice ablation zone.

In Fig. 3, 'winter balance' (August 1994-June 1995), 'summer balance' (June-August, 1995), and annual balance (August 1994-August 1995) along the central flow line of Hare glacier are shown as functions of elevation. All mass balance-elevation curves show large fluctuations in respect to smooth trend lines. The fluctuations are mainly due to uneven distribution of the snow accumulation caused by slope dependent wind drifting. The 1994/95 annual equilibrium line altitude was located near an elevation of 700 m a.s.l.

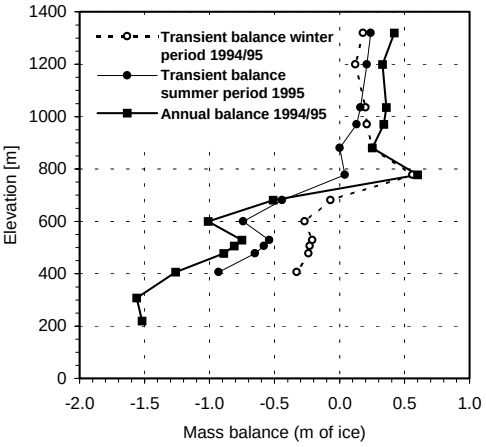

Fig. 3. Measured mass balance as function of elevation in the Hare glacier basin.

Mass Balance Model for Hare Glacier

The model, which is based on the approach described by Reeh (1989), has proven to be a useful driver for time dependent ice-dynamics models (e.g. Huybrechts *et al*., 1991). The model calculates melt rate and snow/ice surface temperature, using parameterisations of annual snow fall, mean annual air temperature and mean July air temperature as input. Melt rates are calculated using positive degree-days, and firn warming (i.e. the positive deviation of the temperature at 10-15 m depth in the firn from the mean annual air temperature) is estimated by means of the model-calculated amount of refrozen melt water in the firn. The parameters of the melt model are determined by means of field data collected on the tongue and in the drainage basin of Hare glacier. The limited extent of this basin justifies to parameterise temperature and snow accumulation only in terms of elevation. For the modelling of the total mass balance of Hans Tausen Iskappe, the parameterisations must be generalised to account also for latitudinal gradients of temperature and snow accumulation.

Annual snow fall

The annual snow fall needed as input to the mass balance model is determined as follows: In the accumulation area, the annual snow fall is put equal to the annual balance. Since part of the annual balance is probably supplied by freezing of rain in the summer season, this results in a slight overestimation of the annual snow fall. In the ablation zone, the annual snow fall is estimated based on soundings of snow depths in June 1995.

Air-temperature

The 1995-summer air temperature records at three sites HT940061 (574 m a.s.l.) HT940075 (777 m a.s.l.), and HT940013 (1320 m a.s.l.) (for location, see map in Fig. 2) are displayed in Fig. 4. Unfortunately, successful recording of air temperature at HT940013 on the local dome lasted only from June 20 to June 25, whereas temperatures were successfully recorded at the two other locations during the entire measurement period from June 20 to August 14. The temperature record for the same period from Kap Molkte, located about 100 kilometres to the south-east of Hans

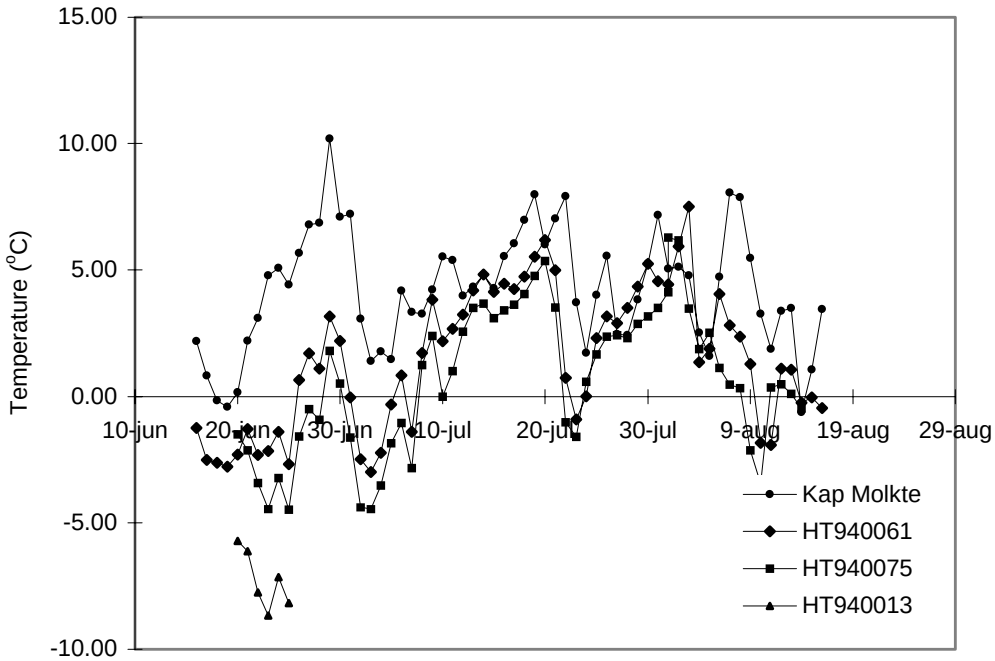

Fig. 4. Air-temperature records observed in the summer of 1995 at stations in the Hare glacier basin (for location, see Fig. 2.) and at Kap Molkte located about 100 kilometre south-east of Hans Tausen Iskappe at an elevation of 13 m.

Tausen Iskappe at an elevation of 13 m, is also shown in Fig. 4. In general, the records show synchronous variations, although discrepancies occur. In Fig. 5 average air temperatures for two periods (June 20-25 and July 1-31) are plotted versus elevation. The first period includes observations from all four sites. The second period, representing peak summer, includes only Kap Moltke, HT940075 and HT940061. It appears that the air-temperature/elevation gradient is more negative in the former period (–0.0081 K/m) than in the latter period (–0.0047 K/m), probably due to generally more humid weather in July than in June. If the distant Kap Molkte data are excluded, the corresponding gradients become –0.0071 K/m and –0.0056 K/m, respectively. We choose the latter value to represent the average gradient in the summer period. This gives the following parameterisation of July air-temperature in the Hare glacier basin:

$$TJM = 5.62 - 0.0056\,E, \qquad (1)$$

where E is elevation.

Unfortunately, mean annual air temperature has not been measured on Hans Tausen Iskappe. Reeh (1989) derived the following parameterisation of mean annual air temperature on the Greenland ice sheet by linear regression of observed ice-sheet mean annual air temperatures *TMA* on elevation E and latitude L:

$$TMA = 48.4 - 0.751\,L - 0.00792\,E. \qquad (2)$$

The temperature inversion occurring at low altitudes in North Greenland (Ohmura, 1987) was accounted for by putting the temperature gradient below 300 m equal to zero north of 75°N. The

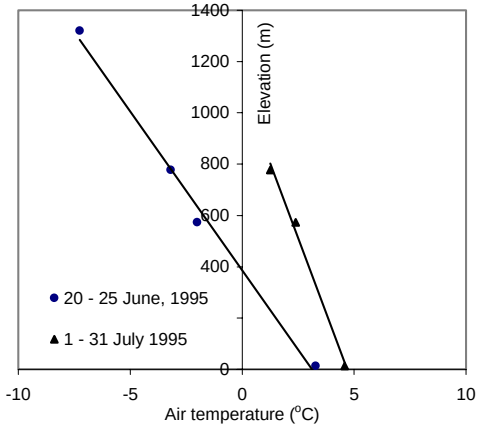

Fig. 5. Air-temperature/elevation relationship observed in the summer of 1995 in the Hare glacier basin. Summer temperatures at Kap Molkte, located about 100 kilometre south-east of Hans Tausen Iskappe at an elevation of 13 m, is also shown.

temperature-latitude gradient of 0.751 K/degree latitude appearing in Equation(2) is in good agreement with the corresponding gradient of 0.7 K/degree latitude derived from temperature records at climate stations in the ice free area in East Greenland (Funder et al, 1998). For Kap Moltke, Equation (2) yields a mean annual air temperature of –15.7°C which is 0.6°C cooler than the 1974-1995-average of the mean annual temperatures measured at Kap Molkte, and 0.8°C cooler than the average (-14.9°C) of the mean annual temperatures at Kap Molkte for the two years of mass balance observations 1994 and 1995. At the mean latitude of Hare Glacier about 0.6 degree of latitude north of Kap Molkte, the mean annual air temperature at sea level for 1994-1995 is accordingly estimated at –14.9 – 0.6*0.751= –15.4°C. Altogether, this leads to the following parameterisation of the mean annual air temperature in the Hare glacier basin for the balance year 1994-1995

$$TMA = \begin{cases} -15.4 \text{ for } E < 300 \text{ m} \\ -15.4 - 0.00792\,(E - 300) \\ \qquad \text{for } E > 300 \text{ m} \end{cases} \qquad (3)$$

10-metre firn/ice temperature

The relationship expressed by Equation(3) is displayed in Fig. 6 together with observed 10-metre firn/ice temperatures. Three sites (HT940013, HT940105, and HT940075) (for location, see map in Fig. 2) show remarkably large positive deviations from the air-temperature curve. These sites are all located in snow-accumulation areas where snow-pit/firn core studies indicate substantial re-freezing of meltwater, causing warming of the firn. Site HT940085 is located in the upper superimposed ice zone, where most of the latent heat produced by the re-freezing process is released to the atmosphere. Consequently, the 10-metre temperature at this site is expected to deviate little

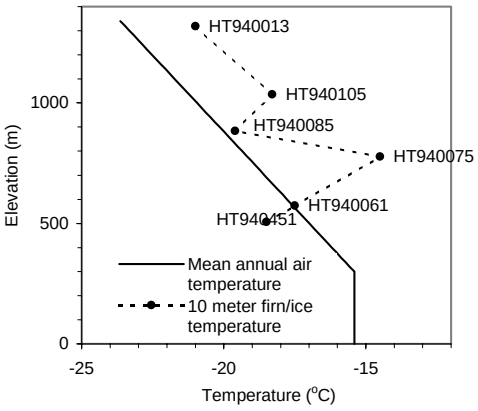

Fig. 6. Model estimated mean annual air temperature and measured 10-metre firn/ice temperature versus elevation in the Hare glacier basin.

from the mean annual air temperature as actually seen in Fig. 6. Sites HT940061 and HT940451 are both in the ablation area, where firn warming does not occur. The negative deviation of the 10-metre temperature from the mean annual air temperature at site HT940451, located several kilometres down-stream from the equilibrium line, is probably due to upward advection of cold ice originating from a site in the higher elevated and consequently colder accumulation region.

Degree-day factors

A degree-day factor for ice melt of 0.0065 m of ice/degree-day (0.0059 m of water/degree-day) is derived from a local detailed stake-farm study (CEC, 1995, Table 2, p7). For snow-melt, the degree-day factor is set to 0.0027 m of ice/degree-day in accordance with the degree-day factor of 0.0025 m of water/degree-day published by Braithwaite (1995).

In order to account for the daily temperature cycle and random temperature deviations from an assumed regular sine-variation of the average annual temperature cycle, a statistic with standard deviation s is introduced in the degree-day calculation (Reeh, 1989). In the Greenland ice sheet study of Reeh (1989), s was set equal to 4.5 K. For reasons to be explained in the following

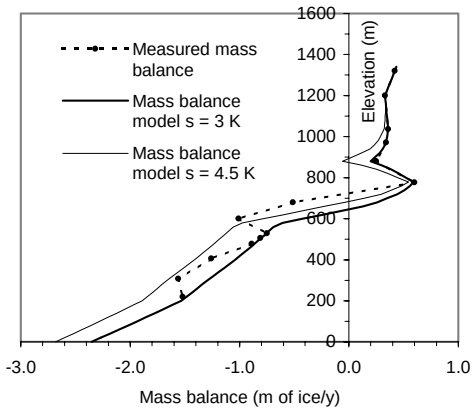

Fig. 7. Comparison of measured and model-estimated mass-balance/elevation relationships for Hare glacier basin.

section, we choose s = 3 K in the melt-rate model for the Hare glacier basin. Another parameter in the mass balance model is the amount of ice (expressed as a fraction P_{MAX} of the total snow fall) formed by re-freezing of melt water in the upper firn before run-off begins. We choose P_{MAX} = 0.6 in accordance with Reeh (1989).

Results

In Fig. 7, the model calculated annual mass-balance elevation relationship for the Hare glacier basin (heavy full curve) is compared to the observed mass balances. The close agreement between model and observations in the accumulation zone reflects the fact that the model predicts that there is no run-off (mass loss) above c. 800 m elevation. This is in accordance with our snow-pit/firn-core observations. In the ablation zone, the model generally underestimates the ablation. By increasing the value of the standard deviation of the statistic s from 3 K to 4.5 K (the value used by Reeh (1989) for the Greenland ice sheet) a better fit (although slightly too high) to the observations in the ablation zone is obtained (thin full curve in Fig. 7). However, with this s-value, the model predicts substantial run-off in the altitude interval 780-1100 m in disagreement with our field observations. Moreover, the model-predicted amount of refrozen melt water in the upper firn greatly exceeds the amount observed in our snow-pit/firn-core study, see Table 2.

In Tables 1 and 2, further comparisons between observations and model results are given. Table 1 shows positive degree-days in the period June 20 to August 14, 1995 calculated by means of the temperature records shown in Fig. 4. The positive degree-days estimated by the mass-balance model are also shown. The increasing excess with decreasing elevation of the model-estimated PDD over the observed PDD can be explained by the limited length of the observation period. The lover the elevation, the more likely is the occurrence of positive temperatures before June 20 and after August 14. The contribution from these temperatures is missing in the calculation of the "observed" PDD, but are included in the model estimate giving the PDD for a full year.

In Table 2, observed 10-metre firn/ice temperature, mean annual air temperature as calculated by Equation(3), and their difference (firn warming) are listed. The weight percentage of ice layers as observed in the snow-pit/firn-cores on June 23 and August 16 1995 and the change of this percentage are also shown in the table. At stake HT940085 located in the upper superimposed ice zone, the change is 100%. The observed amount of re-frozen melt-water is derived by multiplying the annual mass balance with the percentage change of ice layers. Model derived amounts of refrozen melt-water are shown for two different values of the standard deviation s. For s = 3K there is excellent agreement be-

Table 1. Observed (20 June – 14 August, 1995) and model-estimated positive degree-days (PDD).

Station	Elevation (m)	PDD (observation)	PDD (model)
Kap Moltke	13	253	350
HT940061	574	127	150
HT940075	777	91	95

Stake	Elevation (m)	10-metre temp. (°C)	Mean annual air temp. (°C)	Firn warming (K)	Percentage ice June 23	Percentage ice August 16	Change of ice-percentage	Mass balance (m ice/y)	Refrozen melt-water (m ice/y) Observed	Modelled	
										s=3 K	s= 4.5 K
HT940451	506	–18.5	–17.0	–1.5							
HT940061	574	–17.5	–17.6	+0.1							
HT940075	776	–14.5	–19.2	+4.7	10	53	43	0.60	0.26	0.26	0.35
HT940085	883	–19.6	–20.0	+0.4	0	100	100	0.16	0.16	0.15	0.15
HT940105	1035	–18.3	–21.3	+3.0	47	72	25	0.36	0.09	0.13	0.22
HT940013	1318	–21.0	–23.5	+2.5	0	13	13	0.42	0.055	0.055	0.14

Table 2. Observed firn/ice 10-metre temperature, model-calculated mean annual air temperature, and observed and model-calculated amounts of refrozen melt water.

tween observed and modelled values, whereas the modelling with s = 4.5K overestimates the amount of refrozen melt water. In Fig. 8, the amount of refrozen melt water that remains after the summer melt season (expressed as a fraction of the annual snow fall) as estimated from the mass-balance model with s = 3K, is shown together with the observed amount.

Disregarding location HT940085 in the superimposed ice zone where most of the latent heat produced in the refreezing process is released directly to the atmosphere and therefore causes little – if any – warming of the near-surface layer, a regression of firn warming on amount of refrozen melt water (forced to pass through the origin (0,0)), yields a regression coefficient of b_{FW} = 20 K /m ice. This value is close to the corresponding value (27 K /m ice) found in the study by Reeh (1989) using all available 10-metre temperature observations on the Greenland ice sheet. Since the regression coefficient determined in the total Greenland study is based on c. 170 10-metre temperature observations as compared to 3 observations in the present study, we will use the formerly derived value b_{FW} = 27 K /m ice to estimate firn warming also in thus study.

Mass Balance Model for Hans Tausen Iskappe

The modelling of the total mass balance of the Hans Tausen Iskappe requires generalisations of the parameterisations derived for the Hare glacier drainage basin.

Accumulation

The spatial distribution of the annual snow fall (accumulation) on Hans Tausen Iskappe is derived from the snow-pit and stake observations in the Hare glacier basin discussed above. Information is also provided by three firn/ice cores drilled at the central dome in 1994 and 1995 and by two firn/ice cores from the southern part of the ice cap drilled in 1975 and 1976 (Clausen *et al*. 2001). The accumulation data are summarised in the Table 3.

Table 3 displays large accumulation-rate variations both spatially and tempo-

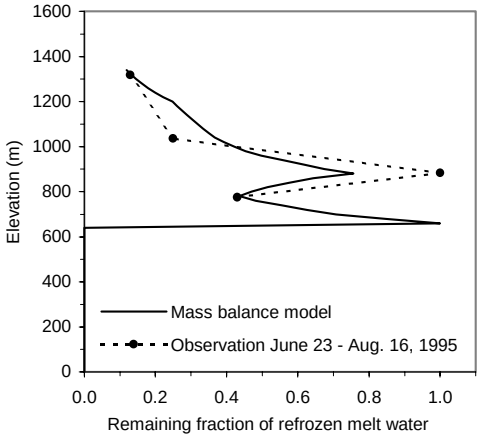

Fig. 8. Observed and model-estimated refrozen amount of melt-water remaining at the end of the 1995-summer season in the Hare glacier basin expressed as a fraction of the annual snow fall.

Table 3. Hans Tausen Iskappe: Mean annual accumulation rates (m of ice per year) in different periods.

Site	°N	°W	Altitude (m)	1994	1912-1975	1783-1975	1975-1995
North Dome	82.79	36.98	1318	0.425			*0.306*
Central Dome	82.51	37.47	1275	0.132	0.120[1)]	0.109[2)]	0.095
BH75	82.38	38.28	1150	*0.171*	0.155	0.147	*0.123*
BH76	82.43	37.50	1125	*0.158*	0.147[3)]	0.141[3)]	*0,116*

Comments: Numbers in regular style are measured values. Italicised numbers are inferred values. [1)] calculated by using mean values for the periods 1912-1995 and 1975-l995. [2)] calculated by using mean values for the periods 1783-1995 and 19751995. [3)] 1976-accumulation included.

rally. Because of the large temporal variations, accumulation-rate values at the different sites must be referred to the same period of time when used to derive the spatial accumulation rate distribution over the ice cap. Unfortunately, this requirement cannot be met by using directly measured accumulation-rate values on Hans Tausen Iskappe for any period of time. However, the accumulation rate record from the central dome has at least one overlapping period with the records from all other sites, and can therefore be used to scale accumulation rates from one period to another.

It is clear from Table 3, that the latitudinal accumulation rate gradient is much larger between the northern and central domes than south of the central dome. A likely explanation is that the storms delivering the major part of the precipitation on Hans Tausen Iskappe come from the north, thus releasing an increasing amount of precipitation as the air masses move up the north-facing mountain-fringed part of the ice cap. The southern slope is at the lee side of the ice cap, and thus receives less precipitation. Here catabatic winds probably play a large role by re-distributing the snow, leading to increasing snow accumulation in the direction of the southern margin, as actually indicated by the large snow drifts seen on aerial photographs.

The different accumulation regimes require different parameterisations of the annual snow fall north and south of the central dome located at 82.51°N. North of this latitude, a snow fall elevation gradient of 0.00036 m ice equiv./m is determined by linear smoothing of the accumulation and winter-snow data from the Hare glacier basin discussed in the previous section. As mentioned previously, surface-slope variations in this basin cause substantial local deviations of snow accumulation from the linear distribution. Although similar deviations are expected all over the ice cap, the limited number of accumulation observations can only justify simple parameterisations in terms of linear dependencies on elevation and latitude. Local deviations from the simple parameterisation will certainly occur, but the deviations will to some extent cancel out in estimates of the overall mass balance of the ice cap.

Using the 1994-values of accumulation rate at the northern and central domes, the latitudinal gradient north of 82.51°N is determined as 0.989 m ice equiv./degree latitude. South of 82.51°N, a linear regression of the accumulation values at the central dome, BH75 and BH76 on latitude and elevation shows that the elevation gradient is insignificant, supporting the idea that orography is of little importance for the snow-distribution on that part of the ice sheet. The snow fall distribution south of 82.51°N is therefore represented by a linear regression of accumulation rate on latitude.

Altogether, this results in the fol-

lowing parameterisation of snow fall on Hans Tausen Iskappe for 1994:

$$ACC=\begin{cases}0.00036\,E+0.989\,L-81.93 & \text{for } L\,(\,82.51°\text{N}\\ -0.307\,L+25.46 & \text{for } L<82.51°\text{N}\end{cases} \quad (5)$$

Table 3 shows that the snow fall on Hans Tausen Iskappe was excessive in 1994. At the central dome, the snow accumulation rate in 1994 (0.132 m ice/year) was 20% higher than the long term (934-1995) mean accumulation rate of 0.110 m ice/year (Clausen *et al.* 2001). 1994 was a year with high accumulation also at the northern dome. This follows from comparing the accumulation-rate value for 1994 (0.425 m ice/year, see Table 3) with the significantly smaller long-term balance values that can be derived from the measured submergence velocity (0.2-0.3 m ice/year) and the local strain net (0.24 m ice/year) at the dome.

The parameterisation of the snow fall on Hans Tausen Iskappe for other periods (e.g. 1975-1995) is determined by multiplying Equation(5) by the ratio between the accumulation rate at the central dome for the period in question and the 1994-value of the accumulation-rate at this location.

Parameterisation of air temperature

The parameterisation of the July air temperature over Hans Tausen Iskappe is obtained by combining the temperature elevation relationship derived for the Hare glacier basin around 82.8°N (Equation(1)) with the July air temperature gradient of --0.4K per degree latitude derived from East Greenland coastal climate stations (Funder *et al.* 1998). This results in the following generalised parameterisation of the 1994 July air temperature

$$TJM= 38.74 - 0.4\,L - 0.0056\,E \quad (6)$$

For the 1994-1995 mean annual air temperature, we use Equation(3) combined with the mean annual temperature gradient of –0.751K per degree latitude given in Equation(2) to obtain

$$TMA=\begin{cases}46.8-0.751\,L & \text{for } E\,(\,300\ m\\ 49.2-0.751\,L-0.00792\,E & \text{for } E>300\ m\end{cases} \quad (7)$$

For the period 1975-1995, air-temperature data are available from Kap Moltke. For this period, mean July and mean annual air temperatures over Hans Tausen Iskappe are derived by adjusting the temperatures given by Equations (6) and (7), assuming that the interannual temperature variations at Kap Moltke are representative also for Hans Tausen Iskappe.

Model Results for Hans Tausen Iskappe

All model runs for the Hans Tausen Iskappe are performed with the same degree-day factors, *s*- and P_{MAX} -values that were used for the Hare glacier basin. Calculations are performed for 1994 and for the period 1975-1995 (in the following used as a reference period) applying the parameterisations of snow fall and air temperature discussed in the previous section.

Mass Balance

The model calculation indicate that, in 1994 the total balance of Hans Tausen Iskappe was negative, viz. –0.08 m ice equivalent/y averaged over the ice cap, corresponding to –42% of the average accumulation rate (0.192 m of ice equivalent/y). For the reference period 1975-1995 with a mean accumulation rate of 72% of the 1994 value and a mean summer temperature 0.26 K lower than the 1994 summer temperature, the total balance was even more negative (–0.14 m of ice equivalent/y). This corresponds to –104% of the mean accumulation averaged over the ice cap. The total mass balances of the ice cap for the year with the warmest summer (1989), and the

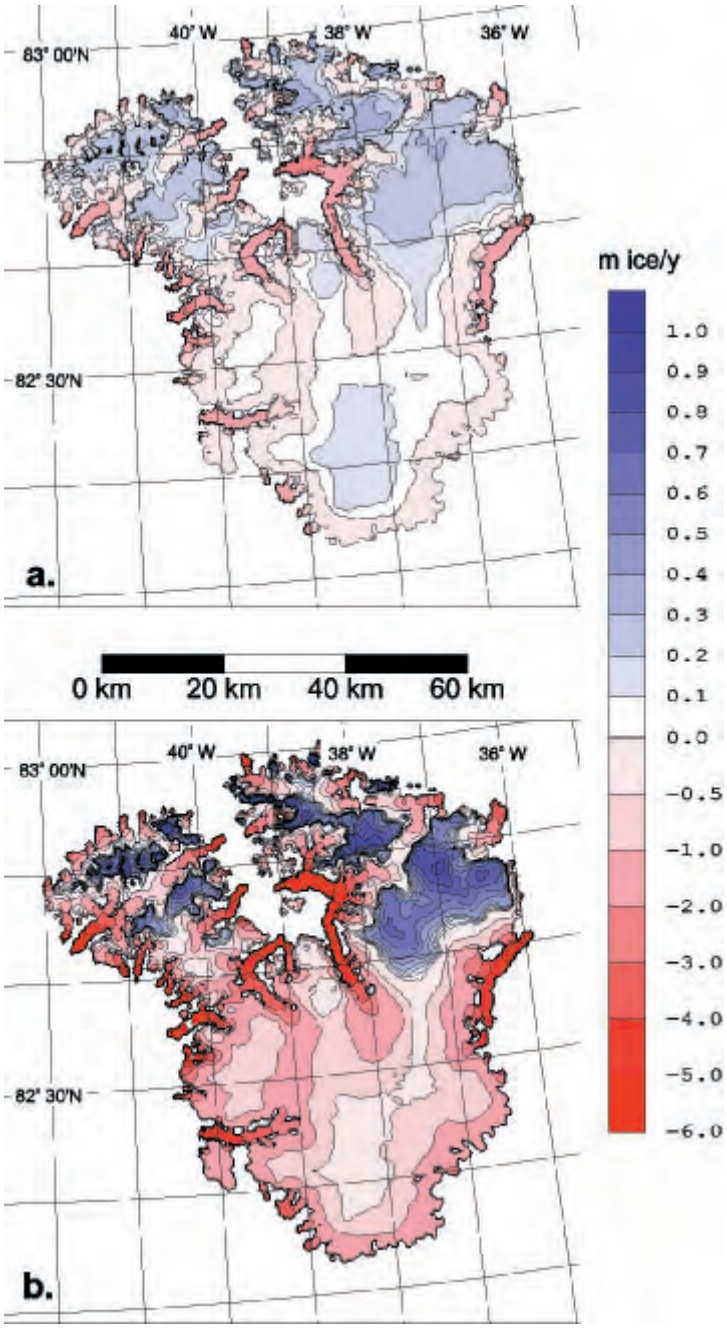

Fig. 9. Model-estimated distribution of mass balance on Hans Tausen Iskappe. a: 1975-1995 mean climate conditions. b: Holocene climatic optimum conditions (5K warmer temperatures and 3 times higher accumulation rate than at present).

year with the coldest summer (1982) are calculated at –0.32 m ice and –0.035 m ice, respectively.

At first sight, these numbers appear rather alarming for the present state of health of the ice cap. Furthermore, the results seem to contradict the conclusion of Keller *et al.* (2001) that the surface elevation of the central dome is presently increasing and probably has been increasing for a long period of time. However, inspection of Fig. 9a, showing the calculated mass balance distribution for Hans Tausen Iskappe for the period 1975-1995, reveals that the mass loss is concentrated at a number of extended outlet glaciers with elevations below 500 metre. These glaciers might be relicts formed in the cool climate of the Little Ice Age and may presently be subject to down-wasting, which seems to be a wide-spread mass-loss mechanism – rather than horizontal recession – for the cold based glaciers in North Greenland (Weidick 2001). Hence, the present mass balance condition for Hans Tausen Iskappe might be thickening of the central accumulation area due to increased snow accumulation associated with the temperature increase after the Little Ice Age, and thinning of the extended low elevated outlet glaciers due to the increased summer warmth, altogether leading to a steeper ice cap. Whether or not Hans Tausen Iskappe with time is able to reach a stable situation under present climate conditions cannot be settled by mass balance considerations alone, but will have to await the results of a planned glacier dynamics model study. Our preliminary conclusion is that, in spite of possible thickening of the central region, Hans Tausen Iskappe is most likely loosing mass under present climate conditions.

Mass Balance Sensitivity

The sensitivity of the mass balance of Hans Tausen Iskappe to climate change is illustrated in Table 4 showing the calculated total mass balance for different changes of the mean annual temperature *(T)* and different percentage changes of snow accumulation per degree change of temperature *(p/(p(T)*. All changes are in respect to the 1975-95 mean values. The table shows that a summer temperature 1.3 K cooler than present will bring the ice cap in balance with the mean

Δp/(pΔT)	*ΔT*=–2 K	*ΔT*=–1 K	*ΔT*=0 K	*ΔT*=+1 K	*ΔT*=+2 K	*ΔT*=+5 K
0 % K-1	0.046	–0.021	–0.141	–0.335	–0.606	–1.874
5 % K-1	0.031	–0.031	–0.141	–0.318	–0.568	–1.759
10 % K-1	0.016	–0.040	–0.141	–0.302	–0.529	–1.620
20 % K-1	–0.008	–0.057	–0.141	–0.270	–0.449	–1.266

Table 4. Total mass balance (m ice/y) of Hans Tausen Iskappe for different changes of the mean annual temperature *ΔT* and different percentage changes of snow accumulation per degree change of temperature *Δp/(pΔT)* in respect to the 1975-1995 mean values.

snow accumulation in the period 1975-1995.

With a temperature increase of 1-2 K in respect to the present temperature, the balance becomes exceedingly negative even if accumulation increases by 10-20% per degree warming. For temperatures 5 K warmer than now and a 20% increase of accumulation per degree warming (a scenario for the Holocene climatic optimum), there is a significant mass loss even from the highest elevated areas of the ice cap. The total annual mass loss for this scenario amounts to 4.3 km^3/y. With a total volume of the present ice cap of 763.5 km^3 (Starzer and Reeh, 2001), the ice cap would under such climate conditions disappear in a few hundred years. Thus the results of our mass balance modelling adds to the evidence that Hans Tausen Iskappe melted away completely during the Holocene climatic optimum.

The mass-balance distribution over the ice cap for an extreme Holocene climate optimum scenario with air temperature increased by 5K and accumulation rate increased by a factor of 3 as compared to their 1975-1995 mean values is shown in Fig. 9b. The figure shows that, even with such a large increase of accumulation rate, most of the ice cap would experience massive melting. Whether or not small areas in the northern part of the ice cap with positive mass balance might survive as small local ice caps cannot be settled by mass balance modelling alone, but will have to await the results of the previously mentioned, planned glacier dynamics model study.

Firn warming

In Fig. 10, calculated firn-temperature distributions of Hans Tausen Iskappe are shown for the climate conditions of the 1975-1995 reference period and for the extreme Holocene climate optimum scenario with temperature 5K warmer than now and accumulation rate three times higher than now. The calculations are performed with a firn-warming coefficient b_{FW} equal to 27 K /m. Fig. 10b shows that even in this extreme climate optimum scenario, firn temperatures in the central region of the ice cap would still be below the freezing point. Lower surface elevations either during the period of deterioration of the ice-age ice cap or during the build-up of the existing ice cap may in periods have caused air/firn temperatures a few degrees higher than those shown in Fig. 10b. Moreover, the geothermal heat flux causes higher temperature at the base of the ice cap than at the surface. Therefore, we cannot exclude the possibility that parts of the central region of Hans Tausen Iskappe – particularly the high accumulation region to the north – were temperate or experienced basal melting during certain periods of the Holocene climatic optimum.

Conclusions

Our study has shown that it is possible to model the observed mass-balance and firn-warming distributions of an outlet glacier basin of Hans Tausen Iskappe by using reasonable values of the model parameters of the degree-day model of Reeh (1989). Application of the mass-

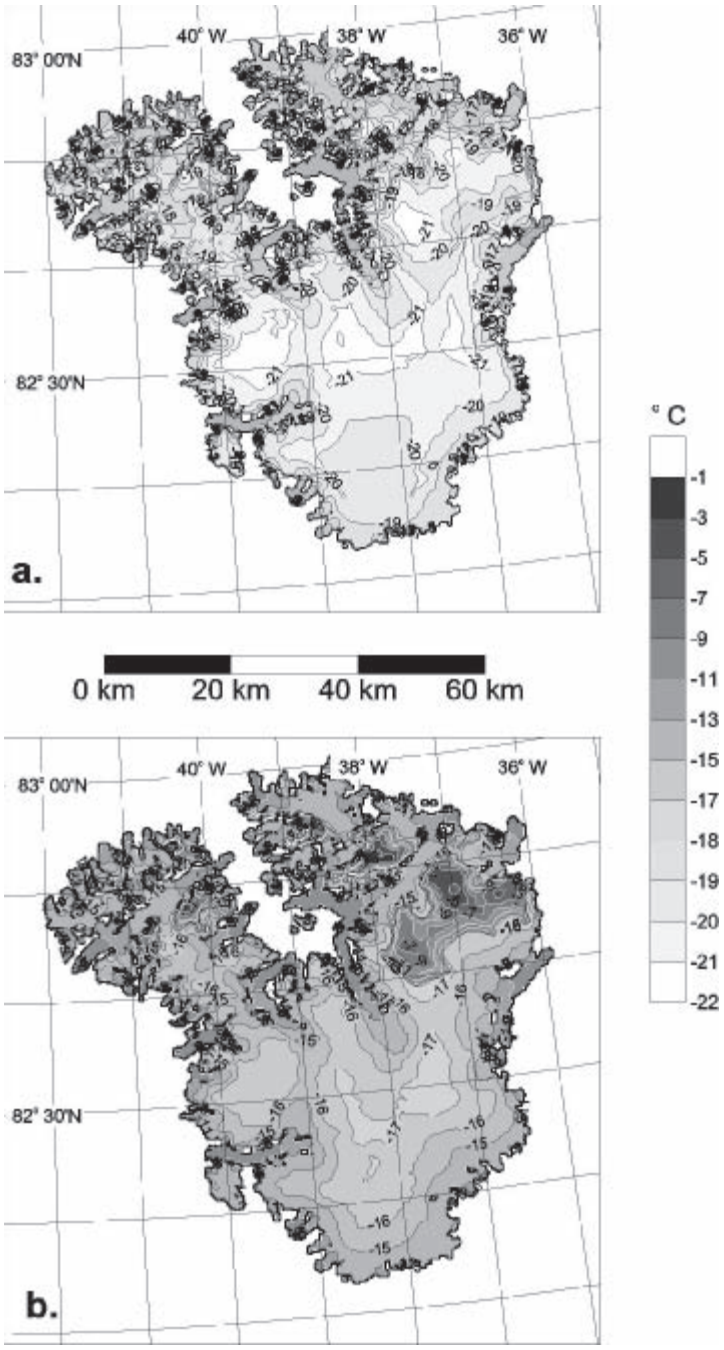

Fig. 10. Model-estimated distribution of firn/ice temperature on Hans Tausen Iskappe. a: 1975-1995 mean climate conditions. b: Holocene climatic optimum conditions (5K warmer temperatures and 3 times higher accumulation rate than at present).

balance model indicates that in 1994 the total balance of Hans Tausen Iskappe was negative, viz. –0.08 m ice equivalent/y averaged over the ice cap, corresponding to –42% of the average accumulation over the ice cap for that year (0.192 m of ice equivalent/y). For the period 1975-1995, the total balance was even more negative (–0.14 m of ice equivalent/y, corresponding to –104% of the mean accumulation for that period averaged over the ice cap).

Keller *et al*. (2001) conclude that the surface elevation of the central dome is presently increasing and probably has been increasing for a long period of time. Hence, at present, Hans Tausen Iskappe might be thickening in the central accumulation area probably due to increased snow accumulation associated with the temperature increase after the Little Ice Age, and at the same time experience thinning of extended low-elevated outlet glaciers due to the increased summer warmth. This will altogether lead to a steeper ice cap. Our preliminary conclusion is that, in spite of the thickening of the central region, Hans Tausen Iskappe is most likely loosing mass under present climate conditions. However, with time, the icecap will probably be able to reach a stable situation with reduced ablation area. A summer temperature only 1.3 K cooler than present will bring the ice cap in balance with the mean snow accumulation in the period 1975-1995, demonstrating the high sensitivity of the icecap's mass balance to summer temperature.

For a temperature 5 K warmer than now and a 20% increase of the accumulation per degree warming (a scenario for the Holocene climatic optimum) model calculations show a significant mass loss even from the highest elevated areas of the ice cap. For this scenario, the total annual mass loss amounts to 4.3 km^3/y. With a total volume of the present ice cap of 763.5 km^3 (Starzer and Reeh 2001) the ice cap would deteriorate in a few hundred years. This supports other evidence that Hans Tausen Iskappe melted away completely during the Holocene climatic optimum.

A calculation of the firn-temperature distributions on Hans Tausen Iskappe, using a climate scenario with a temperature 5 K warmer than now and an accu-

mulation rate three times higher than now (an extreme scenario for the Holocene climatic optimum), gives firn temperatures in the central region of the ice cap a few degrees below the freezing point. This indicates that Hans Tausen Iskappe was a cold glacier during its lifetime. Lower surface elevations, either during the period of deterioration of the ice-age ice cap or during the build-up of the existing ice cap, may have further increased the firn temperature. Also, geothermal heat flow causes higher temperature at the base of the ice cap than at the surface. Therefore, we cannot exclude the possibility that some regions of Hans Tausen Iskappe – particularly the high accumulation region to the north – were temperate or experienced basal melting during certain periods of the Holocene climatic optimum.

Acknowledgement

This research was supported by *The Nordic Environmental Research Programme 1993-1997* of the *Nordic Council of Ministers*. Comments by N. Tvis Knudsen and an anonymous reviewer led to improvements of the paper. Results based on GEUS material is published with permission of the Geological Survey of Denmark and Greenland.

References

Braithwaite, R. J. 1995. Positive degree-day factors for ablation on the Greenland ice sheet studied by energy-balance modelling. *Journal of Glaciology* 41(137): 133-160.

CEC 1995. *Climate and Sea Level Change and the Implications for Europe*. Brussels, Commission of the European Communities. Directorate General for Science, Research and Development, Environment Programme (Final report. Contract EV5V-CT91-0051, DGXII).

Clausen, H. B., M. Stampe, C. U. Hammer, C. S. Hvidberg, D. Dahl-Jensen and J. P. Steffensen 2001. Glacio-Chemical Studies on ice cores from Hans Tausen Iskappe, Greenland. Meddelelser om Grønland Geoscience, this volume, pp. 123-149.

Funder, S., C. Hjort, J. Y. Landvik, S. Nam, N. Reeh and R. Stein 1998. History of a Stable Ice Margin – East Greenland during the Middle and Upper Pleistocene. *Quaternary Science Reviews* 17: 77-123.

Huybrechts, P., A. Létreguilly and N. Reeh 1991. The Greenland ice sheet and greenhouse warming. *Palaeogeography, Palaeoclimatology, Palaeoecology (Global and Planetary Change Section)* 89: 399-412.

Keller, K., C. S. Hvidberg, N. Gundestrup and P. Jonsson 2001. Surface movement of and mass balance of the Hans Tausen drill site determined by use of GPS. Meddelelser om Grønland Geoscience, this volume, pp. 115-122.

Ohmura, A. 1987. New temperature distribution maps for Greenland. *Zeitschrift für Gletscherkunde und Glazialgeologie* 23(1): 1-45.

Reeh, N. 1989 (1991). Parameterisation of melt rate and surface temperature on the Greenland ice sheet. Polarforschung 59/3: 113-128.

Starzer, W and N. Reeh 2001. Compilation of a digital elevation model of surface and subglacial topography at Hans Tausen ice cap, North Greenland. Meddelelser om Grønland Geoscience, this volume, pp. 45-56.

Weidick, A. 2001. Neoglacial glaciations around Hans Tausen Iskappe, Peary Land, North Greenland. Meddelelser om Grønland Geoscience, this volume, pp. 5-26.

Locating the Hans Tausen Drill Site

By Niels Gundestrup, Kristian Keller, Thomas Knudsen and Peter Jonsson

Abstract

Gundestrup, N., K. Keller, T. Knudsen and P. Jonsson 2001. Locating the Hans Tausen Drill Site. Copenhagen, Danish Polar Center. Meddelelser om Grønland Geoscience 39, pp. 71-80.

The Hans Tausen drill site was requested to be on a local dome, as high as possible, with a simple flow pattern and with an undisturbed flow pattern even close to bedrock.

The first mapping of the surface elevation was performed as part of a general mapping of the elevation and gravity over Greenland. Later, NASA performed a few overflights of the ice cap. Combining the passes, it was possible to get the main features: A mountainous northern part with complicated ice flow, and two more flat southern domes. The eastern dome was higher, and thus more interesting.

In 1993, a detailed airborne measurement of the surface elevation and ice thickness was performed. Based on this, the southeastern dome was selected as the best drill site. In 1994, the position of the dome, and additional ice thickness measurements were performed from the surface. This located the exact position of the dome, and allowed staging of drilling material the same year. Finally in 1995, additional measurements of surface elevations over the northern mountains and selected parts of the southeast Dome completed the surface mapping.

The measurement showed that the bedrock was very complicated with a south-north ravine separating the two southern domes. Below the southeast dome however the bedrock was relatively flat with an ice thickness of 345 metres and bedrock changes less than 25 metres. This dome was consequently selected as the site for the drilling to bedrock in 1995.

Keywords: Glaciology; digital elevation model; ice radar.

Niels Gundestrup, Kristian Keller, Thomas Knudsen, Department of Geophysics, University of Copenhagen, Juliane Maries Vej 30, DK-2100 Copenhagen Ø, Denmark

Peter Jonsson, Department of Engineering Geology, Lund University, Box 118, S-221 00 Lund, Sweden

Introduction

Locating a suitable drill site involves a number of compromises. Ideally, the drilling should be performed on a site with minimal ice flow, now and in the past. The site should be cold, and the summer temperatures should be as low as possible because surface melting will influence the records from the ice core. Next, the bedrock should be flat in order not to disturb the ice flow close to bedrock, and thereby the oldest ice records. The accumulation should be within certain limits. If the accumulation is high, the ice core may be dated by counting annual layers, if it is low, the

longest time record is obtained. In practice, not all criteria can be satisfied, and the selection involves significant compromises.

In selecting the Hans Tausen drill site, the dating problem was not considered as significant. A number of well dated volcanic layers in other Greenland cores should be recognisable in the Hans Tausen record, and this should ensure a dating in agreement with the Greenland records. Therefore a low accumulation was of higher priority.

In order to satisfy the criteria about minimal ice flow, the site should be chosen on top of a local dome, or possibly on a gently sloping ice divide. Thus the search for the drill site was concentrated on these points.

Previously, very little was known about the topography of the Hans Tausen ice cap in spite of two shallow drillings in 1975 and 1976 respectively. Both of these drilling sites were chosen based on an old U.S. Army map. Thus the position of the 1975 site is only known with significant errors (several kilometres). The 1976 site was determined by an early Transit receiver.

Recently, the National Survey and Cadastre – Denmark (KMS) has published ortho photo maps of the area. These maps have excellent accuracy and details, except on the ice due to lack of contrast. By examining these maps, it was determined that the ice margin was close to the 900 m contour. Next, three profiles from the American gravity project (Brozena 1991) provided some information. Supplemented by five NASA P3 profiles, it was possible to draw the first map of the ice cap surface topography. In 1993, intensive Twin Otter based surveys revealed surface and bedrock. In 1994, the site was selected, and materials staged on the site. Finally, during the drilling in 1995, several surface traverses supplemented the measurements of the surface topography.

In summary, the selected drill site satisfied most of the criteria: It was on a dome, the bedrock was very flat, the accumulation low and the surface ice velocites low and regular.

Knowledge prior to the 1993 survey

No regular map exists of the Hans Tausen area due to its remote location. Both the 1975 and 1976 shallow drillings used a 1957 U.S. Army map, 1:250.000, Series C501, Sheet NU 19-24,8 Edition 1-AMS. This map has errors in the order of 30 km, in addition to scaling errors. The navigation method used by the helicopters supporting the 1975 and 1976 drilling was dead reckoning, using compass and stopwatch based on a fixpoint on a glacier. This navigation showed its limits, when another outlet glacier was used as fixpoint: Then it was not possible to locate the same points on the ice cap. The 1975 site was chosen as being close to the staging point at Aftenstjernesøen, and on an ice divide as judged from visual observations from the helicopter. The actual position is only known within several kilometres.

In 1976, the same type of navigation was used. But because a prototype Transit geodetic receiver was available, the position of the drill site could be measured. Also a primitive measurement of the ice thickness along a triangular pattern on the southern part of the ice cap was made. Although the radar thickness measurement was limited due to the limited endurance of the helicopter, the sounding revealed a deep trough through the ice cap, dividing it into two separate ice fields. Based on this measurement, the 1976 drill site was chosen on the eastern part of the ice cap with ice thickness less than 300 m. The actual drill site was even further east because of navigation problems.

Both of these years no surface measurements were performed. Thus except for the Transit based fixpoint, no addi-

tional topographic information was collected. In the eighties, KMS produced ortho photo maps of the northern part of Greenland, including the Hans Tausen area. These maps are quite detailed. The accuracy is high due to numerous satellite determined fixpoints. These maps indicated that the ice margin was close to the 900 m contour line, but gave no details for the interior of the ice cap due to lack of contrast.

In 1992, 5 crossings were made by a NASA P3 on our request (Krabill *et al.* 1995). These crossings covered the ice cap reasonably, and were supplemented by 3 crossings by Naval Research Laboratories (NRL). The Navy aeroplane used a radar altimeter, the NASA P3 a scanning laser altimeter. Both soundings had unknown errors due to the long distance to the reference GPS receivers. Also, both of the airborne measurements were referenced to the ellipsoid, whereas the 900 m contour was referenced to sea level. A cross over analysis indicated 5 m internal errors in the NASA measurements, and 20 m for the NRL measurements. In an iterative process, a bias was added to each pass to minimize the crossing errors. Next, a common bias was added to all passes making the crossing agree at the 900 m elevation contour. In this adjustment, crossings that occurred at steep slopes were not used. Finally, the data was gridded and used to produce the topography in Fig. 1. The topography was compared with an ERS1 SAR image of the ice cap. The SAR image was enhanced to show the approximate location of the ice divide, and this agreed well with Fig. 1.

Although the data was limited, the resulting map shows a highly structured ice cap, having 4 different regimes: The Northern part seemed mountainous. The Northern part is connected with the 3 southern domes by a narrow tongue. The larger southern area had 2 clearly defined domes, of which the eastern could be separated in up to 4 individual

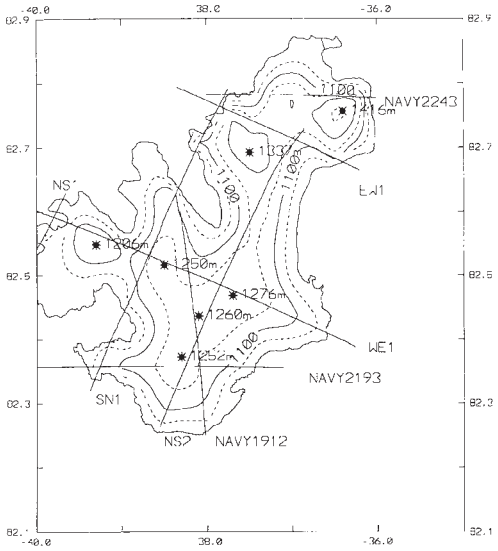

Fig. 1. The Hans Tausen ice cap topography based on 3 Navy radar altimeter crossings, and 5 NASA P3 laser altimeter crossings. The cross over between the flight lines are used to correct the elevation of the profiles, and the resulting topography is adjusted to the 900 m contour line from a ortho photo map. The icecap is highly structured with several potential drilling sites marked.

dome structures, although the elevation difference between the individual domes was minor. All domes seemed possible drilling sites, although the point marked 1276 m seemed the most promising considering its elevation and position along the major ice divide. Although the northern part of the ice cap had higher elevations, it appeared too undulating. In order to select the best site, radar measurements of the ice thickness was needed.

1993 radar survey, description of the equipment

The radar used was the Electromagnetic Institute 1kW pulse radar, originally developed in 1968 (Lintz Christensen *et al.* 1970). The radar has a operating frequency of 60 MHz, and a pulse length from 60 ns to 1µs. Receiver bandwidth is 14MHz to 1 MHz. Originally, the radar output was stored in an analog fashion on films, requiring a later digitalisation process. Although the radar is aging, it was still considered in good working condition. The data treatment however was outdated, and a new digital system had to be developed.

The radar recording consisted of two parts: The position of the aeroplane was

determined by GPS in differential mode. Although the GPS receiver (Trimble 4000) was capable of dual frequency reception, only a single frequency flight worthy antenna was available. The data was recorded each second on a laptop PC, both in the aeroplane and at the reference site at Station Nord.

Originally, the radar output was differentiated prior to recording in order to enhance the forefront of the reflections. It was decided to design a recording system that would store the unprocessed reflections. Also, a direct hardcopy readout was required to verify the radar results.

The averaging and digitalisation of the received waveforms was performed by a Tektronix sampling scope. The scope was interfaced to a laptop PC using an IEEE bus, and the average of 70 waveforms was downloaded each second. The load on the PC was high. Each second, the averaged waveform should be downloaded, saved on disk, differentiated and printed. It required programming optimized for speed in order to accomplish all the tasks, but the resulting system was working very well, and the real time hardcopy profile was of great value. The radar transmitter and receiver share a single antenna. It is a quarter wavelength dipole mounted horizontally out from the aeroplane body, which thus functioned as a vertical mirror. The antenna is the same as used earlier at the Renland recognisance (Johnsen *et al.* 1992). The resulting specifications are:

1. Sample rate
The nominal speed of the ski equipped Twin Otter aeroplane is 140 kn. The take off speed is 60 kn. It is wanted to fly relatively slowly, but also to have some potential for keeping a constant height over the ice cap. Thus, the nominal speed is 100 kn, corresponding to 180 km/h or 50m/s. The total position error should not be more than 100m. Therefore the sample rate is 50m, corresponding to one sample per second.

2. Digitizing rate
The nominal pulse length of the radar is 250nsec and a 4MHz receiver bandwidth with a minimum pulse length of 80nsec and 14 MHz receiver bandwidth. To a 4MHz bandwidth corresponds a time constant of 40ns. Thus, the sampling rate should be a minimum of 40 nsec in order to preserve all information. The wave speed in ice is 170m/μs, and a sampling rate of 40 ns thus corresponds to 170/2*0,04m= 3,4 m.

3. Digitizing window length
From the 1976 survey, the maximum ice thickness expected is 800m. This corresponds to a time delay of 2*800/170 μs= 9,4 μs. The maximum expected flying height is 300 m above the snow surface, corresponding to a 2-way travel time of 2 μs. Finally, the sweep starts 2 μs prior to the transmitted pulse. Thus, the minimum window length is 9,4+2+2 μs= 13,4 μs. Thus, a window of 20 μs ensures sufficient margin. The nominal window length is 500 samples. With a length of 20 μs, the resolution will thus be the requested 40 ns. The 20 μs window allows a maximum ice thickness of 1,3 km to be recorded.

4. Storage requirements
The digitized waveform has a resolution of 12 bits, corresponding to 1:4096. For storage, this was reduced to 3 digits (0 to 999). Because the values are recorded in ASCII format with a delimiter, each sweep generates 3000 bytes. The hourly production is 3000*3600 bytes/hr= 10,8 Mbytes/hr. A 5 hours run will thus produce 54 Mbytes. This amount of data is compatible with a 128MB magneto optical drive.

5. Elevation measurements
In order to get the best possible ice thickness measurements, it is desired to fly at

nearly constant elevation over the ice sheet. The elevation should be as low as possible, considering a safe flight as well as a well defined echo from the surface. The estimated minimum flight elevation is 80m. Because the aeroplane is not flying at constant elevation, it is required to know the 3 dimensional position of the aeroplane in order to calculate the surface elevation height. The performance of the GPS receivers and its associated software is thus critical.

6. Real time profile printout

In order to check the radar performance, and to give a direct printout of the profiles, the Z (differentiated) radar output is printed in real time. The differentiation is performed in software. Because the printer needs to print in real time, an inkjet printer was selected for the output. The capacity of the computer logging the radar returns was limited, and imposed severe restrictions on the processing that could be done during the flights. By using a 2*2 matrix to generate 4 levels of gray, 150 dpi resolution and flying 180 km/hr, a lengthscale of nearly 1:150.000 was achieved. The logging rate was 1 per second, corresponding to 50m. Although primitive, the real time printout worked very well, and made it possible to change flight plans depending on the survey results.

7. Aeroplane specifications

The aeroplane used was a Twin Otter based at Station Nord in Northeast Greenland. The nominal time airborne is 7.5 h using two 300 l ferry tanks, and an air speed of 140 kn or 260 km/h. The fuel consumed per mile is virtually constant down to a velocity of 90 kn, and the fuel consumption is 330 l/h at 140 kn. Additional fuel is also needed for landing on the ice cap Flade Isblink, in case landing at Station Nord is not possible. The two way distance between Station Nord and Hans Tausen ice cap is 700 km, corresponding to 2.7 hrs. This leaves fuel for 7.5 – 1.5 – 2.7 hr = 3.3 hrs over the ice cap at 140 kn, or 4.6 hr at 100 kn. The maximum survey per flight is thus 460 nm or 850 km. In practice, the achieved endurance was less, because the constant change in flight level due to the ice cap topography required much fuel.

Normally GPS satellites with an elevation angle of less than 10^0 are not used in the processing. Thus, the maximum tilting of the aeroplane should be less than 10° in order to keep tracking all satellites while the aeroplane turns. With a speed of 100 kn, this corresponds to a turning diameter of 2.6 km. Thus, the nominal turning diameter was 3 km corresponding to a curve length of 4.7 km and a time of 1,6 min.

1993 airborne survey

The survey had two purposes: to make a general mapping of the ice cap, and a more detailed mapping of the most promising area. Due to the constraints of the turning radius, the main lines were 1,8 km apart, with 900 m line spacing in the key area. The GPS reference was at Station Nord, tied to the local geodetic marker. Prior to the flight, all way points were programmed in the GPS, so in theory the pilots should just follow a straight line, make a curve with 1 nm radius and continue on the next while keeping a nearly constant flight elevation over the ice cap with a minimum elevation of 250 feet. In practice, this was not possible. First, the distances between the way points were so small, that unless the aeroplane was exactly on track and with the correct heading, the GPS navigator would assume that a nearby way point was passed, and switch the route ignoring the intervening tracks! Next, the surface was changing so rapidly that it was not possible to keep a constant distance to the ice cap surface. As a result, the aeroplane had to follow a more gently varying flight level.

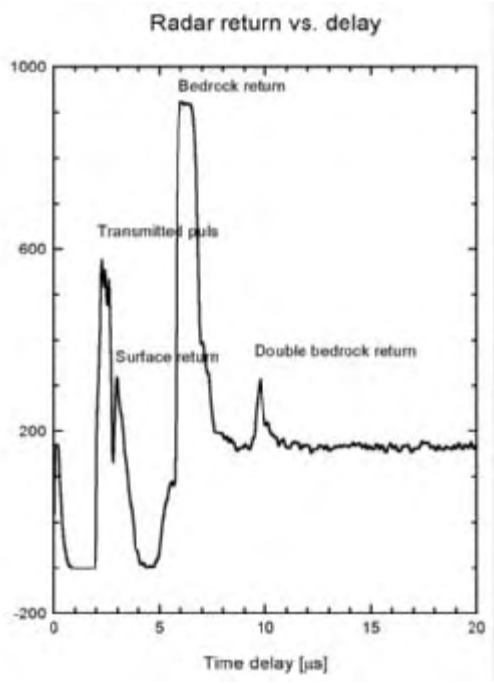

Fig. 2. Radar waveform as recorded during the measurements. The recording starts 2 µs before the pulse is transmitted. The surface return is 0,82µs after the transmission corresponding to a flying height of 123 m. The bedrock return saturates the receiver, and a double bedrock return is also recorded.

It was originally planned to use also a GPS reference at the ice cap. This was only used one day, because first the aeroplane could not land on the ice cap directly from Station Nord due to landing weight restrictions, and secondly the surface was quite warm, demanding much fuel to take off. As a result, all airborne measurements are referenced to the GPS station in Station Nord.

A typical radar return is shown in Fig. 2. The recording is started 2µs before the 250µs pulse is transmitted. On the recording, the transmitted pulse appears jagged. This is caused by attenuation by the transmit/receive switch, and the receiver suppression. The surface echo is recorded 0,82µs later corresponding to a flying height of 123 m. The bedrock echo is very strong, saturating the receiver. It has a two way travel time of 2,93µs. The measured ice thickness is thus 248 m using a wave speed of 169 m/µs in the ice. Finally, a double echo is recorded. This echo is the bedrock reflection as reflected by the aeroplane, and later by the bedrock. No internal layers in the ice cap is recorded. This is partly due to the reduced receiver sensitivity in the first microseconds after the pulse is transmitted. Later, it was learned that the ice cap had little ice accumulation and high summer temperatures. Due to this, the internal layering is difficult to detect with the present radar.

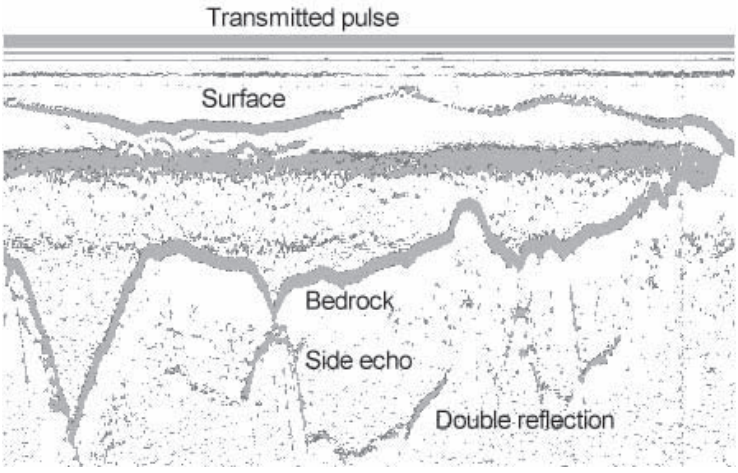

Fig. 3. Profile from a crossing over the drill site. The top line is the transmitted pulse. The surface return shows a changing flight elevation. The dark line is an artifact. West the deep trough is recorded, followed by a profile with almost constant ice thickness. At east, the ice thickness is recorded to the margin of the ice cap.

Fig. 3. shows a recorded west-east profile passing near the drill site. The upper line is the transmitted pulse. It is divided into several lines due to the differentiation of the signal. The surface echo is clear, although weak when the aeroplane passes the crest of the ice cap, and the distance between the aeroplane and surface is minimum. The broad dark line below the surface is an artifact caused by the regulation of the transceiver gain. The deep trough is clearly measured, although the horizontal resolution is limited because the radar always picks up the nearest point. In an area with fast changing bedrock topography, the radar will not be able to resolve the bedrock. It can also be seen, that the trough may in fact be deeper than indicated. Several double reflections are measured, as well as a nearby mountain. The ice thickness is measured to the edge of the ice cap. No internal layering is detected. Although the profile shows several artifacts, both surface and bedrock is easily identified.

The digitized profiled is shown as Fig.

4. At left (west) the trough is shown to be deeper than 600m. It is also clear, that the V-shape may be caused by lack of resolution. The position of the drill site is indicated. It is placed near the center of an almost flat horizontal part of the bedrock. This should assure that the flow of the glacier ice is not disturbed by bedrock undulations.

A corresponding ice thickness profile for the northern part of the ice cap is shown in Fig. 5. The horizontal scale is approximately the same as for Fig. 4, and the track of the profile is indicated in the insert. Compared to Fig. 4, the area is highly mountainous, and the ice flow will be disturbed by the rapidly varying ice thickness. Clearly this area is not optimal for an ice core intended to cover many years of undisturbed ice flow.

Fig. 6. shows the resulting surface topography with all measured points indicated. Most lines are from the airborne sounding, easily recognised by the gentle curvature between the lines. The airborne measurements are supplemented by an intensive grid around the drill site, and some longer surface tracks. One such track goes from the drill site to the northern ice cap. It passes over 4 domes. The northernmost dome was the staging point for the "Hare Glacier" study, and the tracks made by this study indicate the glacial outlet.

The processing of the map was not easy. The 3-dimensional position of the aeroplane was computed by differential GPS with respect to the GPS receiver at Station Nord, and the distance from the aeroplane was obtained from the surface return of the ice radar. In general, the elevation thus measured is accurate to 10m or better, but at times the translocation program (Trimble Post-nav II) had a tendency to be unstable. This resulted in significant elevation errors. In order to assure a high precision of the data, the results from the Trimble program was passed through a filtering program. This program identified all less accurate positions using several methods, including the estimated error from the program, and the vertical velocity of the aeroplane. All doubtful points were removed from the database, and are not indicated here. The parameters in this selection process demanded some trial and error, but as indicated by the shape of the map, it was highly successful. The instability is very likely caused by the use of only a single frequency antenna combined with the relatively long distance to the reference at Station Nord and poor vertical geometry of the GPS constellations.

The surface measurements are referenced to a GPS receiver near the drill site. They are processed kinematically, and have a relative accuracy of 10cm. The 900 m contour line from the ortho photo map is used as border line. Compared with Fig. 1, the map is significantly more detailed, although it is sur-

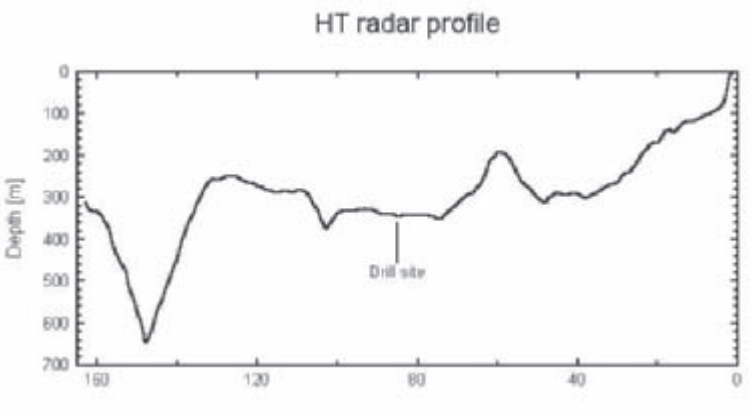

Fig. 4. The same profile digitized. The drill site is marked. Because the radar records the first return, the shape of the trough can not be resolved. It is seen, that the drill site is in area with very smooth bedrock. The profile spans 22 km.

Fig. 5. Profile from the north part of the ice cap. The ground track is indicated in the insert. The area is quite mountainous, with ice thickness rapidly varying between 100 and 400 m.This topography makes the area unsuitable for a drilling to bedrock.

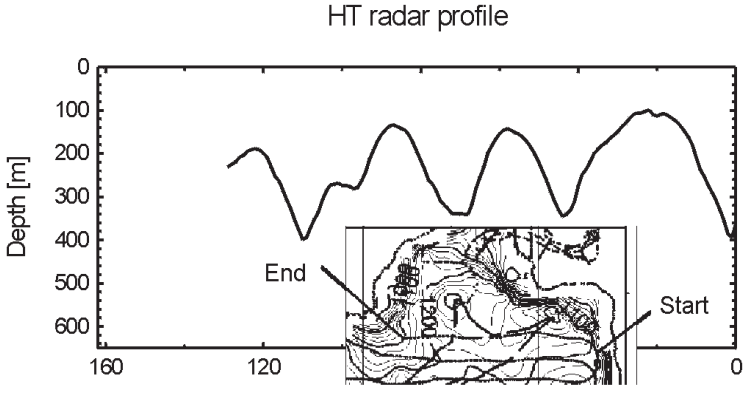

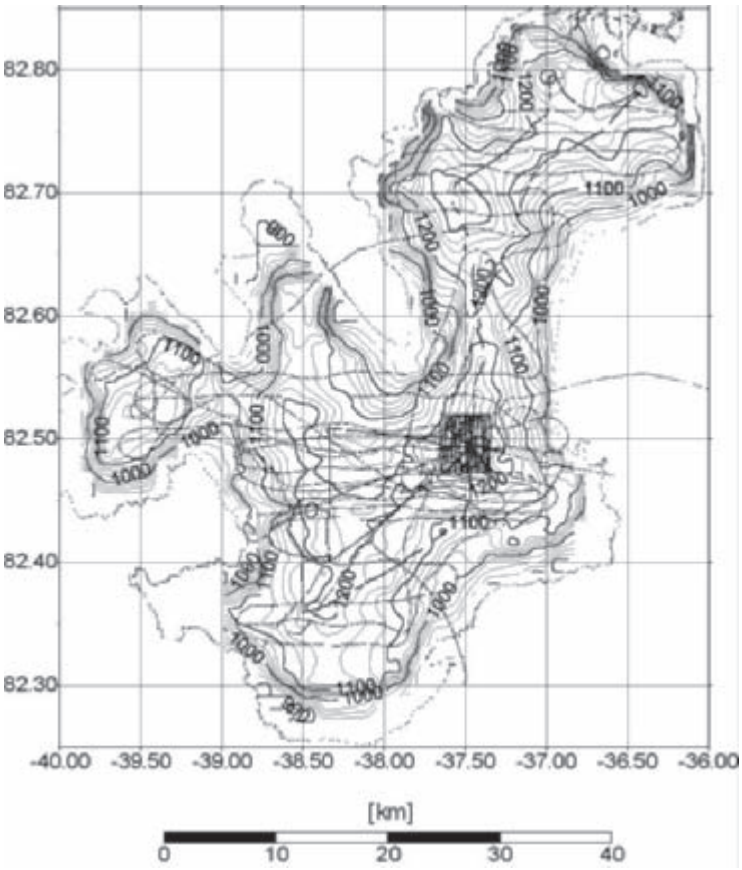

Fig. 6. Surface topography with all measurement lines marked. The densely hatched area is near the drill site. The flight lines have been chosen to give a good representation of the topography of the ice cap, with additional flight lines at the most promising places.

prisingly to see how well Fig. 1 compares with the final map.

The bedrock topography as measured by the airborne soundings is shown in Fig. 7. Only the two southern parts of the ice cap as separated by the deep trough draining the area, has areas which are flat, and thereby useful for the drilling. Based on the surface elevations, the area around 82.5N 37.5W was selected as the position for the drill site.

Based on the 1993 airborne measurements, the general location was thus determined. In 1994, it was the purpose to identify the exact location of the top of the dome, and later to stage material there for the 1995 drilling. Also, the detailed topography of both bedrock and surface should be measured close to the drilling site. The first aeroplane landing at Hans Tausen brought surveying equipment to locate the exact top of the dome. This was easily done because the aeroplane landed very close to the site. The camp was erected, and after a few days, the surface program started. The intention was to measure the topography, and at the same time install poles for a strain net around the drill site.

The resultant surface topography is on Fig. 8. Also, all measurement points are marked. The dome is very regular, indicating a regular ice flow. The surface

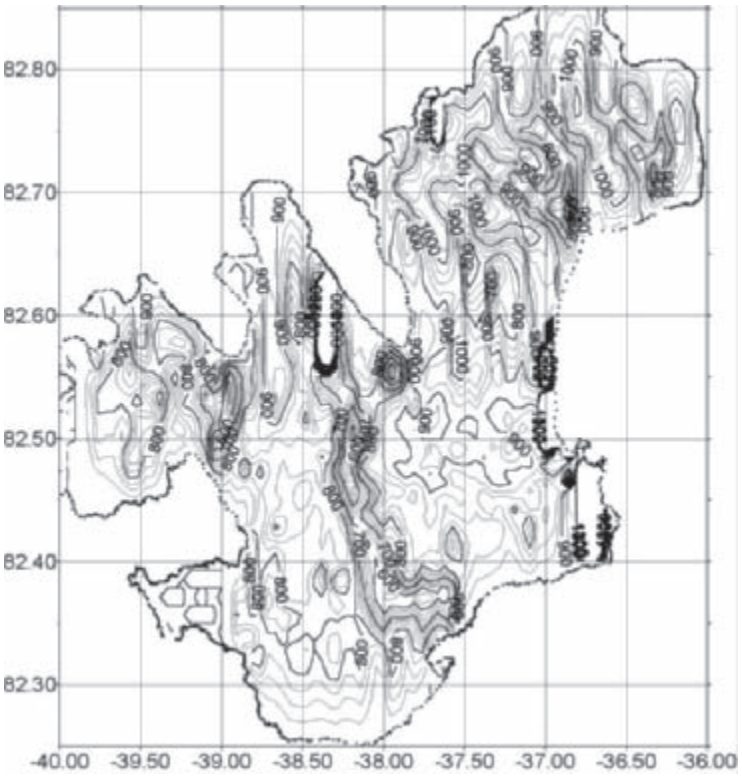

Fig. 7. Bedrock of the ice cap. The mountainous northern part and the deep trough separating the two southern domes are recorded. In general, the bedrock topography is quite irregular, and only around 82.5N 37.5W is there an area with less undulations.

measurement lines were intended to be 300 m apart. However part of the measurements had to be made in low visibility conditions with visibility down to 40 m. Although the navigation was based on GPS receivers, it was very difficult to follow a straight line in white out conditions as seen on the figure.

The bedrock topography is shown in Fig. 9. Although the figure is only based on the airborne measurements, it clearly indicates, that the bottom is flat, with changes not exceeding 20 m (6 percent of the ice thickness) near the drill site.

Summary

Both surface and bedrock of the Hans Tausen ice cap has been measured. In addition to providing a general mapping of the ice cap, a position optimized for the drilling has been found. The selected drill site has a combination of low accumulation, flat bedrock, and local well defined dome, making it close to an optimal drilling site with only few trade offs. The site selection was performed through several steps, taking 3 years. First a preliminary map was constructed from aeroplanes passing the area in connection with other projects. Based on this map, a general airborne survey was executed, later followed by surface measurements for both the exact position of the drill site, and for mapping special features. In summary, all the objective of the site selection process was fulfilled.

Acknowledgements

This program has been sponsored by *The Nordic Environmental Research Programme 1993-1997* of the *Nordic Council of Ministers* under contract 93005. Part of the program has been performed jointly with the GRIP deep drilling program in Central Greenland. The Danish Defence Command allowed the program to be based at the Danish stronghold in Northeast Greenland, Station Nord. The personnel at Nord showed their extremely cooperative attitude allowing us to operate whenever the weather was good, independent of the time of day (or night). In addition, they performed routine radio check both during flights, and later during the drilling.

The airborne survey had not been possible without the skill and dedication of the Flugfelag Nordurland's crew headed by Captain Ragnar Magnusson. The survey required the Twin Otter aeroplane to follow the designated tracks very closely. At the same time, the flight level was changed constantly. Because the aeroplane has no autopilot, this demanded constant attention by the crew.

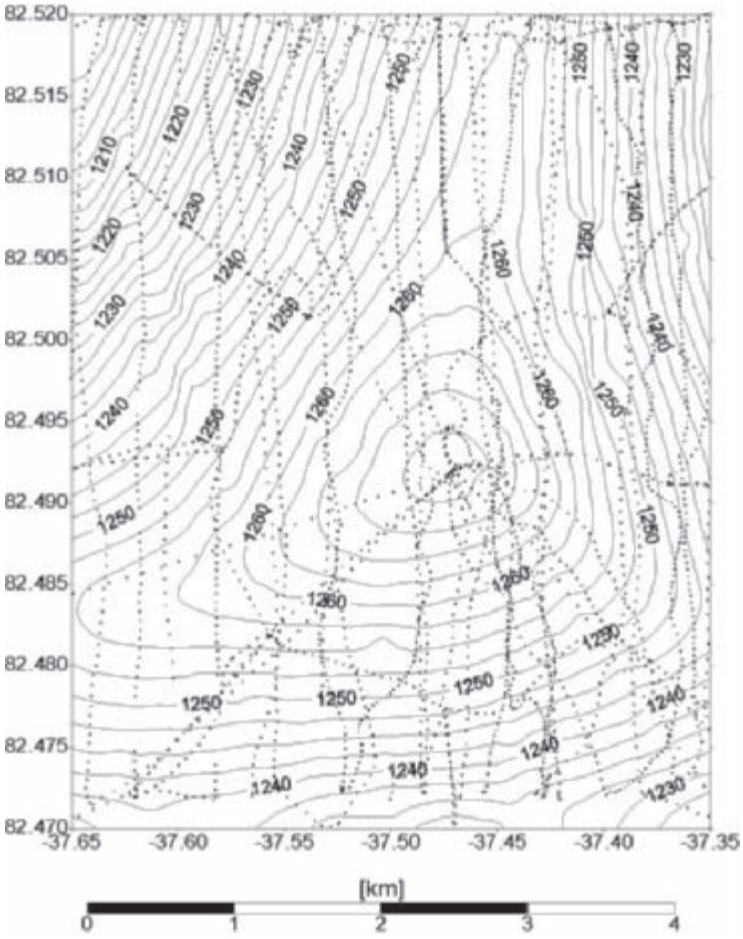

Fig. 8. Surface topography around the drill site based on surface kinematic measurements. All measurement point are marked. The dome is quite regular with a size of around 1 km, or 3 times the ice thickness.

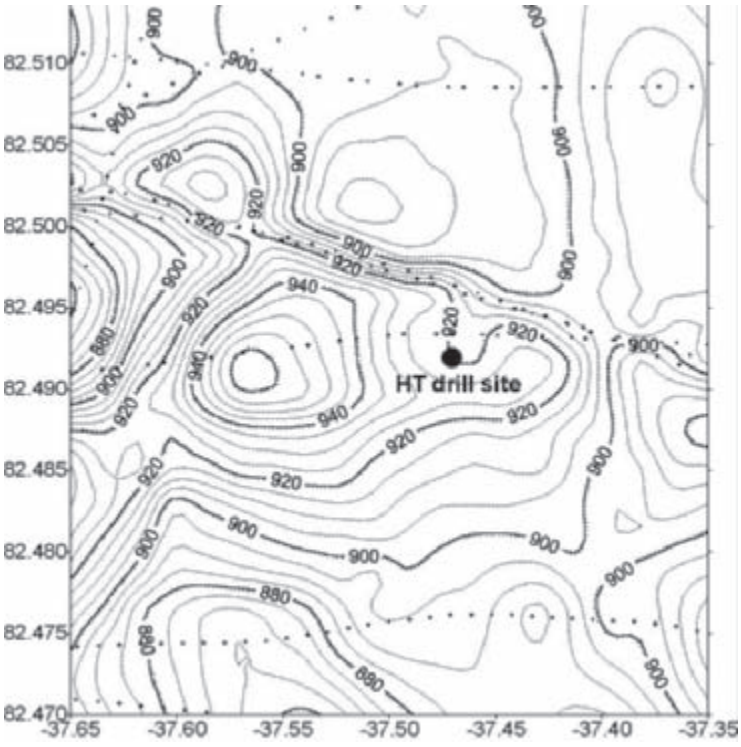

Fig. 9. Bedrock topography around the drill site based on the airborne measurements. All measurements pointes are marked. The contour lines are hatched downstream. The bedrock is relatively flat, with changes of about 20m.

References

The Greenland aerogeophysics project: Airborne gravity, topography and magnetic mapping of an entire continent. In: *From Mars to Greenland: Charting gravity with space and airborne instruments*, pp. 203-214. Springer Verlag.

Gudmandsen, P. E. 1971. Electromagnetic probing of ice. – In: J. R. Wait (ed). *Electromagnetic Probing in Geophysics*, pp 321-348. Galem Press, Boulder, Colorado.

Johnsen, S. J., H. B. Clausen, W. Dansgaard, N. S. Gundestrup, M. Hansson, P. Jonsson, J. P. Steffensen and A. E. Sveinbjörsdottir 1992. *A "deep" ice core from East Greenland*. Meddelelser om Grønland, Geoscience 29: 22 pp.

Krabill, W., R. Thomas, C. Martin, R. Swift and E., Fredrick 1995. Accuracy of laser altimetry over the Greenland Ice Sheet. *International Journal of Remote Sensing* 16: 1221-1222.

Lintz Christensen, E., N. Gundestrup, E. Nielsson and P. Gudmandsen 1970. *Radioglaciology. 60 MHz Radar*. Laboratory of Electromagnetic Theory. Technical University of Denmark.

An impulse radar measurement in NE Greenland

By Peter Jonsson

Abstract

Jonsson, P. 2001. An impulse radar measurement in NE Greenland. Copenhagen, Danish Polar Center. Meddelelser om Grønland Geoscience 39, pp. 81-86.

A snowmobile towed impulse radar measurement was used to produce detailed maps of ice-thickness in two areas, one on a local dome (the Hans Tausen ice cap), and one on an outlet glacier north thereof. A constant spatial sampling was achieved by using a device attached to the snowmobile's odometer. The bedrock reflection was automatically detected in the majority of the data, by using digital signal processing techniques. After merging with differential GPS positions and elevations, a digital database of these parameters and the bedrock reflection times is presented as contour maps.

Keywords: Impulse radar, ice-thickness, constant spatial sampling

Peter Jonsson, Department of Engineering Geology, Lund University, Box 118, S-221 00 Lund, Sweden, email Peter.Jonsson@tg.lth.se

Introduction

The Hans Tausen ice cap, Western Peary Land, Northeast Greenland, has previously been investigated by shallow drillings in 1994 and 1995, and by an airborne radar survey in 1993, as well as earlier (Gundestrup *et al.* 2001). The objective of the survey described in this paper was to produce detailed maps of ice-thickness for two areas, one on the ice cap and one on an outlet glacier north thereof. The ice cap measurements should assist in locating an ice core drilling to bedrock made by the Department of Geophysics, University of Copenhagen, on a dome situated near 82°50'N, 37°50'W, in the SE part of the ice cap. The surveyed outlet glacier is located near 82°80'N, 36°60'W. These measurements were made for the Geological Survey of Denmark and Greenland (GEUS), formerly the Greenland Geological Survey (GGU), along and perpendicular to assumed flow lines, and on a local dome (Thomsen *et al.*, 1996).

Data collection equipment

The measurements were made with a snowmobile towed impulse radar system. All equipment was powered by a gasoline generator and pre-assembled so that the system could be operational in a few hours after arrival. The impulse radar system used was a Geophysical Survey Systems, Inc. (GSSI) model SIR-8, which was modified for glacier soundings to allow for a longer range (7765 ns) than the standard instrument. A technical description of the radar and antenna is found in Morey (1974), while the system performance figures stated below were compiled from Annan and

Davis (1977), Morey and Kovacs (1982) and Schutz (*pers.comm)*.

The transmitter, attached directly to the transmitting antenna, is a high voltage (1 kV) pulse generator, which produces impulses with a pulse repetition frequency (PRF) of 25.6 kHz, an applied peak pulse power of 5 kW, a rise time of 2 ns, and a duration of less than 10 ns. Two identical antennae of folded dipole type, GSSI type 3100, were used in a bistatic mode with an antenna separation of 4 meters. The antennae have a center frequency of 120 MHz, an antenna gain of 2 dB, and an efficiency of –13 dB. The transmitted broadband signal had a total pulse length of 12 ns and an estimated –3dB bandwidth of 60% of the center frequency, or approximately 120±35 MHz. The receiver operates as a repetitive sampling device, synchronized to the PRF. After applying a voltage gain of 19 dB, the signal is downsampled to provide 25.6 sampled signal scans per second. The downsampled scans are in the audio range, and with each downsampled signal scan a start-of-scan strobe is generated. The minimum detectable signal power at the center frequency is estimated to $4 \cdot 10^{-11}$ W, which combined with the parameters above yields a system Q value of –141 dB. The maximum possible range is 7765 ns. To establish the time scale a crystal controlled calibrator that sends out a calibrated 100 MHz signal was substituted for the antennae and recorded after each profile was measured.

The antennae were towed on wooden sleighs behind a snowmobile, separated by 3 m long, 1″ aluminum distance rods. To facilitate downhill measurement the towlines were crossed. This crossing design, in combination with the rigid distance rods, made the antennae sleighs steer in a zigzag pattern, much like a downhill skier, which decreases speed.

To provide data recordings with a uniform spatial sampling distance, a device was used that distributes the recorded signals evenly along the track without loss of synchronization between the radar start-of-scan strobes (see above) and the recorded signals. The device works by blocking the start-of-scan strobes (SOS) from the radar control unit until an adjustable number of pulses have appeared from a rotary sensor fitted to the snowmobile odometer. When the desired pulse count is reached, the next occuring SOS is allowed to pass. The number of odometer pulses that must occur before the device lets a SOS through is adjustable, to allow for different spatial sampling rates, i.e. different scales. The settings used in the measurement gave three recorded pulses per meter of track length. The maximum delay between an odometer pulse and a SOS pulse is less than the distance in time between two SOS, which is 39 ms. At a nominal speed of 1.5 m/s this corresponds to a horizontal, along-track, positioning error of less than 6 cm.

A four-channel audiocassette tape recorder was used to store the data. All received radar scans were stored on one channel, and their corresponding SOS pulses on another. The length scale sorted SOS pulses were stored on a third channel. By storing both sorted and unsorted SOS pulses, maximum flexibility was retained. For example post-processing such as stacking, could be performed without any loss of length scale fidelity.

A hand-held GPS receiver in standard positioning (SPS) mode was used to perform on-site navigation. In addition, stakes and flags were used to define endpoints and flowlines. Positioning of the measured lines was made with kinematic post processed, differential GPS with a precision better than one centimeter, which was provided by Department of Geophysics, University of Copenhagen, in 1994 and by GEUS in 1995. The reference station was established

locally, tied to a reference station at Station Nord.

Data set and post-processing

The data were in field recorded as an analog signal on standard audiocassette tapes, and also on paper, as a backup and for immediate in-field quality control. The ice cap measurement consists of approximately 135 km of profiles on 22 tapes. The outlet glacier data set is slightly more than 70 km of profiles, on 20 tapes.

In the first post-processing stage, the tapes were computer digitized with a sampling frequency of 50 kHz, in a semi-automated process. The recorded analog scans were band pass filtered (200 Hz—10 kHz) prior to digitizing to remove noise, and to provide anti-aliasing. In the digitizing process, each digitized scan was assigned a header with a time-tag showing the time it was collected. Using a lookup-table with time as key and the GPS positions measured in field as values, a position was assigned to each scan.

To identify the bedrock reflection, an automatic method was used. The envelope $E(t)$ of each digitized scan $s(t)$ was calculated as the magnitude of a (complex) synthetic analytic signal:

$$E(t) = |s(t) + j\mathbf{H}(t)|,$$

where **H** denotes the Hilbert transform. After blanking of the first 800 ns of the scan, which contains the transmit pulse and surface effects, the position of the maximum value in the squared envelope of the scan, $E^2(t)$, could be used to detect the bedrock reflection. An example of a digitized profile, named N6, and the detected bedrock reflection, are shown in Fig. 1.

The detection method described above was successfully used for all the ice cap data, but it failed in more than 30% of the outlet glacier data set, mainly due to shallower ice depth, which made the bedrock reflection interfere with the initial part of the signal. The signal-to-noise ratio for the outlet glacier data was also lower in some areas. When automatic detection failed, the segment in question was manually interpreted, and data was interpolated to the same data density as the automatically processed

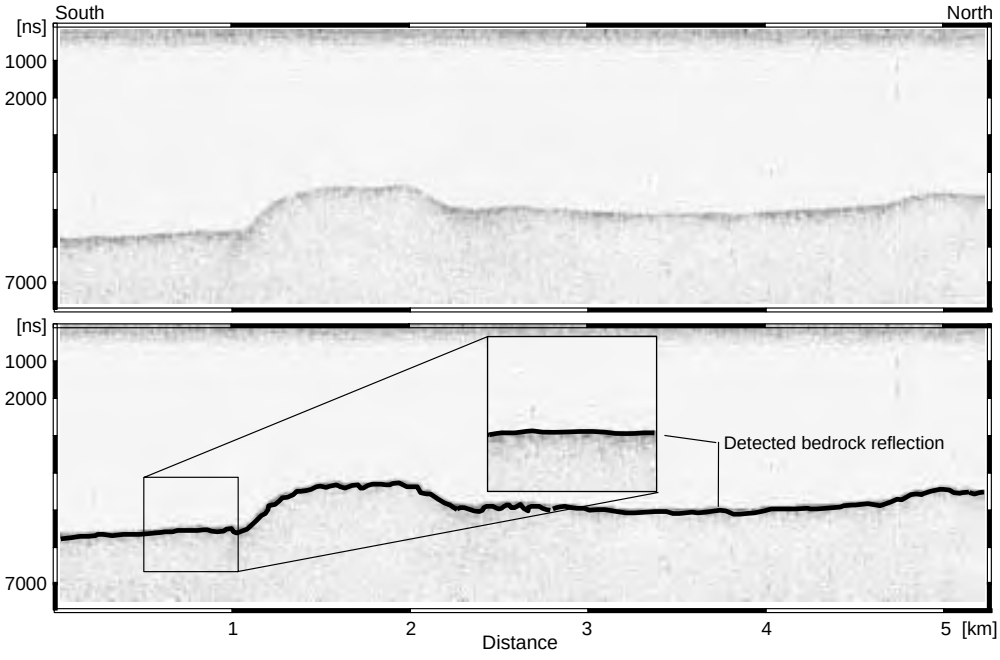

Fig. 1. An example of a digitized profile, northbound N6 in the ice cap dome area – see Fig. 2 for a location map. The two-way time range of the plot is 7765 ns, and the length is 5.2 km. In the upper part of the figure a raw plot of the profile is shown. Below is shown the resulting computer detected bedrock reflection, together with a detail.

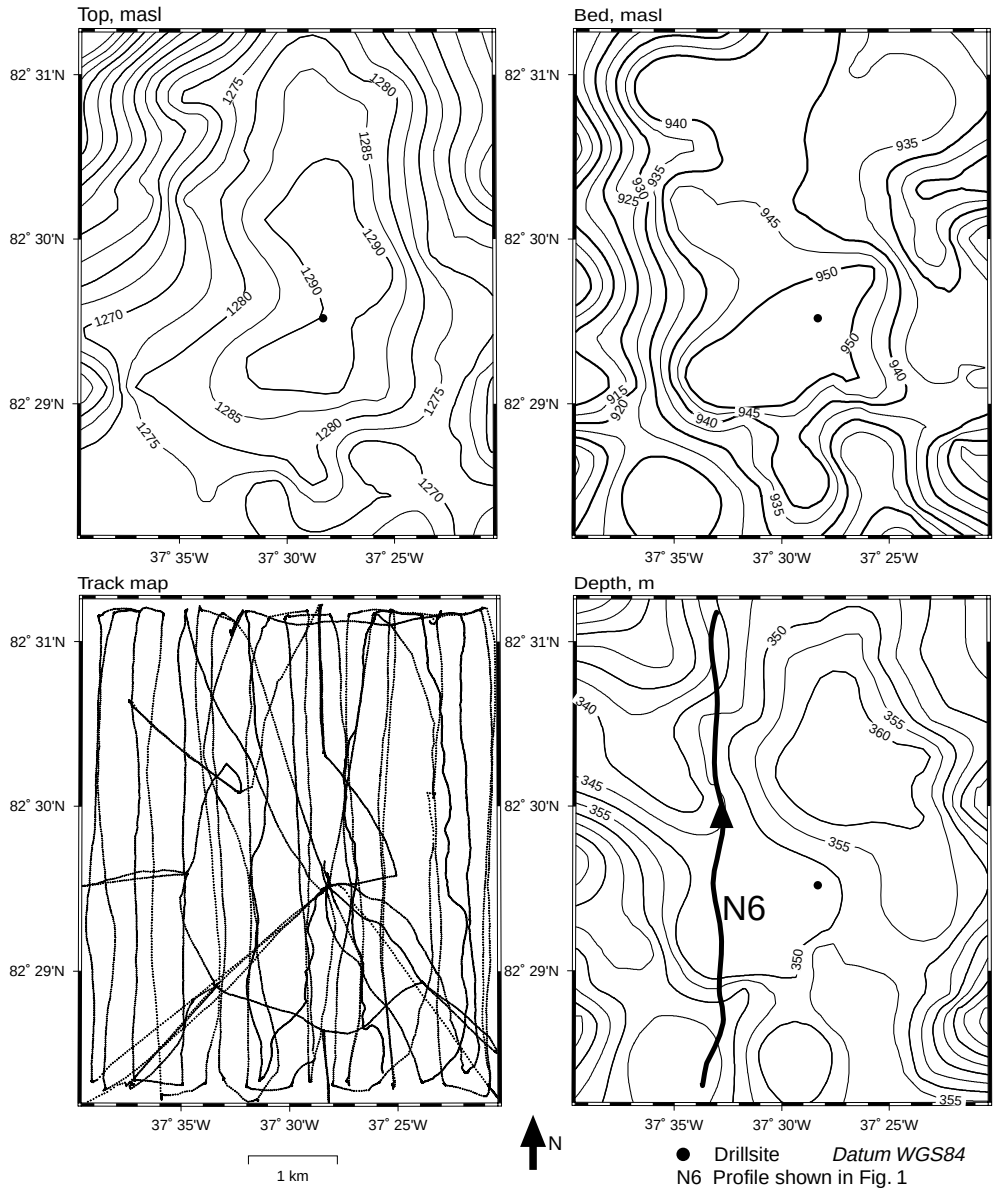

Fig. 2. Result from the evaluation of the measurement in the ice cap dome area. Isoline distance 50 m. The lower left figure shows the surface tracks where profiling was performed, the lower right is the resulting ice depth model (see text). The line N6 in this figure is the location of the profile shown in Fig 1. The upper left figure shows the snow surface elevations from the GPS measurements, while the upper right is the glacier subsurface model, resulting from the elevations and the thickness measurements.

profiles. As a final step, the information in the headers was updated to include the detected time-of-flight to bedrock reflection in nanoseconds. In all profiles, a recorded 100 MHz signal from a calibrator was used to establish the time scale. The result is a database with digitized raw radar scans for each of the two field areas, their corresponding positional data and time of acquisition, and detected bedrock reflex time-of-flight.

To reduce the amount of data, the reflection times were gridded to a lower resolution grid, with divisions of approximately 100x100 m (ice cap data) and 150x150 m (outlet glacier data). The median value of the detected times falling inside a division was used. After gridding, the ice cap data consisted of a database with 8065 entries, whereas the outlet glacier data totals 7203 entries. Each entry consists of a GPS position for the grid division center, the time of acquisition, the height above geoid and the detected bedrock reflex time-of-flight.

To create a model of the subsurface, interpolation with a continuous curva-

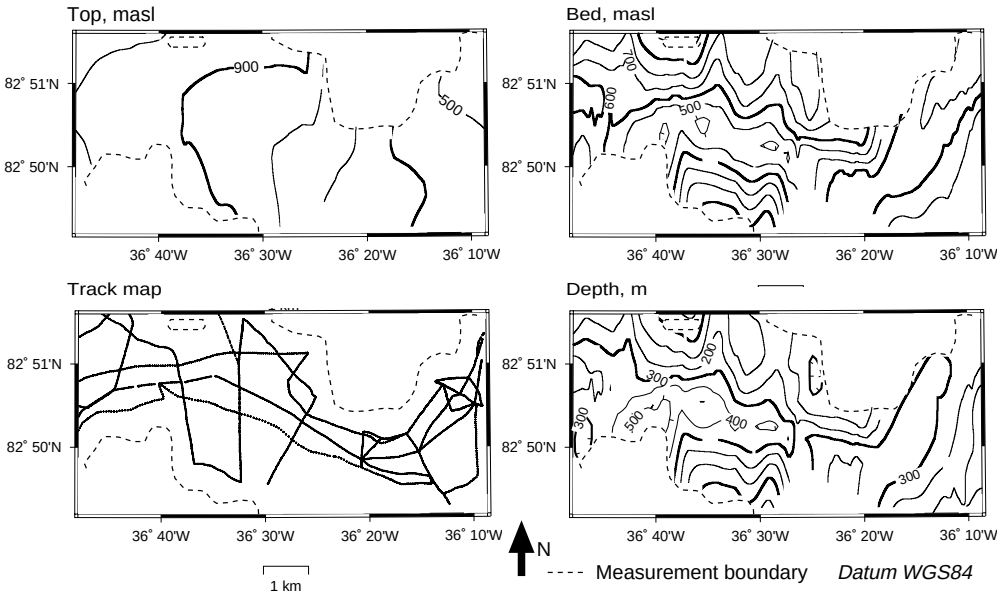

Fig. 3. Result from the evaluation of the measurement in the outlet glacier area. Isoline distance 100 m. The lower left figure shows those surface tracks where profiling was performed, where there was less than 1 km between neighbouring profiles. The lower right figure shows the resulting ice depth model (see text). The upper left figure shows the snow surface elevations from the GPS measurements, while the upper right is the glacier subsurface model, resulting from the elevations and the thickness measurements.

ture method (Smith 1990) was used, which assumed a smooth, relatively level basement under the ice. The interpolated data were then resampled to a regular grid. For conversion between time-of-flight and depth, an average velocity including velocity changes due to ice density variations, of 171±1.5 m/μs was selected rather that the velocity for pure ice of 168 m/μs, based on the compilation of data found in Bogorodsky *et al*. (1985). The used velocity gives a good agreement compared to the depths at the known control points; the core drilling to bedrock on the ice cap by Department of Geophysics, University of Copenhagen, and one hot water drilling performed by GEUS in 1995 (*Thomsen et al*., 1996). Some profiles on the outlet glacier and some lying perpendicular to the assumed flow line were also measured to zero depth.

By analyzing digitized 100 MHz signals from the calibrator, an absolute timing error of less than ±10 ns was estimated. The error in the detection process was estimated to be ±50 ns, based on observations of signals where the antennae were stationary. These error estimates yield an instrumentation related uncertainty in the reflection times to less that ±60 ns, or ±10 m. The depth uncertainty for the selected mean velocity of 171 m/μs compared to a pure ice velocity of 168 m/μs is less than 8 m at the maximum reflection time.

Results

A detailed depth map has been produced for a 5x5 km area on the ice cap, using measurements taken in 1994. The detected two-way reflection times are here between 3220 ns and 4610 ns. This corresponds, with the assumptions above, to a minimum depth of 275 m and a maximum depth of 395 m. A map of the measured tracks is shown in Fig. 2, together with the calculated ice depths and surface elevations, and the resulting model of the ice subsurface in the 5x5 km area.

Reflection times in the northern outlet glacier area range between 0 and 4670 ns, or 0 and 399 m, respectively. Results for this area are presented in Fig. 3.

Acknowledgments

The work has been sponsored by *The Nordic Environmental Research Programme*

1993-1997 of the *Nordic Council of Ministers*. All logistics were provided by the Department of Geophysics, University of Copenhagen, and the Geological Survey of Denmark and Greenland (GEUS), formerly the Greenland Geological Survey (GGU), and the GRIP deep drilling program. GPS data was made available by Department of Geophysics, University of Copenhagen, the National Survey and Cadastre, and GEUS. The friendly and cooperative atmosphere showed to me in the project is gratefully acknowledged. I would also like to acknowledge the reviewers, Preben Gudmandsen at the Technical University of Denmark and Hugh Corr at the British Antarctic Survey (BAS), for their valuable comments on the manuscript.

References

Annan, A. P., J. L. Davis 1977. *Report of activities, Part B*. Geological Survey of Canada, Ottawa, pp. 117-124.

Bogorodsky, V. V., C. R. Bentley, P. E. Gudmandsen 1985. In: *Radioglaciology*. Reidel, Dordrecht, pp. 98-105.

Gundestrup, N., K. Keller and P. Jonsson 2001. Locating the Hans Tausen Drill Site. Meddelelser om Grønland Geoscience, this volume, pp. 71-80.

Morey, R. R. 1974. United States Patent 3,806,795, Geophysical surveying system employing electromagnetic pulses, filed Jan. 3, 1972, issued Apr 23, 1974.

Morey, R. R. and A. Kovacs 1982. *The effects of conductivity on high-resolution impulse radar sounding, Ross Ice Shelf, Antarctica*. CRREL report 82-42. U.S. Army Cold Regions Research and Engineering Laboratory, Hanover, NH.

Smith, W. H. F. and P. Wessel 1990. Gridding with continuous curvature splines in tension. *Geophysics*, Vol. 55 : 293-305.

Thomsen, H. H., N. Reeh, O. B. Olesen and P. Jonsson 1996. Glacier and climate research on Hans Tausen Iskappe, North Greenland – 1995 glacier basin activities and preliminary results. In: Sønderholm, M. & A. K. Higgins (eds.). *Report of Activities 1995*, Bulletin 177. Grønlands Geologiske Undersøgelse, Copenhagen.

The Paleoclimatic Record from a 345 m long Ice Core from the Hans Tausen Iskappe

By Claus Uffe Hammer, S. J. Johnsen, Henrik B. Clausen, Dorthe Dahl-Jensen, Niels Gundestrup, and Jørgen Peder Steffensen

Abstract

Hammer, C. U. *et al.* 2001. The Paleoclimatic Record from a 345 m long Ice Core from the Hans Tausen Iskappe. Copenhagen, Danish Polar Center. Meddelelser om Grønland Geoscience 39, pp. 87-95.

The 345 m long ice core retrieved from the Hans Tausen Ice Cap in 1995 (82,5°N, 38°W) in Western Peary Land was sampled in situ for later paleoclimatic $\delta^{18}O$ measurements in Copenhagen.

The upper 125 m covers a little more than 1000 years and indicates strong persistent warming from the late 1920-ties, a maximum warming in the early 1960-ties and a variable climate with no particular trend since the 1960-ties. The δ record over the past 100 years shows similarities with the temperature records from the Greenland west coast stations, Iceland, and the Faroe Islands.

The 20th century is the warmest in the entire record, while the periode 1700-1900 A.D. is the coldest during the past 2000 years. A maximum of warm climate seems to be reached around 900-1100 A.D. which then declines to the colder conditions around 1700 A.D.

The climatic interpretation of the deepest 105 m of the δ record is more complicated due to the non-steady state of the ice cap: The implication for the paleoclimatic interpretation will be discussed. No glacial ice is present in the bottom ice.

Keywords: Climate; ice cores; North Greenland; Arctic; greenhouse effect; global changes.

C. U. Hammer, S. J. Johnsen, H. B. Clausen, D. Dahl-Jensen, N. Gundestrup, and J. P. Steffensen, Department of Geophysics, Niels Bohr Institute for Astronomy, Physics and Geophysics, University of Copenhagen

Introduction

The Hans Tausen Ice Cap (82.5°N, 38°W) in western Peary Land is believed to be located in a region of high climate variability and its position on a 1000 m high rock plateau north of the present margin of the Greenland Ice Sheet makes it an evident object for paleoclimatic research. It is also the most northern ice cap in the Arctic, but little is known about its stability and history.

The nordic Hans Tausen project (1993-1997) investigated the ice cap and its surroundings in order to obtain paleoclimatic environmental data and to model the dynamic pattern of the ice cap. Part of the project was to drill through the ice cap to obtain an ice core to the bedrock at a suitable drill site. The drill site was

chosen after an intensive survey over the years 1993-1994 (see Gundestrup *et al.* 2001). An overview of the Hans Tausen project is found in Hammer and Højmark (1998).

Below we will concentrate on the main features of the Hans Tausen $\delta^{18}O$ profile along the ice core in order to infer the paleoclimate as far back in time as the core allows.

The preliminary dating of the core (Clausen *et al.* 2001) and other information from the project indicated that the present ice cap is not older than 3500-4000 years, and that the region around the drill site is still growing 4 cm per year (Keller *et al.* 2001), i.e. the ice cap is not yet in a dynamically steady state.

Material and Techniques

The core was sampled in situ for later $\delta^{18}O$ masspectrometric measurements in Copenhagen. Density- and ECM-measurements were also performed in situ; the latter profile has been used to establish a chronology for the past 2000 years by using volcanic reference horizons (Clausen *et al.* 2001; M. Stampe, 1997). The δ sampling was made in the following way:

- From 0-345 m depth each 0.55 m.
- From 0-22 m depth each 0.025 m.
- At various selected depth ranges each 0.025 m in order to investigate the diffusive aspects of the δ profile.

Also a second drilled shallow core down to 35 m and a 2 m pit were sampled for $\delta^{18}O$ in order to estimate the influence of glaciological noise on the δ record and to secure a correct sampling of the upper low density part of the firn surface.

Results

The over all δ profile (0.55 m samples) is shown in Fig. 1. The profile exhibits a number of characteristic features, which can be clearly seen in the figure.

From 345-280 m the δ values are nearly 2‰ lower than the average value over 260 m to the surface. From 260 to around 100 m the values vary around –27‰ but between 60-20 m the δ values are almost 1‰ lower. The upper 10 m represent the highest δ values in the entire record.

Before interpreting the record in terms of past climate changes it is, however, nescessary to invoke other information from the Hans Tausen project.

In Fig. 2 a smoothed version of Fig. 1 is presented along with the timescale established by Clausen *et al.* (2001). This timescale is presently only established back to 244 BC even though we know that the bottom ice is approximately 4 kyrs old. As can be seen from the dates there is nearly no decrease of the annual layer thickness with depth, which indicates that the central dome area must have experienced very low strain rates over a substantial part of the ice caps existence.

Apparently the dome area is presently in a transitionary state approaching steady state as indicated by the findings of Keller *et al.* (2001). The annual accumulation over the past 200 years is 10.8 cm of ice equiv./yr, not much different from the annual layer thickness around 2000 BP.

If the growth rate of the dome area had been equal to the annual accumulation over the past 2000 years, the ice cap would have added some 200 m to its thickness. This estimate is of course too high, because the dome area presently only grows 4 cm/yr. Let us instead assume that the ice cap has grown some 100 m over the past 2000 years (the exact figure is not important in the following). Then the most likely effect on the δ values should be a decrease of the order of some 0.7‰ i.e. if the δ profile in Fig. 2 were to be corrected for elevation changes it would enhance the difference

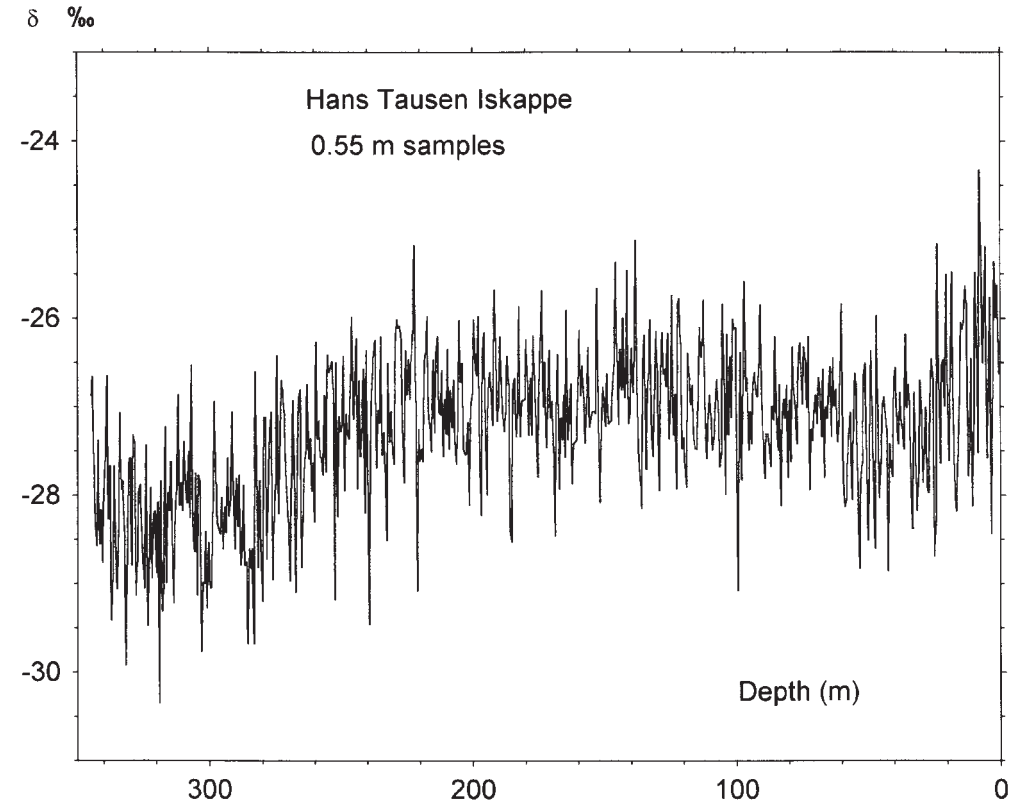

Fig. 1.The Hans Tausen profile versus depth; shown as 0.55 m average samples. Note the high values at 10-20 m and the rather low values over the bottom 60-70 m.

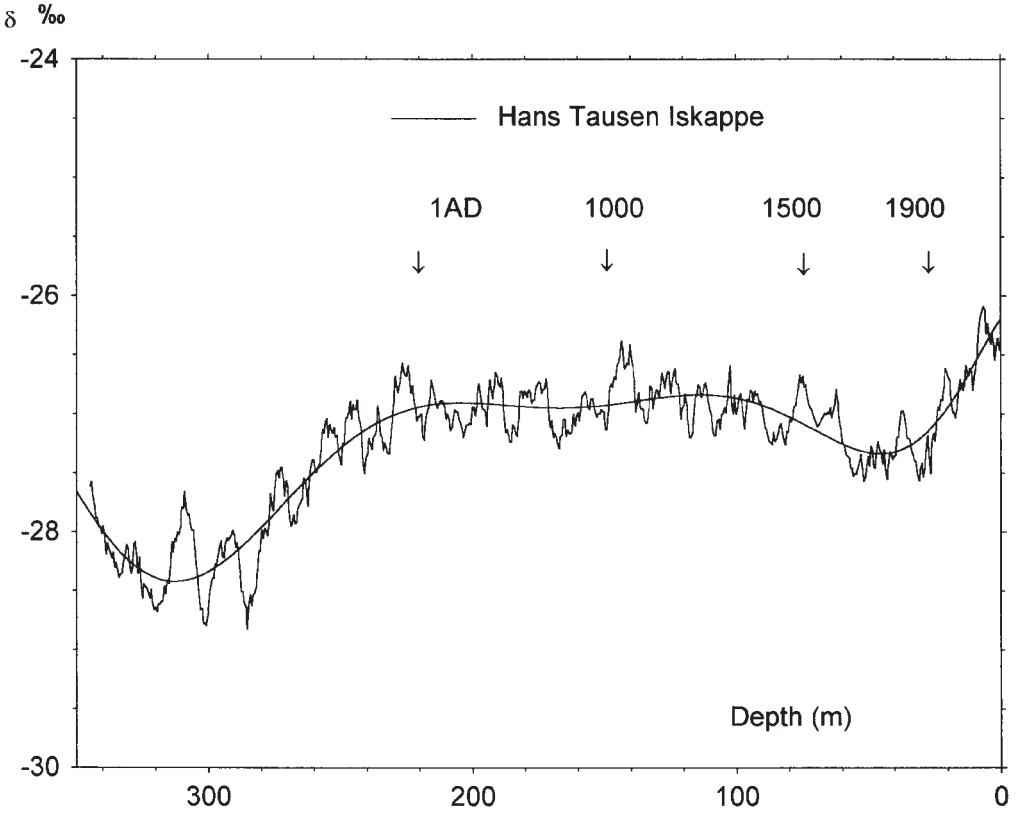

Fig. 2. A smoothed version of Fig. 1 (10 point sliding averages plus a fitted polynomium). Selected dates are indicated (see Clausen et al. 2001).

between the δ values around 2000 years ago and those covering the past century. In other words, the δ values covering the past century would be even higher compared to the values of the older periods.

It is therefore possible to interprete the δ profile, back to 2000 BP, in terms of past climate changes as long as the interpretation concentrates on the qualitative changes. An interpretation in terms of quantitative temperature changes would be rather uncertain both due to our poor knowledge of the orographic influence on the snow deposition, the dynamic history of the rebuilding ice cap and the often forgotten a priori assumption that the seasonal pattern of snowdeposition remains unchanged over time. The latter is especially important for areas of low annual snow accumulation (where a change in the frequency of substantial individual snow deposition events can strongly influence the annual average δ value (Hammer, in press). It should also be remembered that climatic data from ice cores from regions of high summer melt must be interpreted with caution (Koerner 1997) Even with these reservations the Hans Tausen δ record presents us with some intriguing interpretations of relevance to climate research as discussed below.

Interpretation of the δ record

Evidently, it is difficult to relate the deeper parts of the Hans Tausen ice core δ profile to past climate changes. Also there must be a transitionary sequence of the δ profile between the deeper parts up to the layers around 2000 BP old. We have therefore chosen to divide the δ profile into 3 sections, which will be treated independently.

The bottom ice, 345-240 m

While the drill-site is presently on a dome in a fairly "simple" flowregime, this was not the case for this site during the early milleniums of rebuilding. First of all the rebuilding of the ice cap several thousands of years after the Climatic Optimum must have been a wet "summer-affair" during the first few thousand years.

Between 280 m and 250 m the melt-layer percentage in the core is still around 60-70%, and the percentage only falls below some 40% around 200 m depth: The present melt percentage is 8%; increasing with depth to 20% around 120 m. The loss of summer snow accumulation by run-off in the flat dome area is hardly likely, if the melt percentage is below some 30-40% and we therefore assume, that the δ profile reflects climate changes from the surface and down to 220 m depth (of course with the earlier mentioned reservations concerning the growth of the surface elevation).

We must stay clear of interpreting the δ profile below some 220 m in terms of a record of climate change; rather it represents a record related to the rebuilding history of the Hans Tausen Iskappe. It might be possible in the future to extend the usefulness of the δ profile as a climate indicator back to some 260 m, but that would require a substantial amount of new information e.g. from another deep ice core some 5 km from the present drill-site.

1 AD – 1900 AD (200 m – 20 m)

From 1 AD to 1900 AD the smoothed δ profile in Fig. 2 exhibits semi-cyclic variations. The highest values are confined to a short period around 140 m depth while the lowest values are in the depth range 60-20 m (1700-1900 A.D.). How does this compare to the information on the past climate from the Greenland Ice Sheet proper and the Northern Hemisphere in general?

In 1980 only a few ice cores from the Greenland Ice Sheet existed, which reached back to 2000 BP, but an attempt was made to establish a normalized cli-

matic index for the ice sheet back to 550 AD (Hammer *et al.* 1980). This old index concur somewhat with the δ profile of the Hans Tausen ice core i.e. relatively high values until 1300 A.D., followed by declining values until a minimum from 1650-1700 A.D. and general low values between 1700-1900 A.D. The match is not perfect, but the spline in Fig. 2 illustrates the general trend of the δ profile. Hammer *et al.* (1980) also attempted to construct a Northern Hemisphere temperature index, which differed from the ice core index by having a pronounced medieval warm maximum around 1100-1300 A.D.

Since 1980 several new drillings to intermediate depths have been accomplished and the GRIP and GISP2 drillings at the Summit area have added to the climate archive (Greenland Summit Ice Cores 102, C12, 1997). The recent NORTH GRIP drilling 315 km north-north west of the Summit drillings has added yet another δ profile representing the Greenland Ice Sheet.

With all these data it should be possible to compare the δ profile from the Hans Tausen Iskappe to the main features of the Greenland Ice Sheet δ profiles. For the period 1 AD – 1900 AD this is, however, problematic. One could of course normalize the profiles and stack them all together. This has actually been done by Fisher *et al.* (1996), who also included the Canadian ice cores from Devon Island and the Agazzis Ice Cap. The NORTH GRIP core and the Hans Tausen data did not exist at that time. Even though the stacked profile of Fisher *et al.* (1996) explain some of the variance by the EOF technique (Empirical Orthogonal Functions), they reach no firm conclusion as to why the Central Greenland ice cores GISP2 and GRIP show no trend in the Holocene; Fisher *et al.* (1996) link this problem to "the smaller problem" of the past 3000 years. This leads us to a crucial question: Can we a priori assume, that the seasonal distribution of snow fall has not changed over time? There is also the possibility that high and low elevation sites respond differently to climate chances.

In the case of the GISP2, GRIP, and Dye-3 ice cores paleotemperatures obtained from borehole temperature measurements (Cuffey *et al.* 1997; Dahl-Jensen *et al.* 1998) indicate a temperature low some 2000 years ago; high temperatures around 500-1200 A.D. and two minima at approximately 1500 A.D. and mid 19th century; finally ending with a maximum in the 20th century.

The Hans Tausen δ record exhibits some of the same characteristics i.e. high values during the first millenium and low values around 1700-1900 A.D., but it is certainly not a perfect match to either the data from Central Greenland or the stacked data of Fisher et al.

The 20th Century

The number of ice cores from Greenland and Canada covering the past century is substantially higher than the number of cores reaching several thousand years back in time. Also the existence of temperature data from coastal Greenland meteorological stations add to our knowledge of the climatic development during the 20th century in the Greenland region.

In Fig. 3 the Hans Tausen profile (smoothed) covering the periode 1900-1995 A.D. is shown. If we compare this profile to the earlier mentioned data of Hammer *et al.* (1980), Fisher *et al.* (1996), and Dahl-Jensen *et al.* (1998) and the coastal temperature data (from the Danish Meteorogical Institute) we get a much more consistent picture as for the periode 1900-1995 A.D. i.e. cold temperatures (or low (s) in the beginning of the century, higher temperatures (or high δs) during the late 20-ies to 1940 and high values again in the mid 60-ies; finally a slight trend of cooling since the

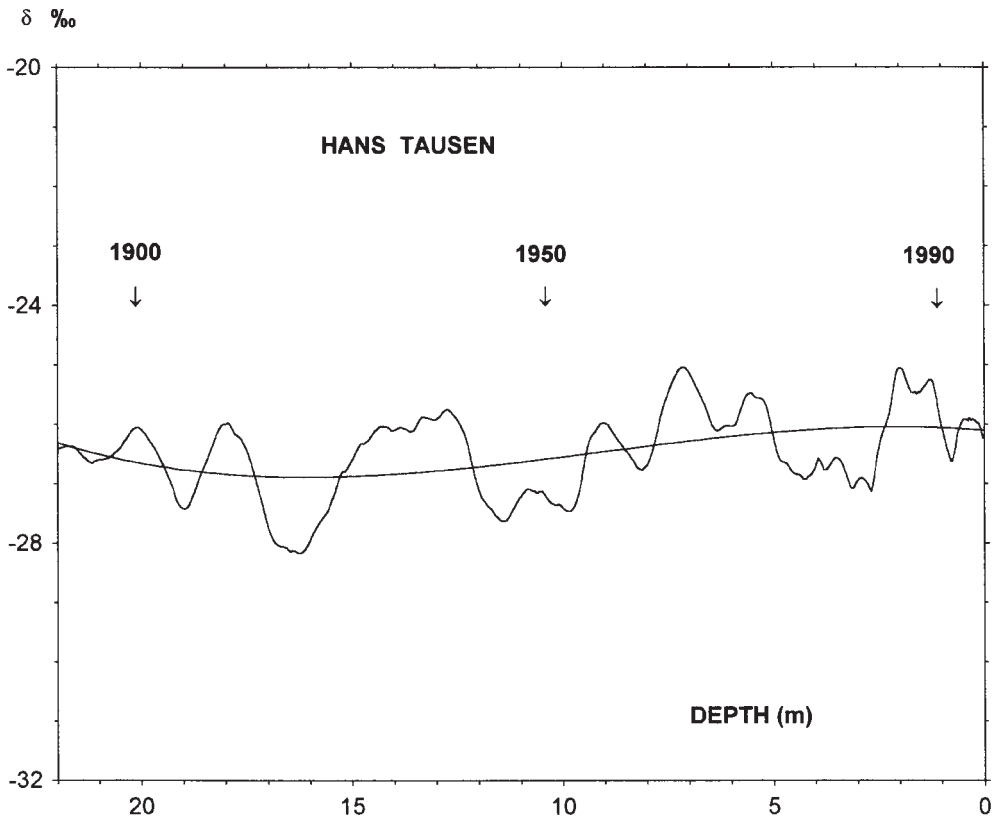

Fig. 3. The upper 22 m of $\delta^{18}O$; smoothed but based on 2.5 cm samples. A fitted polynomium curve of the data is also shown. Dating is based on seasonal variations of $\delta^{18}O$ and a reference horizon from the Katmai eruption 1912 A.D.

mid 60-ties. This is substantiated by a second shallow ice core from the Hans Tausen Southern Dome, i.e. it is not caused by glaciological noise.

More recent ice core data from the GISP2 and GRIP were analyzed by White *et al.* (1997), who also concluded that their stacked δ profiles from 6 ice cores actually reflected several observed features of the 20th century North Atlantic climate.

So we are left with the impression, that the δ profiles in fact do reflect the temperature history at an ice core drill-site in the Greenland-Canadian region. If we analyse the data further back in time the interpretation is harder. Of course this does not change the fact that the δ profiles along deep ice cores indicate glacial periods or the Dansgaard-Oeschger events observed during the last glacial (Dansgaard *et al.* 1993), but it does point to the fact that the δ method is based on certain assumptions.

When dealing with climate changes of the Holocene some of the assumptions do not hold and this can have serious consequences for the δ-T (temperature) relation. It should be noted that Dansgaard's and Johnsen's empirical relation between δ-T for Greenland ice cores (Dansgaard, 1964; Johnsen *et al.* 1989) was established by means of shallow ice cores i.e. while a linear relation was found between δ and T it did not nescessarily mean that it would hold for older ice-strata.

The anthropogenic "Greenhouse effect"

In this paper we have tried to briefly present the Hans Tausen δ profile and its relation to other ice core data from the Greenland and Canadian region. We have also indicated some of the problems involved in relating δ and temperature, but perhaps one of the most

exciting findings of the Hans Tausen project does not require a complete quantitative analysis of the δ profile!

From Fig. 2 it can be clearly seen, that the highest δ values in the Hans Tausen record are observed during the 20th century; the values of the 1930-ies and 1960-ies are even higher than the values of the first millenium and Medieval times. "Is this just a statistical fluctuation over 2000 years or is it indicating that the present human activity is now changing our climate?"

Even though the climate "trend" of the Greenland region since the mid 60-ies has been toward cooling, this "trend" is based on not more than 30 years; could it be that the cooling is just part of a coincidental variation in the semi-cyclic pattern seen in Fig. 2? Actually the low δ values between the 60-ies and the 90-ies are as high as the δ values around medieval times i.e. the 20th century climate seems to be really unique, when compared to the climate changes over the past 20 centuries.

Is there any reason to expect unusual warm conditions since the 1920-ies? There are at least two natural causes which come into play:

1) The absence of volcanic eruptions of climatic significance between 1912 to 1963 A.D. and
2) The Sun's activity (see e.g. ESF project: Solar output and climate during the Holocene, 1995).

While the latter is a highly controversial subject there is no doubt that 1920-1962 A.D. was a period representing a rather clear upper atmosphere (especially stratosphere). It is, however, difficult to explain the high δ values in the Hans Tausen record since the mid 1960-ies without including an anthropogenic "greenhouse effect". If an anthropogenic greenhouse effect is not the explanation we are left with two very complex causes for the high δ values: Either the past 30 years are due to chance fluctuations in the Earth Climate System or some, perhaps oceanic, memory effect of the warm temperatures between the end of the 1920-ies and to the mid 1960-ies is acting in some unknown way.

If compared to all the other information on the Earth climate during the 20th century we feel heavily inclined to accept that human activity in the second half of the 20th century has indeed an effect on the climate.

Conclusions

We have demonstrated that the Hans Tausen ice core δ profile does indeed, in a qualitative way, concur with the general climate change in the Greenland-Canadian region as obtained from other ice core data in the region.

It is, however, clear that the record, as all the ice core records from the region, is not varying entirely in phase. There are good reasons to believe that they should not vary exactly in phase even though the various profiles do indeed show some similar long term trends. We suspect that the differences between the various profiles are partly due to real climatic differences and partly due to a presently unknown change in the seasonal snow deposition pattern.

For the past 100-200 years the δ profile apparently reflects the actual temperature changes in the Greenland-Canadian region rather well. The unusual high δ values during the 20th century seems to be related to both low volcanic activity and since the 60-ies to the anthropogenic greenhouse effect. The latter conclusion could be tested and partly verified by extending the Hans Tausen δ profile i.e. to sample the past 5 years of snow accumulation at the southern dome of the Hans Tausen Iskappe. Only 5 years have passed since the samples from the ice cap were collected, but if the δ values of the past 5 years (1995-2000 A.D.) would still remain as high as during medieval

times – or higher – it could be an important verification of the anthropogenic greenhouse effect. If not, we would be forced to be much more cautious in our interpretation. In other words we would need many more ice core data from the Greenland-Canadian region combined with intensified and improved regional climate modelling to get a more firm basis for our conclusions.

We do, however, base our present conclusion, regarding the anthropogenic greenhouse effect, on the fact that the 20th century data are outstanding when compared to the past 2000 years. It is not proving that the δ profile from the Hans Tausen Iskappe over the 20th century is really unique, but it certainly suggest that the present odds are not in favour of a simple "stastistical fluctuation" of the Earth climate system.

Acknowledgements

The Hans Tausen Iskappe Project received substantial funding from the *Nordic Environmental Program 1993-1997* of the *Nordic Council of Ministers*, the *Danish Natural Science Research Council* (SNF) and the EU DGXII project *MilEClim*. We are grateful to these institutions.

Furthermore we would like to thank the staff at Station Nord in Peary Land for their useful help and cheerfulness during the expedition. A special thank to the twin-otter-team from the Icelandic "Flugverlag", who loved to stay on the ice helping wherever they could.

References

Clausen, H. B., M. Stampe, C. U. Hammer, C. S. Hvidberg, D. Dahl-Jensen and J. P. Steffensen 2001. Glacio-chemical studies on ice cores from Hans Tausen Iskappe, Greenland. Meddelelser om Grønland, Geoscience, this volume pp 123-149.

Cuffey, R. W., G. D. Clow, R. B. Alley, M. Stuiver, E. D. Waddington and R. W. Saltus 1995. Large Arctic temperature change at the Wisconsin-Holocene glacial transition. *Science* 279: 455-458.

Dahl-Jensen, D., K. Mosegaard, S. J. Johnssen, N. Gundestrup and G. Glow 1998: Deep frozen paleotemperatures from the Greenland Ice Sheet. *Science* 282: 268-271.

Dansgaard, W. 1964. Stable isotopes in precipitation. *Tellus* 16: 436-468.

Dansgaard, W., S. J. Johnsen, H. B. Clausen, D. Dahl-Jensen, N. S. Gundestrup, C. U. Hammer, C. S. Hvidberg, J. P. Steffensen, A. E. Sveinbjörnsdottir, J. Jouzel and G. Bond 1993. Evidence for general instability of past climate from a 250 kyr ice core record. *Nature* 364: 218-220.

ESF project: Solar output and climate during the Holocene. Editors B. Frenzel, T. Nanni, M. Galli and B. Gläser. *Paleoclimate Research*, Special Issue 1995: 16.

Fisher, David A., R. M. Koerner, K. Kuivinen, H. B. Clausen, S. J. Johnsen, J. P. Steffensen, N. Gundestrup and C. U. Hammer 1996. Inter-Comparison of ice core $\delta^{18}O$ and precipitation records from sites in Canada and Greenland over the last 3500 years and over the last few centuries in detail using EOF techniques. In: *Climatic Variations and Forcing Mechanisms of the last 2000 Years*. Edited by Philip D. Jones, Raymond S. Bradley and Jean Jouzel. NATO ASI Series I, Vol. 41, pp. 297-328.

Greenland Summit Ice Cores 102, C12. *Journal of Geophysical Research*, special issue, 1997: 26,315-26,886.

Gundestrup, N., K. Keller, T. Knudsen and P. Jonsson 2001. Locating the Hans Tausen drill site. Meddelelser om Grønland Geoscience, this volume, pp. 71-80.

Hammer, C. U., H. B. Clausen and W. Dansgaard 1980. Greenland ice sheet evidence of post-glacial volcanism and its climatic impact. *Nature* 288, pp. 230-235.

Hammer, C. U. and H. H. Thomsen 1998. Fælles nordisk indsats – tæt på verdens top. *Geologi, Nyt fra GEUS* 2: 2-14.

Hammer, C. U. (in press). Holocene Climate and Past Volcanism : Greenland-Northern Europe, Hanse Conference Proceedings.

Johnsen, S. J., W. Dansgaard and J. W. C. White 1989. The origin of Arctic precipitation under present and glacial conditions. *Tellus* ser. B. 41: 452-468.

Keller, K., C. S. Hvidberg, N. Gundestrup

and P. Jonsson 2001: Surface movement and mass balance of the Hans Tausen drilling site determined by use of GPS. Meddelelser om Grønland Geoscience, this volume pp. 115-122.

Koerner, R. M. 1997. Some comments on climatic reconstructrions from ice cores drilled in areas of high melt. *Journal of Glaciology* 43, No.143.

Madsen, K. N. and T. Thorsteinsson: Crystal growth and fabric development in the Hans Tausen ice core. Meddelelser om Grønland Geoscience, this volume pp. 97-114.

Stampe, M. 1997. Vulkanske vidnesbyrd i iskerne fra Hans Tausen. Master thesis, University of Copenhagen, Department of Geophysics, Niels Bohr Institute for Astronomy, Physics and Geophysics.

White, J. W. C., L. K. Barlow, D. Fisher, P. Grootes, J. Jouzel, S. J. Johnsen, M. Stuiver and H. B. Clausen 1997. The climate signal in the stable isotopes of snow from Summit, Greenland: Results of comparisons with modern climate observations. *Journal of Geophysical Research* 102, NO C12: 26,425-26,439.

Textures, fabrics and meltlayer stratigraphy in the Hans Tausen ice core, North Greenland – indications of late Holocene ice cap generation?

By Karen Nørgaard Madsen and Thorsteinn Thorsteinsson

Abstract

Madsen, K. N. and T. Thorsteinsson 2001. Textures, fabrics and meltlayer stratigraphy in the Hans Tausen ice core, North Greenland – indications of late Holocene ice cap generation? Copenhagen, Danish Polar Center. Meddelelser om Grønland Geoscience 39, pp. 97-114.

A thin section study of crystal structure has been carried out on a 345 m long ice core drilled to bedrock on Hans Tausen Iskappe, 1995. In addition a meltlayer stratigraphy was set up, showing how the fraction of meltlayer-ice in the core increases with depth. Main characteristics of crystal structure are increasing mean crystal size from top to bottom in the core and development of a weak single maximum c-axis fabric. The rate of ice crystal growth in the well dated upper half of the core is much lower than expected from studies of the normal grain growth regime in other polar ice cores. Probably the grain boundary movements are impeded by impurities, which are present in relatively high concentrations in the Hans Tausen ice. Asuming the applicability of the calculated growth rate throughout the core, a late Holocene origin of the oldest ice is suggested by the size of the crystals close to bedrock. Presented data furthermore implies that bottom ice temperatures were never near the melting point and it is concluded that there was no ice cap on the Hans Tausen plateau earlier in Holocene.

Keywords: Glaciologi; glacier ice crystals; grain growth: meltlayers; Holocene climate.

Karen Nørgaard Madsen, Department of Geophysics, Niels Bohr Institute for Astronomy, Physics and Geophysics, University of Copenhagen (Now: University of Bergen, Institute of Solid Earth Physics, Norway).

Thorsteinn Thorsteinsson, Alfred Wegener Institute, Geophysics division, Bremerhaven, Germany.

Introduction to Hans Tausen Iskappe

Hans Tausen Iskappe is located on a plateau in Pearyland, North Greenland. This irregularly shaped ice cap stretches out 75 km from north to south and 50 km from east to west, reaching elevations up to 1300 m a.s.l. (Thomsen *et al*. 1996). In the summer of 1995 an ice core was drilled on the southern dome of the ice cap. Drilling reached bedrock and the core retrieved is 345 m long. Temperatures in the Hans Tausen bore hole increase approximately linearly from

–21°C near the surface to –16°C at bedrock (Johnsen, S. J., personal communication 1997).

A visible feature of the core is the frequent occurrence of melt layers formed by refreezing of meltwater in the firn. In the present paper, ice formed in this way will be termed *meltlayer-ice*, while glacial ice formed by gradual compression of firn will be referred to as *firn-ice*. The abundance of meltlayer-ice in the core increases with depth (Fig. 1), attesting to warmer conditions at the surface earlier in the history of the ice cap.

Average $\delta^{18}O$ values of the ice are around $-27^0/_{00}$ in the upper $^3/_4$ of the core decreasing by $1^0/_{00}$ in the deepest part (Hammer *et al.* 2001). Considering the raised fraction of meltlayer-ice in the last part of the core the slight lowering of $\delta^{18}O$ values can hardly be interpreted as a transition to ice age conditions. Thus all ice within the core must have been deposited during the Holocene. For further dating of the ice core, time markers are provided by identified volcanic eruptions. Annual layer thicknesses in the core seem to be almost constant at 10-11 cm at least to the acidic peak at 131.5 m assigned to the 934 AD eruption of Eldgjá (Stampe 1997). Below this depth there are no clear guidelines for the time scale.

The purpose of this paper is to present and interpret data from thin section studies of the Hans Tausen Ice Core and discuss what can be learned about the ice cap from the crystal structure of the ice and the meltlayer stratigraphy. The analysis will be based on the hypothesis that the ice cap formed on the Hans Tausen plateau during the Holocene. Alternatively, the lack of depositions from the last ice age could be explained by melting and run-off from the bottom of the ice cap during the Holocene. This scenario is less appealing considering the present temperature at bedrock, but will however be evaluated in a later discussion of former temperatures in the ice.

Polycrystalline structure of glacial ice

The development of the polycrystalline structure has been investigated in several deep ice cores. Observations of crystal size variations with depth have revealed 3 recrystallization mechanisms, governing the movement or formation of crystal boundaries within the ice under various conditions (Herron & Langway 1982, Alley 1992).

In the top part of the ice cap, where strain and strain rates are small, mean crystal size is increasing with the age of the ice. Reduction in free surface energy by elimination of the smallest crystals provides the driving force for the process dominating, called *normal grain growth*. Following early results from metallurgy, it has been generally accepted to describe the growth of mean crystal size in firn and ice at low strain as function of time by

$$D^2 = D_0^2 + k\,t, \qquad (1)$$

where D_0 and D are mean crystal dimensions at time t_0 and $t > t_0$, respectively (Gow 1969, Alley 1986 et al., Alley 1992). However, it should be borne in mind that theoretical considerations have also led to other growth laws (Atkinson 1988, Alley et al. 1986), for instance with the exponent of 2 raised up to 3. It is very hard to argue for one growth law or the other by data, since the normal grain growth regime often corresponds to a quite limited time interval relative to the slow rate of growth. Put in another way the function relating mean crystal size to time can not be precisely determined because it is constrained by data in a window which is too narrow relative to the scale of its curvature, given the inevitable scatter of data. The local variability of crystal size is not just statistic fluctuations, but reflects the influence of other factors on crystal growth, one of which is impurities in the ice. By impeding crystal boundary migration, impurities lower the growth rate and could possibly change the functional

relationship too (Alley et al. 1986, Alley et al. 1995, Duval & Castelnau 1995).

Adopting equation (1), the growth rate k has been demonstrated to show an Arrhenius type temperature dependence expressed by

$$k = k_0 \, exp \left(\frac{-Q}{RT} \right), \qquad (2)$$

where Q is the activation energy for crystal growth, R the gas constant, T the temperature in Kelvins and k_0 a constant of proportionality (Gow 1969, Duval 1985, Paterson 1994, Li 1995). At temperatures above –10°C, experiments indicate that the grain growth rate increases much faster with temperature than predicted by (2) with k_0 and Q being the constants appropriate for lower temperatures (Li 1995).

Deeper in the ice cap, stored strain energy can provide new driving forces for recrystallization, changing the characteristics of the polycrystalline structure. Succeeding the initial growth a zone of stagnating mean crystal size is observed in several ice cores (Gow & Williamson 1976, Herron & Langway 1982, Alley 1992, Gow et al. 1997, Thorsteinsson et al. 1997). The occurrence of constant crystal size has been explained by the onset of *polygonization*, a process by which deformation induced dislocations arrange themselves into new crystal boundaries, leading to subdivision of crystals and thereby counteracting normal grain growth (Alley 1992, Alley *et al*. 1995).

Finally *dynamic recrystallization*, a process favoured by high strain/strain-rate and temperature is believed to overprint earlier crystal structure close to the bottom of a few drill sites in thick ice sheets. Due to the difference in stored strain energy, new and essentially strain free grains can nucleate in the matrix of highly strained older grains and expand rapidly to form large irregular crystals (Gow & Williamson 1976, Duval & Castelnau 1995, Gow *et al*. 1997).

Methods

The meltlayers are visible in the core as clear bands of essentially bubble free ice and were recorded in the field (H. B. Clausen, personal communication 1997). The total thickness of meltlayers was summed for each 55 cm of core (a bag length), and below the firn/ice transition this is immediately converted into a meltlayer percentage. In the top 60 m of the core the different density of meltlayer-ice and firn must be taken into account in order to obtain a meltlayer percentage, which is independent of the firn compression state. The correct weight percentage is obtained as $\rho_{ice}S_{ice}/(\rho_{ice}S_{ice} + \rho_{firn}S_{firn})$, where ρ and S denote density and core length of ice and firn. However, available density data dictated a more rough calculation of weight percentage replacing the denominator by the bag length times a density at the given depth estimated by the mean density profile of the core (Clausen, H. B., personal communication 1997). If the bag in question contains more (less) than average meltlayer-ice the denominator will be too small (large), thus the amplitude of meltlayer intensity variations is slightly exaggerated in the top.

For the study of ice crystal structure in the Hans Tausen ice core, a total of 34 vertical thin sections were cut parallel to the long axis of the core and evenly spaced from top to bottom. In addition 8 horizontal thin sections, normal to the long axis of the core and evenly spaced from 120 to 330 m were prepared for determining fabric. The coexistence of meltlayer-ice and firn-ice calls for separate analysis to investigate the influence of meltwater percolation on crystal growth. Thus the sampling was done with the aim of obtaining thin sections covering both meltlayer-ice and firn-ice when possible.

Mean crystal sizes were measured on vertical thin sections using the linear

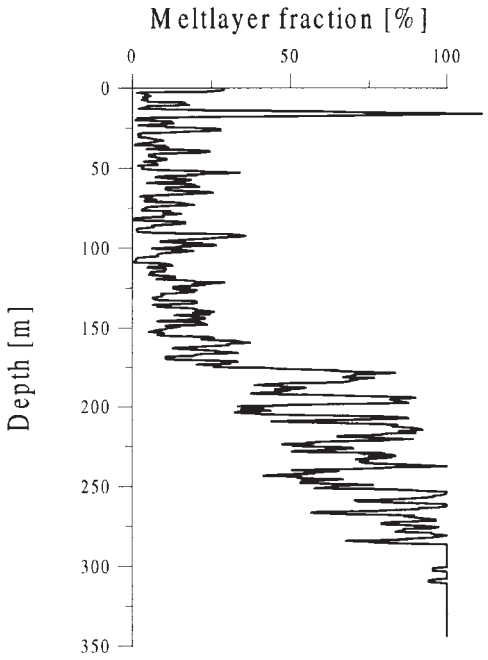

Fig. 1. Percentage by weight of meltlayer-ice in the Hans Tausen ice core, calculated in running mean of 2.20 m. A pronounced shift from high to low fractions of meltlayer-ice is encountered at 175 m depth. A short interval of very high melt is seen in the top at 15-17 m depth. The actual fraction of course does not exceed 100%, this is a consequence of the procedure used for air correction of the firn as explained in the section on methods. The vulcanic time horizon of Katmai 1910 eruption is identified closely below at 17.63 m depth.

intercept method by which the number N of crystal boundaries intersected by a test line of length L is counted. The linear intercept diameter, L/N, was used as a measure of mean crystal dimension. Using test lines parallel and normal to the long axis of the core, vertical and horizontal crystal dimensions D_v and D_h were obtained. Each measurement used several test lines across the thin section, with enough spacing to prevent the same crystal from being counted twice. In most cases this procedure allowed for at least 100 crystals to enter the measurement and the error is then less than 1 mm. The mean crystal diameter was defined as the geometric mean, $D=(D_h\ D_h\ D_v)^{1/3}$, implicitly assuming symmetry around the vertical. For convenience in relation to the growth law (1), D^2 will be referred to as the crystal size.

Crystallographic *c*-axis orientations were measured for the horizontal thin sections using standard operations on a semi automatic Rigsby Stage (Langway 1958, Lange 1988). In addition some extra measurements were carried out on vertical thin sections, noting for each *c*-axis measurement which crystal it belonged to by numbering the crystals on a photograph. This procedure provides the distribution of angles between neighbouring crystals which may reveal the possible recrystallization mechanisms responsible for the existing polycrystalline structure (Alley et al. 1995). If polygonization is happening to a considerable degree, an overweight of low angle boundaries is expected, relative to a sample with the same *c*-axis directions distributed randomly among the crystals. Dynamic recrystallization could also be detected by this method.

Observations

Meltlayer stratigraphy

The variation of meltlayer intensity with depth in the core is shown in Fig. 1. Note that the meltlayer curve is not a direct record of the annual meltwater formation, since the fraction of meltlayer-ice is modulated by changing accumulation. There is however a clear trend of increasing meltlayer abundance with depth, with a pronounced step to higher fractions encountered around 175 m depth. Below this point the oscillations of meltlayer intensity seem to proceed with higher amplitude until the core consists of 100% meltlayer-ice at 285 m depth. The remaining 60 m is superimposed ice interrupted only twice by a few cm of firn-ice.

A significant short term feature of the meltlayer curve is the shallow slim peak at 15-17 m depth. Based on volcanic signals (especially 1910 (Katmai) at 17.63 m and in addition 1873 at 23.05 m to estimate the rate of accumulation (Stampe 1997)) this meltlayer is dated to 1915-1930. The meltwater might have penetrated some meters down in the snow pack, which would make the melt event up to 10 years younger than the meltlayer, considering annual snow accumulation at the drill site.

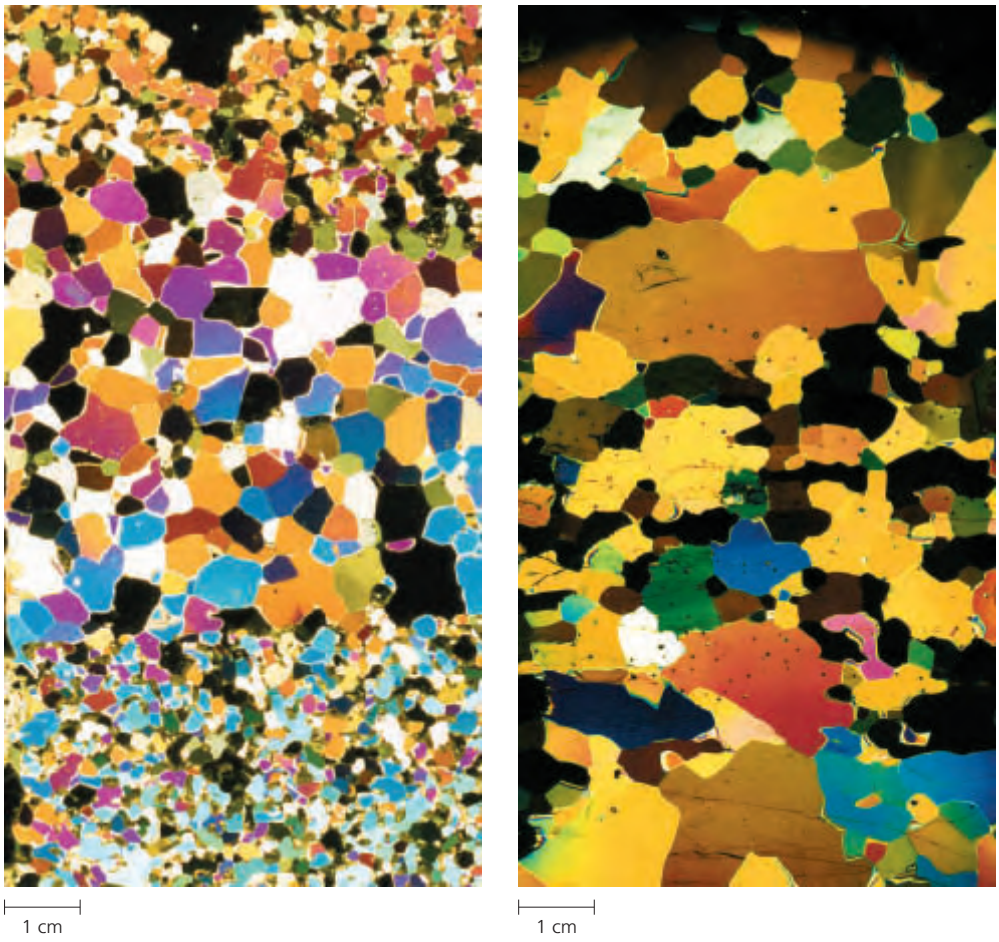

Fig. 2. Thin sections from increasing depths photographed between crossed polarizers. a: 26.40 m. Firn with a meltlayer clearly visible by its larger crystals. b: 209.65 m. Firn layer compressed to glacier ice surrounded by meltlayers with larger crystals. Air bubbles in the firn-ice are still seen. c: 285.50 m. Meltlayer-ice with a distinct difference in crystal size for top and bottom. c-axis measurements and chemistry data reveal that the appearance of smaller crystals is not associated with shear bands, but may be explained by contrasts in impurity concentrations. d: 329.95 m. Meltlayer-ice 15 m above bedrock with crystals being strikingly equant in size and shape.

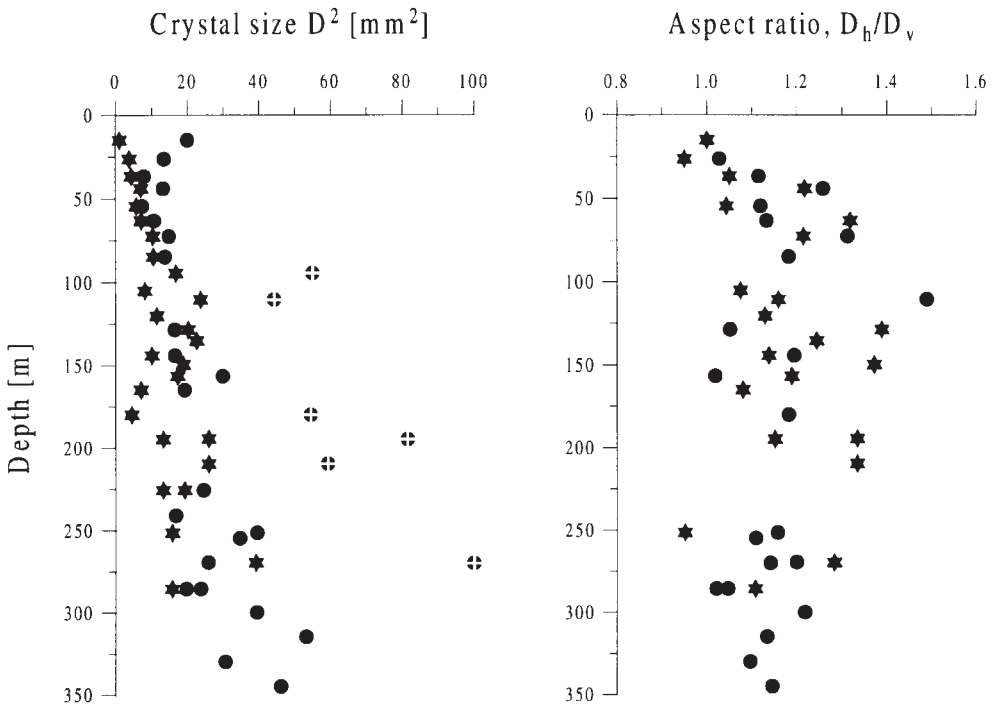

Fig. 3. Development of crystal size (as defined in the method section) and aspect ratios with depth in the core. Stars and dots denote data points obtained from firn-ice and meltlayer-ice respectively. Dots are marked with crosses for a group of outlier points which will be discussed later.

Crystal texture

In Fig. 2 photographs showing selected features of the crystal texture at different depths are reproduced. In the top 50 m, firn is not fully compressed to ice yet and displays small crystals, while the initial crystal size in the meltlayer-ice is considerably larger (Fig. 2a). Pronounced contrast in mean crystal size at the scale of thin sections is observed deeper in the core as well, coinciding with boundaries between meltlayer-ice and firn-ice (Fig. 2b) or totally within one kind of ice, most often meltlayer-ice (Fig. 2c). Strain shadows are observed at depths below 100 m, but become extinct 50 m above bedrock. In the last 50 m of the core, crystals are strikingly equant in size and shape (Fig. 2d), as if grown under very undisturbed conditions.

Fig. 3 shows to the left the crystal size profile along the core. There is a clear trend of mean crystal size increasing with depth and the growth is similar for firn-ice and meltlayer-ice although variations are clearly larger for the latter, featuring examples of outstanding large crystals around 100 and 200 m depth. Crystal elongation measured by the aspect ratio D_h/D_v increases over the top 50 m, but then stabilizes around 1.2, or perhaps decreases slightly towards the bottom.

c-axis distribution

In Fig. 4 the fabric diagrams obtained from *c*-axis measurements on the horizontal thin sections are displayed. All samples except the lowermost from 330 m depth have anisotropic *c*-axis distributions. The *c*-axes cluster in weak single maxima of similar strength throughout the core. Fabric development is summarized in the diagram to the left using the median polar angle θ_m as a measure of fabric strength. Additional data points in 210, 240 and 285 m depth are from measurements carried out on vertical thin sections to investigate if zones of smaller crystals could be shear bands. This was not the case. On

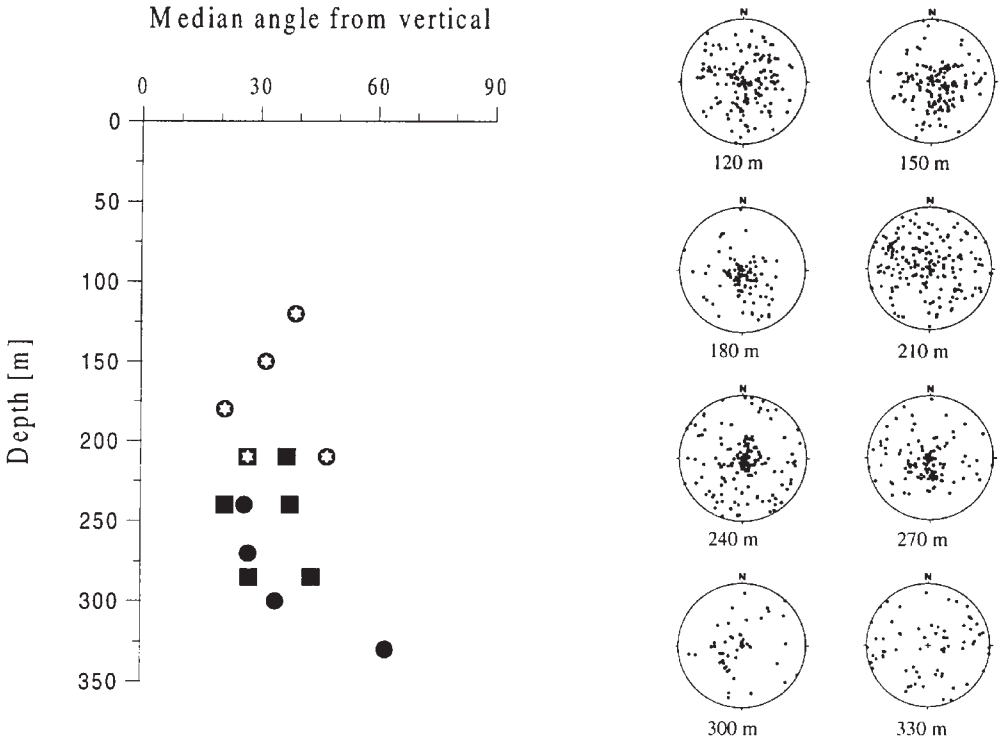

Fig. 4. Fabric diagrams obtained from the 8 horizontal thin sections and the change with depth of fabric strength given by the median angle θ_m, the top half angle in a cone around vertical containing half of the c-axes. A random distribution of c-axes corresponds to θ_m =60° while complete alignment has θ_m = 0°. Symbols with and without white stars denote data points from firn-ice and meltlayer-ice respectively. Extra data points (shown with squares) are obtained from additional measurements on vertical thin sections, rotated so that all data refer to the same coordinate system.

the contrary, the larger crystals in the thin sections from 240 and 285 m depth had the stronger fabric. They were associated with cleaner ice as well, which probably is the reason for the local size difference. In 210 m depth the crystal size contrasts were coincident with meltlayer boundaries and fabric was stronger in the firn-ice with the smaller crystals.

Fig. 5 represents the distribution of angles between *c*-axes of neighbouring crystals in the vertical samples from 210, 240 and 285 m depth. A strong fabric in itself dictates low angles between *c*-axes of individual crystals, whether they are neighbours or not. To investigate the possible influence of polygonization the distribution of angles between *c*-axes of neighbouring crystals must therefore be compared to the distribution of angles between *c*-axes of pairs of crystals picked randomly. This was done by repeating 10000 times a random selection of two crystals from the sample and calculation of the angle between their *c*-axes. The 10 intervals of angles in the figure are adjusted to make 10% of the 10000 angles fall in each interval. With no preferred angles between neighbouring crystals, their mutually angles should also be distributed equally among the 10 intervals and the relative frequencies would all be 1 except for the statistical variation. Dashed lines in the figures indicate the upper and lower fre-

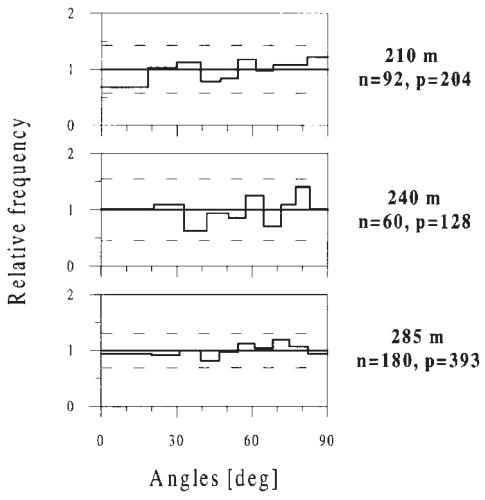

Fig. 5. Distribution of angles between neighbouring crystals in a sample normalized by the distribution of angles between crystals picked at random from the same sample (see text for further explanation). Measurements were carried out on samples from 210, 240 and 285 m depth. In each diagram the number of crystals (n) and neighbouring pairs (p) are noted. Notice that statistics are not equally good for the 3 datasets. Dashed lines indicate the level of significant deviation from a random distribution at 95% confidence level.

quency limits to be exceeded in an interval for the distribution to deviate from random with 95% confidence in a binomial test.

The measurements were carried out on samples from a depth interval where fabric has reached maximum strength according to Fig. 4 and the total deformation thus is expected to be at its highest. However no significant deviation from the random distribution is revealed by the data, especially not a preference for low angle boundaries, as would be expected if polygonization were altering the polycrystalline structure to a considerable degree.

Interpretation of the polycrystalline structure

Deformation and the recrystallization regime

Since the drill site is situated on top of a dome, compression is assumed to be the dominating stress system in accordance with observed fabric pattern. However, single maximum fabrics also form in simple shear. No strong *c*-axis alignment is revealed, which is to be expected for a newly formed ice cap with a limited strain history. An empirical relationship between vertical deformation and strength of the anisotropy developed is well established for relatively weak fabrics, and may be used to estimate the total compression of ice in the Hans Tausen ice core. Measured values of θ_m around 30° from 100 to 300 m depth correspond roughly to a total vertical deformation of 30-40% (Azuma & Higashi 1985, Castelnau et al. 1996). In the top 100 m, where unfortunately no fabric measurements have been carried out, strain is probably decreasing towards zero at the surface.

The random fabric measured in the sample 15 m above bedrock, the disappearance of strain shadows and the equant crystal texture in the last 50 m of the core are all signs of limited deformation of the ice close to the bottom. It may be that the drilled part of the ice cap is sitting in a bedrock depression, but low deformation close to bedrock can also be understood as a result of ice dynamics. If the ice cap has always been frozen to the bed, which seems reasonable considering the present temperature of –16° at bedrock, then vertical strain-rates are predicted to approach zero at the bottom of the ice cap. With a short history of deformation, total strain too is expected to be small close to the bedrock. Thus undisturbed crystal growth conditions for ice in the lowermost part of the core may be accounted for by a simple ice flow model.

As has been observed in other ice cores (Hooke & Hudleston 1981, Lipenkov et al. 1989, Thorsteinsson 1996), the ice crystals are generally less elongated than would be expected considering the inferred total strain. If the crystal structure were stationary except for deformation (that is no grain growth, polygonization, etc) and flattening of each crystal simply followed bulk deformation, the grain boundaries beeing passive strain markers, then the aspect ratio of crystal shape would increase with total strain by uniaxial compression as indicated by the solid line in Fig. 6.

By normal grain growth the material positions of grain boundaries are moving and isotropic growth could be argued to slow down the flattening of crystals, since an elongate crystal becomes rounder by growing the same amount in all directions. The dotted lines in Fig. 6 indicate the development of aspect ratio with total strain for strain rates ranging from 10^{-2} to 10^{-5}. The examples shown are all starting from a spherical crystal of diameter 3 mm and assuming a mean area (in vertical thin section) growth rate of 10^{-2} mm^2/year, which is appropriate for Hans Tausen conditions as will be seen later. What matters for the calculation however is

only the mutual proportions between the rate of crystal growth and the rate of compression. Still using the Hans Tausen ice core as an example it appears that even with the modification introduced by growth of the crystals, the observed aspect ratio 1.2 suggests that total strain should be less than 15%, which is much less than indicated by fabric strength. For a total strain of 30-40% in accordance with general fabric strength measured in the core, the aspect ratio in this model would exceed 1.5. This is more than observed anywhere in the core. Clearly the model is not in agreement with data.

Polygonization operating to some degree along with the normal grain growth could be the mechanism keeping the aspect ratio low by subdividing elongated crystals. In that case the notion of 'onset of polygonization' would be misleading. Rather polygonisation would be an active process well up in zone of crystal growth, gradually gaining influence with increasing depth until a balance with normal grain growth is obtained resulting in a stagnation of crystal size. Another possibility is that some feature of normal grain growth itself counteracts the development of strongly elongated crystals. The possible influence of polygonisation or other process keeping the aspect ratio low in the so called normal grain growth regime is a general problem, which needs further investigation in order to reveal to what extent the crystal growth rate is affected.

The steady growth of mean crystal size with depth in combination with weak single maximum fabrics, are observations that usually are inferred to indicate that normal grain growth is the dominant process controlling the development of the polycrystalline structure. However an effect of polygonization can not be excluded even though a stagnation of crystal sizes is not seen. Depths of 200-300 m are in the zone expected to be most susceptible for polygonization due to a combination of high strain-rate and high strain, but the investigation of the angles between c-axes of neighbouring crystals in this depth interval failed to reveal any influence of polygonization. On the other hand strain shadows observed from 100 to 300 m could be a sign of beginning polygonization. If active, pologonization may or may not change the functional relationship (1). Since too little is known about the influence of polygonization in the zone where crystals are still growing, crystal data will be analyzed assuming the applicability of the normal grain growth law (1). Subsequently some polygonization scenarios and their impact on the conclusions of the analysis will be discussed.

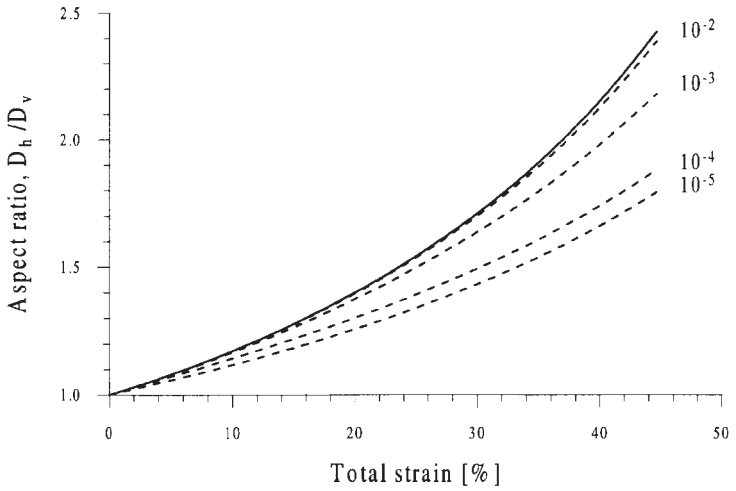

Fig. 6. Aspect ratio of a volume deforming in uniaxial compression as function of total strain ($(a-a_0)/a_0$, a_0 and a being thichness before and after compression). The solid line apply to the bulk of the ice or a crystal following bulk deformation. Dotted lines indicate the development of shape, when isotropic growth of the volume happens simultaneous with the compression. The growth rate and the initial crystal size are chosen to match Hans Tausen conditions ($k=10^{-2}$ mm^2/year and $D_0=3$ mm^2 and strain rates are 10^{-2}, 10^{-3}, 10^{-4} and 10^{-5} year^{-1} respectively).

Factors affecting mean crystal size locally

In the top 50 m of the Hans Tausen ice core, mean crystal size is significantly larger in meltlayers than in the surrounding firn. It seems impossible that temperature enhancement of normal grain growth can account for the initial size difference, even if latent heat released by refreezing of meltwater would raise the temperature close to the

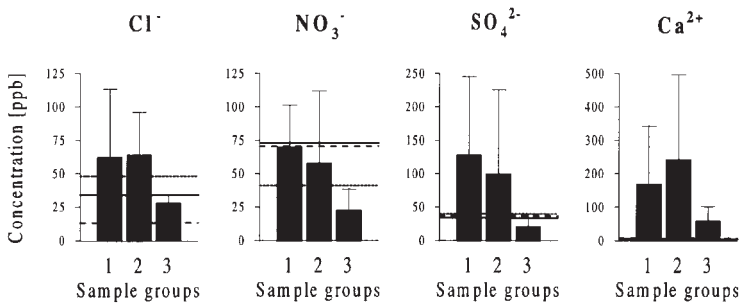

Fig. 7. Mean values and standard deviations for concentrations (ppb) of Cl^-, NO_3^-, SO_4^{2-} and Ca^{2+} in samples 1) firn-ice, 2) meltlayer-ice excluding the outliers of Fig. 3 and 3) meltlayer-ice, outliers. Dashed, dotted and solid lines indicate background levels of the same ions in Holocene ice from Summit (Whitlow et al. 1992), Byrd Station and Camp Century (Paterson 1991) respectively.

melting point. Growth rates as high as 30 mm^2 per year at –0.2°C have been reported (Li 1995), but still months are needed for the crystals in meltlayers to gain the lead of 10-20 mm^2 in crystal size. It is hard to believe that the heat will stay localized in the meltlayer for that long, which would be necessary to explain why the adjacent firn does not grow large crystals. More likely the large crystals are created in the very process of refreezing meltwater.

Deeper in the core the crystal size contrast between firn-ice and meltlayer-ice is often less pronounced or even absent. By equation (1), a blurring of initial crystal size differences with depth is to be expected, since with increasing age of the ice the constant term D_0^2 becomes negligible compared to the growth term $k\,t$. Size contrasts encountered in older ice must owe to local variations in the growth rate. Any difference in growth rate is magnified by the age of the ice, leading to the increased scattering of crystal sizes with depth, revealed by Fig. 3. Local variations of the growth rate are possibly due to different impurity concentrations. Redistribution of impurities is likely to occur with the percolation of meltwater, which might explain why the larger variations of crystal size are associated with the meltlayer-ice.

A comparison of impurity concentrations has been made between samples from the group of outlier points in Fig. 3 and samples from the remaining part of the meltlayer-ice and from firn-ice. Impurities investigated were Cl^-, NO_3^-, SO_4^{2-}, Ca^{2+}, Na^+, K^+, Mg^{2+}, NH_4^+ and micro particles (0.4-2.0 μm). The content of insoluble dust shows no difference among the groups, while all ions excluding ammonia are rarefied in the outlier group, as exemplified by Fig. 7 showing plots of mean concentrations and standard deviations for Cl^-, NO_3^- and SO_4^{2-}. It should be noted that the considerations presented here rest on a meager data material due to the limited amount of data from the group of outliers and furthermore that the redistribution of impurities taking place by meltwater percolation could lead to very localized accumulations of impurities making bulk measurements misleading. However the measurements do support the idea that the outliers are associated with spots of unusually clean ice.

Analysis of the crystal growth

Crystal data were analyzed applying the normal grain growth law (1). To determine the growth rate of mean crystal size, a dating of the ice is required. Furthermore, the influence of temperatures changing with depth and time needs to be evaluated.

Tentative dating of the ice

The eruptions of Laki (1783 AD) encountered at 35.1 m depth and Eldgjá (934 AD) at 131.4 m depth provide two major fix points for the time scale (Stampe 1997, Clausen et al. 2001). Following the hypothesis of a newly formed ice cap, a tentative dating was obtained by modelling the generation of an ice cap which has a thickness at the ice divide given by the length of the Hans Tausen ice core, the time horizons mentioned above placed at right depths and a profile of total strain in accordance with observed fabric strength in the core (Madsen 1997). The growth of a very simplified Hans Tausen ice cap was modelled using a vertically integrated flow model

(Oerlemans 1981). Subsequently the Dansgaard-Johnsen model was invoked to follow the downward movement of individual time horizons within the ice column at the drill site (see e.g. Paterson 1994). Adjusting the dependence of accumulation on elevation, a variety of possible time scales for the older part of the core can be extracted from the modelling. Two examples shown in Fig. 8 will be considered in this paper. The first one ascribe an age of 3500 years to the ice close to bedrock. It turns out from the modelling (or from a rough calculation) that this timescale represents a lower age limit. Generating the present ice thickness considerably faster require early accumulation rates far exceeding present precipitation.

On the other hand stretching the time scale to older ages is possible. The example shown spans 5500 years, and even longer time scales can be obtained.

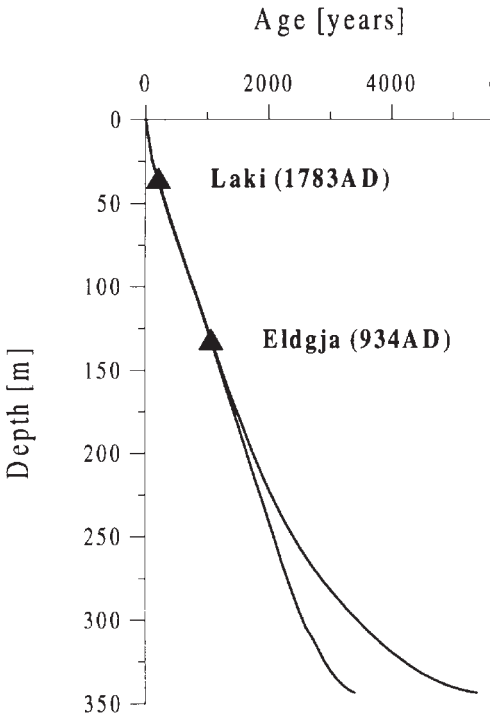

Fig. 8. Two possible time scales of total length 3500 and 5500 years for the Hans Tausen ice core, obtained by modelling the generation of the ice cap. The time horizons provided by eruptions of Laki (1783 AD) and Eldgjá (934 AD) are marked with vulcanic cones.

Temperature correction to crystal growth

Due to the strong temperature dependence of crystal growth given by equation (2), data should be corrected for the different temperature histories experienced by crystals at different depths. Considering only the increasing elevation of the ice surface and using a lapse rate of 0.75°C/100 m, the early ice cap had a temperature around –18.5°C, increasing at the bottom and decreasing at the top as the ice cap grew. The movements of the ice crystals downwards in the ice cap were extracted from the modelling. Temperature profiles back in time were taken to be steady state profiles (see e.g. Paterson 1994), with parameters adjusted to fit the present temperature curve and former surface temperatures based on the modelled surface elevation. Latent heat released by refreezing of melt water has not been taken into account explicitly, and neither has any climatic change been assumed. Invoking the temperature correction, equation (1) is changed to

$$D^2 = D_0^2 + k_0 \sum exp\left(\frac{-Q}{RT}\right) \Delta t, \qquad (3)$$

summing over the time span in which the crystals have existed, or

$$D^2 = D_0^2 + k_0 \bar{A}_t \, t, \qquad (4)$$

where $\bar{A}$ is the time averaged Arrhenius factor for the crystals of age t. The activation energy, Q, was found by regression analysis on data from five other polar ice cores in which crystal growth rates have previously been determined (Fig. 10. The growth rate for Hans Tausen ice core, to be derived in the following, is also displayed but of course not included in this evaluation of Q). According to equation (2) data should define a straight line of slope $-Q/R$ in a plot of k on logarithmic scale versus $1/T$. The fit to data in Fig. 10 is very satisfactory and results in the value Q=58 kJ/mol. Previous analyses using other dataset have suggested lower values of Q (Gow 1969, Duval 1985, Paterson

1994). However this analysis uses data from ice only rather than data from firn or mixtures of data from ice and firn and cores covering both ice and firn. A satisfactory demonstration that ice crystal growth in firn and ice follow the same growth law is not known to the authors.

Furthermore it has been avoided to plot data multiplied by different correction factors used by some authors and an attempt has been made to convert the linear intercept measurements from GRIP to represent results obtained by mean area measurements, which have been used to obtain the other data. For these reasons Q=58 kJ/mol is considered the best value available for this purpose. Using it the present temperature span in the Hans Tausen bore hole make crystal growth 1.7 times faster close to bedrock than in the top of the ice core. By the temperature correction derived above, time averaged crystal growth rates increase from top to bottom by a factor 1.4 using the shorter time scale and slightly less using the longer.

The rate of crystal growth in the upper 200 m

Growth rates were calculated by fitting equation (4) to data. The analysis was restricted to the upper 200 m of the ice core, for which the time scale is well established and the temperature correction small in any circumstance. Data points from firn not yet transformed to ice have been excluded. For firn-ice the growth rate $7.9 \cdot 10^{-3}$ mm^2/year at –21°C was derived from the fit shown to the left in Fig. 9. As already discussed data from meltlayer-ice are more scattered. However from Fig. 3 it is evident that, excluding the outliers, crystal sizes in meltlayer-ice follow the same trend of growth as crystal sizes in firn-ice.

Fig. 9 shows to the right a fit to data from meltlayer-ice in the upper 200 m using the growth rate obtained for firn-ice but taking into account the larger initial size by raising D_0. The fit is good for most of the crystals, while the smaller group of outliers treated separately indicate a much faster growth – perhaps 3 times faster. It should be noted that the

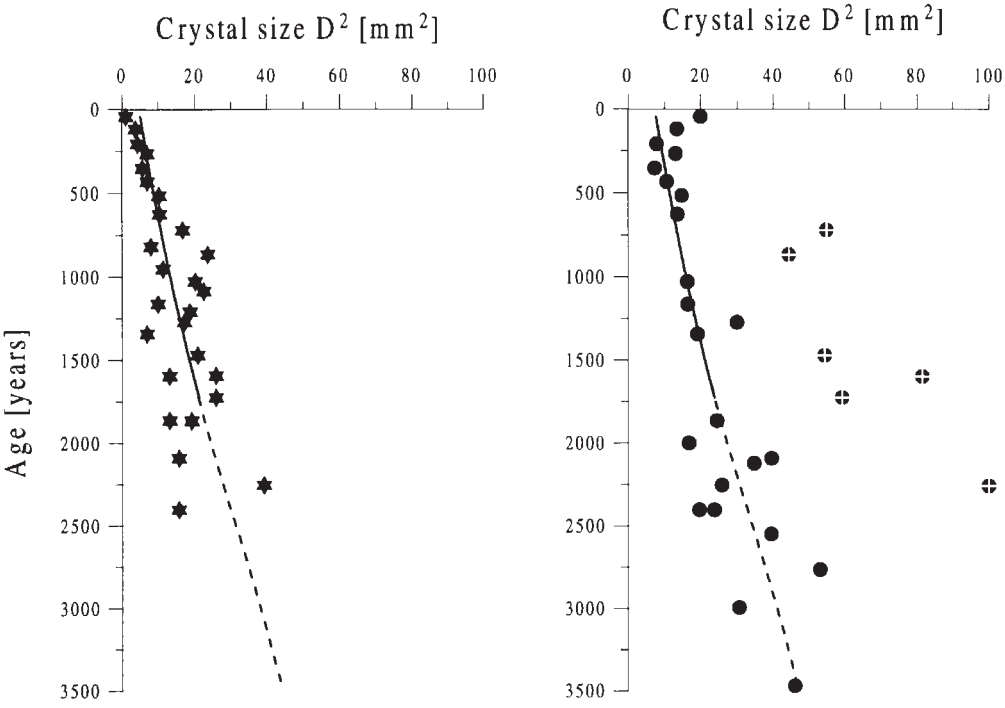

Fig. 9. Crystal sizes (mm^2) versus ascribed age of the ice (years B.P.). The solid line show the best fit of the growth law (3) to data. The timescale used in this figure is the younger of the modelled time scales shown in Fig. 8, but the choice has no importance for the fit which is restricted to the top 200 m, where the time scales are in good agreement. Left: Data from firn-ice. The fit was made excluding the first three data points from firn and data points obtained from ice below 200 m. Right: Data points from meltlayer-ice. The best fit was determined with k_0 fixed at the value found for firn-ice. The fit was made using only data points from the top 200 m and excluding the outliers (marked with white crosses). The dashed line is the extrapolation of the growth law beyond 200 m depth where time control is lost, i.e. it represents the expected crystal size as a function of time. Note that the prediction includes the effect of calculated temperature changes. With the depicted choice of timescale for the older ice, data are well described by this model. Associating the lower datapoints with higher ages (moving them downwards in the figure) would introduce a discrepancy with the model (crystal sizes would be smaller than predicted).

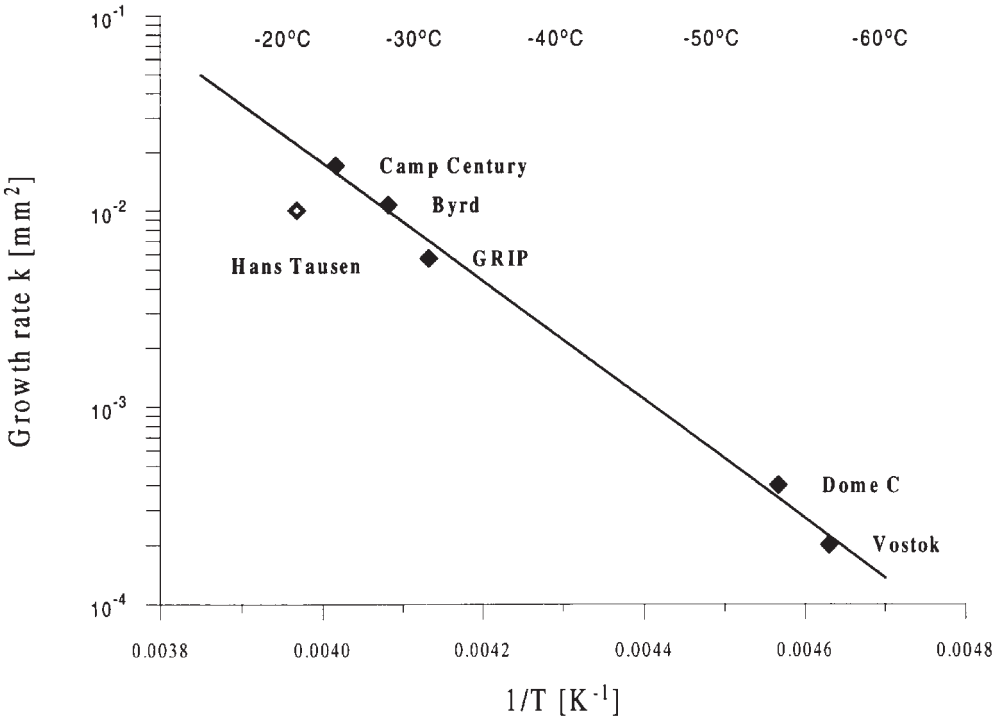

Fig. 10. Crystal growth rates in polar ice. Data points from Vostok (Lipenkov et al. 1989, crystal growth rate estimated by the authors using the published crystal size profile.), Dome C (Duval & Lorius 1980), Byrd (Gow & Williamson 1976), GRIP (Thorsteinsson et al. 1997), Camp Century (Herron & Langway 1982), and the regression line for these data. Also shown is the new data point from the Hans Tausen ice core. Data are given by mean area measurements (number of crystals per area). A correction factor of 1.29 obtained from studies of thin sections from the Hans Tausen ice core, has been applied to convert the linear intercept growth rates from Hans Tausen and GRIP to represent mean area results.

measurements of the largest crystals are inaccurate, since the requirement that crystal size should be much smaller than thin section dimensions is not met.

As can be seen from Fig. 10, the new data point from Hans Tausen ice core deviates appreciably from the regression line of previous data, the growth rate having only half the value expected from the regression line at –21°C. The most obvious explanation for this deviation is offered by the impurities in the ice impeding grain boundary motion. The general impurity level of the Hans Tausen ice core is relatively high compared to the other cores represented in Fig. 10, which are all retrieved from less exposed inland drill sites. The fact that the outlier data points of extremely large crystals in the meltlayer-ice are associated with spots of unusually clean ice lends further support to this explanation. Alternatively polygonization operating to some degree in the upper half of the core, could result in a lowered growth rate. In this case however the question is left why polygonization should not keep crystals small in the cleaner ice as well as in the rest of the core? In fact strain shadows are not absent in the very large crystals.

In case of impurity hindered grain growth, the impurity concentrations in the Hans Tausen samples could be compared with background impurity levels of the other cores from Fig. 10 in order to investigate which impurities have the main impeding effect on crystal growth. In Fig. 7 general concentrations of Ca^{2+}, Cl^-, NO_3^- and SO_4^{2-} in Holocene ice from GRIP, Camp Century and Byrd Station have been marked in the diagrams showing the concentrations in Hans Tausen ice core. In comparison to these two drill sites, the concentration of NO_3^- is not unusually high in Hans Tausen ice. Mean concentrations of Ca^{2+} are an order of magnitude higher in Hans Tausen ice than in GRIP ice, but since this is also the case for the group of outlier samples with high growth rates, Ca^{2+} is probably not the main cause of

impeded grain growth. SO_4^{2-} and to a less extent Cl^- ions are present in elevated concentration except in the outlier samples and thus could be the cause of the lowered growth rate. It may be noted that (Paterson 1991) concluded that elevated concentrations of Cl^- and possibly SO_4^{2-} in ice-age ice relative to Holocene ice kept crystals small and thereby caused the different rheology of the two types of ice.

Implications of data concerning Hans Tausen Iskappe

Age of the ice cap

Age estimates of Hans Tausen Iskappe may be evaluated based on crystal sizes in the ice close to bedrock, using the growth rate $k=7.9 \cdot 10^{-3}$ mm^2/year. From the two examples of time scales shown in Fig. 8, the one dating the oldest ice to 3500 years was selected for Fig. 9 because it happened to fit the data points in the older ice reasonably well. Fig. 11 displays what happens when the time scale is stretched from 3500 to 5500 years. The difference between measured and calculated crystal size is shown as a function of age of the ice for each of the two time scales. The longer time scale tends to predict larger crystals than found, while the shorter time scale leads to an even distribution of crystals being larger and smaller than calculated, and so appears to be a better dating.

The above estimate of the age of Hans Tausen Iskappe rests on the assumption that the growth rate determined in the previous section is applicable throughout the core meaning that temperature and age are the only depth dependent variables controlling crystal size. This involves that the impurity level and the degree of polygonization is approximately constant throughout the core. The concentrations of soluble impurities in the lower samples are comparable to the level in the upper part (excluding the very clean outlier samples), which justifies the growth rate used. As previously discussed, reduction of mean crystal sizes due to polygonization can not be ruled out. The importance of this effect for the age evaluation depends on the distribution of significant polygonization in the core. The age estimate is not affected if polygonization is equally active everywhere so that the functional relationship (2) is preserved and the only influence of polygonization is a smaller (but still constant) k. Data from the top of the core (where strain has not reached its maximum) are used for calculating the growth rate and crystal sizes close to the bottom (where strain apparently is low) are crucial for estimating the time of ice cap initiation. The age evaluation does not depend heavily on crystal sizes in the lower-mid sector where polygonization is likely to be strongest. If significantly more polygonization happens close to bedrock than in the upper part of the core, then the calculated growth rate will be too high for application in the oldest ice and thus the age estimate will be too low. The opposite case of less polygonization at the bottom than in the upper part of the core would lead to overestimating the age. However realistic time of formation can not be much lower than 3500 years.

Paleo ice temperatures

The temperature correction applied in the analysis presented above did not take into account latent heat when estimating former surface temperatures. Released latent heat from refreezing of meltwater may lead to a warming of average 0.266°C per cm meltlayer formed (Reeh 1990). Until 170 m depth the meltlayer fraction is small and similar to present conditions (Fig. 1), and additional warming may be neglected without major errors. Below 170 m the

amount of meltlayer-ice increases to 50-100% and latent heat may have raised the temperature of the ice significantly. Including latent heat in the calculation would add only minor corrections to the calculated growth rate based on the upper half of the core, while temperature enhancement of crystal growth in the older part of the ice has been larger than assumed. Thus the temperature correction applied in the above analysis can be considered a minimum correction.

Explaining observed crystal size by equation (4), a higher temperature correction $\bar{A}_t$ for ice at the bottom implies that the age of the ice is lower by the same factor. As paleo ice temperatures and age of the ice constrain each other in this way, and since the ice cap can not be much younger than the 3-4000 years suggested using the 'minimum' temperature correction, it follows that former ice temperatures can not have been much higher than assumed in the above. Particularly this implies that the total dominance of meltlayer-ice in the bottom of the core should not be interpreted as the remains of a former temperate glacier. Independently of the age estimate it can be argued that according to equation (2) and the results of (Li 1995) the crystal growth rate is one to several orders of magnitude larger at the melting point of the ice than at present temperatures in the bore hole, which means that after a few centuries (or even years) spent close to the melting point, the crystals would have grown larger than observed anywhere in the core. Finally it may be added that removal of older ice by bottom melting involves a substantial temperature drop at bedrock from 0°C when melting ceased to –16°C at present. Allowing the oldest ice in the core some thousands years to sink from the surface to the bottom before melting stops leaves quite a short period for this temperature drop.

In conclusion Hans Tausen Iskappe could have been warmed a few degrees by the latent heat of meltwater in its early days, strengthening the argument for a late formation of the ice cap, but a warming extensive enough to raise the temperature close to 0°C within the ice is not compatible with observed crystal sizes. Thus the lack of depositions from the ice age is hardly due to melting and run-off from the bottom of the ice cap.

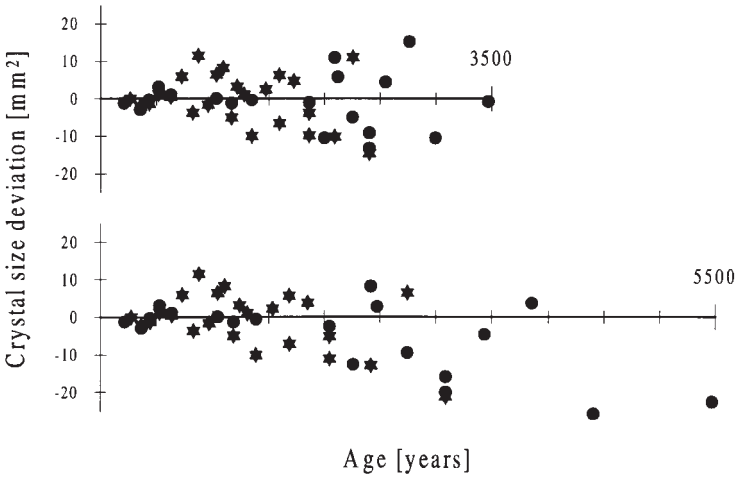

Fig. 11. Deviation of measured crystal size from the size calculated using each of the two timescales of Fig. 8. Stars refer to data from firn-ice and circles to meltlayer-ice. The deviations tend to grow with time, as expected from equation (1), since any initial difference in growth rate is magnified by the age of the ice. Crystals smaller and larger than calculated are evenly distributed in the upper plot, applying the time scale of 3500 years for the data analysis, while negative deviations dominate in the lower plot using the longer time scale of 5500 years.

Paleo accumulation and melt rates

Paleo accumulation rates control the lower limit of the age of Hans Tausen Iskappe, by the time needed to generate the appropriate amount of ice. To account for the deformation indicated by fabric development, mean accumulation is required to be higher than the present 10.8 cm ice equivalent per year if the ice cap is as young as indicated by the crystal data. Evidence that accumulation rates were indeed higher earlier in the history of the ice cap, comes from the constant layer thickness in the core to at least 130 m and probably as deep as 225 m (Clausen et al. 2001). In combination with a vertical compression as revealed by fabric data, this indicate that the accumulation could have been up to twice the amount precipitated at present. A more thorough investigation of fabric strength including the upper 100

m could provide more precise estimates of paleo accumulation.

With the graduation of accumulation mentioned above the meltlayer stratigraphy of Fig. 1 indicates that meltwater formation has decreased over the last thousand years probably around 50%. Provided that accumulation was never appreciably lower than the present, melting activity was even higher further back in time. This pattern conform to the history of a growing ice cap, subject to extensive summer melting until the surface is elevated well above the equilibrium line.

The meltlayer profile holds a climate record of (maximum) summer temperatures (Koerner 1977, Koerner & Fisher 1990). To draw conclusions concerning long term climate from the meltlayer record the effect of changing surface elevation due to the growth of the ice cap must be subtracted. Some studies have been made on the Queen Elizabeth ice caps, Canada (Koerner 1979), which show that the meltwater formation decreases exponentially with ice surface elevation. A quantitative applicability of these results to Hans Tausen Iskappe is questionable, but it seems likely that an exponential or other non-linear relationship between meltwater formation and elevation of the ice surface accounts for some of the highly elevated fraction of meltlayer-ice in the lower half of the core. However the change from approximately 10% to more than 50% meltlayer-ice encountered at 170 m depth in the core still seem so rapid that its explanation must involve some abrupt change, for instance of summer temperatures or accumulation. The higher amplitude of the oscillations in meltlayer intensities coincident with the shift to high meltlayer fractions are also worth noting. Is it attesting to an increased sensitivity of the meltlayer proxy below some critical point or is it the actual record of higher climatic variability in the past? To be able to infer paleo climate and/or the growth history of the ice cap from the meltlayer data, investigation of present meltlayer formation as a function of elevation on Hans Tausen Iskappe would be most useful.

Summary and conclusions

The increase of mean crystal size with depth throughout the Hans Tausen ice core suggests that the development of the polycrystalline structure of the ice is dominated by normal grain growth. Although strain shadows are observed in most of the core, the effect of polygonization seems limited but can not be excluded. The deepest 50 m of the core appear almost unaffected by strain. With the exception of a random *c*-axis fabric measured in ice 15 m above bedrock, fabrics observed below 100 m depth are weak single maximum fabrics which could have been created by vertical compression of the order of 30%. In combination with the knowledge of the thickness of annual layers in the core at least to the horizon of Eldgjá 934 AD eruption, this implies that accumulation has formerly been appreciably higher than present.

The growth rate of mean crystal size was calculated using linear intercept measurements in the well dated upper half of the core. The obtained value of $7.9 \cdot 10^{-3}$ mm^2/year at –21°C is only half the rate expected from previous studies of crystal growth in other polar ice cores. Soluble impurities especially SO_4^{2-} and Cl^- is found in relatively high concentrations in the Hans Tausen ice and may cause the low growth rate by impeding grain boundary motion. Explaning the slow crystal growth by impurities rather than polygonization partially counteracting normal grain growth is supported by the existence of outstanding large crystals associated with spots of unusually clean ice.

Provided that the effect of polygonization is negligible or approximately con-

stant throughout the core, the age of the oldest ice can be evaluated based on mean crystal sizes measured in the lower part of the core. It appears that the crystal size profile is in good agreement with a time scale of length 3500 years, but not with one reaching back 5500 years. Assuming the ice to have formerly been at the melting point at bedrock leads into contradiction with observed crystal sizes in the older part of the core, so the lack of ice age ice in the core is hardly explained by melting and run-off from the bottom of the ice cap. Thus the conclusion of this study is that Hans Tausen Iskappe was absent for a period in Holocene and (re)formed at a time conforming well to the 'Neoglacial' cooling 3500-4500 BP (Crowley & North 1991), which could have caused the initiation of the present ice cap. At the Hans Tausen plateau this climatic cooling could have been reinforced by the isostatic uplift of the area, that has been going on since the retreat of the inland ice at the termination of the last ice age (Funder & Hansen 1996). To learn more about late Holocene climate from the Hans Tausen ice core the meltlayer stratigraphy should be studied further.

Acknowledgements

We thank Marie-Louise Siggaard Andersen for measurements of impurity concentrations and Dorthe Dahl-Jensen and Michael Stampe Skousen for computational assistance and valuable discussions. Contribution no. 1535 of the Alfred Wegener Institute.

References

Alley, R. B. 1992. Flow-law hypotheses for ice-sheet modelling. *Journal of Glaciology* 38(129): 245-256.

Alley, R. B., A. J. Gow and D. A. Meese 1995. Mapping c-axis fabrics to study physical processes in ice. *Journal of Glaciology* 41(137): 197-203.

Alley, R. B., J. H. Perepezko and C. Bentley 1986. Grain growth in polar ice: I. Theory, II. Application. *Journal of Glaciology* 32(112): 415-433.

Atkinson, H. V. 1988. Theories of normal grain growth in pure single phase systems. *Acta Metallurgica* 36(3): 469-491.

Azuma, N. and A. Higashi 1985. Formation processes of ice fabric pattern in ice sheets. *Annals of Glaciology* 6: 130-134.

Castelnau, O., T. Thorsteinsson, J. Kipfstuhl and P. Duval 1996. Modelling fabric development along the GRIP ice core, central Greenland. *Annals of Glaciology* 23: 194:201.

Clausen, H. B., M. Stampe, C. U. Hammer, C. S. Hvidberg, D. Dahl-Jensen and J. P. Steffensen 2001. Glacial chemical studies on ice cores from Hans Tausen Iskappe. Meddelelser om Grønland Geoscience, this volume, pp 123-149.

Crowley, T. and G. R. North 1991. *Paleoclimatology* Oxford University Press. pp. 67-68, 92-94.

Duval, P. and O. Castelnau 1995. Dynamic recrystallization of ice in polar ice sheets. *Journal de Physique IV* 5(C3): 197-205.

Duval, P. 1985. Grain growth and mechanical behaviour of polar ice. *Annals of Glaciology* 6: 79-82.

Duval, P and C. Lorius 1980. Crystal size and climatic record down to the last ice age from antarctic ice. *Earth and Planetary Science Letters* 48: 59-64.

Funder, S and L. Hansen 1996. The Greenland ice sheet – a model for its culmination and decay during and after the last glacial maximum. *Bulletin of the Geological Society of Denmark* 42: 137-152.

Gow, A. J. 1969. On the rates of growth of grains and crystals in south polar firn. *Journal of Glaciology* 8(53): 241-252.

Gow, A. J., D. A. Meese, R. B. Alley, J. J. Fitzpatrick, S. Anandakrishnan, G. A. Woods and B. C. Elder 1997. Physical and structural proporties of GISP2 ice core: A review. *Journal of Geophysical Research* 102(C12): 26, 559-26, 575.

Hammer, C. U., S. J. Johnsen, H. B. Clausen, D. Dahl-Jensen, N. Gundestrup and J. P. Steffensen 2001. The paleoclimatic record from a 345 m long ice core from the Hans Tausen Ice Cap. Meddelelser om Grønland Geoscience, this volume, pp. 87-95.

Herron, S. L. and C. C. Langway 1982. A

comparison of ice fabrics and textures at Camp Century, Greenland and Byrd Station, Antarctica. *Annals of Glaciology* 3: 118-124.

Hooke, R. L. and J. P. Hudleston 1981. Ice fabric from a borehole at the top of the south dome, Barnes Ice Cap, Baffin Island. *Geological Society of American Bulletin Part I*, 92: 274-281.

Koerner, R. M. 1977. Devon Ice Cap: Core stratigraphy and paleoclimate. *Science* 196: 15-18.

Koerner, R. M. 1979. Accumulation, ablation and oxygen isotope variations on the Queen Elizabeth Islands ice caps, Canada. *Journal of Glaciology* 22: 25-41.

Koerner, R. M. and D. A. Fisher 1990. A record of Holocene summer climate from a Canadian high-arctic ice core. *Nature* 266: 508-511.

Lange, M. 1988. A computer-controlled system for ice-fabric analysis on a Rigsby Stage. *Annals of Glaciology* 10 : 92-94.

Langway, C. C. 1958. *Ice fabrics and the universal stage*. Thecnical Report 62, U. S. Army snow and permafrost establishment.

Li, J. 1995. *Interrelation between flow proporties and crystal structure of snow and ice*. PhD thesis, The University of Melbourne.

Lipenkov, V. Y., N. I. Barkov, P. Duval and P. Pimienta 1989. Crystalline texture of the 2083 m ice core at Vostok Station. *Journal of Glaciology* 35(121): 392-398.

Madsen, K. N. 1997. *Hans Tausen iskernen – studier af krystalstruktur, datering og smeltelagsstratigrafi*. Master of Scince thesis, University of Copenhagen.

Oerlemans, J. 1981. Some basic experiments with a vertically integrated ice sheet model. *Tellus* 33: 1-11.

Paterson, W. S. B. 1991. Why ice-age ice is sometimes 'soft'. *Cold regions Science and Technology* 20: 75-98.

Paterson, W. S. B. 1994. *The physics of glaciers*. Pergamon, 3. edition.

Reeh, N. 1991. Parametrization of melt rate and surface temperature on the Greenland ice sheet. *Polarforschung* 59(3): 113-128.

Stampe, M. 1997. Vulkanske vidnesbyrd i en iskerne fra Hans Tausen. Master of Science thesis, University of Copenhagen.

Thomsen, H. H., N. Reeh and O. B. Olesen 1996. *Glacier and climate research on Hans Tausen Iskappe, North Greenland – 1995 glacier basin activities and preliminary results*. Bulletin Grønlands geologiske Undersøgelse.

Thorsteinsson, T. 1996. *Textures and fabrics in the GRIP ice core, in relation to climate history and ice deformation*. PhD thesis, Alfred-Wegener-Institut für Polar und Meeresforschung.

Thorsteinsson, T., J. Kipfstuhl and H. Miller 1997. Textures and fabrics in the GRIP ice core. *Journal of Geophysical Research* 102(C12): 26,583-26,599.

Whitlow, S. P., A. Mayewski and J. E. Dibb 1992. A comparison of major chemical species seasonal concentration and accumulation at the South Pole and Summit, Greenland. *Atmospheric Environment* 26A: 2045-2054.

Surface Movement and Mass Balance at the Hans Tausen Drill Site determined by use of GPS

By Kristian Keller, Christine S. Hvidberg, Niels Gundestrup and Peter Jonsson

Abstract

Keller, K., C. S. Hvidberg, N. Gundestrup and P. Jonsson 2001. Surface Movement and Mass Balance at the Hans Tausen Drill Site determined by use of GPS. Copenhagen, Danish Polar Center. Meddelelser om Grønland Geoscience 39, pp. 115-122.

During the deep drilling at Hans Tausen Iskappe in Peary Land, North Greenland, the ice cap has been mapped with GPS. Kinematic GPS and ice penetrating radar measurements were done at the southeast dome extending to approximately 3 km from the drill site at the top of the dome, 82.5°N; 37.5°W (Gundestrup et al. 2001). Furthermore a strain net was established consisting of a center pole at the top of the dome and three rings, each of eight poles, at distances 0.3, 1.5, and 3.0 km from the center.

The bottom and surface topography, ice surface velocities from the strain net and precipitation data were used to calculate the present mass balance of the dome. The present mass balance of the dome was found to be +0.04±0.02 m of ice/year, i.e. the ice thickness at the dome increases with a rate of about one third of the annual accumulation. The result is highly consistent and independent on assumptions regarding the ice flow. Our result shows that the central part of the ice cap is far from steady state, implying that simple models cannot be used to determine the time scale of the ice core and the thinning of annual layers.

Keywords: GPS; strain net; ice flow model; mass balance; North Greenland.

Kristian Keller, National Survey and Cadastre (KMS), Rentemestervej 8, DK-2400 København NV, Denmark

Christine S. Hvidberg and Niels Gundestrup, Department of Geophysics, University of Copenhagen, Juliane Maries Vej 30, DK-2100 København Ø, Denmark

Peter Jonsson, Department of Engineering Geology, Lund University, S-221 00 Lund, Sweden

Introduction

Before the ice core drilling at the Hans Tausen Iskappe (Ice Cap) in 1995, an airborne radar survey was performed in 1993 in order to map the ice cap. The radar survey was supplemented with a surface survey in 1994 in order to select the drill site at the exact top of the southeastern dome (Gundestrup *et al*. 2001). This paper presents a height model of the ice surface topography around the dome. The 1994 survey found the exact

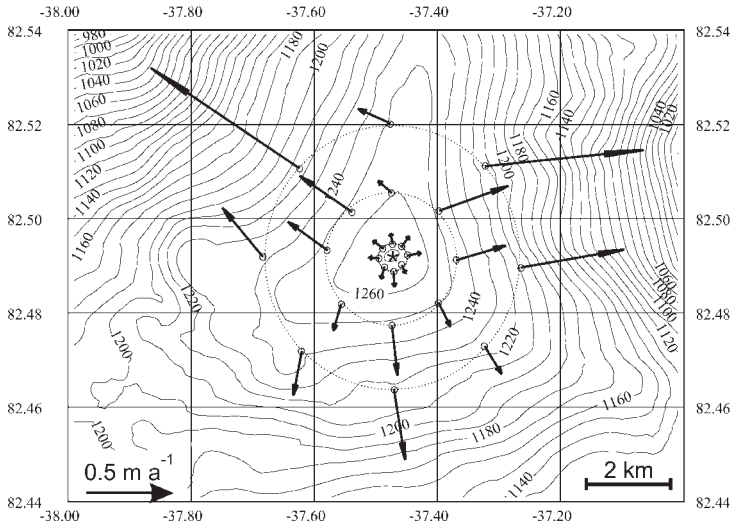

Fig. 1. Ice surface topography and annual velocity. Strain net poles are marked with an open circle, the reference pole at the drill site is marked with an asterix. The dotted lines indicate the strain net rings described in the text. The arrow at the lower left corner corresponds to velocities of 0.5m/year and the scale bar in the lower right corner shows horizontal distance. The contour interval is 10 m.

position of the dome and allowed a strain net to be erected and precisely positioned by relative GPS observations. The area covered by the strain net is approximately 6 km by 6 km. In 1995, GPS measurements of the strain net were repeated and ice surface velocities were computed. The strain net data enable us to determine the mass balance of the Hans Tausen Iskappe at the drill site.

The present mass balance of Hans Tausen Iskappe is important for understanding the history and state of the ice cap. In this context, the mass balance at the dome is a supplement to observations along the margins (Thomsen *et al.* 2001). Furthermore, changes over time in ice thickness in the central part will influence the ice flow pattern and the thinning of annual layers. The mass balance at the dome is therefore relevant for interpretation of data from the ice core drilled at the dome.

The mass balance is determined with three different glaciological approaches; two based on the continuity equation combined with results from a thermo-mechanically coupled ice flow model, one based on the surface principal strain rates. We obtain a consistent estimate of the mass balance at the drill site. The high quality of the result is partly due to the accurate and comprehensive data set, partly to the geometry of the ice cap with an horizontal bedrock around the drill site.

The surface survey

In June 1994, the exact top of the dome was identified (Gundestrup *et al.* 2001). At the top, an aluminum pole was erected as a local reference point. This point was tied into the geodetic benchmark KMS No. 1001 (81°36'01.43065"N; 16°39'19.84959"W; H (ellip)=72.883 m; WGS84) at Station Nord, 250 km east of the drill site, by multiple GPS sessions in both 1994 and 1995 with an accuracy of approximately 0.05 m.

During skidoo traverses in 1994, ice thickness and height measurements were collected simultaneously along north south going lines with an intended spacing of 300 m. The surface survey was extended by traverses to erect strain net poles, which supplemented the data; in total more than 8000 height measurements were obtained. Because of RF-interference from a satellite std-C telex, the reference GPS data had many gaps, and the static initializations were lost. Nevertheless, it was possible to process all the GPS data using Trimbles software: GPSurvey, ver. 2.0 using the 'On-The-Fly' mode. We obtained very accurate height measurements with an estimated overall rms-error of less than 0.05 m. This result is very fine especially considering, that the geometrical configuration of the GPS satellites causes GPS height measurements to be approximately three times less accurate than the horizontal positions.

A height model is presented in Fig. 1. It is composed by two data sets: The data from the surface survey in 1994, combined with data from the airborne radar survey of the Hans Tausen Iskappe in 1993 (Gundestrup *et al.* 2001). The model was made using the software

Surfer (Golden Software) by detrending the data manually by a fitted paraboloid, then gridding the residuals by kriging interpolation and finally adding the gridded values onto the paraboloid.

The accuracy of the model is 0.05 m within the strain net (3 km from the dome), and 5-10 m outside the strain net area. All heights are reduced from ellipsoidal heights to mean sea level heights by using the Greenland geoid 'Geoid 94a' (Forsberg 1996). The geoid height at the Hans Tausen drill site is approximately 28.5 m.

The ice surface topography around the dome is very regular with smoothly varying surface contour lines (Fig. 1). This is a result of the relatively flat and smooth bedrock in the area (Gundestrup *et al.* 2001). The overall structure of the dome is, however, rather complicated. Three ridges radiate from the dome with troughs in between, where particularly the northern ridge is very narrow and lengthy.

The ice thickness in the measured profiles varied between 300 and 393 m with an estimated accuracy of ±5 m. The mean thickness is 350 m. In general the thickness varies between 340 and 360 m. When converting the measured times to depths, a velocity of 171 m/μs was used, and correction for the firn layer was assumed to be constant within the strain net. The radar measured thickness is tied to the logged depth by a profile measured in close proximity to the drill hole (Jonsson 2001).

Number	Height	Distance	Az.	d-lat N	d-long E
	m	m	deg.	cm	cm
11	1269,16	312,4	358,6	6,0	–1,0
12	1269,18	301,6	40,8	6,4	4,7
13	1268,53	350,6	84,4	1,5	7,9
14	1268,55	286,1	132,0	–4,4	2,1
15	1267,45	342,4	177,2	–8,9	0,6
16	1268,99	301,6	221,3	–7,1	–1,9
17	1269,43	322,0	264,3	0,5	–5,6
18	1269,36	291,4	311,7	4,7	–6,0
21	1259,37	1519,9	359,2	6,9	–8,0
22	1245,82	1552,2	45,1	14,4	39,9
23	1245,08	1507,6	92,8	8,4	28,5
24	1249,83	1527,9	134,8	–14,0	7,0
25	1247,43	1615,2	180,7	–29,0	3,2
26	1255,88	1652,6	227,8	–15,7	–4,6
27	1252,09	1552,8	275,9	16,6	–23,0
28	1252,17	1439,6	317,9	20,8	–30,2
31	1251,76	3164,5	359,1	8,6	–18,9
32	1211,61	3065,4	45,4	9,3	91,5
33	1209,38	3050,4	94,6	10,3	59,4
34	1225,82	3031,3	134,0	–16,3	10,0
35	1217,57	3120,1	179,6	–41,0	6,5
36	1239,74	3102,2	224,2	–25,6	–4,9
37	1237,42	3076,1	270,1	28,4	–23,5
38	1214,21	3047,5	313,6	57,8	–85,8

Table 1. GPS data at the 24 surface points shown at Fig. 1: Pole number, height, horizontal position and surface movement over 337 days (1994-1995). The position of the reference pole is 82°29'30.6"N; 37°28'20.6"W; H=1270.54 m.a.s.l.

Strain net

The strain net was put up during the surface survey in 1994. It consists of three concentric rings with eight poles in each ring, around the reference pole in the center. The distances to the rings from the center are 0.3 km, 1.5 km and 3.0 km, corresponding to one, five and ten ice thicknesses. In 1995, GPS observations of the strain net were collected again, giving the movement of the poles relative to the reference pole over a period of 337 days. The horizontal movement of the strain net poles relative to the reference pole are listed in table 1, and illustrated at the map in Fig. 1.

The movement of the reference pole was found to be few centimeters (3.5 cm North, 1.4 cm East), i.e. within the accuracy of the location of the pole. This confirms that the reference pole is placed at the top of the dome. We also estimated the location of the top of the dome from the surface velocities with a simple model: For each pole in the inner ring of the strain net, we calculated an estimate of the center point assuming that the direction to the center is in the opposite direction of the velocity, and that the ice flow is simple axi-symmetric flow (model parameters as in the circular mass balance model below). The average of these points is found to be within few meters of the reference pole, again confirming that the reference pole is at the top of the dome. In the mass balance calculation below, we therefore assume that the reference pole is located at the ice flow center, i.e. the velocity of the reference pole is vanishing.

The overall ice flow pattern (Fig. 1) shows highly divergent flow along the ridges, while the flow is plane or convergent in the troughs. The velocities increase with distance from the center, with high velocities in the troughs, low along the ridges. In general, the surface velocity vectors point in the steepest downward direction.

Mass balance at the drill site

The mass balance is calculated in the following way: Flow lines from the dome to each strain net pole are determined. The equation of continuity is solved along each flow line to give the mean rate of ice thickness change $(\partial H/\partial t)_p$ along that flow line. These ice thickness changes are assumed to be representative for the geographic direction from the dome to the strain net pole. The rate of ice thickness change at the dome is calculated as a weighted average of the mean rates along the flow lines at the surface.

In order to solve the continuity equation along a flow line, we assume that the direction of the flow does not change with depth, and that the flow lines are perpendicular to the surface contour lines, and we neglect shear stress transverse to the flow line (more details in Hvidberg *et al.* 1997; Reeh 1988). The equation of continuity is here written,

$$\frac{\partial q}{\partial x} + \frac{q}{R} = a - \frac{\partial H}{\partial t} ,$$

where x is the horizontal distance along the flow line, $q=q(x)$ is the depth integrated ice volume flux per unit width, H is the ice thickness, t is time, and $a=a(x)$ is the net mass balance, and $R=R(x)$ is the radius of curvature of the surface contour lines at intersections with the flow line. The flux may be written $q=u_m \cdot H = f \cdot u \cdot H$, where u_m is the depth average of the horizontal velocity, u_s is the horizontal surface velocity, and $f=u_m/u_s$ is the shape factor of the horizontal velocity profile. In order to calculate the mean rate of ice thickness change along the flow line, we need to know the following parameters: The course of the flow lines, a and R along the flow lines, and H and f at the strain net poles.

The ice thicknesses around the drill site are determined from maps of sur-

face and bedrock topography (Gundestrup *et al.* 2001; Jonsson 2001). The uncertainty of the ice thickness is ±5 m.

The accumulation rate is determined at the drill site by identified volcanic horizons in the electric conductivity record of the ice core (Clausen *et al.* 2001). We use a long term average of the accumulation rate from 1912 AD (Katmai eruption) to 1995 AD (year of drilling) determined at the dome, and at two previous drill sites in the area (1975 and 1976, situated at about 13 km SW and 5 km S of the dome, at 125 m and 150 m lower elevations, respectively; (Clausen *et al.* 2001) in order to set up an elevation dependent accumulation rate, $a(z) = (-2.63 \cdot 10^{-4} z + 0.448)$ *m of ice equiv./year* (z in meters), which we have used here. This gives $a = 0.114$ *m/yr* at the drill site. Accumulation rates based on the 1783 AD horizon (Laki eruption) give accumulation rates at about 0.08 m of ice/year. The uncertainty of the accumulation rate is set to ±0.02 m of ice/year. The accumulation rate is assumed to vary linearly along the flow lines from the value at the drill site to the calculated value at each strain net pole.

Glaciological studies in the northern part of the Hans Tausen Iskappe show that the accumulation rate at the north dome (about 35 km north of the 1995 drill site) is 0.42 m of ice/year (Thomsen *et al.* 2001). This indicates large accumulation gradients, probably strongly related to the local topography. We do not take accumulation data from the northern part of the ice cap into account here, as we do not know the local variation of the accumulation rate, e.g. the NS ridge radiating from the southeast dome may well introduce a strong local variation.

The shape factor of the horizontal velocity, f is calculated for Hans Tausen conditions. We have used a steady state, thermo-mechanically coupled ice flow model based on Glen's flow law (Hvidberg 1996; Hvidberg *et al.* 1997). f has been calculated for an ideal circular ice cap with ice divide thickness and temperature conditions as at the drill site. The temperature difference between surface and bedrock of only about 5% (personal communication with S. J. Johnsen) results in values of f from 0.58 at the dome to 0.8 in the outer ring, 3 km from the center; which is only slightly higher than calculated theoretically for isothermal conditions (giving 0.5 at the divide (Reeh 1988), 0.8 away from the divide (Paterson 1994)). The uncertainty of f is set to ±0.15.

As a first and simple approach, it is assumed that the flow lines are straight lines radiating from the dome in the center of the strain net to each of the poles. It is further assumed that the flow is axi-symmetrical, i.e. $R = x$. The uncertainty of the distance along the flow line is set to ±15 m. The calculation only consider the radial component of the horizontal surface velocity at the strain net poles. We call this *the circular model*. This approach is naturally used here, where the strain net poles are placed in (or close to) three concentric circles around the drill site at the center. For each strain net pole, the mean rate of ice thickness change along the corresponding flow line is calculated (Fig. 2). For each of the three strain net rings an estimate of the regional mass balance is calculated. Each of these estimates equals the mass balance found as the difference between the total accumulation within the circle and the mass flux across the perimeter of the circle. The average mass balance at the dome found as the mean of the results of the three rings, and its accuracy (2 standard deviations) is calculated to be

$$\langle \partial H/\partial t \rangle = 0.035 \pm 0.015 \text{ m of ice equivalent / year. (circular model)}$$

To the uncertainty, a, f, and u_s all contribute equally with about 1/3, while the contributions from H and R are negligible.

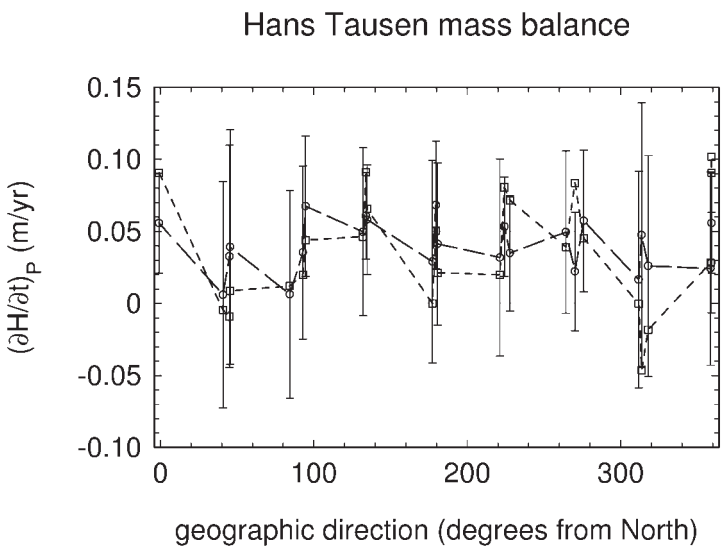

Fig. 2. The mean rate of ice thickness change $(\partial H/\partial t)_p$ along the flowlines from the drill site at the dome to the strain net poles, plotted as a function of the geographic direction from the dome to the strain net pole. The results are from the topographic model (full line) and the circular model (dotted line), see description of the models in the text. Error bars (topographic model only) indicate one standard deviation.

In a second approach, we utilize the mapped surface topography (Fig. 1) to derive information about the ice flow pattern and the flow lines. The flow lines are determined from the map by assuming that they radiate from the dome, and that they are perpendicular to the surface contour lines, i.e. that the ice flows in direction of the steepest surface slope. Because of the complex topography around the dome, the flow lines are curved in this approach, not straight lines as in the circular model above. The horizontal distance x is measured along the flow line from the dome to the corresponding strain net pole, and the uncertainty of x is set to ±10%. $R(x)$ is derived from the map with the uncertainty set to ±50%, which is relatively high partly due to uncertainties in the map introduced by the interpolation routine, but most importantly due to uncertainties in measuring the curvature. As seen at Fig. 1, the measured surface velocities are in the direction of the steepest surface slope, and therefore parallel to the flow lines in this approach. We call this *the topographic model*. As for the circular model, the results are shown at Fig. 2. The average mass balance found as the mean of the results from the three rings, and its accuracy (2 standard deviations) is calculated to be

$$\langle \partial H/\partial t \rangle = 0.039 \pm 0.017 \text{ m of ice equivalent / year. (topographic model)}$$

The uncertainty is not much higher than in the circular model despite the low accuracy of R and x. The difference is, however, caused by the contribution from R, which constitute about 1/3 of the uncertainty, while a, f, and u_s all contribute with about 1/6.

The results for the strain net poles of the two models are compared at Fig. 2. The circular model shows high rates of ice thickness change along the ridges where the surface velocities are low, and vice versa in the troughs. As expected, the results of the circular model oscillates around the results of the topographic model, which are more constant, since the topographic variations are taken into account. The average mass balance of the two models equals, showing that all directions (ridges, troughs) are well represented in the circular model, and furthermore that the topographic model does describe the flow in a satisfactory way. An important reason is the relatively horizontal bedrock within the strain net. Two points in the inner circle in the NE and E direction from the center have exceptionally low values in both models. The relative uncertainty is large at these points, because the velocities are only about double the uncertainty, so the relatively large velocities (as seen at Fig. 1) may be overestimated.

Finally, as a third approach, the average mass balance is calculated from the principal strain rates at the surface, independent of the ice flow geometry. The sum of the surface principal strain rates at the dome is found to be $\dot{\varepsilon}_1+\dot{\varepsilon}_2=(3.72\pm1.8)\cdot10^{-4}\ yr^{-1}$ based on all the strain net stakes. In steady state this would balance the vertical strain rate. The rate of ice thickness change at the

dome is found from: $<\partial H/\partial t>=a-H\cdot f\cdot(\dot{\varepsilon}_1+\dot{\varepsilon}_2)$ (derived from Paterson, 1994, equation 33, p. 257). We assume *a=0.114(0.02 m/yr*, *H=330(5 m*, and *f=0.58(0.08* at the dome, and calculate the average mass balance to be

$<\partial H/\partial t>$ = *0.04 (0.04 m of ice equivalent / year. (from principal strain rates)*

With three different approaches, we reach the same result for the mass balance at the southeast dome of the Hans Tausen Iskappe. The result depends on two critical parameters, which occur in all three models: the accumulation rate *a* and the shape factor *f*. As mentioned above, a longer time average of *a* would reduce the result with 0.03 m/yr, and *a* may vary locally in a way which could influence the result. The shape factor *f* is a modeled parameter without any direct bounds from data. However, the fact that we reach similar results for points at different distances from the center (Fig. 2), and that the calculation of $<\partial H/\partial t>$ based on the principal strain rates gives the same result, does indicate consistence in the variation of *f*. An additional reservation is that the three results are based on the same strain net data set with its possible deficiencies.

Discussion and conclusions

This paper presents a surface topography map around the drill site at the southeast dome of the Hans Tausen Iskappe based on a GPS survey. Furthermore, the surface movement of the ice cap around the drill site is mapped with GPS in a strain net consisting of 3 rings with 8 poles in each ring.

The data show that the ice thickness at the dome is increasing with a present rate of +0.04±0.02 m/year. The result is highly consistent and independent on assumptions regarding the ice flow. Important reasons for the successful calculation of the mass balance are the relatively high precision of the surface velocity data, and also the horizontal bedrock in the area, which secures a regular and smooth flow pattern.

Other glaciological investigations show that the Hans Tausen Iskappe disappeared during earlier changes in climate, and later emerged again (Landvik and Hansen 2001; Thomsen *et al. 2001*; Hammer *et al*. 2001). Our calculation of the mass balance show that the ice cap has not yet reached a steady state, but is still thickening. We calculate a thickening rate of about one third the present accumulation rate. Identified volcanic horizons in the electric conductivity measurements (ECM) record of the ice core show that the annual layer thickness is almost constant with depth down to about 100 m above the bed (Clausen *et al. 2001*). This supports that the ice cap is thickening, but the thickening rate may be as high as the accumulation rate, or lower if the accumulation rate is decreasing with time. Non-vanishing surface velocities show that the annual layers must be thinning, and studies of the crystal structure indicate that some deformation of the layers have occurred (Madsen *et al. 2001*); therefore, constant annual layer thickness with depth indicate that the accumulation rate must have been higher back in time, possibly as a result of the lower surface elevations back in time. A review of the available data from the Hans Tausen Iskappe suggests realistic scenarios with increasing ice thicknesses and decreasing accumulation rates (D. Dahl-Jensen, personal communication), where our calculated thickening rate is in agreement with the results from ice core analyses.

Acknowledgments

This programme has been sponsored by *The Nordic Environmental Research Programme 1993-1997* of the *Nordic Council of Ministers* under Contract No. 93005.

References

Clausen, H. B., M. Stampe, C, U. Hammer, C. S. Hvidberg, D. Dahl-Jensen and J. P. Steffensen 2001. Glacio-chemical studies on ice cores from Hans Tausen Iskappe, Greenland. Meddelelser om Grønland Geoscience, this volume, pp. 123-149.

Forsberg, R. 1996. The Geoid of Greenland – a reference surface for remote sensing. In: Olesen, O.B. (ed.). *Mass balance and related topics of the Greenland Ice Sheet*: 27-31. Report 1996/53, Geological Survey of Denmark and Greenland.

Gundestrup, N., K. Keller, T. Knudsen and P. Jonsson 2001. Locating the Hans Tausen drill site. Meddelelser om Grønland Geoscience, this volume. pp. 71-80.

Hammer, C. U., S. J. Johnsen, H. B. Clausen, D. Dahl-Jensen, N. Gundestrup and J. P. Steffensen 2001. The paleo-climatic record from a 345 m long ice core from the Hans Tausen Iskappe. Meddelelser om Grønland Geoscience, this volume, pp. 87-95.

Hvidberg, C. S. 1996. Steady state thermomechanical modeling of ice flow near the centre of large ice sheets with the finite element technique. *Annals of Glaciology*, 23: 116-123.

Hvidberg, C. S., K. Keller, N. S. Gundestrup, C. C. Tscherning and R. Forsberg 1997. Mass balance and surface movement of the Greenland Ice Sheet at Summit, Central Greenland. *Geophysical Research Letters*, 24 (18): 2307-2310.

Jonsson, P. 2001. An Impulse radar measurement in NE Greenland – equipment, methods and results. Meddelelser om Grønland Geoscience, this volume, pp. 81-86.

Landvik, J. and A. Hansen 2001. The last glaciation of Peary Land, North Greenland, as seen from the glacial history of the Hans Tausen Iskappe. Meddelelser om Grønland Geoscience, this volume, pp. 27-44.

Madsen, K. N. and T. Thorsteinsson 2001. Crystal growth and fabric development in the Hans Tausen ice core. Meddelelser om Grønland Geoscience, this volume, pp. 97-114.

Paterson, W. S. B. 1994. *The Physics of Glaciers*. *Third Edition*. – Pergamon Press, New York: 480 pp.

Reeh, N. 1988. A flow-line model for calculating the surface profile and the velocity, strain-rate, and stress fields in an ice sheet. *Journal of Glaciology*, 34(116): 46-54.

Reeh, N., O. B. Olesen and H. H. Thomsen 2001. Measurements of mass balance, ice temperature and velocity on Hans Tausen Iskappe in Central North Greenland. Meddelelser om Grønland Geoscience, this volume pp. 57-69.

Glaciological and Chemical Studies on ice Cores from Hans Tausen Iskappe, Greenland

By Henrik B. Clausen, Mia Stampe, Claus Uffe Hammer, Christine S. Hvidberg, Dorthe Dahl-Jensen and Jørgen Peder Steffensen

Abstract

Clausen, H. B., M. Stampe, C. U. Hammer, C. S. Hvidberg, D. Dahl-Jensen and J. P. Steffensen 2001. Glaciological and Chemical Studies on ice Cores from Hans Tausen Iskappe, Greenland. Copenhagen, Danish Polar Center. Meddelelser om Grønland Geoscience 39, pp. 123-149.

The paper presents studies of various chemical and isotopical parameters from ice cores drilled in the northernmost located ice cap, Hans Tausen Iskappe, Pearyland, Greenland (HT). The 346 m main ice core (MC95) was drilled to bedrock in 1995 as well as a 35 m shallow core (SC95). A 60 m shallow core (SC75) and a 51 m shallow core (SC76) was drilled at two different positions in 1975 and 1976, respectively. A 6 m shallow core (SC94) was drilled in 1994. Continuous stable isotope records exist for all of these cores, total β-activity only from SC75 and SC76. Continuous ECM inferred acidity records exist along the 1995 cores (MC95 and SC95) and finally detailed records of dust and water soluble ion concentrations exist on selected parts of MC95.

To determine a time scale for the ice core is an important prerequisite for the interpretation of other records. The age scale is based on acid layers, caused by known volcanic eruptions, and by comparison of the chemical composition of these layers to that found in ice cores from other arctic locations. The total β-activity data from SC75 and SC76 provide fixed points to the time scale because a pronounced increase in total β-activity is related to the thermo-nuclear tests in the atmosphere in the early 1960'ies. Many of the investigated parameters exhibit seasonal variations e.g. $\delta^{18}O$, acidity, Cl^- and dust, therefore the study of the accumulation history of the ice cap improves our knowledge of the question if the mass balance of the Hans Tausen Iskappe is in equilibrium or not.

In the upper half part of the ice core the MC95 ECM record reveals several events of high acidity which can be connected to volcanic events known from other Greenland ice core records. Among the identified volcanic events are AD 1912 (Katmai, Alaska), AD 1815 (Tambora, Indonesia), AD 1783 (Laki, Iceland), AD 934 (Eldgjà, Iceland) and e.g. the signals of AD 1259 and 49 BC. The two latter signals originate from major volcanic eruptions of unknown eruption sites with a probable location close to the Equator in the case of the AD 1259 event. Some of the volcanic events are selected for an analysis of dust and water soluble chemical components, including F^-, $CH_3SO_2^-$, Cl^-, NO_3^-, SO_4^{2-}, Na^+, NH_4^+, K^+, Mg^{2+} and Ca^{2+}. Coulter counter technique was used for the dust measurements and the chemical analysis were carried out by ion chromatography.

Keywords: Ice cores; volcanism; ion chemistry; radioactivity; dating; precipitation.

H.B. Clausen, M. Stampe, C. U. Hammer, C. S. Hvidberg, D. Dahl-Jensen and J. P. Steffensen, University of Copenhagen, Department of Geophysics, Juliane Maries Vej 30, DK 2100 Copenhagen Ø, Denmark

Introduction

The Hans Tausen Iskappe (83°N, 38°W) in Pearyland, NE Greenland is one of the northernmost located glaciers in the world. This unique location close to the Greenland Sea and the Arctic Ocean combined with the fact that little information exists on past climate from this region, makes the Hans Tausen Iskappe a well suited place for performing palaeo-climatic and palaeo-environmental investigations by analysis of ice cores. For this reason ice cores have been drilled through 4 seasons: 1975-76 and 1994-95. The drilling sites are shown on Fig. 1, and the actual positions of the drilling sites, the length of the individual ice cores and their identifications (MC95, SC75 etc.) are given in Table 1.

In this work we want to concentrate on comparing the different records of ECM, water soluble ion chemistry, $\delta^{18}O$ and total β-acitivity in order to establish a reliable time scale and further to study the temporal and spatial distribution of the various components, e.g. the rate of annual accumulation and the acid deposition related to major volcanism.

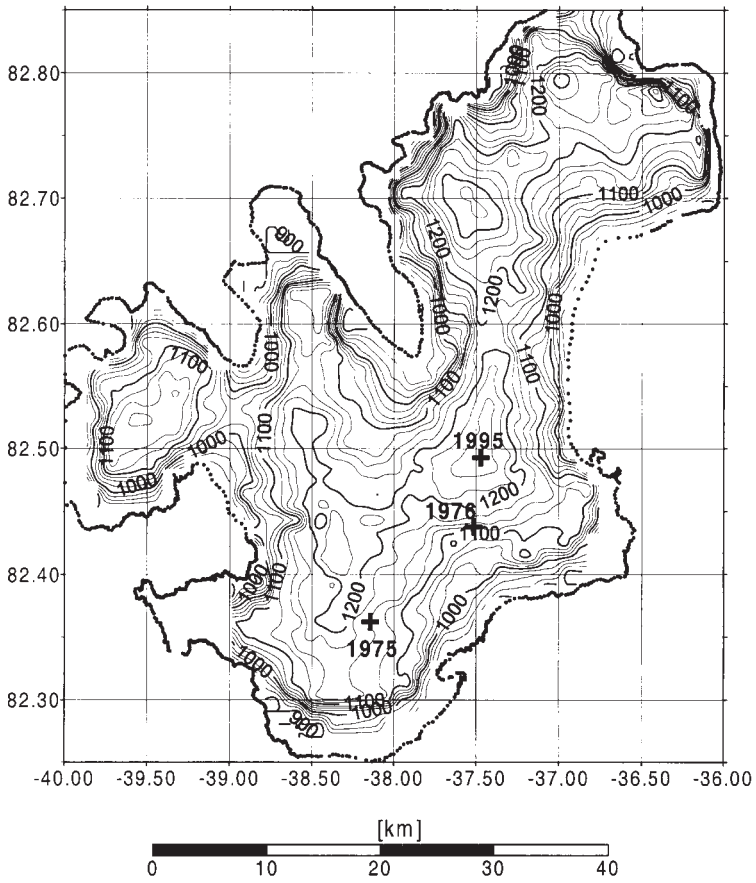

Fig. 1. The map shows the altitudes of the Hans Tausen Iskappe with 25 m contour lines and the positions of the 1975, 1976 and 1995 drilling sites presented in Table 1.

The ECM record

The ECM method reveals the acidity of polar ice by the measured electrical current on solid ice. The H^+ concentration is calculated based on an empirical relation between the electrical current and the H^+ concentration (Hammer 1980), (Clausen *et al.* 1995). The ECM record reveals several high acidity peaks which often are related to major volcanic eruptions in the northern hemisphere (see next section, The volcanic record).

In spite of the fact that Hans Tausen Iskappe is located at a high northern latitude (83°N) with an annual mean temperature of –21°C at a relative high altitude, 1275 m a.s.l., the summer air temperature often reaches 0°C or warmer, and rain occurs. These conditions imply that melting often takes place, and the water phase combined with a presence of alkaline dust, mainly from nearby local sources, has a great impact on the acid concentration of the snow pack, and causes neutralisation of the strong acids.

Year of drilling	Position °N	°W	Altitude m.a.s.l.	Type of core		Length of core, m	Rate of accumulation, m of ice equiv./year		Mean $\delta^{18}0$ per mil	Figs.
							0.162	1970-1975	–27,02	Figs. (22,23)
							0.152	1963-1975	–27,19	Figs. (22,24)
1975	82.38	38.28	1150	Shallow	SC75	60	0.152	1953-1975	–27,24	Figs. (22,24,26)
							0.155	1912-1975	–27,60	Fig. (26)
							0.147	1783-1975	–28,11	Fig. (26)
1976	82.43	37.50	1125	Shallow	SC76	51	0.147	1912-1976	–27,96	Figs. (24,26)
							0.141	1783-1976	–26,05	Figs. (24,26)
1994	82.51	37.47	1275	Handaugered	SC94	6	0.094	1975-1994	–26,27	Fig. (25)
							0.118	1970-1975	–26,05	Fig. (25)
							0.095	1975-1995	–26,31	Fig. (25)
							0.111	1970-1975	–25,53	Fig. (25)
				Main core	MC95	360	0.104	1963-1975	–25,84	Fig. (3)
1995	82.51	37.47	1275	and			0.113	1953-1975	–26,17	Figs. (3,24,26)
				shallow	SC95	35	0.114	1912-1995	–26,56	Figs. (3,24,26)
							0.108	1783-1995	–26,84	Figs. (3,26)

Table 1. Tabulates the positions of the different drilling sites shown on Fig. 1, as well as some compiled data of accumulation and $\delta^{18}O$ mean values for common periods represented in the different ice cores with references to the relevant figures.

The concentration of the strong acids in the snow precipitation is generally ~1-2 µequivalent H^+/kg snow, and the acids are mainly nitric acid and sulphuric acid.

The effect of the high summer air temperature is clearly seen in the melt layer percentage of the ice core. This parameter is some 5% at the surface layers, increasing to 15% at 150 m, to 70% at 250 m and reaches 100% at 275 m (Madsen and Thorsteinsson 2001). The ECM signal is seriously affected by the amount of melting. The frequency of high ECM signals decreases with the increased amount of the alkaline melt layers, thus at the depths below 250 m no distinct ECM signals appear (Fig. 2).

Another effect which makes it difficult to interpret the ECM signal is caused by the high air temperatures during part of the field season when the main core (MC95) was processed and the ECM measurements were performed. We use a reference temperature for ECM measurements at –14°C. MC95 was often measured at temperatures higher than –5°C. At these temperatures surface conductance may also occur through a water film, and the temperature correction factor which corrects the measured currents does not apply at these temperatures. The level of the ECM-signal exceeds by far the level of a signal measured at –14°C. However, the record can still be used to identify possible past major volcanism, but at 6 depth intervals hiatuses exist due to this temperature problem (Fig. 2 and Table 2). The shallow core SC95 was drilled, processed and ECM measured at the end of the field season at temperatures around –10°C, and this record shows "normal ECM behaviour" i.e. allows measured currents to be converted into H^+ concentrations by a conversion equation.

The comparison of the two ECM records from MC95 and SC95 over the last 230 years common in both records, is shown in Fig. 3 and Table 3. Normally we show the ECM records from ice cores in H^+ concentrations based on the actual measured currents, i, (in µAmp) corrected to –14°C and converted into concentrations (µequiv. H^+/kg of ice) by the original conversion equation:

$H^+ = 0.045 \cdot i^{1.73}$ (Hammer 1980). Due to the high temperature during the ECM

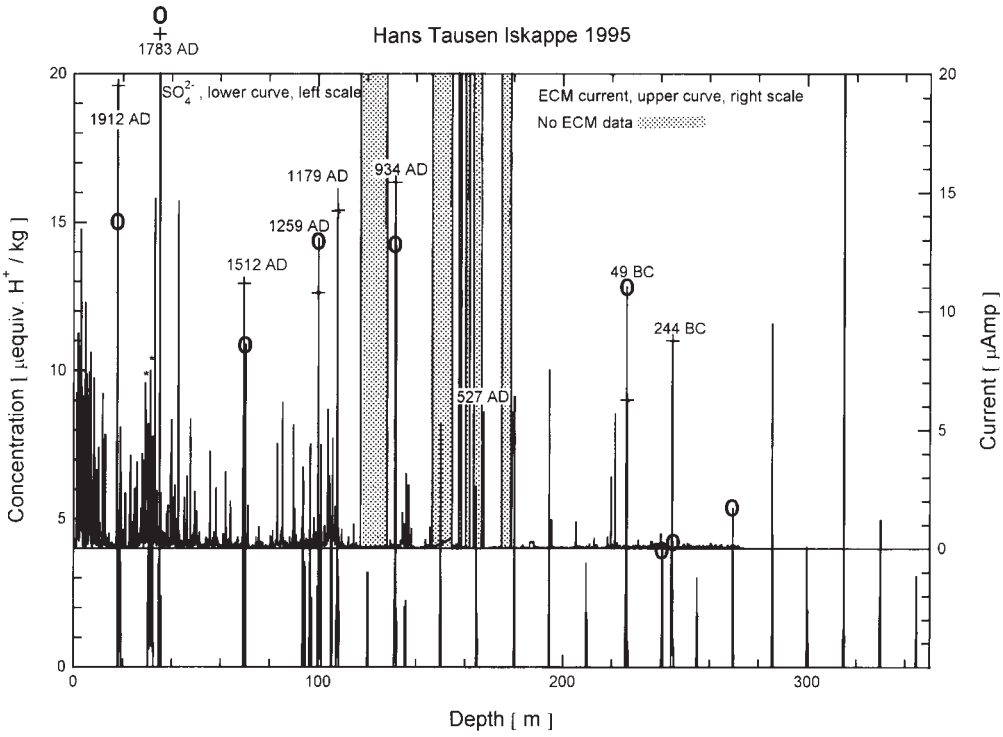

Fig. 2. The upper curve shows (on a depth scale) a continuous record of the actual measured ECM current (in µAmp, scale to the right). The data represent a resolution of 1cm. No ECM data exist for the dotted area, and the corresponding depth intervals are listed in Table 2. The lower curve shows (on the same depth scale) the actual measured sulphate concentration of selected depth intervals in 5 cm resolution. Some major volcanic signals are shown by their year of appearance in the ice core record. In the cases of overlap between current and concentration signals (above 250 m), two symbols are used to separate the signals:
o *means the maximum of the sulphate concentration value*
\+ *means the maximum of the current value.*
The peak values of the AD 1783 event are 39 units and 33 units for sulphate and current, respectively.

The two asterisks around 30 and 31 m correspond to the volcanic signals of AD 1816 and AD 1810. A detailed version of the current for the top 40 m is shown in Fig. 3, and detailed sulphate values for 4 depth intervals around the AD 1512, AD 1179, 49 BC and 244 BC events are shown on Figs. (15, 17, 19, 21), respectively.

measurements and the high content of alkaline material in the ice, we use the actual measured currents corrected to –14°C in the case of SC95, and in the case of MC95 we use the actual measured currents because the currents are generally measured at temperatures above –5°C. Fig. 4 exhibits the effect of the high temperature on the actual measured electrical currents. 5 prominent volcanic events (exhibited in Fig. 3 as #4, 5, 10, 11 and 12) from the last 200 years are used in the comparison which shows that at temperatures above –5°C a substantial and uncontrollable surface conductance takes place through a water film, and this effect is not accounted for by the ordinary calibration curve.

The actual measured temperatures are

Table 2. Exhibits the depth intervals of the missing ECM data from MC95, and the corresponding ages of the ECM hiatuses which are presented as dotted areas on Figs. 2 and 6.

Depth Interval m	Time Interval Age, year AD
117.15-128.15	1080-965
146.30-154.55	766-673
156.75-158.40	649-630
160.05-161.70	613-594
163.35-166.65	575-538
174.90-178.75	456-418

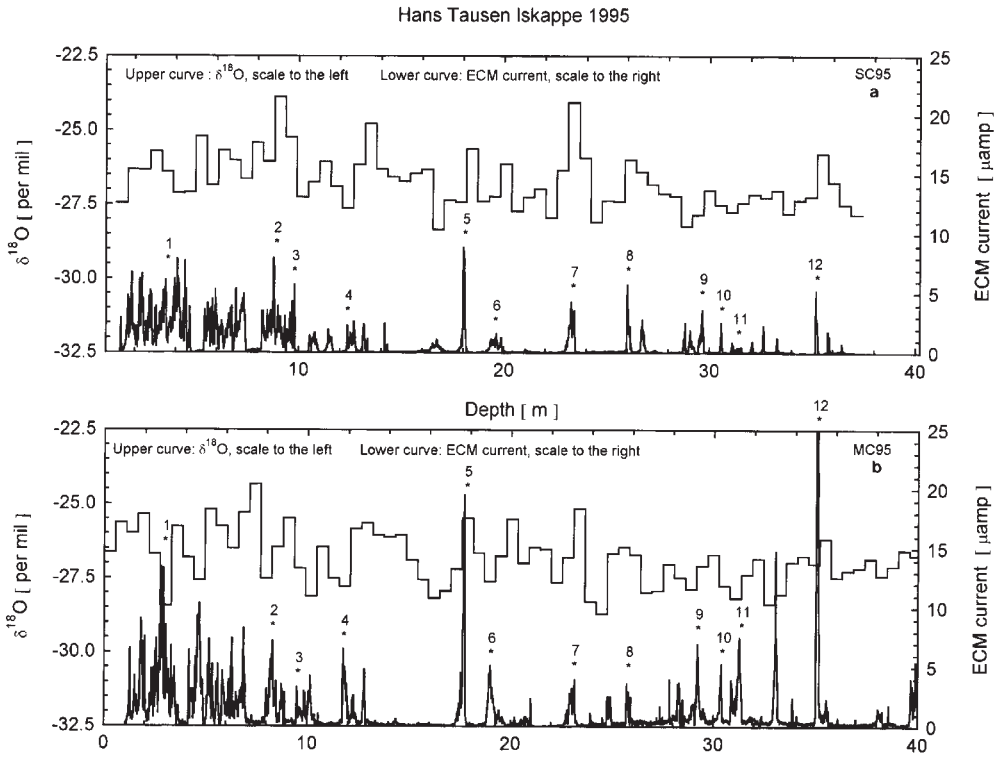

Fig. 3. The $\delta^{18}O$ records in 55 cm resolution from HT95SC and HT95MC are shown at the top of figs. a and b, respectively. The bottom curve of fig. a shows the actual measured ECM-currents referenced to –14°C, in the case of fig. b the actual measured ECM currents are shown. The numbered asterisks (#1-#12) correspond to common events in the two records: #5 and #12 : the Katmai 1912 and the Laki 1783 eruptions. These major volcanic events are used to lock the two records together. For both records the actual surface at the time of drilling serves as the depth reference, thus the difference in the depth for the same event in the two records is due to the different drilling time of MC95 and SC95. The MC95 core is drilled at the start of the season, and SC95 some 6 weeks later when new snow falls had added some 60 cm of snow at the surface.

According to (Simkin and Siebert 1994) 13 out of the 16 largest explosive volcanic eruptions of the 19th and the 20th century took place north of 20°S. Of these 13 events 7 were located between 20°S and 20°N: 1991, Pinatubo, Philippines; 1982, El Chichon, Mexico, (1); 1902, Santa Maria, Guatemala, (6); 1883, Krakatau, Indonesia; 1835, Cosiguina, Nicaragua; 1822, Galunggung, Indonesia, (9) and 1815, Tambora, Indonesia, (10), one event between 20°N and 50°N:1980, Mt. St. Helens, USA and 5 events at higher latitudes than 50°N: 1956, Bezymianny, Kamchatka, (3); 1912, Katmai, Alaska, (5); 1907, Ksudach, Kamchatka; 1875, Askja, Iceland, (7) and 1854, Sheveluch, Kamchatka, (8).

The numbers in parentheses correspond to the asterisk # of the figure.

Besides these events, #2, 4 and 11 are assigned to 1963, Agung, Indonesia; 1947, Hekla, Iceland and 1810, unknown, respectively.

shown in Fig. 5 where the numbers 1 through 12 correspond to those of Fig. 3.

The volcanic record

Major volcanic eruptions emit large amounts of acid gasses into the atmosphere, mainly SO_2 which eventually ends up as H_2SO_4. The acid is deposited at the snow surface by precipitation and can in an ice core be identified by the ECM method as layers with increased H^+ concentration. A continuous record of major volcanism of the last 4000 years, obtained by an ice core from the GRIP site in central Greenland, reveal some 50

Table 3. Displays the average ice thickness of the annual layers (λ) between the fixed points for the common periods in MC95 and SC95 based on acid volcanic layers determined by ECM.

		MC95 λ			SC95 λ	
Age year AD/BC +/–	**Depth at signal**	**from fixed point to 1995**	**between fixed points**	**Depth at signal**	**from fixed point to 1995**	**between fixed points**
		m of ice/year			**m of ice/year**	
1995	0			0		
1983	1.06	0.008	0.088	1.34	0.112	0.112
1963	3.68	0.115	0.131	3.95	0.123	0.131
1947	5.66	0.118	0.124	6.02	0.125	0.130
1912	9.49	0.114	0.109	9.68	0.117	0.104
1816	19.08	0.107	0.100	19.24	0.108	0.100
1810	19.81	0.107	0.122	20.03	0.108	0.131
1783	22.99	0.108	0.118	23.09	0.109	0.113
1512	54.65	0.113	0.117			
1259	84.50	0.115	0.118			
1179	92.12	0.113	0.095			
934	115.74	0.109	0.096			
527	152.03	0.104	0.089			
-49	210.55	0.103	0.102			
-244	229.06	0.102	0.095			

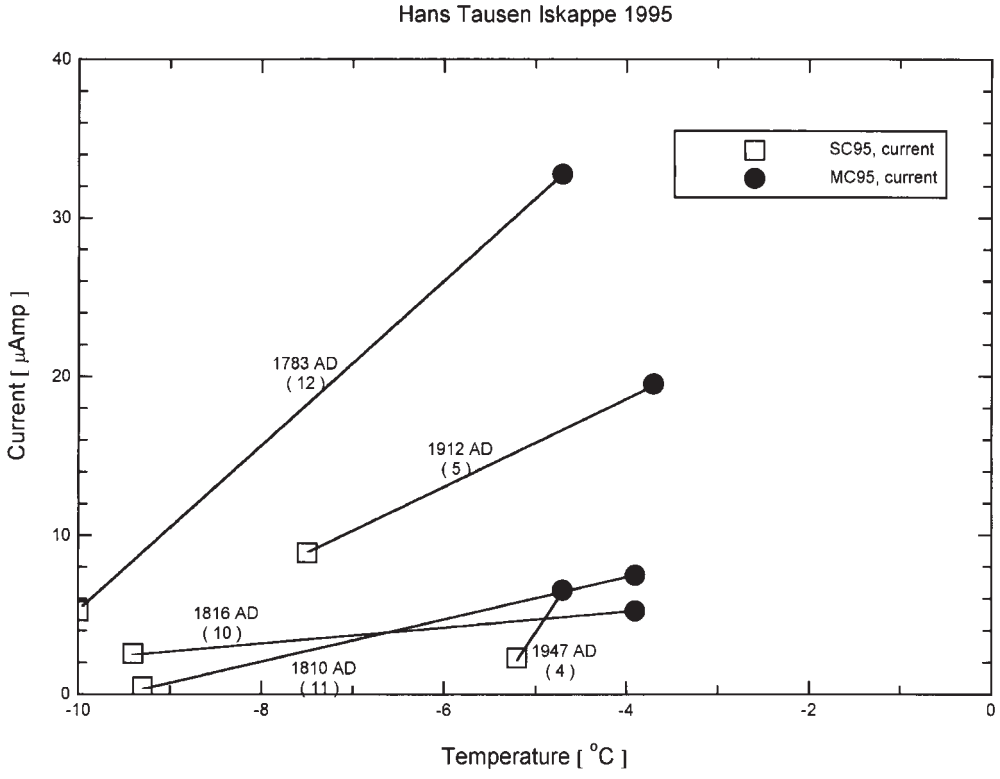

Fig. 4. The peak values of the ECM currents for 5 different volcanic events, identified in HT95SC and HT95MC, are plotted versus the temperature of the ECM measurements. The currents are corrected to –14°C for the HT95SC values. The graph clearly exhibits the uncontrollable effect of the high temperature on the ECM currents. The numbers in parentheses correspond to the numbers of Fig. 3.

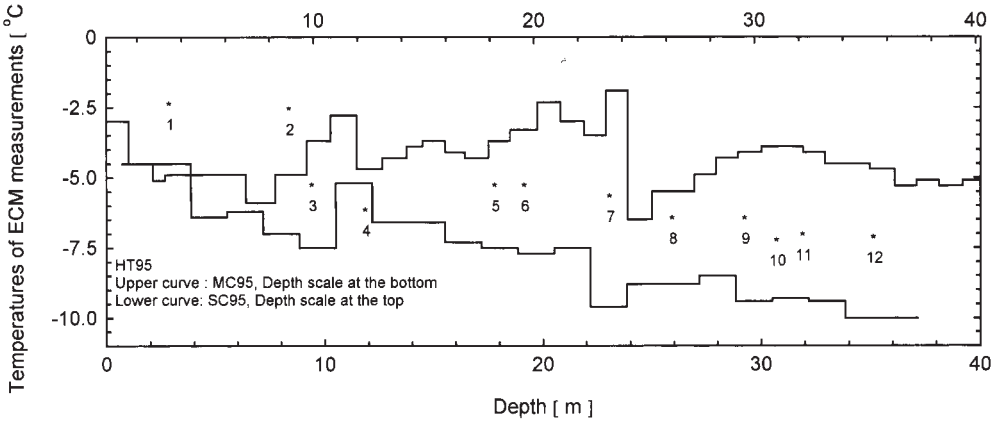

Fig. 5. The actual temperatures of the ECM measurements. The numbered asterisks correspond to the numbers shown in Fig. 3.

major volcanic events from the last 2000 years (Clausen *et al.* 1997) which are relevant for the comparison in this paper. Of these 50 events, 13 belong to the category of the strongest signals characterized by a strong acid deposition rate on the ice surface of more than 3 times the natural acid background deposition rate, and a duration of increased acidity over a time interval of one year or more. Fig. 3 exhibits among others 4 of these 50 volcanic events: AD 1912, 1816, 1810 and 1783, found in the time interval common of HT95MC and HT95SC. Fig. 6 shows at the top: the peak current values of the continuous HT95MC ECM record (shown as upper curve in Fig. 2) on a time scale, and at the bottom: the sulphuric acid deposition at GRIP on the same time scale. Of the 13 major events mentioned above: AD 1783, 1512, 1259, 1229, 1179, 934, 871, 645, 527, 514, 159, 49 BC and 244 BC, the 8 underlined events are used as fixed points for the time scale.

Ages of the acid signals located

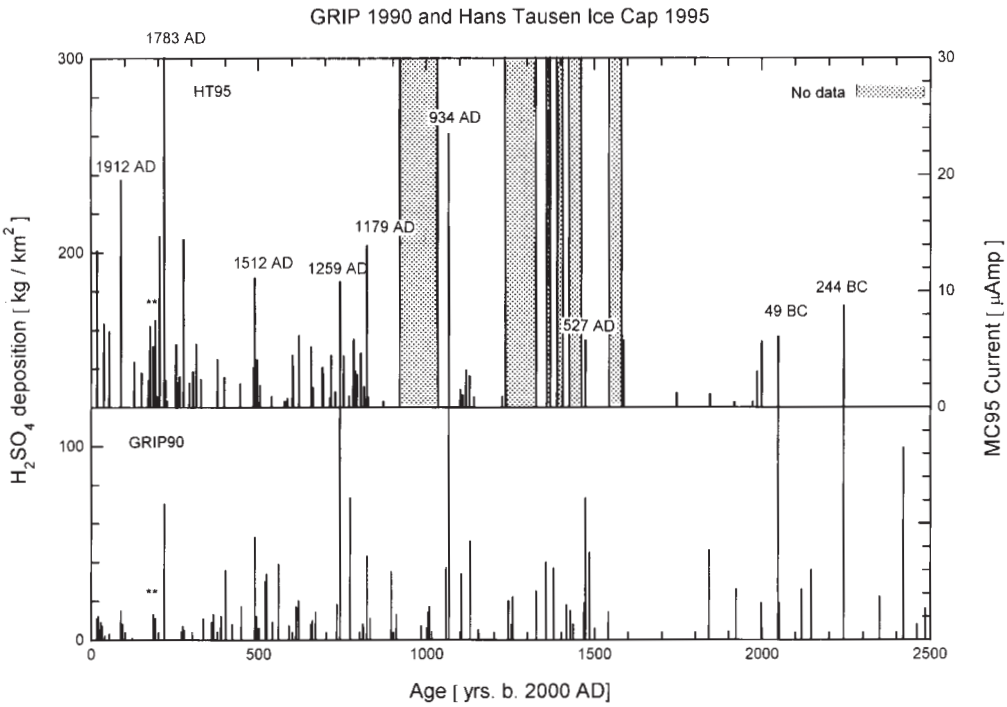

Fig. 6. The upper curve shows (on a time scale) the maximum value of the observed electrical currents of the ECM measurements (scale to the right). Table 4 lists these currents as well as the ice temperature during the ECM measurements. The dotted area correspond to the depths intervals listed in Table 2. The lower curve shows (on the same time scale) the volcanic H_2SO_4 deposition at the GRIP site in central Greenland (scale to the left). The basis of the time scale is the major volcanic eruptions given by their year of appearance in the GRIP ice core record (Clausen et al. 1997).

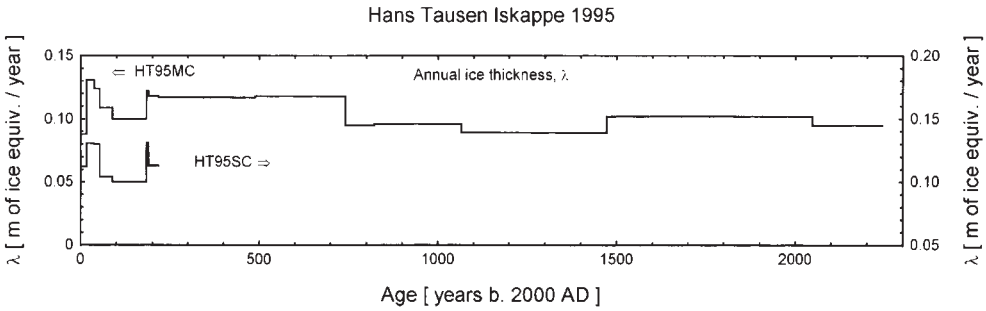

Fig. 7 exhibits the annual ice thicknesses, λ, for the 95MC and the 95SC ice cores based on the fixed points given in Tables 3 and 4.

between the fixed points are found by linear interpolation based on the rate of the annual ice thickness determined by the depths of the fixed points. An interesting observation is that no significant thinning of annual layers versus depth is observed. This indicates that Hans Tausen Iskappe is not in mass balance, and analysis of surface movements in relation to the accumulation rate by Keller *et al.* (2001) shows that the ice cap is not in mass balance at present. The annual ice thicknesses are displayed in Table 3 and shown in Fig. 7 for the common periods of HT95MC and HT95SC.

Table 4 shows it in details for the period AD 1995 to 244 BC, and we see that of the 5 major volcanic events: AD 1229, 871, 645, 514, and 159, not accounted for above, the 3 underlined show up as AD 1232, 871, and 156, respectively. Besides these events we also see other prominent volcanic signals known from GRIP, like AD 1601, 1554, 898 and 79, show up as AD 1605, 1557, 898 and 83, respectively. As to the discussion of the chemical composition of the volcanic signals, see next section.

The chemical record

Determination of the concentration of water soluble inorganic components have been performed on selected sections of the ice core and the intervals of sampling are shown on the lower curve in Fig. 2 by the sulphate concentrations together with the ECM currents on a common depth scale. The ionic concentration measurements are performed by ion chromatography and the insoluble particle (dust) concentrations done on the snow pit samples are determined by Coulter counter technique.

First we discuss the various components, their interaction, and compare the records to values measured on the GRIP ice core. This study is based on some 570 samples (each 5 cm) representing the depth intervals of the ice core shown on Figs. 2 and 8-12. A compilation of the data is presented in Table 5.

All chemical concentration data are given in the unit µequivalent per kg of ice (µequiv./kg) and the components discussed here are the anions and cations listed below with their natural sources given in decreasing order of importance:

Mg^{2+}	terrestrial, marine
Ca^{2+}	terrestrial, marine
Na^{+}	marine, terrestrial
Cl^{-}	marine, volcanic, terrestrial
F^{-}	volcanic
SO_4^{2-}	volcanic, biological (terrestrial and marine), terrestrial
NH_4^{+}	biological (terrestrial)
NO_3^{-}	atmospheric
K^{+}	terrestrial
$CH_3SO_3^{-}$ (MSA)	marine

For references to the sources see e.g. Clausen and Langway (1989), Legrand *et al.* (1997) and Wolff (1995).

Age year AD/BC +/–	Depth at signal m of snow	Depth at signal m of ice	λ from fixed point to 1995 m of ice/year	λ between fixed points	Current i µAmp	Measured temp. °C
1995*	0	0				
1983*	2.790	1.061	0.088	0.088	13.46	– 4.9
1963*	8.280	3.680	0.115	0.131	7.20	– 4.9
1947*	11.760	5.660	0.118	0.124	6.54	– 4.7
1912*	17.710	9.490	0.114	0.109	19.54	– 3.7
1873	23.150	13.411		0.100	3.88	– 1.9
1852	25.800	15.480		0.100	2.94	– 5.5
1831	28.490	17.550		0.100	2.30	– 4.3
1826	29.200	18.120		0.100	6.99	– 4.1
1816*	30.370	19.075	0.107	0.100	5.24	– 3.9
1813	30.850	19.475		0.122	3.93	– 3.9
1810*	31.250	19.805	0.107	0.122	7.50	– 3.9
1806	31.890	20.328		0.118	0.82	– 3.9
1802	32.370	20.726		0.118	0.92	– 4.1
1797	33.040	21.284		0.118	14.74	– 4.5
1783*	35.070	22.994	0.108	0.118	32.75	– 4.7
1780	35.520	23.376		0.117	2.30	– 4.7
1749	39.650	26.940		0.117	4.02	– 5.1
1748	39.880	27.145		0.117	5.43	– 5.1
1743	40.490	27.681		0.117	2.08	– 5.1
1737	41.300	28.395		0.117	2.63	– 4.5
1726	42.700	29.628		0.117	14.45	– 4.5
1708	45.140	31.822		0.117	2.08	– 4.5
1698	46.370	32.933		0.117	3.05	– 4.9
1688	47.700	34.141		0.117	5.47	– 4.9
1674	49.520	35.805		0.117	2.37	– 3.5
1625	55.600	41.452		0.117	4.11	– 3.9
1605	58.120	43.809		0.117	2.57	– 3.0
1557	64.030	49.418		0.117	2.01	– 2.3
1516	69.090	54.273		0.117	3.38	– 2.8
1512*	69.480	54.648	0.113	0.117	11.16	– 2.8
1509	69.920	55.073		0.118	3.16	– 2.8
1506	70.240	55.381		0.118	4.07	– 2.8
1497	71.300	56.406		0.118	1.85	– 2.6
1462	75.580	60.556		0.118	0.92	– 2.6
1399	83.100	67.898		0.118	4.43	– 3.7
1399	83.180	67.976		0.118	2.44	– 3.7
1398	83.290	68.084		0.118	3.48	– 3.7
1380	85.390	70.143		0.118	6.18	– 3.7
1343	89.790	74.470		0.118	5.20	– 1.9
1338	90.380	75.051		0.118	1.68	– 1.9
1310	93.720	78.345		0.118	3.43	– 1.1
1308	93.930	78.552		0.118	2.88	– 1.1
1284	96.750	81.338		0.118	4.43	– 1.5

Table 4. Shows the ages of the acid layers of the MC95 record from AD 1995 back to 244 BC. The ages of the acid signals located between the fixed points (marked by asterisks) are found by interpolation based on the rate of the annual ice thickness (λ) determined by the depths of the fixed points. Also presented are the actual measured maximum electrical currents of the individual acid peaks (in the units µAmp), and the actual temperature of the ice during the ECM measurements.

Table 4. Cont.

Age year AD/BC +/–	Depth at signal m of snow	Depth at signal m of ice	λ from fixed point to 1995 m of ice/year	λ between fixed points m of ice/year	Current i μAmp	Measured temp. °C
1272	98.240	82.811		0.118	1.29	– 1.9
1259*	99.950	84.504	0.115	0.118	10.80	– 2.3
1248	101.050	85.593		0.095	4.38	– 2.3
1232	102.520	87.050		0.095	0.95	– 2.3
1219	103.820	88.348		0.095	2.44	– 1.9
1218	103.900	88.427		0.095	5.86	– 1.9
1213	104.330	88.854		0.095	3.05	– 1.9
1209	104.700	89.211		0.095	2.76	– 1.9
1197	105.850	90.351		0.095	4.64	– 1.6
1187	106.850	91.374		0.095	1.76	– 1.1
1179*	107.630	92.118	0.113	0.095	13.93	– 1.1
1130	112.350	96.807		0.096	0.49	– 6.6
934*	131.360	115.739	0.109	0.096	15.47	– 2.6
900	134.370	118.742		0.089	1.51	– 2.3
898	134.550	118.921		0.089	1.01	– 2.3
893	135.030	119.400		0.089	1.03	– 2.3
883	135.880	120.248		0.089	3.16	– 1.4
872	136.870	121.236		0.089	2.69	– 1.4
775	145.530	129.930		0.089	0.91	– 3.7
527*	167.630	152.030	0.104	0.089	5.76	– 4.7
417	178.810	163.210		0.102	1.24	– 12.4
414	179.110	163.510		0.102	5.76	– 12.4
255	195.360	179.760		0.102	1.20	– 8.5
156	205.380	189.780		0.102	1.12	– 9.0
83	212.840	197.240		0.102	0.42	– 5.0
29	218.290	202.690		0.102	0.47	– 4.8
16	219.610	204.010		0.102	3.05	– 4.7
1	221.210	205.610		0.102	5.69	– 4.3
– 49*	226.150	210.550	0.103	0.102	6.07	– 4.3
–244*	244.660	229.060	0.102	0.095	8.75	– 7.3

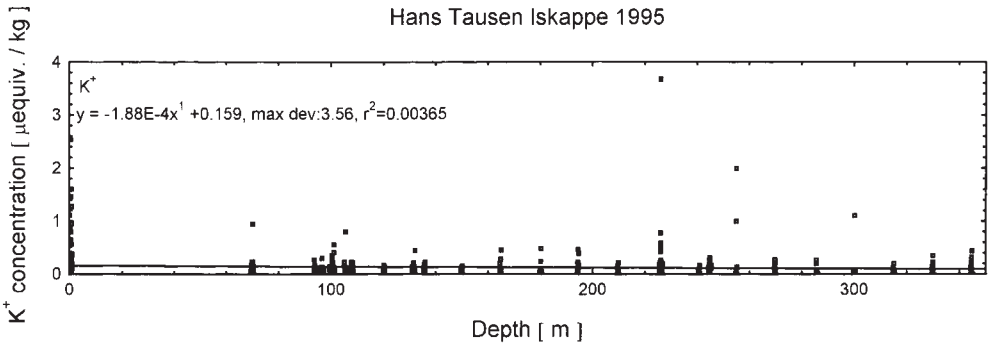

Fig. 8 shows a slightly decreasing concentration of the terrestrial component K^+ versus depth.

Compound	Mean values of concentration [µequiv. / kg]			Figs.
	Measured	Graphic		
Cl^-	1.29	0.88 – 1.84, 1.36	Increase vs. depth	Fig. 10
Na^+	0.96	0.64 – 1.24, 0.94	Increase vs. depth	Fig. 10
Na^+_{ss}	0.89			
Ca^{2+}	5.47	1.07 – 11.05, 6.06	Increase vs. depth	Fig. 9
Ca^{2+}_{nss}	5.43			
Mg^{2+}	2.37	0.44 – 4.54, 2.49	Increase vs. depth	Fig. 9
Mg^{2+}_{nss}	2.17			
SO_4^{2-}	2.08	1.82 – 2.18, 2.00	Increase vs. depth	Fig. 11
$SO_4^{2-}{}_{nss}$	1.97			
NO_3^-	1.18	1.36 – 0.94, 1.15	Decrease vs. depth	Fig. 12
K^+	0.14	0.16 – 0.09, 0.13	Decrease vs. depth	Fig. 8

Table 5. Compiles the mean value of various chemical compounds with references to the relevant figures.

The chemical data sets are corrected for their marine contributions:

$$Na^+_{ter} = 0.5K^+ \quad (1)$$

$$Na^+ = Na^+_{ss} + Na^+_{ter}\,;\, Na^+_{ss} = Na^+ - 0.5K^+ \quad (2)$$

$$Cl^-_{ex} = Cl^- - 1.166\, Na^+_{ss} \quad (3)$$

$$Mg^{2+}_{nss} = Mg^{2+} - 0.228Na^+_{ss} \quad (4)$$

$$Ca^{2+}_{nss} = Ca^{2+} - 0.0436Na^+_{ss} \quad (5)$$

$$SO_4^{2-}{}_{nss} = SO_4^{2-} - 0.120\, Na^+_{ss} \quad (6)$$

Here the chemical symbol (e.g. Na^+) means the actual measured concentra-

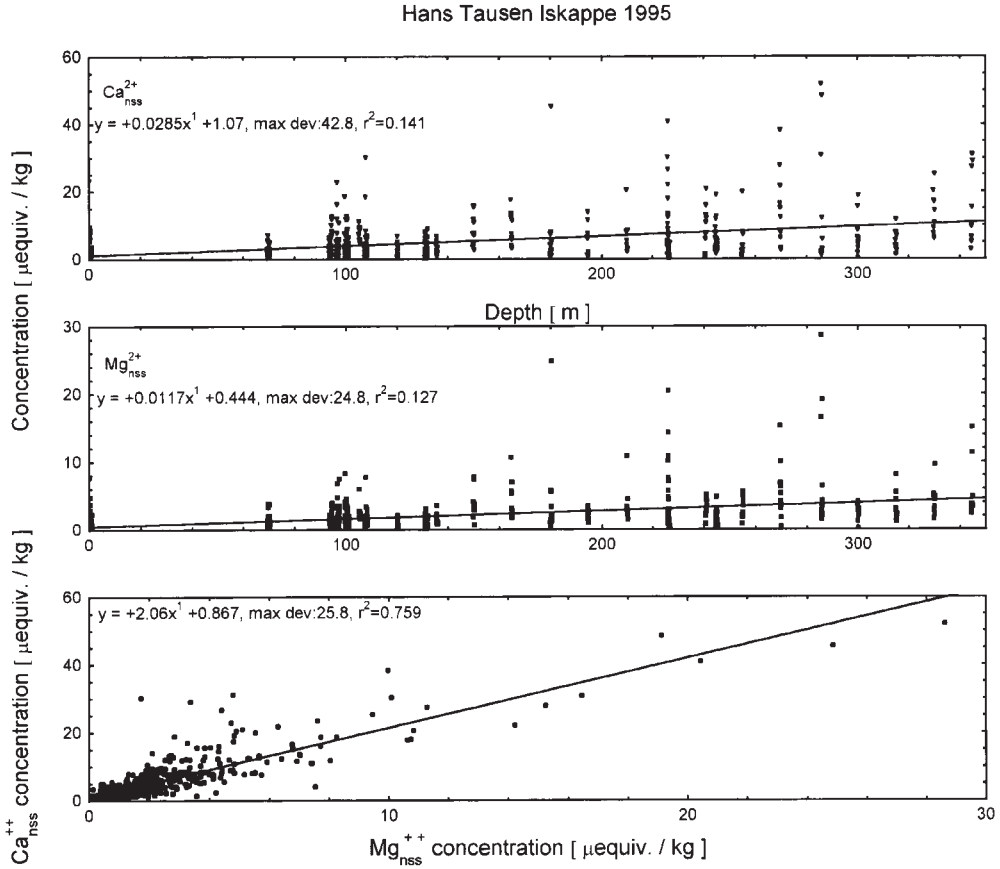

Fig. 9 shows an increasing concentration of non sea salt Ca^{2+} and Mg^{2+} versus depth, and Ca^{2+}_{nss} plotted versus Mg^{2+}_{nss} determines a concentration ratio around 2 for these dominating impurities, indicating a dolomite type of impurity source.

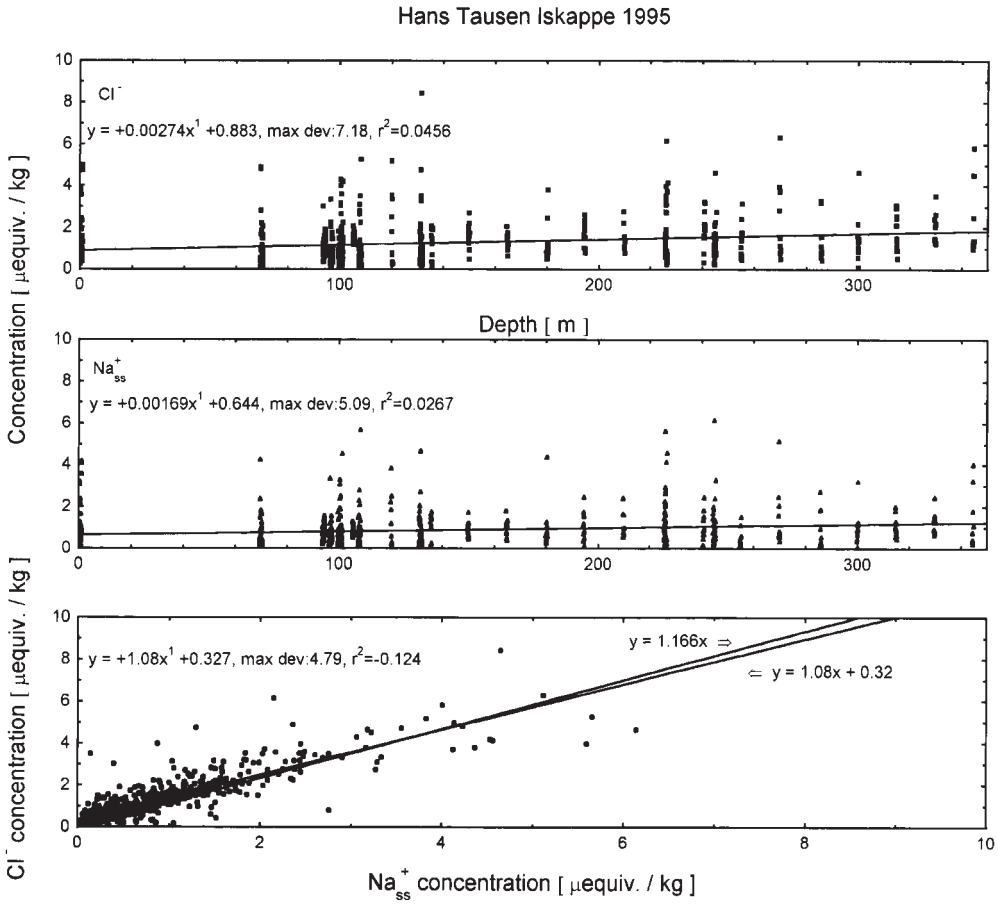

Fig. 10 shows an increasing concentration of Cl^- and sea salt Na^+ versus depth, and Cl^- plotted versus Na^+_{ss} determines a concentration ratio typical for sea salt.

tion, and the chemical symbols provided with the lowered symbols **ss**, **nss** , **ter**, and **ex** refer to the element concentration of sea salt, non sea salt, terrestrial matter and excess amount, respectively. The sea salt concentration ratios, based on the unit µequiv./kg, for the different components relative to Na^+_{ss} are 1.166, 0.120, 0.228 and 0.0436 for Cl^-_{ss}, SO^{2-}_{4ss}, Mg^{2+}_{ss} and Ca^{2+}_{ss}, respectively (Sverdrup *et al.* 1942). Thus Cl^-_{ex} means Cl^-_{nss}, e.g. present as HCl.

K^+ is of terrestrial origin, with an average concentration level of 0.15 µequiv./kg over the entire ice core varying from 0.16 to 0.10 µequiv./kg at the top and bottom, respectively (Fig. 8) with a maximum deviation of some 4 µequiv./kg. The concentration is higher than at GRIP where the typical concen-

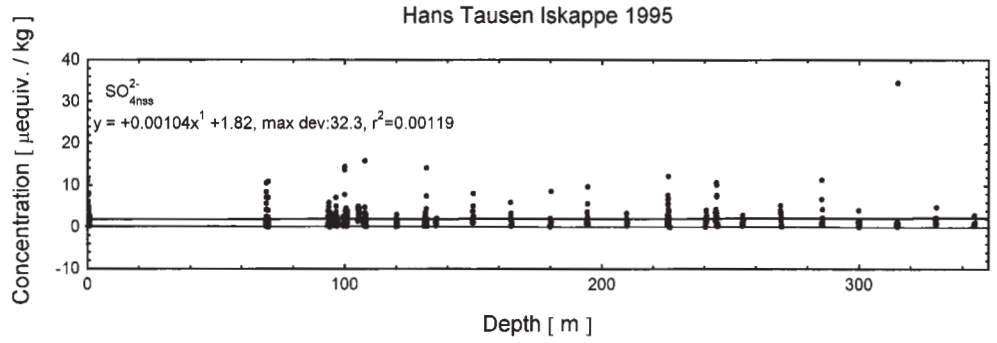

Fig. 11 shows a slightly increasing concentration of non sea salt sulfate versus depth.

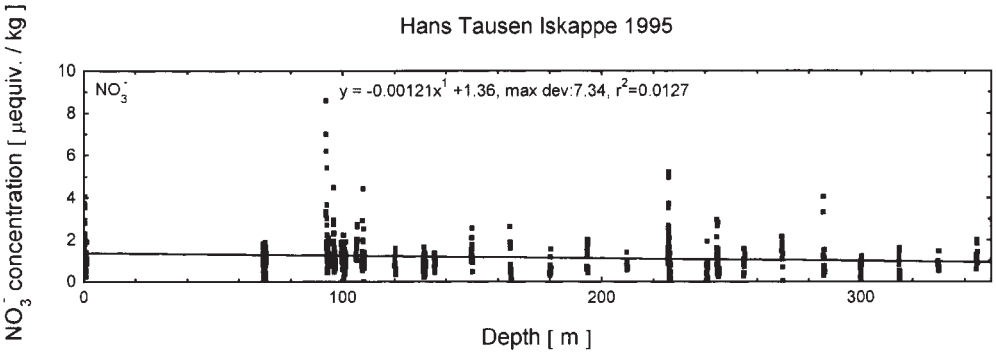

Fig. 12 shows a nearly constant concentration level of the atmospheric component NO_3^- versus depth, indicating that no essential source strength variations has occurred during the time period represented in the record.

tration levels are around 0.05 µequiv./kg.

Na^+ is mainly of marine origin, and for Holocene ice from central parts of Greenland the concentration of this component can be used to correct the concentration of other ions like SO_4^{2-}, Mg^{2+} etc. for their sea salt contribution. Hans Tausen Iskappe is located close to the ice free margin of the Greenland ice cap, therefore the concentrations of ions originating from local terrestrial sources exceed by far those found in ice from central parts of the ice cap (Steffensen *et al.* 2001). Ca^{2+} and Mg^{2+} are the main components of the impurities of the HT ice core (Fig. 9). The main source of these components are limestone and dolomite with some shales which are present in the HT glacier area of NE Greenland. (Blaker and Peel 1997). Because a considerable amount of K^+ is found, we use this component to correct the Na^+ content for its terrestrial contribution. According to Handbook of Geochemistry (Wedepohl 1969) we use a value of 0.5 for the Na^+/K^+ ratio of dolomite sediments to correct the Na^+ for the terrestrial component (1). The actual measured Cl^- / Na^+ ratio is in average 1.4, and for Na^+ corrected for Na^+_{ter} according to (2), we get 1.5 (Table 5) compared to a seawater ratio of 1.17 which is the typically value determined in ice from central parts of Greenland where deviations from this value in the form of excess Cl^- (Cl^-_{ex}) are especially observed in the acid ECM peaks related to Icelandic volcanism (Clausen *et al.* 1997). Fig. 10 suggests a Cl^-/Na^+ ratio of 1.08, which like the above mentioned values are not significant different from the sea water ratio considering the large deviations of the values displayed in Fig.10.

Fig. 9 and Table 5 show a Ca^{2+}_{nss} / Mg^{2+}_{nss} ratio of 2-2.5 and a concentration increase of the two elements versus depth. This ratio is a strong indicator that dolomite is the main contributor of the Ca^{2+} and Mg^{2+} impurities. The increasing rates of concentration with depth indicate that the altitude of the glacier surface has been increasing during the life time of the glacier (Keller *et al.* 2001; Hammer *et al.* 2001).

Fig. 11 and Table 5 show an average SO^{2-}_{4nss} concentration of 2-2.5 equiv./kg with slightly increasing values versus depth. A substantial amount of the sulphate content is conneceted to the terrestrial source.

Fig. 12 and Table 5 show an average NO_3^- concentration of 1.2 µequiv./kg with a constant level versus depth. The shown decrease versus depth can not be considered to be significant due to the high variability. The concentration level is similar to levels found at other Greenland locations, and the high variability is due to the frequent melting at the HT site (Clausen *et al.* 1995).

Secondly we discuss the concentration of various ions with special emphasis on

Table 6. Displays the annual ice thicknesses around 4 distinct volcanic events (AD 1179, AD 1512, 49 BC and 244 BC) based on the chemical components Ca^{2+} and Mg^{2+}, Na^{+} and Cl^{-}, NH_4^{+} and NO_3^{-} which all show seasonal variations (see Figs. 14-21). The values, based on only 5-10 years, are not inconsistent with the values (in parentheses) from Table 3.

Depth Interval of 2,5 cm samples m	Age of volcanic event Year AD / BC	Number of annual layers based on: Ca^{2+} / Mg^{2+}	Na^{+} / Cl^{-}	NH_4^{+} / NO_3^{-}	Average of annual ice thickness cm of ice eq./year
69.30- 70.40	AD 1512	10 ± 1	10 ± 1	10 ± 1	11 ± 1 (11.7)
107.25-108.35	AD 1179	10 ± 1	10 ± 1	10 ± 1	11 ± 1 (9.5)
225.80-226.35	49 BC	6 ± 1	6 ± 1	6 ± 1	9 ± 1 (10.2)
244.35-244.90	244 BC	5 ± 0.5	5 ± 0.5	5 ± 0.5	11 ± 1 (9.5)

the dating of the ice core. The data for this are detailed chemistry profiles (2.5 cm per sample) from a snow pit study covering the top one meter of snow (Fig. 13), and from 4 depth intervals around pronounced acid signals originating from the distinct volcanic eruptions of AD 1512, AD 1179, 49 BC and 244BC given in Table 6 and shown in Figs. 14-21. Fig. 13 show a detailed $\delta^{18}O$ profile from a surface snow pit. The profile clearly exhibits the seasonality of the years 1992 to 1994.The seasonality is also seen in the Na^{+} and Cl^{-} profiles with the characteristic peak in the winter precipitation (in the $\delta^{18}O$ minimum). A Cl^{-} to Na^{+} ratio of 1.14 is close to the sea salt ratio of 1.17 for the two elements. The seasonality is also observed in the Ca^{2+} and Mg^{2+} concentrations with a ratio around 2. In snow from central parts of Greenland the seasonality exhibited by the dust concentration (insoluble particles) varies in parallel with Ca^{2+} concentration with maximum in early spring precipitation (Hammer 1977). This be-

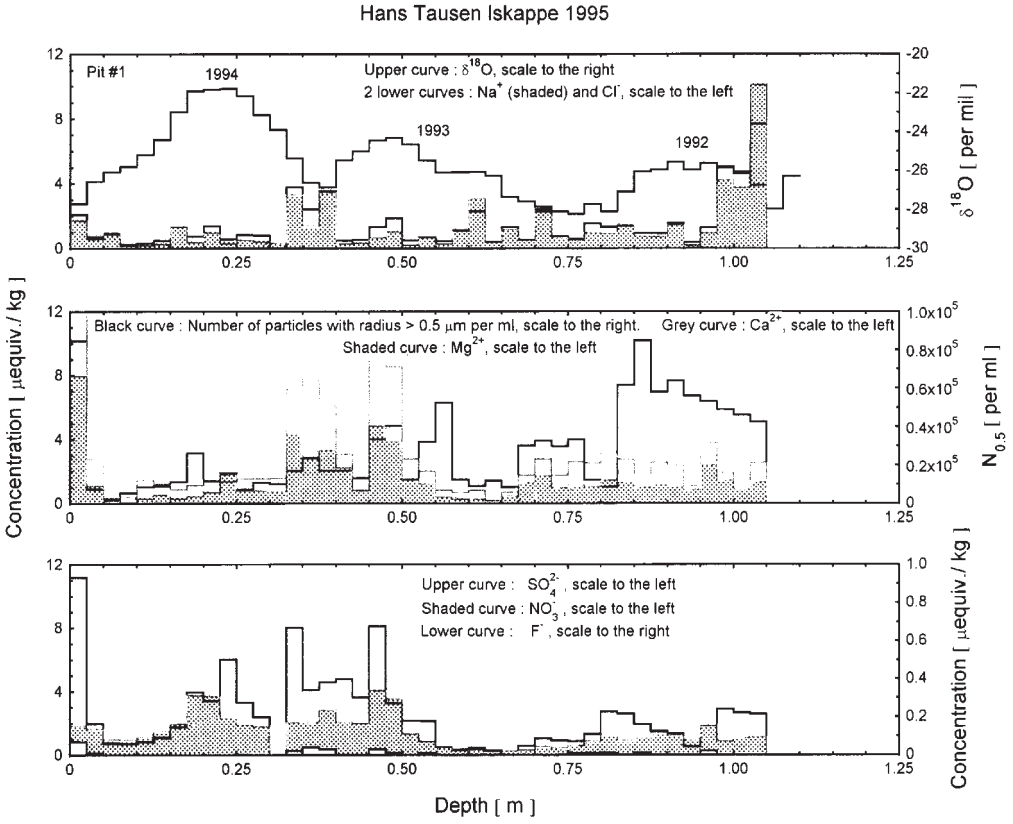

Fig. 13 presents detailed profiles of $\delta^{18}O$, insoluble particles and 7 water soluble chemical components (Na^{+} and Cl^{-}, Mg^{2+} and Ca^{2+}, NO_3^{-}, SO_4^{2-} and F^{-}). The $\delta^{18}O$ curve is shown with calendar years at the summer positions. The winter layers are indicated by the maxima of the Na^{+} and Cl^{-} concentration, and the spring layers by maximum of Mg^{2+} and Ca^{2+} concentration and of dust concentration. The summer layers are exhibited in the NO_3^{-} peaks (see the text for details).

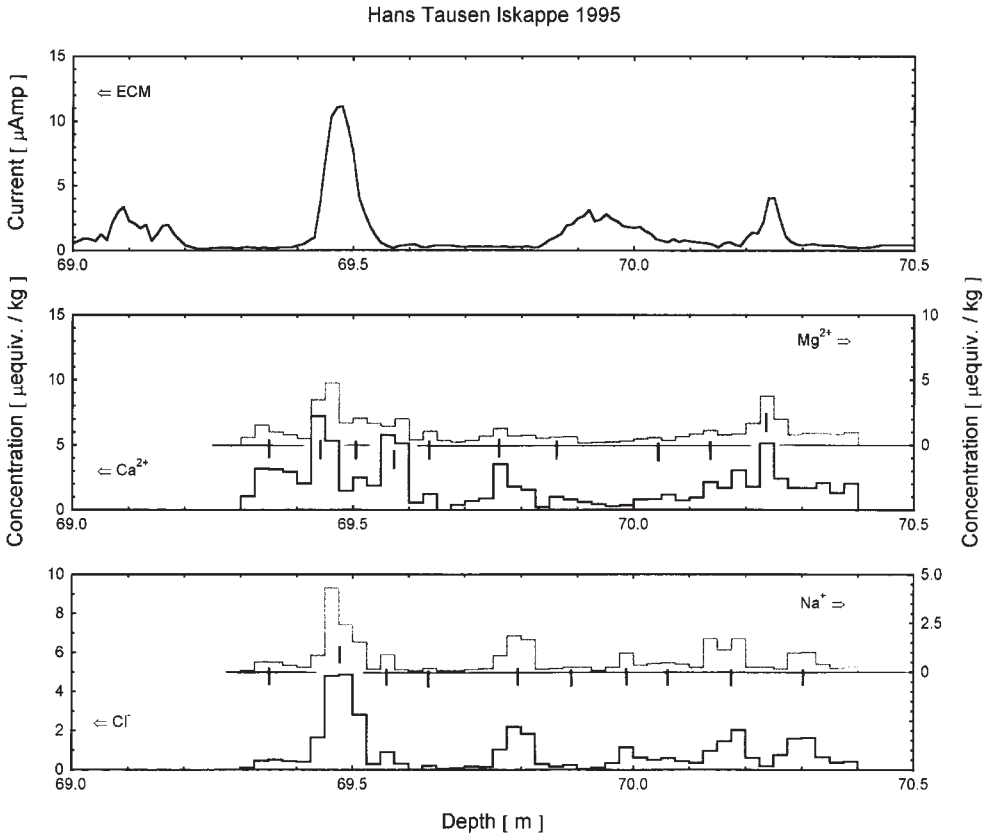

Fig. 14.

Figs. 14, 16, 18 and 20 show detailed profiles of ECM current, Mg^{2+}, Ca^{2+} and Na^{+}, Cl^{-} concentrations at 4 depth intervals around the distinct volcanic events of AD 1512, AD 1179, 49 BC and 244 BC. In the case of the AD 1179 event (Fig. 16) a detailed δ18O record is shown as well. The vertical marking on the records with a resolution of 2.5 cm per sample, indicate the seasonality of the components, and the corresponding yearly ice thicknesses are listed in Table 6 (see the text for details).

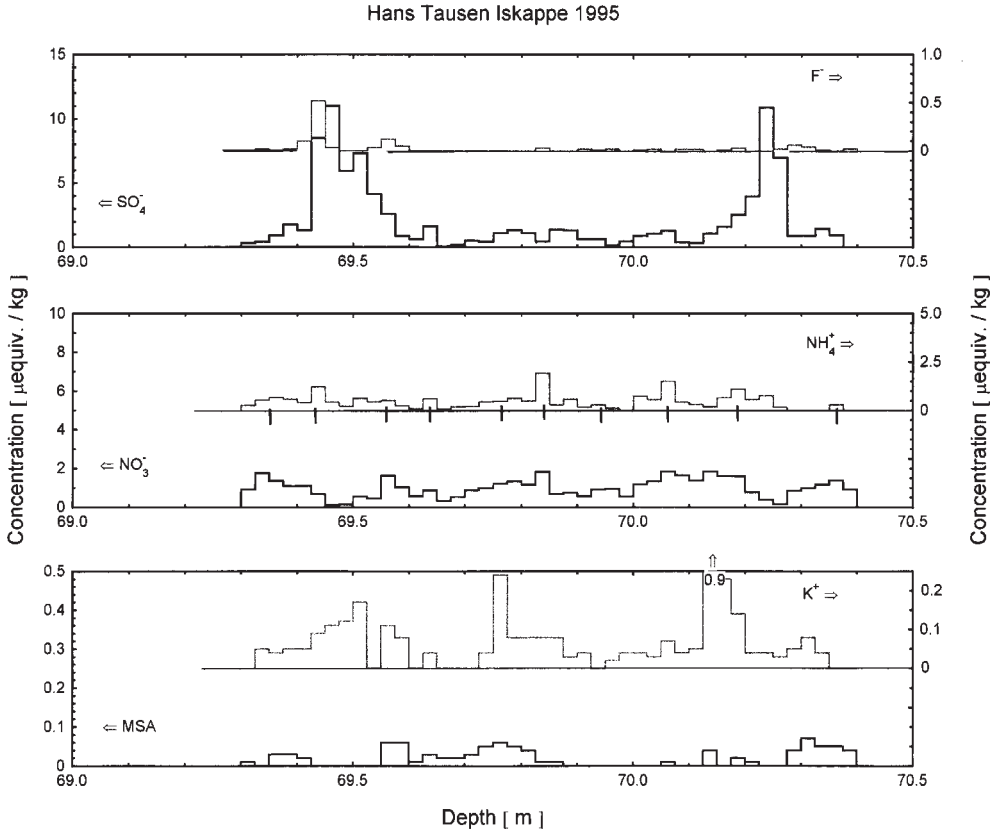

Figs. 15, 17, 19 and 21 show the concentration of F^{-} and SO_4^{2-},NH_4^{+} and NO_3^{-}, K^{+} and MSA at the same depth intervals as those in Figs. (14, 16, 18 and 20). The seasonality is demonstrated by the vertical marking on the NH_4^{+} and NO_3^{-} curves, and the results are listed in Table 6 (see the text for details).

Fig. 15.

Fig. 16.

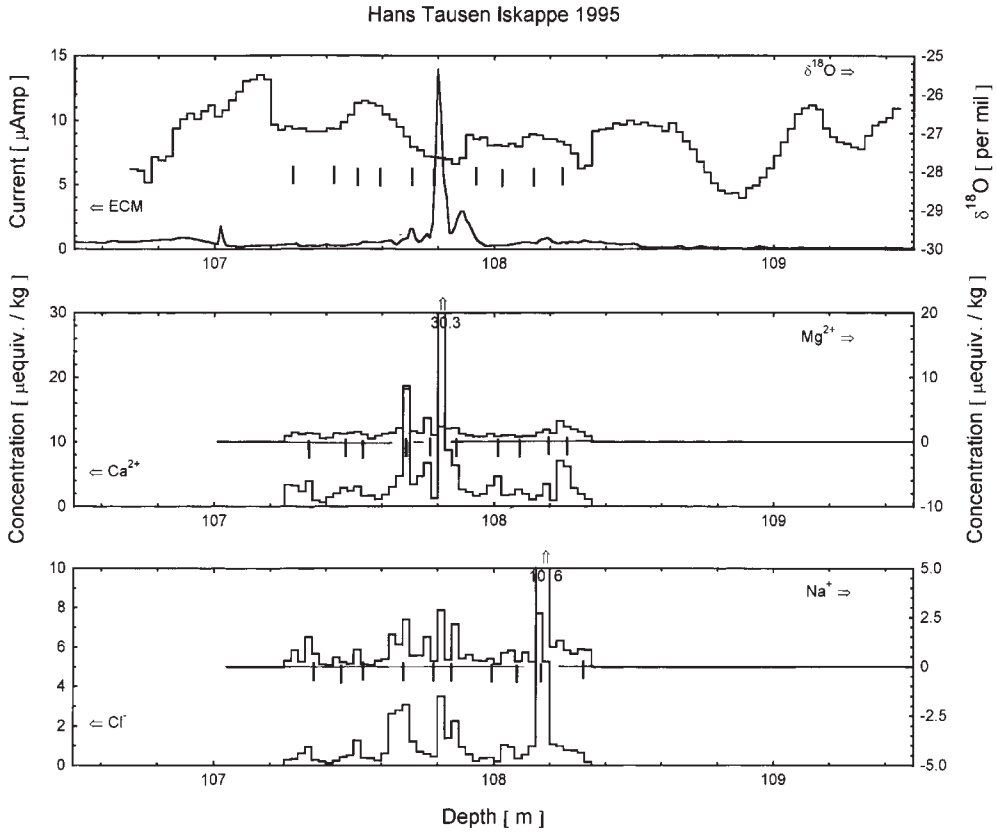
Hans Tausen Iskappe 1995
Current [μAmp]
⇐ ECM
δ18O ⇒
δ18O [per mil]
Concentration [μequiv. / kg]
⇐ Ca2+
30.3
Mg2+ ⇒
⇐ Cl-
10.6
Na+ ⇒
Depth [m]

Fig. 17.

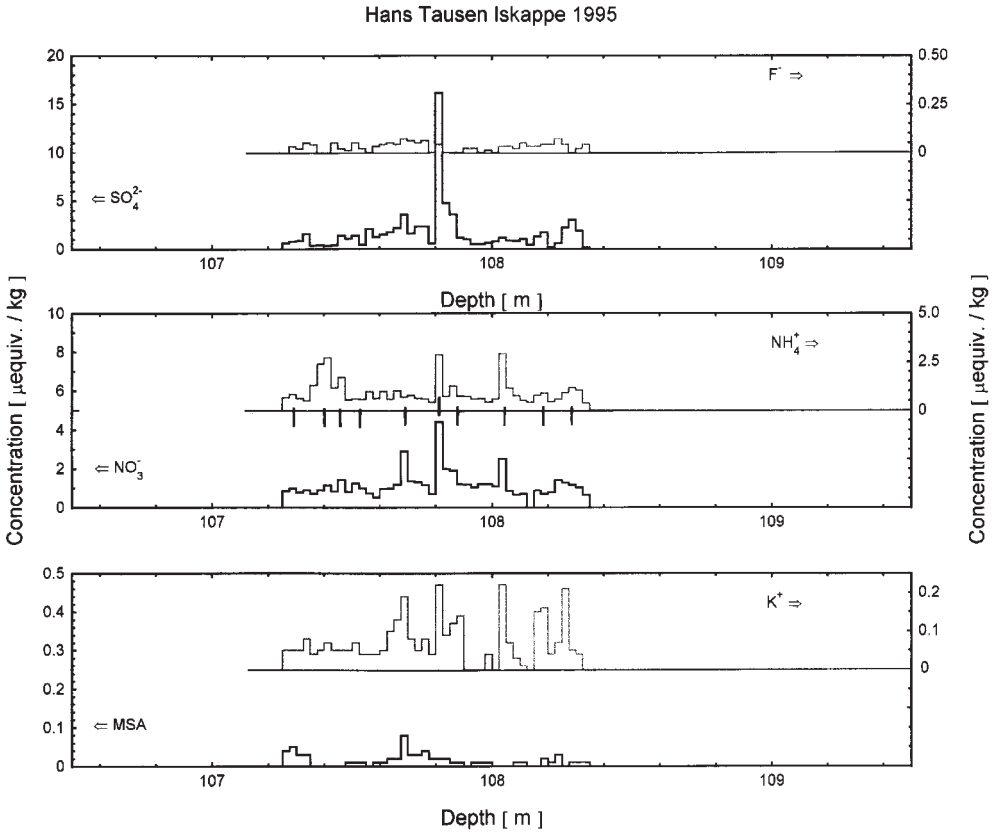
Hans Tausen Iskappe 1995
⇐ SO4 2-
F- ⇒
Depth [m]
Concentration [μequiv. / kg]
⇐ NO3-
NH4+ ⇒
⇐ MSA
K+ ⇒

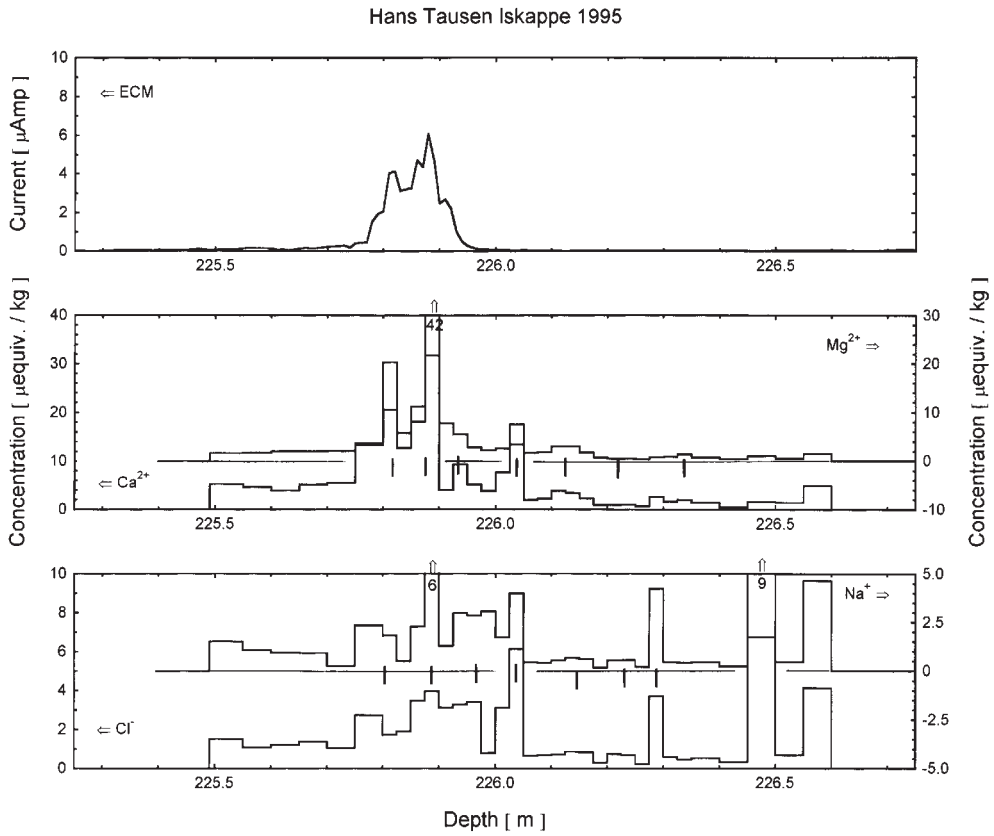
Hans Tausen Iskappe 1995
Current [μAmp]
⇐ ECM
Concentration [μequiv. / kg]
42
Mg2+ ⇒
⇐ Ca2+
6
9
Na+ ⇒
⇐ Cl-
Depth [m]

Fig. 18.

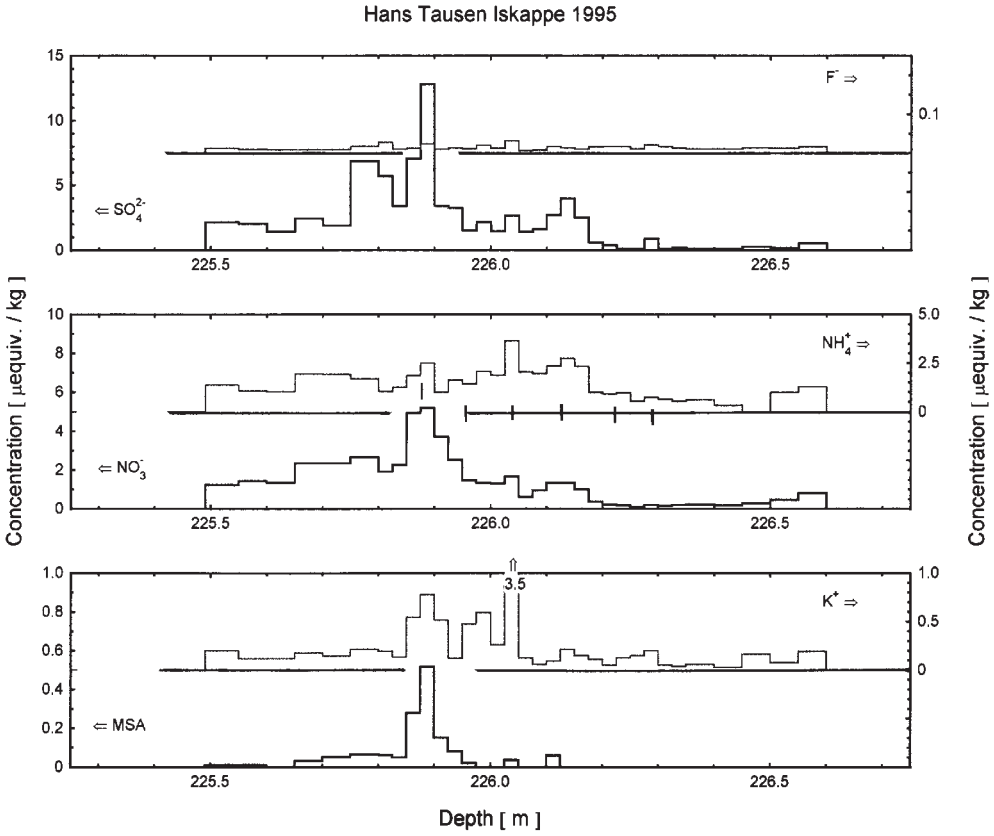
Hans Tausen Iskappe 1995
F- ⇒
⇐ SO4 2-
Concentration [μequiv. / kg]
NH4+ ⇒
⇐ NO3-
3.5
K+ ⇒
⇐ MSA
Depth [m]

Fig. 19.

Fig. 20.

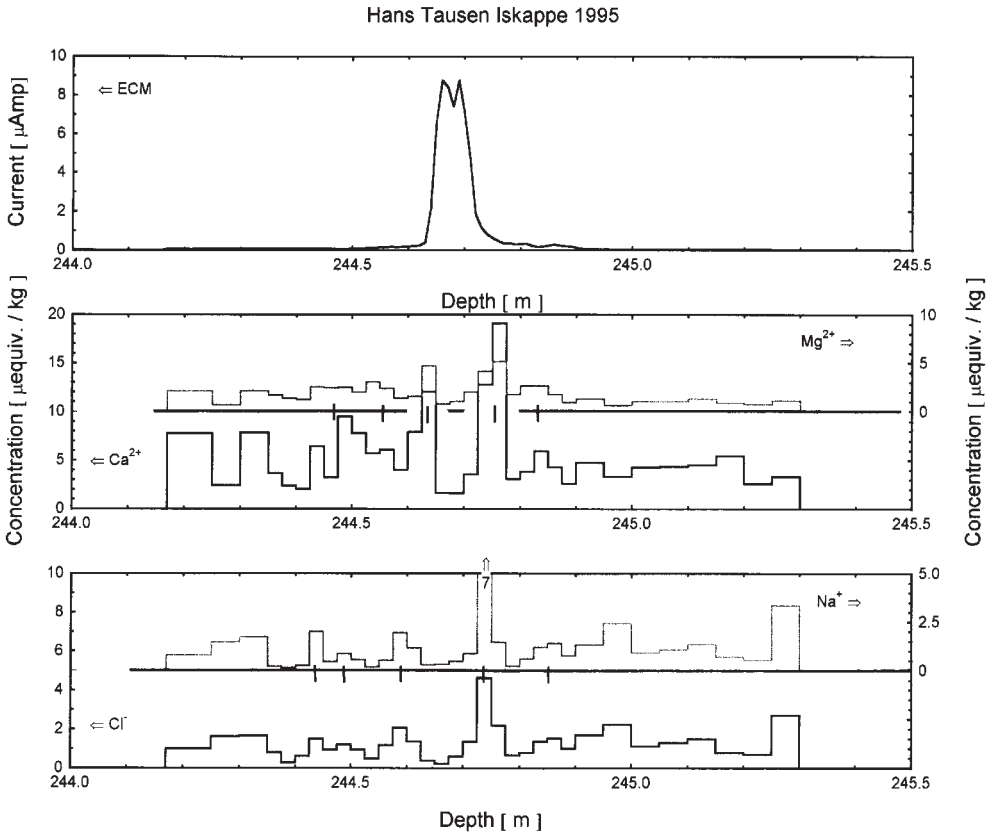
Hans Tausen Iskappe 1995
⇐ ECM
Current [µAmp]
Depth [m]
Concentration [µequiv. / kg]
Mg2+ ⇒
⇐ Ca2+
Na+ ⇒
⇐ Cl-
Depth [m]

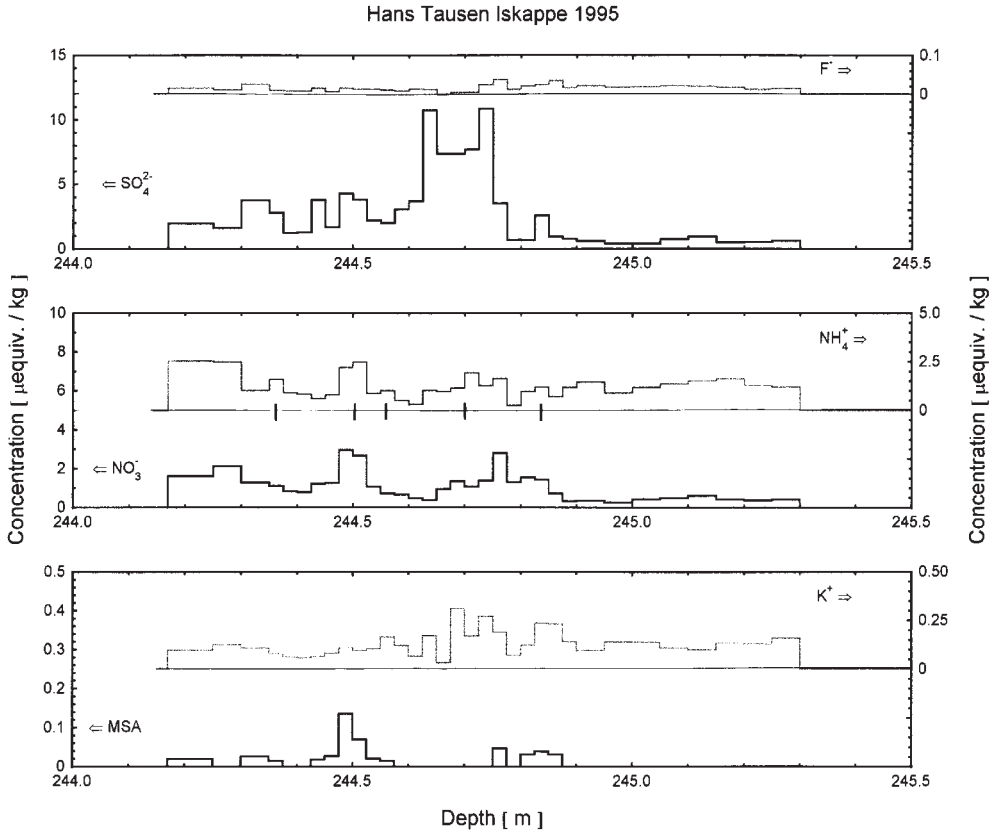
Hans Tausen Iskappe 1995
F- ⇒
⇐ SO4 2-
NH4+ ⇒
⇐ NO3-
K+ ⇒
⇐ MSA
Concentration [µequiv. / kg]
Depth [m]

Fig. 21.

haviour is not clearly demonstrated in the pit samples partly due to the high content of the dust which at HT amounts an order of magnitude higher than at GRIP, in average some 50,000 particles per ml at HT against some 5,000 per ml at GRIP (Steffensen *et al*. 1996). Also the frequent surface melting and the refreezing of the meltwater in the cold winter snow below can blur the stratigraphy by redistribution of water soluble ions. NO_3^- concentration shows distinct seasonal variation in polar ice (Risbo *et al*. 1981) with maximum in late summer precipitation (in the $\delta^{18}O$ maximum). In snow representing the last 50 years the seasonality pattern of NO_3^- has changed due to an anthropogenic input which partly has doubled the concentration (Mayewski *et al*. 1986), and partly changed the season signal into a double peak with an additional peak showing up in the early spring precipitation (at the Ca^{2+} and dust peaks) (Finkel *et al*. 1986). In Greenland ice the SO_4^{2-} signal does not show an unambiguous seasonal signal as found in Antarctica ice. This is mainly due to the difference in the relative strength of the active SO_4^{2-} sources. But what is observed in Greenland is a similar pattern as found in the NO_3^- with a pronounced early spring peak due to an anthropogenic input starting some 100 years ago and with a four time concentration increase in present precipitation.

In order to further investigate the seasonality of the chemical components in ice older than 100 years, we use the chemical data from the 4 depth intervals listed in Table 6 and based on a resolution of 2.5 cm per sample. This is the case for 88 samples of Figs. 14 – 21 where the 10 chemical components and the ECM current are arranged in the same way in all the figures, except for Fig. 16, where a detailed $\delta^{18}O$ profile is shown on the ECM current figure.

Mg^{2+} and Ca^{2+} show maximum in the spring, like dust (Figs. 14, 16, 18, 20).

Na^+ and Cl^- show maximum in the winter (Figs. 14, 16, 18, 20).

NH_4^+ and NO_3^- show maximum in the summer like $\delta^{18}O$ (Figs. 15, 17, 19, 21).

The vertical lines on the figures indicate the seasonality and the amounts of years in the records. Table 6 compiles these data and compare the consequent annual ice thicknesses with those determined by the acid volcanic layers from Table 3. The values based on the chemical series are not inconsistent with those based on ECM. It is interesting that the seasonality of the above 6 components show up considering that the annual resolution is based on only some 4 samples per year. This relative low resolution combined with the frequent melting, which causes redistribution of the water soluble ions, does not allow any conclusion on how the peaks show up within a year:

Na^+ and Cl^- before Mg^{2+} and Ca^{2+} before NH_4^+ and NO_3^-.

K^+ follows Mg^{2+} and Ca^{2+} and peaks at the same time. This is not marked by vertical lines on Figs. 15, 17, 19, 21 as it does not provide an independent yearly resolution because the main source of K^+ is terrestrial like for Mg^{2+} and Ca^{2+} in the HT ice.

F^- with volcanism as the dominant source does not show any seasonality (Figs. 15, 17, 19, 21).

SO_4^{2-} does not exhibit seasonal variations as distinct as e.g. NO_3^- (Figs. 15, 17, 19, 21). This is due to the varying strength of the various sources of SO_4^{2-}, with volcanism in a predominant role partly by major volcanism which creates high SO_4^{2-} peaks, and partly by non explosive emission of sulphurous gases which contribute to the sulfate background. Other sources to SO_4^{2-} in Greenland are terrestrial and marine biological processes. An important marine biological source is Dimethylsulfide [DMS, $(CH_3)_2S$] which is emitted from the ocean to the atmosphere where it is oxidized partly to methanesulfonic acid [MSA,

Table 7. Compares the amount of the deposited acid (as sulphuric acid) at HT and GRIP from 4 volcanic eruptions (VAD), and the corresponding magnitudes of the eruptions.

Event	Hans Tausen Iskappe		GRIP	
	VAD	Magnitude	VAD	Magnitude
	kg H_2SO_4/km^2	Mton H_2SO_4	kg H_2SO_4/km^2	Mton H_2SO_4
AD 1512	39	79	53	77
AD 1179	32	66	45	65
49 BC	38	77	140	194
244 BC	39	79	40	51

CH_3SO_3] and partly to SO_2. The branching ratio of this process is not well known (Saltzman 1995). Because the MSA concentrations at HT and at central Greenland sites like Crete and GRIP are low (~0.03 µequiv./kg) and at the same level (Osada and Langway 1993), (Legrand *et al.* 1997), the biological marine sources of MSA are remote and their contribution to the sulfate background is of less importance. This is quite different from Antarctica, where the marine biological processes are the dominant SO_4^{2-} source (Mulvaney and Peel 1988).

The data sets of Table 6 are also used in the discussion of the chemical composition of the volcanic signals and for the comparison to the corresponding volcanic signals in the GRIP ice core. The study comprises the volcanic events of:

AD 1512, Figs. 14-15; AD 1179, Figs. 16-17; 49 BC, Figs. 18-19 and 244 BC, Figs. 20-21.

The amount of deposited sulphuric acid per km^2 from volcanic eruptions depends upon the site of eruption and the magnitude of the eruption. To estimate the magnitude we compare the amount of volcanic acid deposited per km^2 (VAD) to the deposited amount of total β-activity from known atmospheric nuclear bomb tests (Clausen and Hammer 1988). VAD is calculated by integrating the amount of acid above the background value during the period of elevated acidity. VAD and the magnitude expressed in Mton H_2SO_4 are listed in Table 7 where we for comparison have assumed a high northern latitude (HNL) eruption site for the four events. The factor that converts HT VAD values into magnitude for a HNL eruption is $2.04 \cdot 10^9$ (see total β-activity section). The comparison to the magnitudes determined for GRIP (Clausen *et al.* 1997) shows agreement except for the 49 BC event where a factor of 2 occurs, however deviation of this size has been observed in other cases (Langway *et al.* 1988).

Generally for the chemistry of the four events we find sulfate as the dominant component and in the case of the AD 1512 and AD 1179 events we find significant amounts of F^- as found in the GRIP ice cores. The F^- records show the F^- distributed in the well recognised symmetrical pattern on the flanks of the sulfate peaks due to the post depositional replacement of F^-. Both events are assigned to high northern latitude eruption sites: The AD 1512 event is only seen in Greenland ice core records from the GRIP region and north of this location like the AD 1912 eruption of Katmai in Alaska. The AD 1179 event is, like all major Icelandic eruptions, found in all Greenland records covering this time period, and the event is assigned to the Katla eruption of AD 1179. The 49 BC event is like in other Greenland records a "pure" sulfate signal. The chemical composition of the 244 BC event differs from that found in the GRIP record. The GRIP signal consist of a substantial amount of Cl^- and F^- besides the sulfate. The lack of the Cl^- and F^- is probably

	Pit		AD 1512		AD 1179		49 BC		244 BC	
	HT	GRIP	HT	GRIP	HT	GRIP	HT	GRIP	HT	GRIP
Component	Concentration [µequiv./kg]									
F-	0.007	0.007	0.028	0.031	0.028	0.048	0.014	0.022	0.015	(0.109)
MSA	0.019	0.016	0.019	0.034	0.014	0.029	0.044	0.033	0.015	0.023
Cl^-	1.48	0.95	0.88	0.34	1.21	0.37	1.90	0.39	1.29	(4.47)
NO_3^-	1.40	2.12	1.00	1.20	1.17	1.29	1.41	1.41	1.07	1.03
SO_4^{2-}	2.50	2.62	2.09	1.26	1.67	1.38	2.31	1.37	2.90	2.90
Na^+	1.30	0.45	0.66	0.18	1.04	0.26	1.75	0.33	1.15	0.47
NH_4^+	1.15	0.40	0.45	0.46	0.93	0.58	1.43	1.02	1.24	0.28
K^+	0.58	0.08	0.08	0.02	0.07	0.05	0.31	0.09	0.13	0.05
Mg^{2+}	1.43	0.19	1.07	0.17	1.55	0.14	3.35	0.22	1.91	0.11
Ca^{2+}	2.95	0.39	1.94	0.40	3.88	0.37	6.55	0.49	5.46	0.37

Table 8. Compares the concentration values of 10 chemical compounds from common time intervals in the HANS TAUSEN and GRIP ice cores. For the parentheses at the 244 BC GRIP values, see text.

due to the strong hydrophilic character of these components, also the 244 BC signal is the last acid peak of the ECM record where the ice core at this depth consists of some 75% refrozen meltwater.

Other volcanic signals like Laki AD 1783 and Eldja AD 934 found in the HT95 Ice core are discussed by Stampe (Stampe 1997).The HT chemical data sets presented in Figs. 13-21 are compared to GRIP data which represent the same time intervals as the HT data, and the data are presented in Table 8. The HT data deviate from those presented in Table 5, especially the SO_4^{2-} values due to the presence of major volcanic signals in the data sets.

The $\delta^{18}O$ record

Detailed $\delta^{18}O$ records with annual resolutions exist from HT75, HT76, HT94 and HT95 and are shown on Figs. 22-25 provided with time markers from recognizable events. The sample frequency of the 4 records corresponds to 50, 50, 20 and 40 samples per m, respectively. Other $\delta^{18}O$ records presented here are the records of HT75, HT76, SC95 and MC95 which is only given to the same age level as covered in SC75 and SC76. The 4 latter $\delta^{18}O$ records are presented in Figs. 3 and 26 in resolutions from 2 to 6 samples per m. Table 1 shows the mean annual accumulation rates and the $\delta^{18}O$ means of common time intervals represented in the ice cores. Generally the data show increasing $\delta^{18}O$ and accumulation values from AD 1783 to 1975, and the opposite trend during the period 1975 to 1995. The $\delta^{18}O$ mean value of –26.2 per mil and the mean annual temperature of –21°C for HT95, places Hans Tausen Iskappe on the Greenland far North and North East line of the $\delta^{18}O$ – temperature curve, which includes locations like Spitsbergen and Station Nord, and indicates that the air masses take up some water vapour from the Arctic oceans (Dansgaard *et al.* 1973). The entire $\delta^{18}O$ record of MC95 is discussed by Hammer *et al.* (2001).

The total β-activity record

In the 1950'ies and the early 1960'ies mainly the Americans and the Russians performed thermonuclear bomb tests in the atmosphere. Radioactive debris from these tests was deposited on the polar ice caps by precipitation, and the polar ice became stratified by the radioactive isotopes from the debris. Today mainly the radioactive isotopes ^{90}Sr and ^{137}Cs remain, and these isotopes were identi-

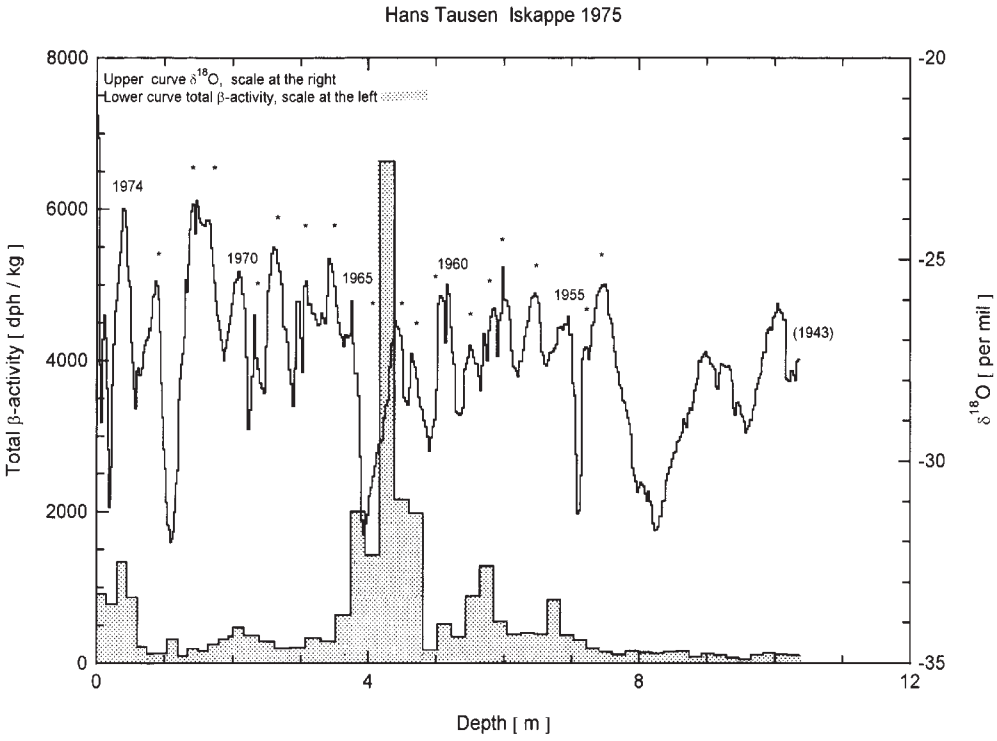

Fig. 22. A detailed $\delta^{18}O$ record (in 2.5 cm resolution) of the top 10 m of the HT75 ice core (scale to the right), and a total β-activity record (scale to the left), provide the ice core with a calendar year dating back to 1953, and suggest 1943 at the bottom depth 10.4 m of the detailed sampling.

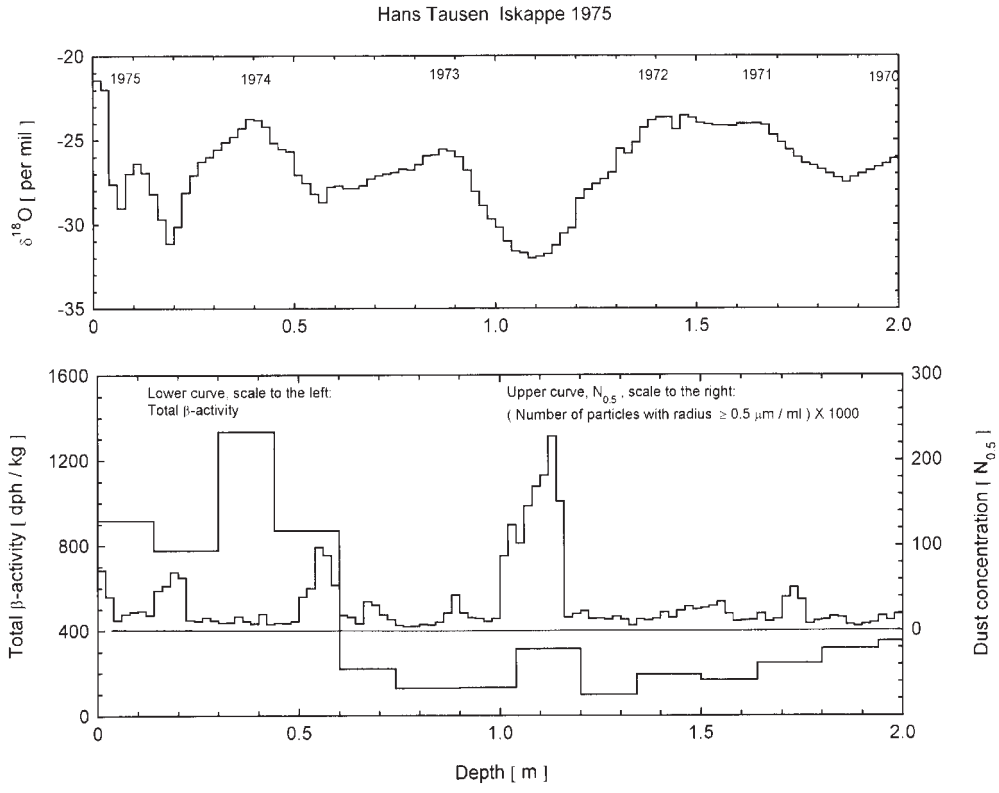

Fig. 23. The figure shows a blown up version of the top 2 m presented in Fig.22 ($\delta^{18}O$ and total β-activity) and a high resolution dust concentration profile (scale to the right) which supports the calendar year dating placed on the $\delta^{18}O$ curve, by the clear early spring peaks of 1971 to 1975.

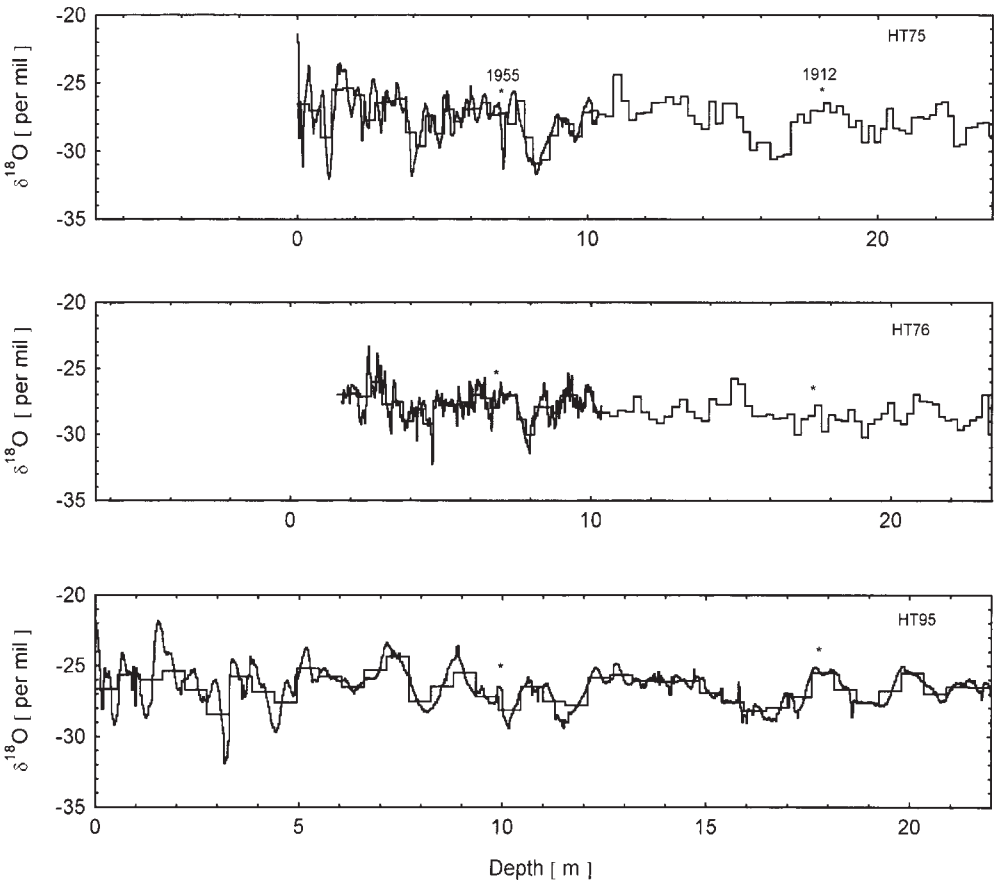

Fig. 24 shows the $\delta^{18}O$ of HT75, HT76 and HT95 (Fig. 25 contains in details the top 6 m of the HT95 record). The 22 m long record of the HT95 represents the length of the detailed (2.5 cm) $\delta^{18}O$ sampling, and the HT75 and HT76 records are locked to the HT95 record at the fixed points of 1955 and 1912 (marked by asterisks at the HT76 and HT95 records). Besides the detailed $\delta^{18}O$ curves, also the $\delta^{18}O$ curves in a lesser resolution are shown. The resolution is 55 cm per sample in the case of HT95, and some 24 cm in the case of HT75 and HT76.

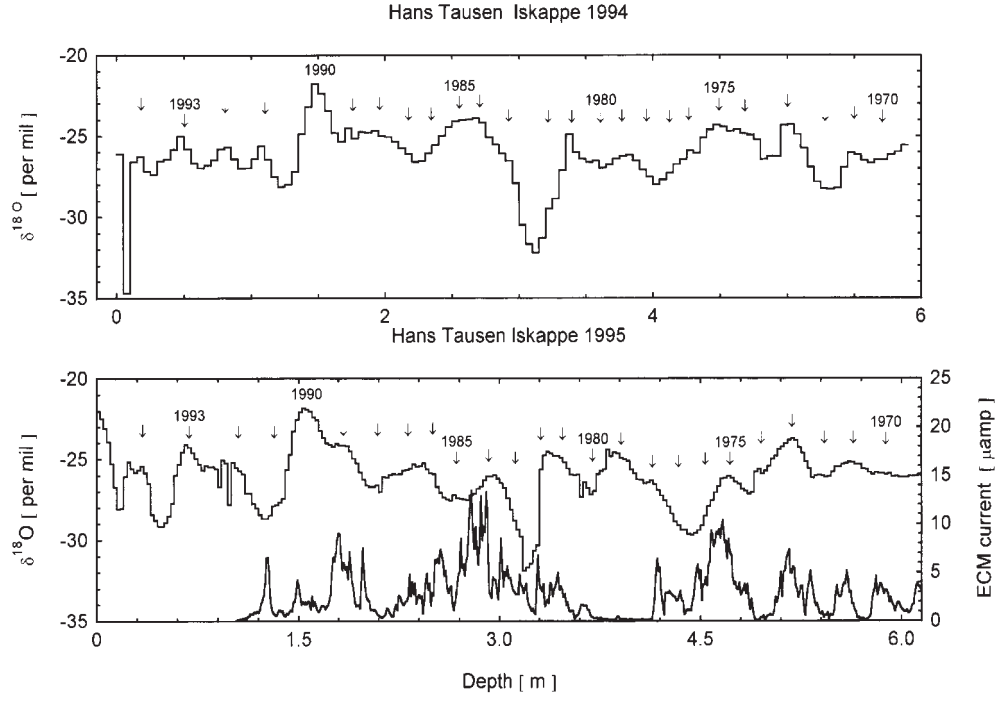

Fig. 25 presents the $\delta^{18}O$ curves of the HT94 (in a 5 cm resolution) and the top 6 m (in a 2.5 cm resolution) of the MC95 profile (see also Fig. 24) provided with the ECM current (lower right scale). The two depth scales are locked together at 1990 and 1975. The arrows suggest the summer positions of a calendar dating of the two records, and the ECM curve supports this dating.

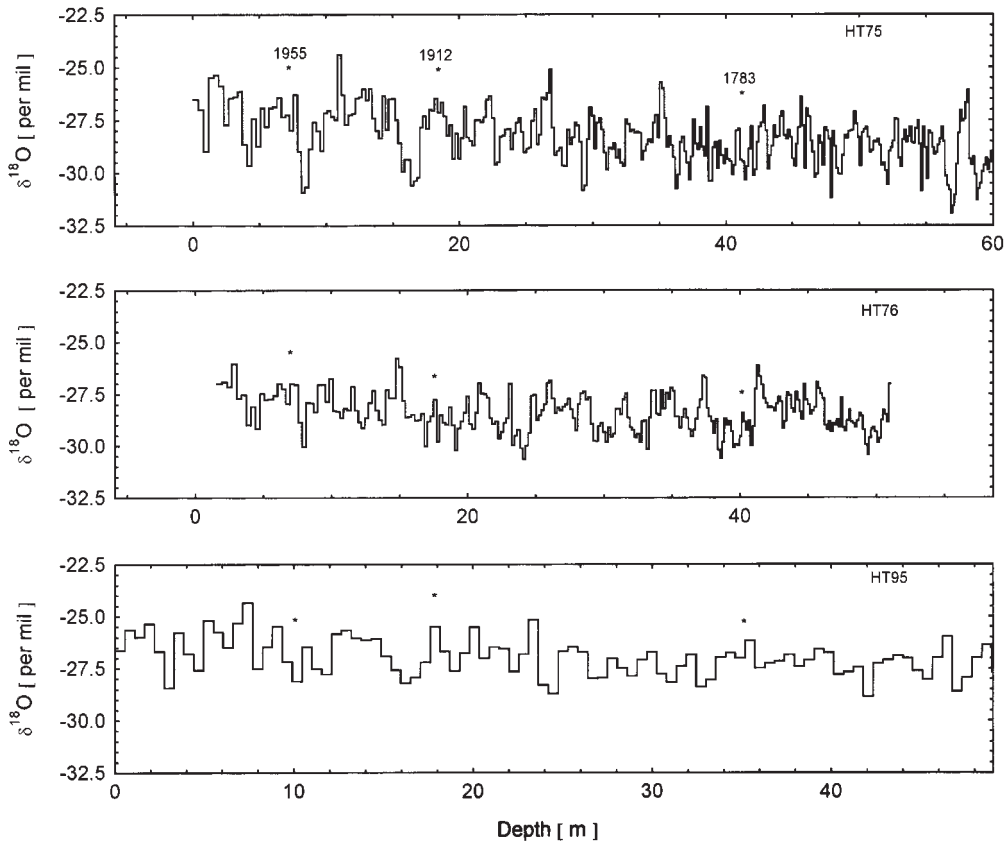

Fig. 26 shows the entire $\delta^{18}O$ records of the HT75 and HT76 ice cores in a resolution of some 15-16 cm of ice equivalent per sample. These curves are locked to the HT95 record at the fixed points of 1955, 1912 and 1783 shown by asterisks on the HT76 and HT95 records. The top some 20 m are shown in details in Fig. 24.

fied by measurement of the total β-activity of ice core samples.

Fig. 22 shows an example of a total β-activity record and a detailed $\delta^{18}O$ record from HT75, and exhibits the typical shape of the total β-acivity records known from other Greenland locations (Clausen and Hammer 1988). This shape includes the raise in 1954 to above the natural total β-activity background which mainly consists of ^{210}Pb (due to the American test series at low northern latitudes (LNL) in the early 1950'ies), a relative minimum (due to the declared moratorium on nuclear testing from November 1958 to September 1961) and the absolute maximum (mainly due to the Russian test series at high northern latitudes (HNL) in the early 1960'ies). Also the record shows a maximum and an increase around 1970 and 1974, respectively. These peaks are probably due to the Chinese test series at 40° N at Lop Nor and they are found in ice cores from other Greenland sites as well (Clausen and Hammer 1988). The total β-acivity records can be used to estimate the magnitude of major volcanic eruptions from known eruption sites. At Hans Tausen Iskappe we find a total β-acivity deposition of 11.1 mCi / km^2 originating from the amount of 22.6 MCi injected into the atmosphere by the Russian test series at HNL in 1962-66. This determines the factor of $2.04 \cdot 10^9$ used in the chapter of the chemical records. The corresponding factor for an eruption site at LNL is $5.89 \cdot 10^9$ based on a deposition of 1.63 mCi / km^2 from 9.6 MCi injected into the atmosphere by the American test series at LNL in 1953-55.

Dating of the ice core

The dating of the ice cores is based on the records of acidity (ECM), water soluble ion concentrations (e.g. nitrate and sodium), $\delta^{18}O$ and total β-activity. Table

	HT 1994 Snow pit			HT 1995 Snow Pit #1			HT 1995 Snow Pit #2			HT 1995 Main Core			Mean-annual rate of-accumulation
	Depth, start of year		Annual rate of	Depth, start of year		Annual rate of	Depth, start of year		Annual rate of	Depth, start of year		Annual rate of	
Year AD	m of snow	m of ice	accumu-lation	m of snow	m of ice	accumu-lation	m of snow	m of ice	accumu-lation	m of snow	m of ice	accumu-lation	m of ice/year
1995				0			(0.125	0.043	0.043)	(0.175	0.061	0.061)	
1994	(0.30	0.104	0.104)	0.400	0.140	0.140	0.550	0.194	0.151	0.475	0.167	0.106	0.132
1993	0.65	0.229	0.125	0.775	0.274	0.134	0.975	0.346	0.152	0.950	0.337	0.170	0.145
1992	0.95	0.337	0.108	1.075	0.382	0.108	(1.100	0.391	0.045)	1.250	0.444	0.107	0.108
1991	1.25	0.444	0.107	(1.100	0.391	0.009)				1.400	0.507	0.063	0.085

Table 9. Shows the annual rate of accumulation at 4 different locations around the HT95 drilling site. The dating in calendar years is based on the $\delta^{18}O$ records, dust measurements and chemical components like Ca^{2+}, Mg^{2+} and Na^{+}, Cl^{-} and NH_4^{+}, NO_3^{-} (see Fig. 13, which exhibits the data from snow Pit#1). The 1995 density record is used for all sites, and the resolution of the records is 5 cm for the HT94 record and 2,5 cm for the HT95 records. Parenthesis means an incomplete year in the record.

9 shows the annual rate of accumulation for the period 1991-95 determined by $\delta^{18}O$ measurements performed on snow pit samples from 4 different locations at the HT95 drilling site and the data from snow pit #1 are exhibited in Fig. 13. Fig. 27 shows the HT95 time scale as defined by the volcanic fixed points plotted versus a depth scale in m of ice equivalent. Fig. 6 shows ECM pins on a time scale from GRIP and Hans Tausen. The fixed points of the dating (marked by asterisks) are from the $\delta^{18}O$ records (see above): 1947, 1963 and 1983, and from major volcanic eruptions known from other Greenland ice core ECM records covering the last 200 years: e.g. AD 1912, 1816, 1810 and 1783. For ice cores representing precipitation over the last 1000 years especially the period AD 920 to AD 1275 is interesting, because in this time interval we find three large volcanic signals at AD 934, 1179 and 1259 and they are among the largest signal found during the last 11,500 year long Holocene period (Clausen *et al*. 1997). The three signals are found in all Greenland ice core records which reach the depth corresponding to these ages, and in average one signal of this type appears per century. The AD 1259 signal is, besides being a fixed point for dating of artic ice cores (also found in Canadien ice cores (Fisher and Koerner 1988)) also identified in antarctic ice cores and thus serves as an interhemispheric fixed point (Langway *et al*. 1988). For the time period between 1000 and 2000 years ago we find acid signals corresponding to AD 527, 49 BC and 244 BC (Clausen *et al*. 1997), and as mentioned in the ECM section no ECM peak signals are seen below the depth of 250 m.

Conclusion

Information from the ECM measurements and the chemical analyses are available despite the large impurity content from local sources and the relatively high temperatures during part of the ECM measurements. Major volcanic eruptions can be identified and used as time markers. Seasonal variations are preserved in the $\delta^{18}O$ records from the top layers, and chemical compounds like e.g. NO_3^{-}, Ca^{2+} and dust measured on discrete core sequences, show seasonality. The average annual ice thickness (λ) is some 10 cm of ice equivalent per year down to the depth of 244 m, and a detailed dust profile covering some 5 m close to bottom indicates almost an unchanged λ at this depth (Hammer *et al*. 2001). This suggests an age of some 3000 years for the bottom near layers. The observation that no significant thinning of annual layers is

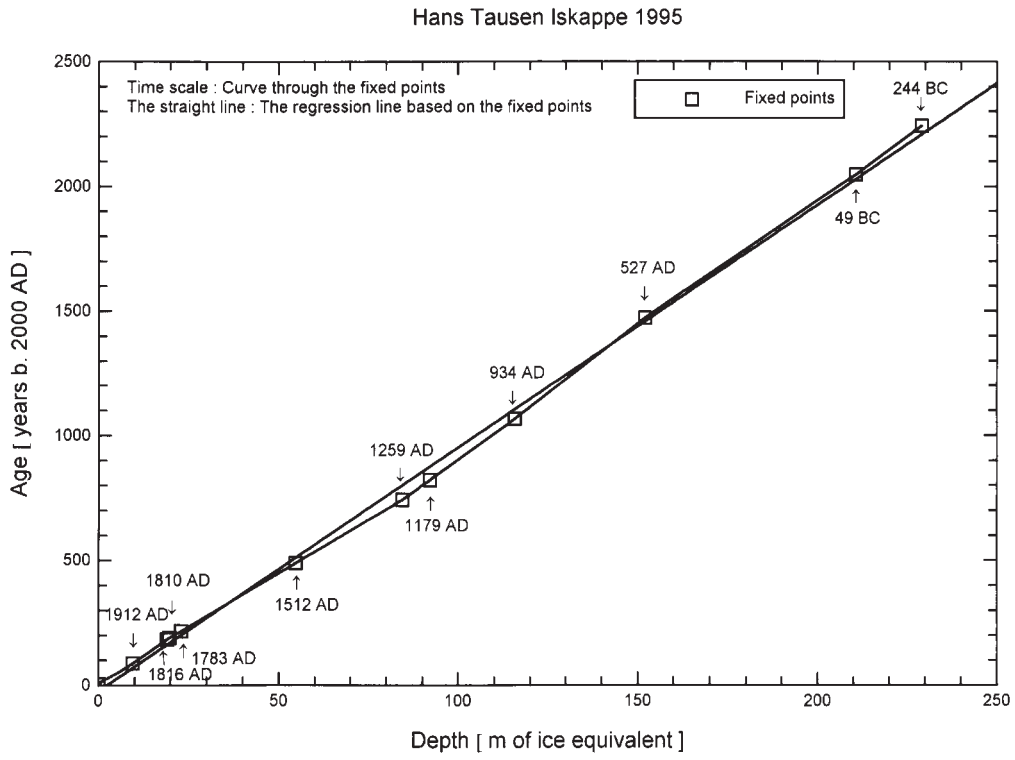

Fig. 27 presents a time scale (the line segments though the origin and the squares) for the HT95 ice core based on 11 prominent volcanic eruptions also listed in Tables (3 and 4). The regression line based on the fixed points: y = 9.74x –23.1 corresponds to an average annual ice thickness of 10.3 cm of ice equivalent per year for the time period represented by this depth interval.

observed, supports other findings (Keller *et al.* 2001) that the Hans Tausen Iskappe is not in mass balance.

Acknowledgments

We want to thank the *Danish Natural Science Research Council* (SNF), *the Climate Change Research Program* under the *Nordic Environmental Research Program* (the *Nordic Council of Ministers*) and the EU DGXII project *MilEClim* for financial support. Also we want to thank the personnel at Station Nord for hospitality and logistic support.

References

Blaker, M. R. and J. S. Peel 1997. Lower Cambrian trilobites from North Greenland. Meddelelser om Grønland Geoscience 35: 1-145.

Clausen, H. B. and C. U. Hammer 1988. The Laki and Tambora eruptions as revealed in Greenland ice cores from 11 locations. *Annals of Glaciology* 10: 16-22.

Clausen, H. B. *et al.* 1995. 1250 years of global volcanism as revealed by Central Greenland Ice Cores. In: *Ice Core Studies of Global Biogeochemical Cycles*. R. J. Delmas. New York, Springer-Verlag. 30: 175-194.

Clausen, H. B. *et al.* 1997. A comparison of the volcanic records over the past 4000 years from the Greenland Ice Core Project and Dye3 Greenland ice cores. *Journal of Geophysical Research* 102(C12): 26707-26723.

Clausen, H. B. and C. C. Langway, Jr. 1989. The ionic deposits in polar ice cores. In: *Dahlem Konference: The Environmental Record in Glaciers and Ice Sheets*. H. Oeschger and C. C. Langway, Jr. New York, John Wiley: 225-248.

Dansgaard, W. *et al.* 1973. *Stable Isotope Glaciology.* Meddelelser om Grønland 197(2): 5-53.

Finkel, R. C. *et al.* 1986. Changes in precipitation chemistry at Dye 3, Greenland. *Journal of Geophysical Research* 91(D9): 9849-9855.

Fisher, D. A. and R. M. Koerner 1988. The effects of wind on $\delta^{18}O$ and accumulation give an inferred record of seasonal $\delta^{18}O$ amplitude from the Agassiz ice cap, Ellesmere Island, Canada. *Annals of Glaciology* 10: 34-37.

Hammer, C. U. 1977. Dating of Greenland ice cores by micro-particle concentration analyses. In: *Proc. of Symp. on Isotopes and Impurities in Snow and Ice, I.U.G.G. XVI, General Assembly, Grenoble Aug. Sept., 1975*. Washington D.C.: 297-301.

Hammer, C. U. 1980. Acidity of polar ice cores in relation to absolute dating, past volcanism, and radio-echoes. *Journal of Glaciology* 25: 359-372.

Hammer, C.U, S. J. Johnsen, H. B. Clausen, D. Dahl-Jensen, N. Gundestrup and J. P. Steffensen 2001. The paleo-climatic record from a 345 m long ice core from the Hans Tausen Iskappe. Meddelelser om Grønland Geoscience, this volume pp. 87-95.

Keller, K., C. S. Hvidberg, N. Gundestrup and P. Jonsson 2001. Surface Movement and Mass Balance at the Hans Tausen Drill Site determined by use of GPS. Meddelelser om Grønland Geoscience, this volume pp. 115-122.

Langway, C. C., Jr. *et al.* 1988. An inter-hemispheric volcanic time-marker in ice cores from Greenland and Antarctica. *Annals of Glaciology* 10: 102-108.

Legrand, M, *et al.* 1997. Sulfur-containing species (methanesulfonate and SO_4) over the last climatic cycle in the Greenland Ice Core Project (central Greenland) ice core. *Journal of Geophysical Research* 102(C12): 26663-26679.

Madsen, K. N. and T. Thorsteinsson 2001. Texture, fabrics, and melt layer stratigraphy in the Hans Tausen Ice Core, North Greenland – indications of late Holocene ice cap generation? Meddelelser om Grønland, Geoscience, this volume pp. 97-114.

Mayewski, P. A. *et al.* 1986. Sulfate and Nitrate Concentrations from a South Greenland Ice Core. *Science* 232: 975-977.

Mulvaney, R. and D. A. Peel 1988. Anions and cations in ice cores from Dolleman Island and the Palmer Land plateau, Antarctic Peninsula. *Annals of Glaciology* 10: 121-125.

Osada, K. and C. C. Langway 1993. Background levels of formate and other ions in ice cores from inland Greenland. *Geophysical Research Letters* 20 (23): 2547-2650.

Risbo, T. *et al.* 1981. Supernovae and nitrate in the Greenland Ice Sheet. *Nature* 294: 637-639.

Saltzman, E. S. 1995. Ocean/Atmosphere Cycling of Dimethylsulfide. In*: Ice Core Studies of Global Biogeochemical Cycles.* R. J. Delmas. New York, Springer-Verlag. 30: 65-89.

Simkin, T. and L. Siebert 1994. *Volcanoes of the World.* Tucson, Ariz., Geoscience Press.

Stampe, M. 1997. *Vulkanske vidnesbyrd i iskerne fra Hans Tausen*. Master of Science thesis, University of Copenhagen, Geophysical Department, Niels Bohr Institute, 93 pp.

Steffensen, J. P. *et al.* 1996. On the spatial variability of impurity content and stable isotope composition in recent Summit snow. In: *Chemical Exchange Between the Atmosphere and Polar Snow.* E. W. Wolff and R. C. Bales. New York, Springer-Verlag. 43: 607-616.

Steffensen, J. P. *et al.* 2001. Microparticles, soil derived chemical components and sea salt in the Hans Tausen Iskappe ice core from Peary Land, North Greenland." Meddelelser om Grønland Geoscience, this volume pp. 151-160.

Sverdrup, H. U. *et al.* 1942. *The Oceans.* New York, Prentice Hall Inc.

Wedepohl, K. H., Ed. 1969. *Handbook of Geochemistry.* New York, Springer-Verlag.

Wolff, E. W. 1995. Nitrate in polar ice. In: *Global Biochemical Cycles in Polar Ice*. R. J. Delmas. New York, Springer-Verlag. 30: 195-224.

Microparticles, soil derived chemical components and sea salt in the Hans Tausen Ice cap ice core from Peary Land, North Greenland

By Jørgen Peder Steffensen, Marie-Louise Siggaard-Andersen, Mia Stampe and Henrik B. Clausen

Abstract

Steffensen, J. P., M-L. Siggaard-Andersen, M. Stampe and H. B. Clausen 2001. Microparticles, soil derived chemical components and sea salt in the Hans Tausen Ice cap ice core from Peary Land, North Greenland. Copenhagen, Danish Polar Center. Meddelelser om Grønland Geoscience 39, pp. 151-160.

Selected segments of the 344 m deep ice core from Hans Tausen ice cap in Peary Land, North Greenland have been stratigraphically analyzed for chemical impurities and insoluble microparticles (Dust). Two different components of the microparticles have been identified by their different sizedistributions: A component of small particles from remote sources, and a component of large particles from local sources. The abundance of large particles increases with depth (and age) in the ice core resulting in an increase in total dust mass. Very high dust mass in the lowest 100 m of the core are believed to be a result of melt water run-off. Compared to Central Greenland ice cores the Hans Tausen ice is strongly enriched in soluble crustal material from local sources manifested by high concentrations of Ca^{2+} and nss. Mg^{2+}. In the bottom 100 m section our results indicate a loss of Ca^{2+} and Mg^{2+} relative to dust due to melt water run-off. Sea salt concentrations show little variation with depth, and our results indicate, that the sea salt in Hans Tausen ice is from remote sources. The North Polar Sea has not been a significant source of sea salt in the life time of the Hans Tausen ice cap. All our results are consistent with the hypothesis that the Hans Tausen ice cap was formed sometime during the Holocene: It started as a small ice cap of superimposed ice with heavy melting and strong influence of local dust sources. With time the ice cap grew, both horizontally and vertically, the surface got colder with less melting and the influence from local sources got weaker. Today the impurity content of Hans Tausen snow is comparable to that of the Central Greenland ice sheet with the exception of the influence of soluble crustal material from the ice free Peary Land area which remains.

Keywords: Ice core; microparticles; sizedistributions; sea salt; melting/refreezing.

Jørgen Peder Steffensen, Marie-Louise Siggaard-Andersen, Mia Stampe and Henrik B. Clausen. Department of Geophysics, Niels Bohr Institute for Astronomy, Physics and Geophysics, University of Copenhagen, Copenhagen, Denmark.

Introduction

Stratigraphic analysis of ice cores from polar ice caps provide important palaeoclimatic information. In ice cores originating from sites where melting never occurs changes with depth in e.g. stable isotopic composition or concentrations of chemical impurities and insoluble microparticles (dust) reflect changes in past atmospheric composition and climate. Over large areas in the interior of the Greenland ice sheet, including ice core drilling sites such as GRIP (Johnsen *et al.* 1992), GISP2 (Grootes *et al.* 1993) and NGRIP (Dahl-Jensen *et al.* 1997), melting at the surface is very rare. However at sites where summer melting occurs, the ice core stratigraphy may be disturbed by melting and refreezing processes. At sites where this summer melting is limited, the melt water refreezes in the cold spring and winter snow below. In the firn this can be observed as blue layers of ice in the white firn. In ice cores, these layers show up as clear layers without gas bubbles. Although the chemical composition and the dust content may change due to melting/refreezing there is no loss of material and mixing between annual layers is limited. Ice cores from such sites still provide reliable palaeoclimatic information, but great care should be exercised in the interpretation of stratigraphical details since some features of the stratigraphical profiles may be due to melting and not a consequence of atmospheric changes. Ice core drilling sites such as Dye-3 (Dansgaard *et al.* 1982) and Renland (Johnsen *et al.* 1992) fall into this category. At sites where summer melting is heavy the snow below the surface melt layer may become saturated with melt water and material may be lost due to run-off. Here, the chemical composition, the dust content and even the stable isotopic composition may be altered over large sections of the stratigraphical profiles to such degrees that these cores contain very little reliable palaeoclimatic information. A large number of ice cores from smaller ice caps in the north polar region originate from such sites (Koerner 1997).

In the Hans Tausen ice cap ice core layers of refrozen meltwater are found in abundance. The percentage of layers showing melting/refreezing increases with depth from about 10% close to the surface until it reaches 100% in the deepest 10% of the core (K. Nørregaard Madsen 2001). Here the ice core is completely clear without any bubbles from trapped atmospheric air. The stratigraphical profiles of stable isotopic composition, chemical compostion and the dust content from this core therefore have to be interpreted with great care in order to separate "real" climatic and atmospheric signals from the effects of melting/refreezing.

Experimental

The Hans Tausen ice cap ice core was drilled in the summer of 1995 on a local dome at 82° 30′ N, 37° 28′ W, 1271 m a.s.l. on the Hans Tausen ice cap in Peary Land in North Greenland. The core reaches to bedrock at 344.85 m depth. Immediately after drilling the core was logged and the visible stratigraphy, such as melt layers, recorded. Electric Conductivity Measurement (ECM) was performed as well as the cutting of samples for stable isotopic composition before the core was cut into 55 cm core segments. The core segments are called "bags" in reference to the numbered plastic bags they are packed into. The bags were packed in insulated boxes for shipment in frozen condition to the cold storage in Copenhagen. 30 selected segments of the core were sampled in Copenhagen for chemical and dust analysis. The segments were cleaned and sampled under laminar flow by cutting away the outer surface using a steel microtome knife in the cold room. The

samples were stored in Coulter Accuvettes and kept frozen until analysis. Measurement of the concentrations of ionic components, such as Na^+, Cl^-, Mg^{2+} and Ca^{2+} was done on a Dionex 4000i ionchromatography system capable of measuring both anions and cations on the same aliquot. Measurement of the sizedistribution of microparticles between radii 0.4 µm and 6.5 µm was done on a Coulter Multisizer II. A total of more than 700 samples each of them 5 cm long were measured this way. 55 cm averages of the sizedistribution data were made and the results fitted to a log-normal distribution (Steffensen 1997).

The log-normal distribution:

$$\frac{dV}{d\log r} = \frac{V_T}{\sqrt{2\pi}\log\sigma} \exp\left(-\frac{1}{2}\left(\frac{\log r - \log\mu}{\log\sigma}\right)^2\right)$$

V(r) is the volume concentration of particles larger than r. r is particle radius in µm. In this distribution the volume is normal (or Gaussian) distributed as a function of log r. log µ plays the role of the mode, thus µ is called the log-normal mode and log σ plays the role of the standard deviation, thus σ is called the log-normal standard deviation. V_T is the total volume concentration of particles. In this distribution 70% and 95% of the total volume is inside the radius intervals:

$$[\exp(\log\mu - \log\sigma) \;;\; \exp(\log\mu + \log\sigma)] \quad (70\% \text{ of } V_T)$$
$$[\exp(\log\mu - 2\log\sigma) \;;\; \exp(\log\mu + 2\log\sigma)] \quad (95\% \text{ of } V_T)$$

Logarithms to base "e" was used.

Also, the total dust mass (in µg/kg) and the mass fraction of large particles (2.5 µm < r < 6.5 µm) to the total particle mass was calculated.

Results

Mean concentrations in 55 cm ice core segments ("bags") of ionic components and dust data are presented in Table 1. The total dust mass for individual samples is presented in Fig. 1. Although there are large variations in dust mass between individual samples there is an increase in dust mass with depth. Below 300 m the dust mass is more than 10 times higher than at 100 m. Six 55 cm mean dust sizedistributions are shown in Fig. 2, including the fit of the data to log-normal distributions. For comparison, a sizedistribution from GRIP has been included. With increasing depth the sizedistributions are shifted towards larger particles. This is reflected by the mode parameter, µ, of the log-normal fit that shifts from 0.8 µm to around 2.6 µm and the increasing mass fraction of large particles, that shifts from 5% to around 50%.

In the two ice cores from GRIP and Dye-3 there was a clear correlation between total dust mass and the concentration of Ca^{2+} which is believed to be due to the common continental origin and shared atmospheric transport of these species (Steffensen 1997). In Fig. 3 the Hans Tausen results are presented. As can be seen there is very little correlation between Ca^{2+} and dust mass in the Hans Tausen core. And compared to GRIP and Dye-3, the Hans Tausen ice is strongly enriched in Ca^{2+}. Five outliers are marked with their corresponding depths. Four of them are from great depth.

Also, at GRIP and Dye-3 the concentrations of non sea salt (nss.) Mg^{2+} and Ca^{2+} correlated. This correlation also is believed to be due to a common origin and shared transport (Steffensen 1997). A significant amount of Mg^{2+} in the ice may originate from sea salt. So the sea salt fraction of Mg^{2+} has to be calculated to obtain nss. Mg^{2+}. The Hans Tausen nss. Mg^{2+} concentrations are plotted as a function of Ca^{2+} concentrations in Fig. 4. In the Hans Tausen ice nss. Mg^{2+} and Ca^{2+} do correlate; but the molar ratio of nss. Mg^{2+} to Ca^{2+} is 0.43 which is 3.5

Depth	Bag #	Na^+	Cl^-	Mg^{2+}	Non sea salt Mg^{2+}	Ca^{2+}	Dust mass 0.4<r<6.0	Dust mass 0.4<r<2.5	Mass fraction of 2.5<r<6.0	Relative amount of melt layers
[m]	μ	[μequiv/kg]	[μequiv/kg]	[μequiv/kg]	[μequiv/kg]	[μequiv/kg]	[μg/kg]	[μg/kg]	[%]	[%]
0.55	1	0.90	1.22	1.87	1.68	4.09				2
1.1	2	1.78	1.82	1.04	0.65	1.91				4
18.15	33			1.90		3.54	114	108	5	1
18.7	34			2.81		5.57	47	43	10	2
19.25	35			1.39		2.14	55	51	7	0
30.8	56			1.95		3.64	76	73	4	5
31.35	57			0.82		1.74	49	47	4	1
31.9	58			1.93		4.07	108	105	3	9
32.45	59			0.82		1.74	86	81	5	6
35.2	64	2.14	1.89	2.86	2.38	4.28	76	72	6	1
35.75	65	1.26	1.23	0.88	0.61	1.85	51	49	5	0
69.85	127	0.78	1.07	1.25	1.08	2.38	88	85	4	0
70.4	128	0.54	0.69	0.88	0.76	1.50	36	34	4	2
94.05	171	0.67	0.95	0.97	0.82	2.57	60	53	12	40
94.6	172	1.38	1.53	2.31	2.01	5.25	26	25	2	26
96.8	176	0.69	0.85	1.82	1.67	4.51	34	31	9	7
97.35	177	0.67	0.80	1.79	1.64	3.24	101	81	20	1
100.1	182	0.51	0.56	2.02	1.91	3.71	91	84	7	3
100.7	183	1.16	1.68	2.05	1.79	5.01	103	100	3	9
101.2	184	0.78	0.99	1.10	0.93	2.53	80	75	6	12
105.6	192	1.01	1.60	2.72	2.50	7.99	228	168	26	2
107.8	196	0.65	0.83	1.65	1.51	3.40	86	80	7	0
108.4	197	1.44	1.41	1.45	1.13	4.36	153	125	18	1
120.5	219	1.13	1.59	1.18	0.94	2.79	303	189	38	0
131.4	239	1.07	1.72	1.47	1.23	3.24	88	85	3	4
132	240	0.46	0.64	0.77	0.67	2.62	92	85	7	1
135.9	247	0.99	1.23	1.54	1.32	3.30	126	102	19	2
150.2	273	0.99	1.63	3.94	3.72	8.48	190	127	33	22
165	300	1.08	1.39	4.69	4.46	9.09	477	250	48	27
180.4	328	0.96	1.16	4.41	4.20	7.21	182	109	40	69
194.7	354	1.16	1.68	2.46	2.20	5.94	37	33	10	67
210.1	382	0.95	1.31	4.13	3.92	6.20	284	241	15	29
226.1	411	1.41	1.66	4.92	4.61	12.82	133	90	32	44
226.6	412	1.43	1.35	1.20	0.89	1.95				91
240.9	438	1.09	1.94	3.16	2.92	9.57	88	81	7	24
244.8	445	1.08	1.21	2.10	1.86	5.72				20
245.3	446	1.24	1.40	1.64	1.37	5.11				86
255.2	464	0.51	1.31	2.94	2.83	5.53	78	72	7	100
270	491	1.53	2.30	6.30	5.97	15.28	192	165	14	76
286	520	0.88	1.36	8.41	8.22	14.78	71	67	7	100
300.3	546	1.04	1.48	2.60	2.37	7.04	2009	1078	46	100
315.2	573	1.09	1.74	3.28	3.04	5.24	543	310	43	100
330	600	1.28	1.97	4.39	4.11	12.99	1986	1421	28	100
344.8	627	1.33	2.00	5.30	5.01	12.82	487	467	4	100

Table 1. Note: All values represent 55 cm mean values of between 11 and 22 individual samples.

times higher than the ratio at GRIP of 0.12. No significant changes in the ratio of magnesium and calcium with increasing depth is observed.

The sea salt correction on the concentrations of Mg^{2+} appear to be reasonable because all Na^+ and most of Cl^- in Hans Tausen ice is believed to be from sea salt. In Fig. 5 the Cl^- concentrations are plotted versus Na^+. Chloride and sodium are correlated, and the molar ratio of chloride and sodium is close to the ratio in sea salt: $[Cl^-]/[Na^+] = 1.17$. There are several points that show an excess of chloride, but chloride has other sources than sea salt. In particular, volcanic eruptions may contribute HCl, and since several samples were taken across volcanic eruptions, a slight excess of chloride is expected. However, there are very few outliers with excess sodium so that the bulk of sodium can be assumed to originate from sea salt and nss. Mg^{2+} can be calculated using the sea salt molar ratio between sodium and magnesium: $[Mg^{2+}]/[Na^+] = 0.22$. The mean sea salt concentration in Hans Tausen ice does not show significant variation with depth. The Hans Tausen concentrations are 0.5 – 1.5 µequiv./kg as compared to GRIP Holocene values of 0.3 – 0.4 µequiv./kg, i.e. 2-3 times higher.

Discussion

The mean dust mass of the upper part of the Hans Tavsen core is around 80 µg/kg. This is significantly higher than the 40 µg/kg in GRIP Holocene ice (Steffensen 1997). On the other hand, annual accumulation is 0.11 m ice/yr as compared to GRIPs 0.22 m ice/yr. Thus the dust fluxes at Hans Tausen and GRIP are comparable. The size distributions are comparable with modes of 0.9 µm at Hans Tausen and 0.85 µm at GRIP. The dust in the GRIP core is of remote origin, since the site is on the central part of the Greenland ice sheet far removed from any local dust source areas. In fact, isotope studies on the dust particles from the nearby GISP2 core suggest an Asian origin of the dust (Biscaye *et al.* 1997). Since GRIP and Hans Tausen sizedistributions and dust fluxes are comparable it suggests that the dust in the upper part of the Hans Tausen ice core is also of remote origin.

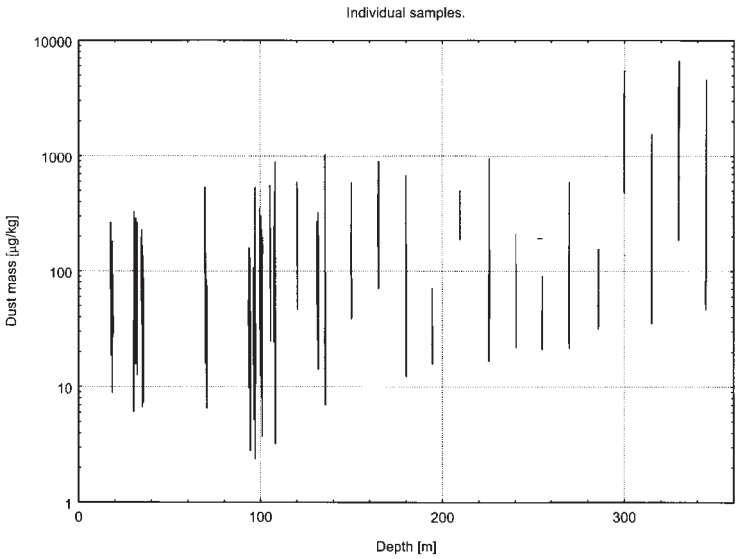

Fig. 1. Dust mass as function of depth for individual 5 cm samples in the segments analyzed. The variation in dust mass within each segment causes the results to appear as vertical lines, which gives an idea of the variability of dust mass. Note, that the dust mass scale is logarithmic.

The GRIP dust sizedistributions and concentrations show very little variation in the Holocene period. Since the dating of the Hans Tausen ice core and the stable isotopic profile indicate that the whole ice core is from the Holocene (C.U. Hammer *et al.* 2001) then the increase in dust mass with depth in the Hans Tausen core has no counterpart in GRIP, and it is caused by increasing mass of large particle fraction. The mass ratio of large particles is high at high dust mass in the Hans Tausen core, which is contrary to the low mass ratios at high dust mass in the GRIP core. The large particle fraction with modes of 2 µm or more appears sporadically through the Hans Tausen profile but becomes more and more dominant with depth. Below 300 m it dominates completely. The mean sizedistributions have modes close to 2.5 and such distributions have not been observed at GRIP or at Dye-3 at all.

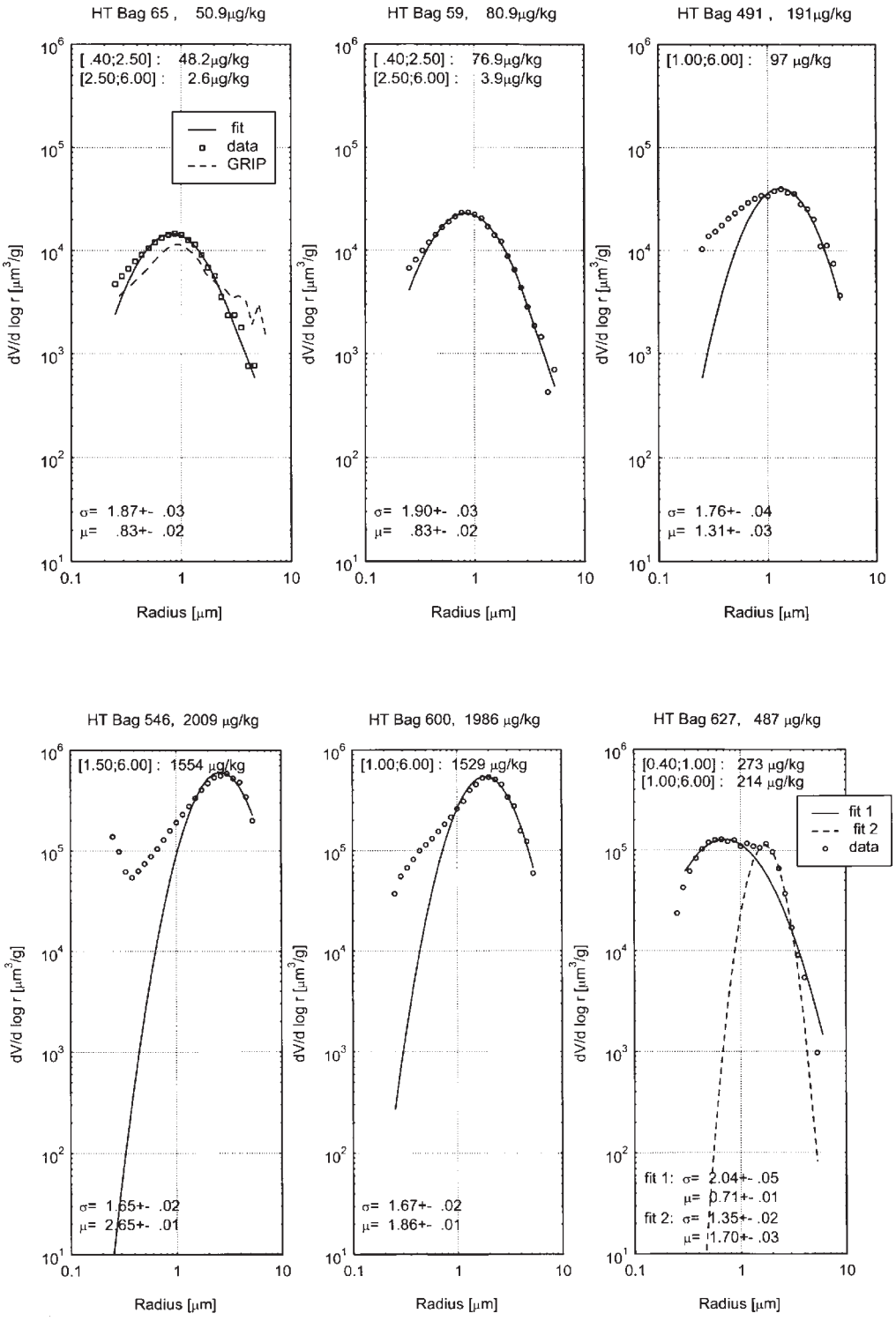

Fig. 2. Mean microparticle size distributions of six selected 55 cm ice core segments. Bag numbers refer to the numbers in Table 1. Total dust mass is given above each plot. Dust mass in selected particle radius intervals are also indicated. The data points represent measurements. The full lines are the log-normal distributions fitted to the data. The mode and standard deviation of the log-normal fits are given at the bottom of the plots as "µ" and "(" respectively. The GRIP Holocene mean sizedistribution has been added for comparison.

Measurements of the sizedistribution of dust particles in air over arid dust producing areas in the U.S. yield log-normal distributions with modes of 2 – 3 µm (Patterson and Gillette 1977). They argued, that these distributions are consequences of the physical mechanisms of wind action on the surface particles to produce dust aerosol. Dust aerosols in the free troposphere, i.e. 3-5 km altitude

have modes of about 1 µm (Patterson *et al.* 1980). The 2-3 µm mode dust aerosols have been modified by gravitational settling and removal by condensation in clouds of primary the large particles. Therefore, we may assume that the large particle fraction in Hans Tausen are of local origin. We investigated if the presence of very large particles was due to changes by melting and refreezing processes, but we found also large particles in ice outside the melt layers. The dust in Hans Tausen ice appears to have two components: Dust from remote sources with log-normal modes of around 1 µm, and dust from local sources with modes around 2 µm. In most cases, one or the other component dominates; but in Bag 627 we were lucky to identify both components (see Fig. 2). The very large concentrations below 300m occur in ice with 100% indication of melt and could be caused by two things:

1) The ice cap was smaller at the time of deposition (C.U. Hammer 2001; Keller 2001) local sources were therefore closer, and
2) The layers below 300m have experienced significant run-off by melting.

This would cause the water phase to run off and leave the microparticles behind, increasing the dust concentration (Koerner 1997). This could also explain why Ca^{2+}/dust ratio points from great depth in Fig. 3 are outliers. The Ca^{2+} has been washed out; but the dust remained.

Both factors appear to be significant. The decreasing frequency of dust layers with large particles with time (increasing frequency with depth) can be explained by less likelihood of local dust being blown unto the snow due to the growing of the ice cap and increased snow cover over the local sources. The "jump" in concentrations at 300m may mark a time in the development of the Hans Tausen ice cap where run-off by melting stopped. This is also indicated by the shift in the stable isotopic profile around this depth (C. U. Hammer *et al.* 2001) and the end of the 100% indication of melt layers in the core (K. Nørregaard Madsen 2001)

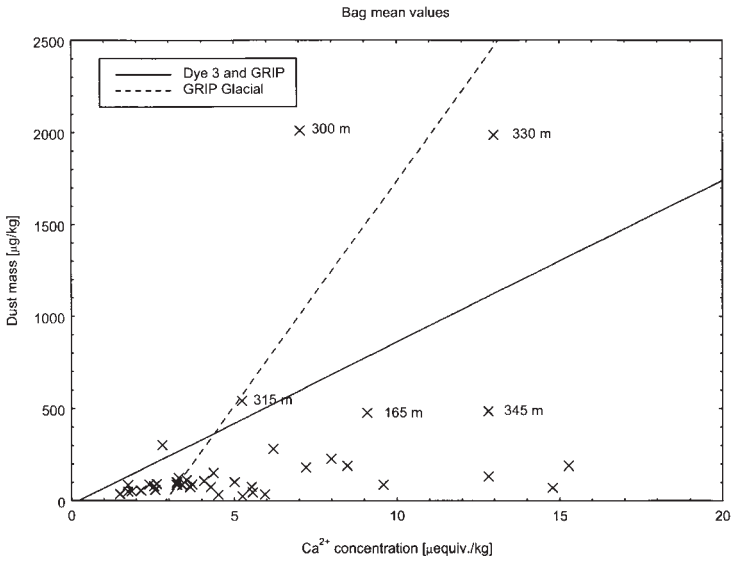

Fig. 3. Dust mass plotted as function of Ca^{2+} concentration for 55 cm ("Bag") averages. Data are given in Table 1. For comparison the correlation between Ca^{2+} and dust for Dye-3 and GRIP (Holocene) and GRIP (Glacial ice) are shown as lines. Five outlying points are labeled with their corresponding depths.

There is far more Ca^{2+} in Hans Tausen than at GRIP. Also the relative concentration of nss. Mg^{2+} to Ca^{2+} is much higher. At the same time, the ECM measurements and ionic balance calculations indicate that the Hans Tausen ice generally is slightly alcaline. This is most likely due to the presence of large enough amounts of dissolved (Mg,Ca)-carbonates in the ice samples to neutralize the strong acids such as sulfuric acid and nitric acid. Only in layers containing very large amounts of acid fallout from volcanic eruptions the Hans Tausen ice is acidic (H. B. Clausen pers. comm.). At Dye-3 and GRIP the ice from the Holocene remains acidic. The strong presence of dissolved (Ca,Mg)-carbonates in Hans Tausen ice is most likely from local sources of soluble carbonate dust particles from exposed carbonate rich sediments such as dolomite which are abundant in the Peary Land area (Dawes 1976).

With respect to sea salt, the high sea salt concentrations at Hans Tausen compared to GRIP is not surprising. Herron (1982) showed that sea salt concentra-

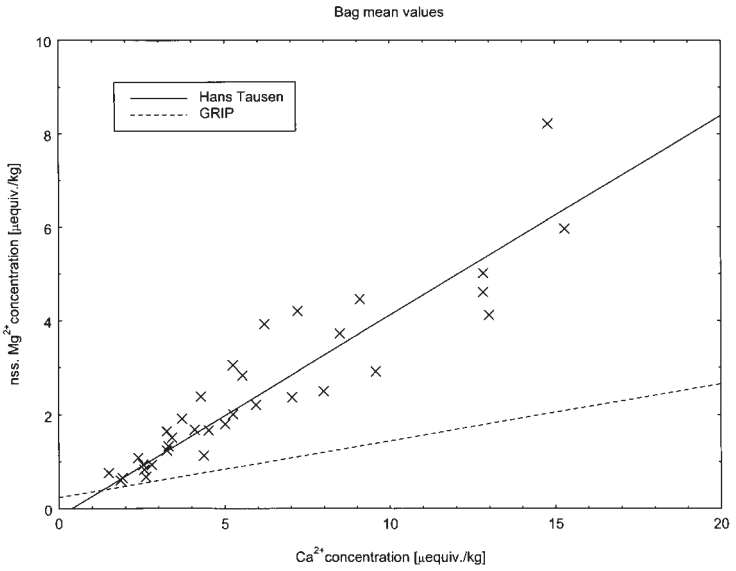

Fig. 4. Non sea salt (nss.) Mg^{2+} concentrations plotted as function of Ca^{2+} concentrations for 55 cm ("Bag") averages. Data are given in Table 1. The full line represents linear regression of the Hans Tausen points. The dashed line is a similar regression line for GRIP data for comparison.

tions decrease with altitude. However, the concentrations at Hans Tausen are slightly lower than estimated by the relationship of Herron. Also, Herron only discussed concentration data. If sea salt fluxes are calculated by inferring observed annual accumulations, the sea salt flux at Hans Tausen is significantly lower than would be expected at this altitude.

The Hans Tausen ice core is the only core from the northern coast of Greenland studied so far. The north coast borders the North Polar Sea. This ocean is mainly ice covered throughout the year, and it is not believed to be a significant source of marine sea salt aerosol. The sea salt flux at Hans Tausen ice cap (100 µequiv./m^2/yr of Cl^-) is comparable to the flux on the Central Greenland ice sheet (80 µequiv./m^2/yr of Cl^-). A detailed pit study at the drilling site revealed that in the surface snow at Hans Tausen ice cap the seasonal variation of sea salt concentrations shows winter highs and summer lows. This is similar to the seasonal pattern observed in Central Greenland (Steffensen 1988) and in aerosol measurements at Station Nord (on the Greenland North coast) (Heidam *et al.* 1993). This contrasts the seasonal pattern of sea salt concentrations in the aerosol at the coastal sites of East and West Greenland with summer highs and winter lows which is believed to be a consequence of the changing sea ice cover in the local sea (Heidam 1984). Thus the sea salt in the Hans Tausen ice core is believed to be from remote sources and in terms of sea salt the Hans Tausen ice resembles the Central Greenland ice cores. NaCl is readily soluble so in periods of heavy melting and run-off the sea salt is expected to run-off at the same degree as water. This means, that the concentration of sea salt is not expected to change due to heavy melting. This may explain why we do not see a change in sea salt concentration with depth in the Hans Tausen ice core. On the other hand, the lack of change with depth also indicates, that the North Polar Sea has never been a significant source of sea salt in the snow here, and has therefore probably not been ice free in the life time of the Hans Tausen ice cap.

Conclusions

Sodium is well suited as indicator of sea salt in the Hans Tausen core. The sea salt flux to the Hans Tausen ice cap is comparable to the flux to the Central Greenland ice sheet. The seasonal variation of sea salt concentrations in Hans Tausen snow shows winter highs and summer lows which is in agreement with the seasonal variations observed in Central Greenland and at Station Nord on the north coast of Greenland; but not in agreement with observations at coastal sites in West and East Greenland. The sea salt in Hans Tausen ice cap is believed to be from remote sources and not from the North Polar Sea. It appears, that the North Polar Sea has not been a significant source of sea salt for the Hans Tausen ice cap during its lifetime.

For the first time in Greenland we have identified two different fractions of microparticles characterized by their log-normal modes. Local dust with a

log-normal mode of 2 – 3 µm and dust from remote sources with modes around 1 µm. The influence of local dust decreases over time. Very high dust concentrations close to bedrock are thought to be due to run-off of melt water during the initial build-up of the ice sheet. Influx of soluble carbonate rich particles from local sources makes the ice slightly alcaline. The ratio between dust mass and Ca^{2+} has been changed in the deep part of the core due to melting and run-off. Sea salt and dust concentrations in the younger snow are comparable with Central Greenland concentrations. All together, these results support the overall interpretation that the Hans Tausen ice cap has been developing from a small glacier where melting and influence from local sources was dominant, into a larger glacier where the impurity content in the ice from the atmospheric aerosol is comparable with the contents in Central Greenland ice. The only "Hans Tausen finger print" that remains in modern Hans Tausen snow as opposed to Central Greenland snow is the high concentrations of (Ca,Mg)-carbonates from local sources.

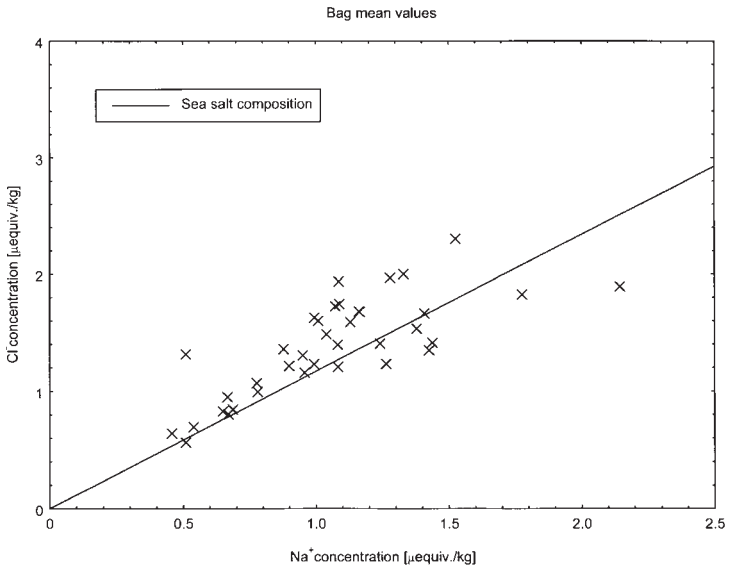

Fig. 5. Cl^- concentrations plotted as function of Na^+ concentration for 55 cm ("Bag") averages. Data are given in Table 1. The full line indicates mean sea salt composition with a molar ratio between chloride and sodium of 1.17.

Acknowledgements

The Hans Tausen ice cap project was funded by *The Nordic Environmental Research Programme 1993-1997* of the *Nordic Council of Ministers*. We wish to express our gratitude to the Danish military personnel at Station Nord for their helpfulness and hospitality during the fieldwork on Hans Tausen ice cap.

References

Biscaye, P. E. *et al.* 1997. Asian provenance of glacial dust (stage 2) in the Greenland Ice Sheet Project 2 Ice Core, Summit, Greenland. *Journal of Geophysical Research* 102(C12): 26765-26781.

Dahl-Jensen, D. *et al.* 1997. A search in north Greenland for a new ice-core drill site. *Journal of Glaciology* 43(144): 300-306.

Dansgaard, W. *et al.* 1982. A new Greenland deep ice core. *Science* 218(4579): 1273-1277.

Dawes, P. R. 1976. Precambrian to Tertiary of northern Greenland. In*: Geology of Greenland*. A. Escher and W. S. Watt (eds.). Denmark, The Geological Survey of Greenland: 248-303.

Grootes, P. M. *et al.* 1993. Comparison of oxygen isotope records from the GISP2 and GRIP Greenland ice cores. *Nature* 366(6455): 552-554.

Hammer C. U. *et al.* 2001. Meddelelser om Grønland Geoscience, this volume pp. 87-95.

Heidam, N. Z. 1984. The components of the Arctic aerosol. *Atmospheric Environment* 18(2): 329-343.

Heidam, N. Z. *et al.* 1993. Arctic aerosols in Greenland. *Atmospheric Environment* 27A: 3029-3036.

Herron, M. M. 1982. Impurity Sources of F^-, Cl^-, NO_3^- and SO_4^{2-} in Greenland and Antarctic Precipitation. *Journal of Geophysical Research* 87(C4): 3052-3060.

Johnsen, S. J. *et al.* 1992. Irregular glacial interstadials recorded in a new Greenland ice core. *Nature* 359(6393): 311-313.

Johnsen, S. J *et al.* 1992. *A "deep" ice core from East Greenland*. Meddelelser om Grønland Geoscience 29: 1-22.

Keller, K. *et al.* 2001. Surface Movement and Mass Balance at the Hans Tausen Drill Site

determined by use of GPS. Meddelelser om Grønland Geoscience, this volume pp. 115-122.

Koerner, R. M. (1997). Some comments on climatic reconstructions from ice cores drilled in areas of high melt. *Journal of Glaciology* 43(143): 90-97.

Madsen, K. N. and T. Thorsteinsson 2001. Texture, fabrics, and melt layer stratigraphy in the Hans Tausen Ice Core, North Greenland – indications of late Holocene ice cap generation? Meddelelser om Grønland Geoscience, this volume pp. 97-114.

Patterson, E. M. and D. A. Gillette 1977. Commonalities in measured size distributions for aerosols having a soil-derived component. *Journal of Geophysical Research* 85(15): 2074-2082.

Patterson, E. M. *et al*. 1980. Global measurements of aerosols in remote continental and marine regions: Concentrations, size distributions and optical properties. *Journal of Geophysical Research* 85(C12): 7361-7376.

Steffensen, J. P. 1988. Analysis of the seasonal variation in dust, Cl^-, NO_3^-, and SO_4^{2-} in two Central Greenland firn cores. *Annals of Glaciology* 10: 171-177.

Steffensen, J. P. 1997. The size distribution of microparticles from selected segments of the Greenland Ice Core Project ice core representing different climatic periods. *Journal of Geophysical Research* 102(C12): 26755-26763.

Biological Microparticles in the Hans Tausen Ice Cap, North Greenland

By Sabine Gruber and Ruprecht Jaenicke

Abstract

Gruber, S. and R. Jaenicke 2001. Biological Microparticles in the Hans Tausen Ice Cap, North Greenland. Copenhagen, Danish Polar Center. Meddelelser om Grønland Geoscience 39, pp. 161-163.

Samples from three different depths in the Hans Tausen ice core (82.5°N, 37.5°W) in Peary Land, North Greenland were examined. The aim was to determine the size distributions of the total and biological particles in the size range 0.2 µm < radius < 41.2 µm. To date, the concentration of the whole spectrum of biological microparticles including viruses, bacteria, spores, pollen, plant debris and animal fragments in ice is still unknown. Biological particles were distinguished from non-biological ones by single particle analysis. The mean concentration of the total insoluble particles in ice was 1.02E+05 per ml, of these, 3.20% were biological.

Keywords: Hans Tausen ice cap; particle size distribution; biological particles.

Sabine Gruber, Institut für Physik der Atmosphäre, Universität Mainz, Germany. (Now: Chemistry Department, University of Reading, UK).

Introduction

Particles included in an ice cap are deposited atmospheric aerosol particles. Assuming that the mechanisms of deposition (wash-out by precipitation or dry fallout) are constant in time, the particle concentration in ice mirrors the concentration in past air masses. Changes in the concentration and/or composition of the particles reflect as well changes in sources and sinks of particles as changes in the atmospheric circulation. Biological particles are of special interest for climate change studies. The biosphere reacts very sensitive to variations in the temperature and therefore changes in the concentration of biological particles might indicate a temperature change (Bennike *et al*. 1990).

Biological particles in ice cores may originate both from local and remote source areas. The Arctic is not a vast abiotic frozen desert. A great variety of living organisms have adapted to the cold environment. Fredskild (1966) and others found altogether 105 different species of vascular plants in Peary Land. Bennike *et al*. (1990) isolated 60 plant and 120 insect remains from the pliopleistocene Kap København Formation, a sediment in north-east Peary Land. But there are also biological particles found which derive recognizably from sub-Arctic areas. As Greenland lies north of the tree line, all tree pollen found in the ice must have been transported over a long distance. Fredskild *et al.* (1974) discovered, that in addition to local herb and grass pollen, pine *(pinus)*, birch *(betula)* and alder *(alnus)* pollen were

also found in the Camp Century ice core (77.1°N, 61.1°W). Pine, birch and ragweed pollen also occurred in the Dye-3 ice core (65.1°N, 43.5°W) in southern Greenland (Bourgeois 1990).

Methods

The ice cores were kept frozen at –80°C until analysis. The surface of the ice core was contaminated by drilling and handling processes so that it could not be used for microparticle analysis. Hence the ice had to be cleaned by cutting off the outer parts of the core with a stainless steel knife. Because of the wide size range of the particles suspended in the ice, two different methods were used to determine the size distributions of the total and biological particles. Particles with radii $r > 2.0$ µm were investigated in a light microscope. For this, the ice was melted at room temperature and a protein dye (Matthias-Maser *et al*. 1994) was added. Biological particles were stained blue, while non-biological particles were not stained. Particles with radii $0.2\ \mu m < r < 2.0\ \mu m$ were analysed in a scanning electron microscope (SEM) which was combined with an energy dispersive X-ray spectrometer (EDX). Biological particles often showed a characteristic morphology (spheres with rods or cavities) in the SEM, but not in all cases this information was sufficient to distinguish them from non-biological particles. The elemental composition of the particles was very important for identification. Biological material was characterised by a high background spectrum which was overlapped by peaks of the elements phosphorus, sulphur, potassium, calcium and sometimes chlorine. Some biological particles were unstable under the electron beam during EDX and shrank or disappeared. For classifying biological particles in the SEM/EDX, the morphology, elemental composition and the behaviour during the analysis must be considered. The total and the biological particles were counted in nine size classes. The number-, volume- and mass size distributions were calculated for both the total and the biological particles. Additionally the percentage of the particles with biological origin was determined.

Results

The size distribution of insoluble particles in the Hans Tausen ice core was determined for the size range $0.2\ \mu m < \text{radius} < 41.2\ \mu m$. Ice samples from different depths were analysed and a mean value was calculated. In Fig. 1 the mean size distributions for the total and the biological particles are plotted together with the percentage of the biological particles. In the left plot the number size distributions dN/dlogr are shown. In the Hans Tausen ice core around 10^5 insoluble particles per ml ice were found. The ratio of biological to non-biological particles rises with increasing radius. While only 3% of all particles with sizes below 2.0 µm were biological, the biological percentage rises up to 26% at radii between 10 µm to 15 µm. The smaller particle sizes are characteristic of viruses and bacteria which are mostly found in urban areas. As Peary Land is a very remote area, these small biological particles are not found and hence the biological percentage in this size range is relatively low. Spores of lichens, mosses, fungi and algae have radii larger than 0.5 µm, whilst pollen and fragments are in excess of 5 µm in radius. These particles, that are typical for remote continental regions (Matthias-Maser 1998), appear in the Hans Tausen ice cap in a much higher percentage than bacteria. Regarding the volume and mass size distributions (Fig. 1, centre and right plot) it is obvious, that the main mass is due to particles larger than 3 µm radius. This is in agreement with particle measurements in snow from South Greenland

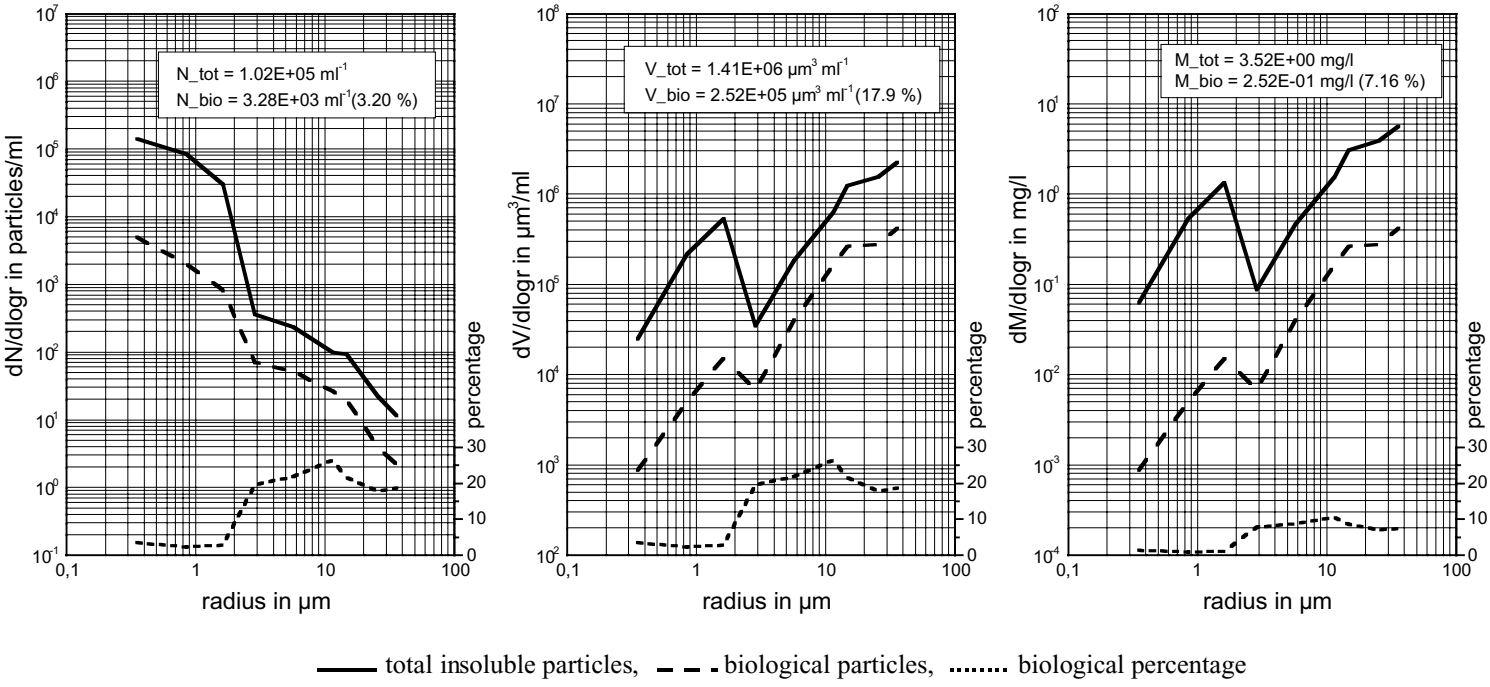

Fig. 1: Left plot: Number size distributions; centre plot: Volume size distributions; right plot: Mass size distributions (density of total particles $\rho\_tot = 2.5\ g/cm^3$, density of biological particles $\rho\_bio = 1.0\ g/cm^3$).

(Steffensen 1985). It is remarkable, that biological particles comprise nearly 18% of the total particle volume in the ice core. This corresponds to 7% of the total particle mass. Again, this is caused by the higher biological percentage in the giant particle fraction. These preliminary results show, that there exists a great variety of biological material both from local and remote sources in northern Greenland ice.

Acknowledgements

The ice samples have kindly been provided by Claus Uffe Hammer from the Niels Bohr Institute, University of Copenhagen, Denmark. The Hans Tausen project was part of the *Nordic Environmental Research Programme 1993-1997* and was funded by the *Nordic Council of Ministers* and the *Danish Science Research Council*.

References

Bennike, O. and J. Böcher 1990. Forest-Tundra Neighbouring the North Pole: Plant and Insect Remains from the Plio-Pleistocene Kap København Formation, North Greenland. *Arctic* 43(4): 331-338.

Bourgeois, J. 1990. A Modern Pollen Spectrum from Dye 3, South Greenland Ice Sheet. *Journal of Glaciology* 36: 340-342.

Fredskild, B. 1966. *Contributions to the Flora of Peary Land, North Greenland.* Meddelelser om Grønland 178 (2): 1-23.

Fredskild, B. and P. Wagner 1974. Pollen and fragments of plant tissue in ice core samples from the Greenland Ice Cap. *Boreas* 3: 105-108.

Matthias-Maser, S. and R. Jaenicke 1994. Examination of Atmospheric Bioaerosol Particles with Radii r > 0.2 µm. *Journal of Aerosol Science* 25: 1605-1613.

Matthias-Maser, S. 1998. Primary biological aerosol particles: Their significance, sources, sampling methods and size distribution in the atmosphere. In: *Atmospheric Particles* (ed. R.M.Harrison and R.Van Grieken). John Wiley and Sons Ltd.

Steffensen, J.P. 1985. Microparticles in snow from the South Greenland ice sheet. *Tellus* 37 B: 286-295.

MONOGRAPHS ON GREENLAND

PUBLISHED BY THE DANISH POLAR CENTER

The Hans Tausen Iskappe (ice cap) in the extreme north of Greenland owes its existence to the relatively cool conditions over the past 4000 years. The area is sensitive to global climate changes, and the ice cap will melt away if the climate becomes a few degrees warmer.

From 1993 to 1997 a group of Nordic researchers set out to investigate the history and dynamics of this most northernly ice cap of the hemisphere. Geophysicists, geologists and geographers mapped the ice cap, drilled through it and searched for the history of its past by analyzing the annual ice layers.

Some of the findings have added significantly to our understanding of the consequences of Global Change. The major findings are presented in this volume.